Wetting phenomena and foam drainage on complex substrates

Wetting phenomena and Foam drainage on complex substrates

by
Nektaria Koursari

Department of Chemical Engineering

Loughborough University, United Kingdom

(August 2020)

A doctoral thesis submitted in partial fulfilment of the requirements for the award of Doctor of Philosophy of Loughborough University

ABSTRACT

The interaction of foam and droplets with multiple substrates is investigated. This research is divided into the following areas (1) Equilibrium of droplets on deformable substrates: Equilibrium conditions (2) Hysteresis of contact angle of sessile droplets on deformable substrates: Influence of Disjoining pressure (3) Foam drainage on thin porous layer (4) Drying of foam under Microgravity conditions and (5) Modelling of foamed emulsion drainage.

Equilibrium conditions of droplets on deformable substrates are investigated and it is shown for the first time that for equilibrium the Jacobi's condition must be satisfied. It is shown that the deduced solution for both droplet and deformed substrate the Jacobi's necessary equilibrium condition is satisfied. It is shown that the deduced profiles of the equilibrium droplet and deformable substrate satisfy the Jacobi's condition and provide the minimum to the excess free energy of the system.

A theory of contact angle hysteresis of sessile droplets on deformable substrates is developed in terms of the disjoining pressure isotherm. It is shown that calculated values of both advancing and receding contact angles for droplets on deformable substrate depend on droplet volume and decrease with increasing substrate elasticity.

A theory of foam drainage placed on thin porous layer is developed by considering mobile upper foam surfaces and taking into account the presence of surface viscosity. The rates of drainage and imbibition into porous layer are predicted. Conditions and duration of free liquid layer formation on the foam-porous layer interface have been theoretically predicted. The theoretical predictions are compared with experimental observations and comparison showed a good agreement. The effect of model parameters on the kinetics of the drainage/imbibition process and the existence of three different imbibition regimes are evaluated and discussed.

A new method of drying foams under microgravity conditions is suggested for the first time. It is known that gravity affects the foam formation, its evolution and stability by causing flow of liquid from higher to lower parts of the foam (drainage). However, under microgravity conditions the drainage is impossible because only capillary forces are involved. That is, drying of foams is impossible under microgravity conditions. A new method is suggested for drying of foams under microgravity conditions. According to the suggested method of foam drying the foam is placed on porous layer which will result in liquid absorbance from the foam driven by capillary suction. Model predictions are compared with experimentally obtained data with reasonable agreement.

The drainage of foamed emulsions (also considered as complex multiphase systems) has been investigated both experimentally and theoretically. Foamed emulsions have been prepared using mixture of sodium dodecyl sulphate and oil, using the double syringe method. A theoretical model is developed, taking into account both surface viscosity and non-Newtonian behaviour of the foamed emulsion describing the kinetics of the drainage process. Theoretical predictions of rate of drainage, foam height and liquid volume fraction for foamed emulsion systems of various oil volume fractions are compared with experimental observations and comparison shows a reasonable agreement.

ACKNOWLEDGMENTS

I wish to express my deepest gratitude to my supervisor Prof Victor Starov for his consistent support, guidance and advice throughout these three years. I have been extremely lucky to be offered the opportunity to work with such an exceptional scientist and person and receive patient and constructive advice.

I equally would also like to pay my special regards to my co-supervisor Dr Anna Trybala for inspiring me to initiate this research project and for all the continuous professional and personal support, scientific advice, and encouragement.

I would like to recognize the assistance and advice provided by my co-supervisor Dr Hemaka Bandulasena during the third year of my PhD.

I am also extending my warmest gratitude towards Prof Tatiana Gambaryan-Roisman, coordinator of CoWet project and my colleagues and co-authors of joint research, Mr Phillip Johnson, Dr Omid Arjmandi-Tash, Dr Gulraiz Ahmed, Dr Maryam Parsa, Dr Longquan Chen, Mr Elmar Bonaccurso, Professor Yapu Zhao and Dr Maxime Schneider for their wonderful collaboration, discussions and efforts.

I gratefully acknowledge the funding received towards my PhD from EU CoWet project; Procter & Gamble, Brussels; EPSRC, UK, grant EP/J010596/1; PASTA and MAP EVAPORATION projects, European Space Agency; and COST project MP1106.

Gratitude towards the School of Aeronautical Automotive Chemical and Materials Engineering, Loughborough University for a doctoral scholarship.

I equally wish to acknowledge the support and inspiration I received from my family, my husband Jonathan; my daughter Nefeli; my son Jason; my beloved parents and my brother Spyros. This work would not have been possible without their input.

Contents

LIST OF TABLES

Table of Figures

CHAPTER 1

INTRODUCTION

Overview

The increasing interest on the investigation of parameters that affect the interaction between liquid droplets, foams and foamed emulsions with complex substrates (rigid, deformable or porous substrates), is related to numerous industrial, biological and technical applications. The properties of these fluids, the properties of the substrates and the way they interact when in contact are highly important when referring to specific applications and product development. The properties of the components, e.g. concentration, liquid volume fraction, rheological properties, can be altered depending on the application, setting the complexity of such systems as an incentive for further theoretical and experimental analysis(1).

Liquid droplets occur everywhere in nature and technology. Water droplets can be found anywhere on earth from the clouds above to the ground below(2). Aqueous thin films also refer to as 'wetting films', are ubiquitous in nature. A solid substrate exposed to its environment is always covered by a very thin liquid film which, in most cases, is unable to be seen with naked eye(3). The process of 'Wetting' of solid substrates by thin liquid films is highly related to the existence of the so-called apparent three-phase contact line, which is the region where the three phases, liquid, air and solid meet. At the region of the three-phase contact line the thickness of the liquid film becomes too small allowing for some special Colloidal forces, refer to as surfaces forces, to act and influence the process of wetting and spreading. Efficient wetting and spreading of liquid droplets on multiple substrates is highly important for various applications including coating, inkjet printing, spray painting, tertiary oil recovery, surface cooling, medicine and offset printing (4), (3). When for instance we are referring to the process of inkjet printing a liquid ink droplet has to be applied equally and steadily on a sheet of paper while in medical applications a liquid antibiotic has to be applied directly down in the lungs for respiratory disease treatment (2). The investigation of the parameters of the liquid droplet and the wetted substrate when interacted in relation to the action of forces in thin layers can lead to progress in the area of colloidal science and potential technological advances and product development.

Foams are also a popular type of colloidal system, consisting of both liquids and bubbles stabilised by surfactants and/or polymers (foaming agents). Foams can be produced with several methods including blowing gas through a nozzle into a liquid phase, shaking, beating a liquid or blending (2). Aqueous foams have a wide range of industrial and domestic applications including acoustic thermal insulation, fire-fighting processes, packaging solutions and constituents of structural foam materials and food, cosmetic and medical products (5). Foams are favourable in the industry due to their properties and ability to act as chemical carriers for cleaning purposes, as effective firefighting materials able to attack the three causes of fire (fuel, oxygen and heat) and for decontamination processes in nuclear reactors (2). Foam products are also ideal for penetration and imbibition into porous media, such as gas and oil recovery and irrigation (6,7) . It has been recently reported that foams are ideal products for the delivery of topical active agents such as antibacterial, skin corticosteroids, antiviral agents and local anaesthetic agents and act as ideal dug carriers for various dermatological applications (8–10).

Foamed emulsions with oil are also commonplace in a wide range of products including food foams, cosmetics, pulp and paper and water treatment processes where emulsions are used for the production of more stable foams and as antifoams (11). In the pharmaceutical industry several foamed emulsions have

been created for the effective delivery of active ingredients and controlled release for topical and oral applications for the provision of therapeutic benefits (11,12). Foamed emulsions can be created by several types of emulsions. In most of emulsions one phase is usually oil and the other one is water, so that the two most common types of emulsions are oil-in water (O/W) or water-in -oil (W/O) where oil is the dispersed phase or water is the dispersed phase respectively. As foams with oil droplets are notoriously unstable, emulsification is an interesting way of creating stable foams of various oil volume fraction (13–15).

Foams are thermodynamically unstable systems and foam stability is highly significant for product development and stability control for several applications. The major processes taking place during foam collapse are mainly i) drainage ii) coarsening (interbubble diffusion of gas) and iii) coalescence (lamella rupture and burst of bubbles). Foam drainage is the process of liquid flow in between gas bubbles through Plateau borders, nodes and films and it occurs from the very beginning of foam formation (16). Foam drainage and imbibition into porous substrate has also attracted interest as a highly important process for biological and industrial applications where the substrate is porous (hair, skin, textile and rocks). The interaction of foam with porous material is applicable for use in drug delivery processes (8,17,18). Surprisingly a theoretical investigations of foam interaction with porous substrates was undertaken only recently (19).

Considering the vast amount of applications related to the interaction between fluids with multiple substrates of such complexity it is important to further investigate the properties that affect the behaviour of these systems. Throughout this thesis features of wetting and spreading of droplets on rigid and deformable substrates will be presented and common problems of the interaction between foam and foamed emulsions with porous substrates will be discussed.

1.1 Motivation and scope of the research

Recent research in the area of interfacial science has shown a fast-growing interest on wetting of deformable substrates and foam drainage on multiple substrates. The increasing interest originating by a multiplicity of industrial and biological applications related to these processes has developed the motivation of this research aiming on expanding our knowledge on:

i)Static wetting of deformable substrates considering the effect of surface forces in the vicinity of the three-face contact line. Wetting of elastic substrates such as elastic solids, polymeric material, cosmetics, gels and melts is commonplace in several applications such as pesticide spraying, surface coating and inkjet printing. Although recent progress on the development of experimental microscopic imaging techniques (20–22),(23) has allowed determination of interfacial droplet and substrate profiles and several theories (24–27) have been developed to describe the interaction between the two phases, yet the effect of the action of surfaces forces has been ignored. Surface forces are predominant when the thickness of the liquid layer becomes as small as 0.1μm and their action cannot be disregarded. Manifestation of surface forces that appear in thin liquid layers is the disjoining/conjoining pressure. The research focuses on developing a new modelling technique to describe the droplet profile and the deformation of the substrate where the influence of the action of surface forces on the deformation is considered. Contact angle hysteresis (advancing and receding contact angles) and equilibrium conditions of droplets on deformable substrates are theoretically investigated via the physical characteristics of the disjoining/conjoining pressure isotherm for the first time.

ii)Foam drainage and foam drainage/imbibition into porous substrates.
Aqueous foams are widely used in industrial and domestic applications including the production of shaving foams, firefighting foams, foam materials, food, cosmetics and medical products (11).

Foam products are also ideal for imbibition and penetration into porous substrates such as skin and hair acting as carriers for the delivery of topical active agents used for dermatological applications (8–10,28,29). One of the major processes taking place during foam collapse is foam drainage which is the flow of liquid through Plateau borders, nodes and films driven by the simultaneous action of gravity and capillarity (30–34).

The process of foam drainage is highly related to the stability of foam systems and it has been theoretically investigated by several research groups (33–39).

The process of foam drainage is governed by simultaneous factors yet not fully understood setting an era for further theoretical and experimental analysis on the parameters that affect the kinetics of the process.

Recognising the significance of the process of foam drainage for several technological and medical applications, this research is devoted on developing a theory able to describe the process of foam drainage on a thin porous layer such as skin or hair. In this case, the drainage process is a combination of a drainage caused by gravity/capillary action inside the foam and a capillary suction applied by the pores from the porous substrate (40).

The latter developed mathematical model is then modified to describe a method of foam drying under microgravity conditions where the drained liquid is absorbed by a porous material based on capillary forces. Investigating the behaviour of foams under microgravity conditions also allows overcoming the instability barriers imposed when gravity forces are present (41), leads to optimisation of terrestrial processes and is linked to applications where gravitational drainage is not desirable (42–44).

Foamed emulsion drainage is also investigated both theoretically and experimentally. Foamed emulsions are commonplace in the development of a variety of industrial products including food products, pharmaceuticals, and cosmetics where the rate of drainage is pivotal for their stability, behaviour and texture (11,45,46)**.** This research was motivated by a most recent experimental study by Schneider et al(14) where the complexity of foamed emulsion systems was identified, and the necessity of further experimental and theoretical investigation was recognised. We have developed a new analytical model to describe the kinetics of drainage process of foamed emulsion systems containing emulsified oil, taking into account of both the non-Newtonian behaviour of the foamed emulsion and the mobility of the gas/liquid interface. Theoretical model predictions for all investigated systems are compared with experimentally obtained results.

1.2 Aims and Objectives

The study aims to investigate the parameters that affect the interaction between droplets, foams, and foamed emulsions, with rigid, deformable, and porous substrates. The parameters of the liquid and the parameters of the substrate have a profound impact on the processes taking place during the interaction between the two phases.

More specifically our research has focused on:

i) Investigating equilibrium conditions of droplet on deformable substrate using Jacobi's sufficient condition. A mathematical model is developed of droplet on deformable substrate by considering the action of the disjoining/conjoining pressure. The obtained equilibrium profiles of the droplet and the support are investigated based on the necessary and sufficient conditions of equilibrium and the validity of Jacobi's condition is verified for the first time.

ii) Create a theory of contact angle hysteresis of a liquid droplet on deformable substrate in terms of the disjoining/conjoining pressure isotherm. The parameters of the liquid and the support that affect the values of both advancing and receding contact angles are investigated.

iii) Develop a mathematical model of foam drainage on a wettable thin porous layer by considering the effective slip caused by the effect of surface viscosity. The existence of three different regimes of spreading/imbibition is predicted and the kinetics of drainage/imbibition are investigated based on seven dimensionless model parameters. Theoretical predictions are compared with experimental observations.

iv) Create a method of foam drying under microgravity conditions. The research focuses on developing a theoretical model to investigate the kinetics of foam spreading on several porous supports only under the action of capillary forces. Model predictions are compared with experimentally obtained measurements.
v) Experimental and theoretical investigation of foam drainage for foam created using Non-Newtonian emulsions. The theoretical model developed describes the time dependencies of free liquid layer formation, foam height and liquid volume fraction for various foamed emulsion systems.

1.3 Thesis layout

This thesis is divided into eight chapters. Chapter 1 is an Introduction with seven subsections including i) Background information ii) Motivation and scope of the Research, iii) Research Aims and Objectives, iv) Thesis layout v) Dissemination from the PhD thesis, vi) Participation in scientific meetings and vii) Prizes. Chapter 2 is a literature review followed by Chapters 3-7 where the Theoretical and Experimental research undertaken is presented and results are discussed. Chapter 8 is the Conclusions and Future research section where an i) overall summary and ii) suggestions for further investigation are provided.

The research studies presented in Chapters 3-7 are published in 5 journals papers and are listed in section 1.4.1. More specifically each chapter contains the following information:

Chapter 1is an Introduction which provides with general information for the research undertaken, outlines the significance of the study in relation to common industrial, technical, and medical applications and provides with a list of the most relevant background research. In this Chapter the motivation and scope of the research studies are also outlined in section 1.1 and the aims and objectives are discussed in section 1.2.

Chapter 2 is a literature review where information on the most recent theoretical and experimental research on i) Static wetting on deformable substrates and ii) Foam drainage and Interaction of foam with porous substrates is provided.

In Chapter 3 equilibrium conditions of droplets on deformable substrates are investigated. A mathematical model is developed under consideration of the action of surface forces and a simplified disjoining/conjoining pressure isotherm is adopted for calculations. The purpose of the study is to investigate the validity of Jacobi's necessary equilibrium condition which proves that the obtained solutions really provide with the droplet and deformable substrate equilibrium profiles. This is the first time that Jacobi's necessary equilibrium condition has been verified.

In Chapter 4 a mathematical model of hysteresis of contact angle of sessile droplets on deformable substrates is presented in terms of the disjoining/conjoining pressure isotherm. The parameters that affect the advancing and receding contact angles of droplets on deformable/soft substrates are theoretically investigated.

In Chapter 5 foam drainage on thin porous layer is investigated both from a theoretical and experimental point of view. The mathematical model developed aims on investigating the process of foam drainage/imbibition and the parameters that affect the interaction between the foam and the porous layer. Model predictions are compared with experimental findings.

In Chapter 6 a new method of drying of foam under microgravity conditions is developed and the kinetics of foam spreading on various porous layers are presented. Model predictions for time relations of wetted radius are compared with experimental results of foam created using Triton X-100 non-ionic surfactant in contact with porous layer of various grades.

In Chapter 7 the kinetics of foam drainage of foam created by emulsions of sodium dodecyl sulphate (SDS) and rapeseed oil are investigated. The developed mathematical model is able to describe the time evolutions

of liquid volume fraction, foam height and the thickness of the drained layer taking into account both the non-Newtonian behaviour of the foamed emulsion and free slip condition. Theoretical results are compared with experimental findings for four investigated emulsions.

1.4 Dissemination from the PhD thesis

1.4.1 Journal paper publications

(1) Chen, L.; Bonaccurso, E.; Gambaryan-Roisman, T.; Starov, V.M; **Koursari, N**.; Zhao, Y. Static and Dynamic Wetting of Soft Substrates. Curr. Opin. Colloid Interface Sci. 2018, 36, 46–57**.**

(2) Ahmed G., **Koursari N.**, Trybala A. and Starov V.M, Sessile Droplets on Deformable Substrates, Colloids Interfaces 2018, 2(56), 1-16**, (Chapter 2, section 2.1.2)**

(3) Ahmed, G.; **Koursari, N.**; Kuchin, I. V.; Starov, V. M. Hysteresis of Contact Angle of Sessile Droplets on Deformable Substrates: Influence of Disjoining Pressure. Colloids Surfaces A Physicochem. Eng. Asp. 2018, 546 (March), 129–135, (**Chapter 4)**

(4) **Koursari, N.**; Ahmed, G.; Starov, V. M. Equilibrium Droplets on Deformable Substrates: Equilibrium Conditions. Langmuir 2018, 34 (19), 5672–5677, **(Chapter 3)**

(5) Trybala, A.; **Koursari, N.**; Johnson, P.; Arjmandi-Tash, O.; Starov, V. Interaction of Liquid Foams with Porous Substrates. Curr. Opin. Colloid Interface Sci. 2019, 39, 212–219, **(Chapter 2, section 2.2)**

(6) **Koursari, N.**; Arjmandi-Tash, O.; Johnson, P.; Trybala, A.; Starov, V. M. Foam Drainage Placed on Thin Porous Layer. Soft Matter 2019, 15, 5331–5344, **(Chapter 5)**

(7) **Koursari, N.,** Arjmandi-Tash, O., Trybala, A. *et al.* Drying of Foam under Microgravity Conditions. *Microgravity Sci. Technol.* 31, 589–601 (2019), **(Chapter 6)**

(8) **Koursari N.,** Johnson P., Parsa M., Schneider M., Trybala A., Starov V.M., Modelling of foamed emulsion drainage, Colloids Surfaces A Physicochem. Eng. Asp. (2020), **(Chapter 7)**

1.4.2 Participation in Scientific meetings

1. Darmstadt Germany-Short course on complex wetting (COWET), 11-13 October 2017, (attendance)
2. 16th IACIS Conference Rotterdam 21-25 May 2018, title: 'Hysteresis of Contact Angle on Deformable Substrates: Influence of Disjoining Pressure, (poster presentation)
3. Durham University, Workshop on Multiscale Modelling of Wetting Phenomena, 12 September 2018 (attendance)
4. Loughborough University School Research Day, 19 June 2019, title: Droplets on deformable substrates: equilibrium and hysteresis contact angles (poster presentation)
5. 8th Conference B&D Bulgaria, Sofia, title: Droplets on deformable substrates: equilibrium and hysteresis contact angles, 24-28 June 2019 (oral presentation)

1.4.3 Prizes and nominations

1. School of AACME research student development fund (2018)
2. Loughborough Doctoral College Student Prize 2019-Supervisor's Nomination (April 2019)

CHAPTER 2

LITERATURE REVIEW

Overview

This chapter is divided into two sections.

In the first section equilibrium droplets on rigid and deformable substrates are discussed and a summary of the most recent experimental and theoretical research on static wetting on deformable substrates will be provided. The effect of the action of the surface forces (disjoining/conjoining pressure) near the apparent three-phase contact line on the interfacial behaviour between a liquid droplet and an elastic substrate will be considered.

In the second section of this review a description of foam, foam structure and the process of foam drainage will be provided, and the most recent studies of foam drainage/imbibition of foam placed on porous substrates will be reviewed.

The information provided in Sections 2.1.2 is published in Colloids and Interfaces and re-used below with permission from corresponding author, Professor Victor M. Starov(v.m.starov@lboro.ac.uk). The information provided in section 2.2 is published in Current Opinion in Colloid & Interface Science, and reused below with permission from corresponding author, Dr. Anna Trybala(a.trybala@lboro.ac.uk).

2.1 Static wetting of deformable substrates

2.1.1. Equilibrium droplets on rigid and deformable substrates- The role of the disjoining/conjoining pressure

There has been a considerable increase of interest in wetting and spreading phenomena during the last decade mainly related to a broad range of industrial, environmental, and medical applications(47). Thomas Young first derived an equation to predict equilibrium contact angle, θ_e, on a rigid solid substrate(48):

$$cos\theta_e = \frac{\gamma_{sv} - \gamma_{sl}}{\gamma_{lv}} \qquad (2.1)$$

Youngs equation connects three interfacial tensions, liquid-solid γ_{sl} , liquid-vapor γ_{lv} , and vapor-solid, γ_{sv}, in consideration of the balance of horizontal forces.

When a droplet is deposited on a solid substrate, three different cases could be met. The droplet could spread out either partially with a contact angle between 0 and π/2, completely or immediately form a droplet with a contact angle greater than π/2. These three cases are referred to as partial, complete, and non-wetting respectively. As shown above, Youngs equation reduces the three spreading cases to the determination of three interfacial tensions. Under equilibrium conditions the excess free energy, Φ,

$$\Phi = \gamma_{lv} \cdot S + P_e \cdot V + \pi R^2(\gamma_{sl} - \gamma_{sv}) \qquad (2.2)$$

of the droplet should be at its minimum value, where $P_e = P_a - P_l$ the excess pressure inside the liquid droplet, P_a the pressure in the ambient air and P_l the pressure inside the liquid, S excess of the vapour-liquid interfacial area, V the excess volume and R the radius of the drop base. At equilibrium, the excess pressure inside the droplet(P_e) should be at any negative value in the case of a liquid droplet. Only in the case when the minimum of the excess free energy is reached then the contact angle can be evaluated by Young's equation (3). For the excess free energy to be at its minimum value four necessary conditions should be satisfied:

(i) The first variation of the excess free energy, $\delta\Phi$, should be zero
(ii) The second variation, $\delta^2\Phi$, should be negative
(iii) The transversality condition at the perimeter of the droplet at $r = R$ at the three-phase contact line should be satisfied
(iv) Jacoby's necessary condition should be satisfied(49)

In addition to the above statements it also should be mentioned that Youngs equation does not consider neither the role of droplet volume nor the excess pressure inside the liquid droplet which could be any negative value. According to Kelvin's equation, the excess pressure inside the liquid droplet is expressed as:

$$P_e = \frac{R_g \cdot T}{V_m} ln \frac{P_s}{P} \qquad (2.3)$$

where V_m molar volume of the liquid, P_s pressure of the saturated vapor at temperature T, R_g the gas constant and P the vapor pressure. As P_e should be negative at equilibrium, this means that the right-hand side of the above equation should be negative or $P > P_s$ and therefore a droplet can only be at equilibrium with oversaturated vapor. The latter means that it is very difficult if not impossible to investigate equilibrium droplets experimentally. Based on the above consideration every previously obtained contact angles correspond to static advancing and static receding contact angles and not equilibrium contact angles (3).

In addition, we should now refer to the requirement of the existence of a transition zone from the flat equilibrium film ahead of the droplet to the solid substrate. The presence of this transition explains the existence of the so called three phase contact line (TPCL) where the action of surface forces comes into effect. Surface forces are highly related to the wetting properties of droplets on solid substrates and are well known in the area of colloidal and interfacial science. At the TPCL the thickness of the liquid profile tends to zero, $h(r) < 10^{-5} cm$, and this is when surface forces start to act. Derjaguin's pressure is a manifestation of surface forces acting near the TPCL and are named after Boris Derjaguin (50). At the TPCL the thickness of the droplet profile is too small allowing for Derjaguin's pressure to act.

Derjaguin's pressure has three components: 1) The molecular component 2) The electric double layer and 3) The electrokinetic phenomena. But let us refer to each one of them in more detail below:

1) The molecular component of surface forces

   According to the Derjaguin–Landau–Vervey–Overbeek, or DLVO theory(50) the molecular contribution of Derjaguins pressure is expressed as:

$$\Pi_M = \frac{A}{6\pi h^3} \quad (2.4)$$

where $A = -A_H$ the Hamaker constant which depends on the three phases, liquid, air and solid phase and could be either positive (repulsion) or negative (attraction).

2) The structural component of Derjaguin's pressure, which is caused by the water molecules orientation in the aqueous solution-solid interface or the aqueous solution-air interface. If the interface is negatively charged then the positive parts of the water dipoles are attracted to the interface leading to the creation of a negatively charged layer outside the interface (directed onwards). In the next layer the water dipoles will be in contact with the negatively charged dipole parts. According to (47,51,52) the total structural force is expressed as:

$$\Pi_s(h) = K_1 e^{-h/\lambda_1} + K_2 e^{-h/\lambda_2} \quad (2.5)$$

where K_1, K_2, λ_1, λ_2 are experimentally obtained constants related to a magnitude and characteristic length of structural forces. Subscript 1 corresponds to the short-range and subscript 2 to the long-range interactions.

3) The electrostatic component of the Derjaguin's pressure

In the case of two charged surfaces (e.g aqueous electrolyte solutions) the surfaces might be equally or oppositely charged which means that there is an electrical double layer near each of the surfaces.

In the case of low ζ potential of both surfaces the electrostatic component of Derjaguin's pressure is expressed as:

$$\Pi_e(h) = \frac{\varepsilon\kappa^2}{8\kappa} \frac{2\zeta_1\zeta_2 cosh\kappa - (\zeta_1^2 - \zeta_2^2)}{sinh^2\kappa h} \quad (2.6)$$

where ε the dielectric constant of water and $\frac{1}{\kappa} = R_d$ and R_d the thickness of the Debye layers.

If the surfaces are oppositely charged, then the following expression is used:

$$\Pi_e(h) = -\frac{\varepsilon}{8\pi} \frac{(\zeta_1 - \zeta_2)^2}{h^2}, \quad (2.7)$$

which corresponds to attraction always in relation to the distance between the surfaces. Attraction could change to repulsion as distance between surfaces decreases(50).

The sum of the above mentioned three components corresponds to the Derjaguin's pressure of thin liquid films as shown in the following expression:

$$\Pi(h) = \Pi_E(h) + \Pi_s(h) + \Pi_M(h) \qquad (2.8)$$

The dependency between Derjaguin's pressure on the flat liquid films thickness is presented in the following Figure 2.1:

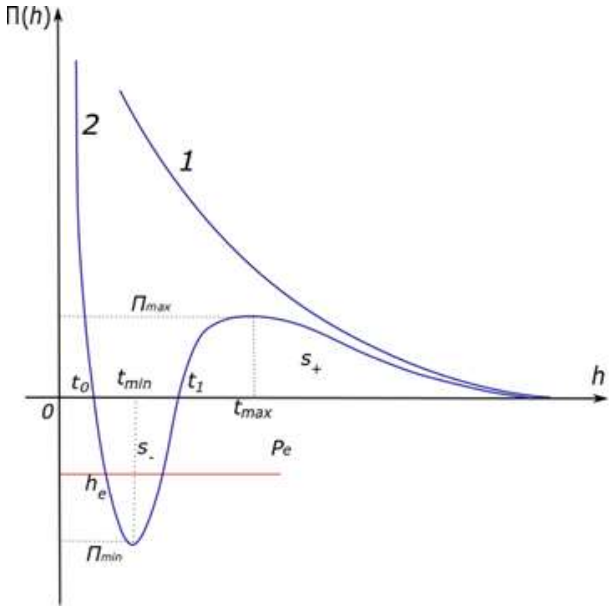

Figure 2. 1 : Disjoining/conjoining pressure isotherms: 1, complete wetting; 2, partial wetting, where h_e is the equilibrium flat thin film(53)

The excess pressure P_e given by kelvins equation $P_e = \frac{R_g T}{v_m} \ln \frac{p_s}{p}$ is an equality of the chemical potentials of water molecules in the vapor and liquid phases and P_e is a function of the thickness of the equilibrium film, h_e. At equilibrium, the excess free energy of the system should be at its minimum value: 1) $\frac{d\Phi}{dh_e} = 0$ which results in $P_e = \Pi(h_e)$ and 2) $\frac{d^2\Phi}{dh_e{}^2} > 0$ which results in $\frac{d\Pi(h_e)}{dh_e} < 0$ where $\Pi(h)$ the Derjaguins pressure.

$P_e = \Pi(h_e)$ is a relation between the thickness of the equilibrium film h_e and Derjaguin's pressure and equation $\frac{d\Pi(h_e)}{dh_e} < 0$ corresponds to the stability condition of flat equilibrium films (3,50).

2.1.2 Sessile droplets on deformable substrates

2.1.2.1 Introduction

Wetting of deformable substrates has gained significant interest over the last decade, particularly due to its wide range of applications. These applications occur both naturally (include biological processes) and via industrial processes. Elastic solids including foams, cosmetics, paper, polymeric materials, gels and melts have been incorporated in several applications such as inkjet printing applications(4), forensics (54), surface coating, pesticide spraying and spray painting (55).

The well-known Young's equation has been widely used to predict equilibrium contact angle, θ_e, on rigid solid substrates(48). It gives a relationship between solid-liquid, liquid-vapor, and vapor-solid surface tensions and is based on consideration of the balance of horizontal forces. However, Young's equation cannot be used when the substrate is deformable, where the vertical component ($\gamma \sin \theta_e$) of the surface tension remains unbalanced. Substrate deformation should balance this extra force in the case of deformable substrate. However, even after modification, Young's equation still cannot be applied directly as it gives rise to deformation singularity (surface deformation goes to infinity) near the three-phase contact line (25,26,56–60).

To avoid the singularity, several researchers have tried different approaches. It was initially suggested that surface tension should be uniformly distributed near the contact line to mitigate the singularity (56–59).

Lester was the first to model a sessile droplet on an elastic substrate where the Neuman's triangle is considered (25). The author identified the significance of a vertical component of liquid surface tension applied at the three-phase contact line. Neumann's triangle, as firstly introduced by Neumann(61) is a triangle of forces distributed in a certain way over the contact line so that the resultant force vanishes(25). Using the same concept, Style and Dufresne, generalized a three-dimensional configuration confirming the validity of Neumann's triangle for small droplets(26). However, it is important to mention that Neumann's triangle of forces applied near the three-phase contact line could only be regarded as valid in the case an equilibrium configuration(25) as long as the necessary equilibrium conditions are satisfied (60).

Unfortunately, Neumann's approach (despite being widely used) is in a contradiction with thermodynamics because it ignores the full thermodynamic equilibrium of liquid with vapor and solid substrate (see the full discussion in (53)), but most importantly, according to Neuman's approach, a vapor pressure at which the droplet is at equilibrium is not specified. That is, according to Neumann's equation, the droplet can be at equilibrium even with undersaturated vapor. The latter is in a drastic contradiction with Kelvin's equation: according to Kelvin's equation, droplets can be at equilibrium with over saturated vapor only. It is also important to mention that Neumann's equation ignores surface forces action in the vicinity of the apparent three phase contact line. It is worth remembering that surface forces come into play as soon as the thickness of the liquid layer is <0.1 μm. Manifestation of surface forces action appear in thin liquid layers (<0.1 μm, that is in the vicinity of the apparent three-phase contact line) of disjoining/conjoining pressure (53). Note that the term "apparent three-phase contact line" is used to emphasize that there is no real sharp contact line but instead there is a transition zone, where capillary and surface forces act simultaneously (53). The disjoining/conjoining pressure acts in the vicinity of the apparent three phase contact line in both rigid and deformable substrates. That is, surface forces action in the vicinity of the apparent three-phase contact line is compulsory in both rigid and deformable substrates. Consideration of action of disjoining/conjoining pressure in the vicinity of the apparent three-phase contact line in the case of rigid substrates allows calculating via disjoining/conjoining pressure isotherm equilibrium the droplet profiles, equilibrium contact angles (53) and hysteresis of contact angle (static advancing and static receding contact angles) (47). Recently, surface forces effect near the apparent contact line for droplets on deformable substrates are taken into account (47,49,53,60,62–64). The most recent theoretical and experimental studies are reviewed in this article and a brief description is provided of equilibrium and hysteresis contact angles of sessile droplets where disjoining/conjoining pressure is taken into account(49,63,64).

2.1.2.2 Theoretical and experimental analysis

Several experimental studies on droplet wetting of deformable substrate have gained a lot of interest, primarily due to technological advances in imaging techniques(21–23,65–67).

The high-resolution cameras allow capturing droplet profiles in the vicinity of the three-phase contact line and subsequent substrate deformations. This has allowed developing understanding of theoretical concepts underlying the experiments (24,68,69).

In the most recent experimental studies, Style et al characterised the indentation of glass particles using confocal microscopy (69) while Camara et al. experimentally investigated the effect of Laplace pressure on deformation caused by drops of 1-butyl-3-methylimidazolium hexafluorophosphate ionic liquid on a silicone elastomeric polymer(23). The authors continued also by experimentally investigating the effect of the film thickness on the deformation of the substrate and found that for thinner films the solid support located underneath the drop affected both the wetting ridge and the dimple below the liquid(66). Jerison et al also used confocal microscopy to measure the displacement of water on an elastic substrate and described a symmetric model that fits these profiles(66). In the past few years, it has been possible to record high resolution images both in temporal and spatial coordinates.

Andreotti et al (24) presented recent advances of solid capillarity. The authors discussed that stretching the interface causes the energy to increase in proportionally to the surface energy(24). However, the Shuttleworth effect arises when the surface energy depends on the strain and in this case the derivative of surface energy also affects the surface stress(70,71). Other related materials, e.g. polymer melts and their thermodynamic properties, e.g. glass-transition temperature in relation to their mechanical properties are also discussed(70). It has been reported that the glass transition temperature of a polymer melt can be reduced depending on the boundary conditions (70,72,73). The relationship between surface stress and bulk deformation was also discussed in (70). In the same article(70) the significance of the critical elastocapillary length on the capillary effects, measured on nano scale for polymers and micro scale for gels, is also discussed.

In consideration of the static wetting problem the relationship between surface stress and surface energy has also been analyzed in a recent review article by Style et.al.(74). In this review paper the authors used the term “elastocapillarity” to describe the phenomenon of solid deformation as affected by mechanical properties of the substrates. The surface stresses theory is outlined and the importance of elastocapillary length on surface stress and elasticity is identified. Surface stress causes a stress jump across the interface of the deformable solid. Surface stress causes a stress jump across the interface of the deformable substrate(74). However, in the above-mentioned theories, the most important phenomena, the action of surface forces near the apparent three-phase contact line and the influence of the surface forces on the deformation of soft solids, are ignored.

In the next section, a new modeling technique for the investigation of wetting of soft substrates is reviewed, where surface forces action near the apparent three-phase contact line is considered. Surface forces are introduced using simplified disjoining/conjoining pressure isotherm. Although the selected configuration of the disjoining/conjoining pressure isotherm is simplified, it is still able to capture essential properties of a real disjoining/conjoining isotherm: (i) surface forces are present over short range; (ii) partially wetting droplets are referred to when appropriate values of parameters are selected; and (iii) the regions of influence of surface forces have stable thin fluid films. Elasticity of the soft substrate is introduced using Winkler’s model(73). Substrate’s deformation and the droplet profile are deduced via the physical characteristics of the disjoining/conjoining pressure isotherm and substrate’s elasticity(63).

For the droplet to be at equilibrium, four conditions have to be satisfied: (i) first variation of excess free energy is equal to zero; (ii) second variation is greater than zero; (iii) transversality condition is satisfied; (iv) Jacobi’s sufficient condition is fulfilled. The fourth condition is usually neglected by researchers in this area. In (63), a solution is deduced for both droplet and deformable substrate profiles, where disjoining/conjoining pressure action in the vicinity of the apparent three phase contact line was taken into account. For the first time in (49), the essential Jacobi’s condition for the solution of the liquid droplet on a soft substrate obtained in (63) is verified. In section 2.1.2.4 (analyzed in Chapter 3) the verification of the Jacobi’s sufficient condition for already obtained solution of equilibrium droplets on deformable substrates is undertaken.

Contact angle hysteresis (advancing and receding contact angles) is frequently connected to surface roughness and surface heterogeneities. However, these are not the only causes for the existence of contact angles hysteresis. Lately researchers have illustrated that hysteresis exist on smooth homogeneous solid substrates (75–77). It has been observed that contact angle hysteresis on a rigid substrate is dependent on surface forces action in the vicinity of the three-phase contact line (47). Recently, this theory has been

extended and applied to investigation of contact angle hysteresis of droplets on deformable/soft substrates(64). In Section 2.1.2.5(analyzed in Chapter 4), the findings of these quasi-equilibrium states that exist on deformable substrates are discussed.

2.1.2.3 Equilibrium of droplets on soft substrates

In this section a new approach for wetting of soft substrates is developed by introducing, surface forces action in the vicinity of three-phase contact line of the droplet. A simplified linear disjoining/conjoining pressure isotherm, Π, and elasticity of the substrate through Winkler's model(73,77)are used in this section. According to the Winkler's model, the deformation in the soft substrate is regional and has a direct relation with the applied pressure, P (63):

$$h_s = -KP, \tag{2.9}$$

where, K is the elasticity coefficient, h_s is the local deformation of the substrate due to the applied pressure from the fluid above, see Figure 2.2.

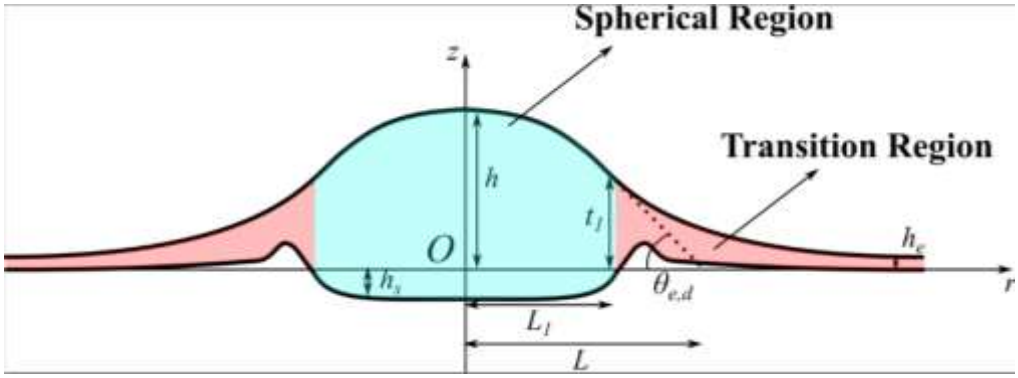

Figure 2. 2:Schematic diagram of droplet on a deformable substrate, Spherical (Bulk) region - $\Pi(h-h_s)=0$, and Transition region - $\Pi(h-h_s)\neq 0$, h - the liquid profile; h_s - deformation of the substrate; h_e- equilibrium flat film; θ_e- apparent equilibrium contact angle; t_1- height of the droplet at which surface forces (disjoining/conjoining pressure) start to act; L_1- radial length corresponding to t_1; L- Effective radius of the droplet; r, $z-$ co-ordinate system. Source: (78)

Assume P_{air} to be the ambient pressure in the air. Under the influence of the ambient air pressure the soft solid deformation is given by:

$$h_{se} = -KP_{air}. \tag{2.10}$$

Equilibrium thin film of fluid covers the deformed soft substrate, which is calculated according to a combination of the Kelvin's equation and disjoining/conjoining pressure isotherm (53):

$$\Pi(h_e) = P_e = \frac{R_g T}{v_m} \ln \frac{p_{sat}}{p}, \tag{2.11}$$

where, v_m is the molar volume of the liquid, T is the temperature in K, R_g is the gas constant, vapor pressure, p, which is higher than the saturated pressure p_{sat}. Reminder, a droplet is deemed to be at equilibrium under oversaturated vapor only according to Kelvin's equation. The excess free energy of the equilibrium thin film on the deformed solid in front of the liquid droplet per unit area is given by(53,63):

$$\frac{F_{e,film}}{S_{film}} = \gamma + \gamma_s + P_e h_e + \frac{h_{se}^2}{2K} + \int_{h_e}^{\infty} \Pi(h) dh, \qquad (2.12)$$

where, $P_e = P_{air} - P_{liquid}$, γ and γ_s are vapor-liquid and liquid-solid surface tensions. This free energy should be subtracted from the free energy of the droplet on the deformable substrate; otherwise the excess free energy of the droplet is infinite(53,63). Hence, the excess free energy of the droplet on a deformable solid substrate is as follows (see Figure 2.2):

$$F - F_{e,film} = \gamma \Delta S + \gamma_s \Delta S_s + \Delta V + F_{surface\ forces} + F_{deformation}, \qquad (2.13)$$

where Δ means "as compared with a flat equilibrium film".
Eq. 2.13 can be rewritten as:

$$F - F_{e,film} = 2\pi \int_0^{\infty} f(h, h', h_s, h_s') dr, \qquad (2.14)$$

where

$$f(h, h', h_s, h_s') = r \left[\begin{array}{c} \gamma\sqrt{1 + h'^2(r)} - \gamma + \gamma_s \sqrt{1 + h_s'^2(r)} - \gamma_s + \\ P_e(h - h_s) - P_e h_e + \frac{h_s^2}{2K} - \frac{h_{se}^2}{2K} \\ + \int_{h-h_s}^{\infty} \Pi(h) dh - \int_{h_e}^{\infty} \Pi(h) dh \end{array} \right]. \qquad (2.15)$$

In above equations, r is the length along radial direction. For equilibrium conditions, the excess free energy in Eq. 2.14 should attain minimum value. To fulfil this condition the first variation Eq. 2.14 should equal to zero, which leads to two Euler equations, i.e. for liquid and substrate profiles:

$$\frac{\gamma}{r} \frac{d}{dr} \frac{r h'}{(1 + h'^2)^{1/2}} + \Pi(h - h_s) = P_e, \qquad (2.16)$$

$$\frac{\gamma_s}{r} \frac{d}{dr} \frac{r h_s'}{(1 + h_s'^2)^{1/2}} - \Pi(h - h_s) - \frac{h_s}{K} = -P_e. \qquad (2.17)$$

Eqs. 2.16 and 2.17 form a system of two interlinked differential equations for two undetermined profiles: the fluid droplet, $h(r)$, and deformed soft substrate, $h_s(r)$. Low slope approximation, $h'^2 \ll 1$, $h_s'^2 \ll 1$, which is acceptable for small contact angles, is used below. It is important to observe that Eq. 2.16 is unlike the usual capillary equation for the non-deformable substrate, because it now has contribution of h_s in the disjoining/conjoining pressure, which can be determined using Eq.2.17. Eqs. 2.16 and 2.17 are interconnected and, in general can be solved numerically only. It is the reason why the problem is further simplified with use of linear disjoining/conjoining pressure isotherm to obtain analytical solutions.

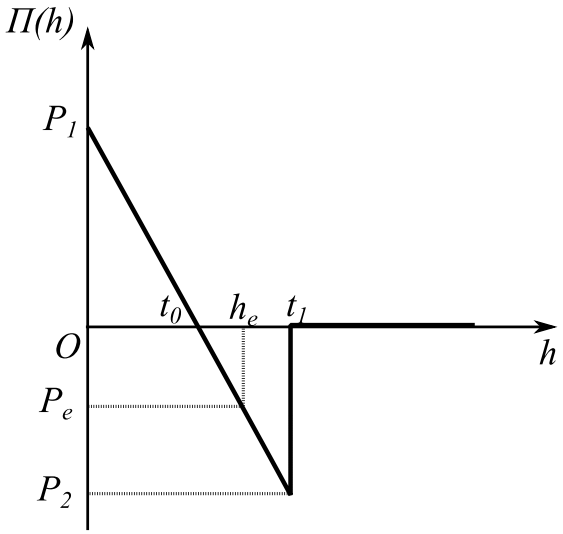

Figure 2. 3:Disjoining/conjoining pressure isotherm adopted for calculations. Source: (78)

$$\Pi(h) = \begin{cases} P_1 - ah & at \;\; h \le t_1 \\ 0 & at \;\; h > t_1 \end{cases}. \qquad (2.18)$$

where P_1 and t_0 are defined in Figure 2.3, t_1 is the radius of influence of surface forces, a is the slope of disjoining/conjoining pressure isotherm. The subsequent radial length from the origin to the point t_1 is L_1, see Figure 2.2. The selected linear dependency of disjoining/conjoining pressure isotherm $\Pi(h)$ on h according to Eq. 2.18 still captures the essential properties of the disjoining/conjoining pressure isotherm in spite of substantial simplification: (i) it satisfies the stability condition, $\Pi'(h) < 0$ when $h < t_1$; (ii) the influence of surface forces is short ranged and the radius of its action is defined by t_1; (iii) it corresponds to the partial wetting case at the proper choice of parameters(63).
Disjoining/conjoining pressure cannot be ignored near the apparent three-phase contact line; therefore, substrate deformation is linked directly with the parameters of the disjoining/conjoining pressure isotherm, see Table 2.1.

Table 2. 1: Physical properties: fluid surface tension, γ ,Disjoining/Conjoining pressure isotherm parameters t_1, t_0, Disjoining/Conjoining pressure isotherm slope a ,elasticity coefficient, K ,equilibrium excess pressure, P_e, and substrate surface tension, γ_s, used for calculation of droplet profile and deformation in the substrate. 1dyne=10^{-5}N. Source:(78)

Physical Property	Value
γ	72 dyne/cm
t_1	3×10^{-6}cm
t_0	7×10^{-7} cm
a	1×10^{11} dyne/cm^3
K	1×10^{-11} cm^3/dyne
P_e	-1×10^{5} dyne/cm^2
γ_s	1 dyne/cm

Effect of variation of P_e, a, K and γ_s on substrate deformation and its subsequent effect on the droplet profile is investigated below.

2.1.2.3(a) Effect of variation of excess pressure, P_e

Excess pressure is changed according to $0 \leq |P_e| \leq |P_2|$. Figure 2.4 illustrates shapes of the droplet and substrate with variation in P_e. An increase in P_e causes equilibrium thin film height, h_e, to reduce. This consequently influences the height and span of the droplet to increase. Hence, causing the extent of the deformation in the radial direction to grow, but generates a reduction in the depth which the substrate gets deformed to.

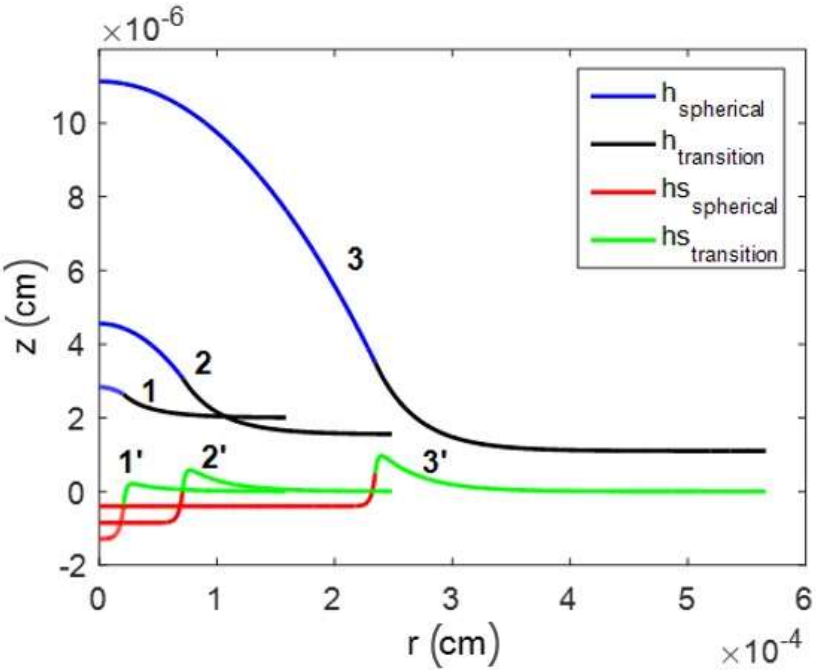

*Figure 2. 4:Calculated profiles of the droplet and substrate deformation:*1, $1' - |P_e| = 130000$ *dyne/cm2*, 2, $2' - |P_e| = 85000$ *dyne/cm2*, 3, $3' - |P_e| = 40000$ *dyne/cm. Source:*(78)

2.1.2.3(b) Effect of variation of slope of the disjoining/conjoining pressure isotherm, a

The value of a is varied in the following range $1 \times 10^{11} \leq a \leq 1 \times 10^{12}$ dyne/cm^3 to see its impact on depth to which the substrate gets deformed and profile of the fluid droplet. Figure 2.5 demonstrates that slope a also effects the droplet shape: increasing the gradient of the disjoining/conjoining pressure isotherm, the maximum height of the droplet increases which correspondingly increases the effective radius of the droplet. The equilibrium contact angle for droplet on a deformable substrate increases as a increases. Slope of the adopted disjoining/conjoining pressure isotherm does not affect the extent/height to which the soft substrate gets deformed.

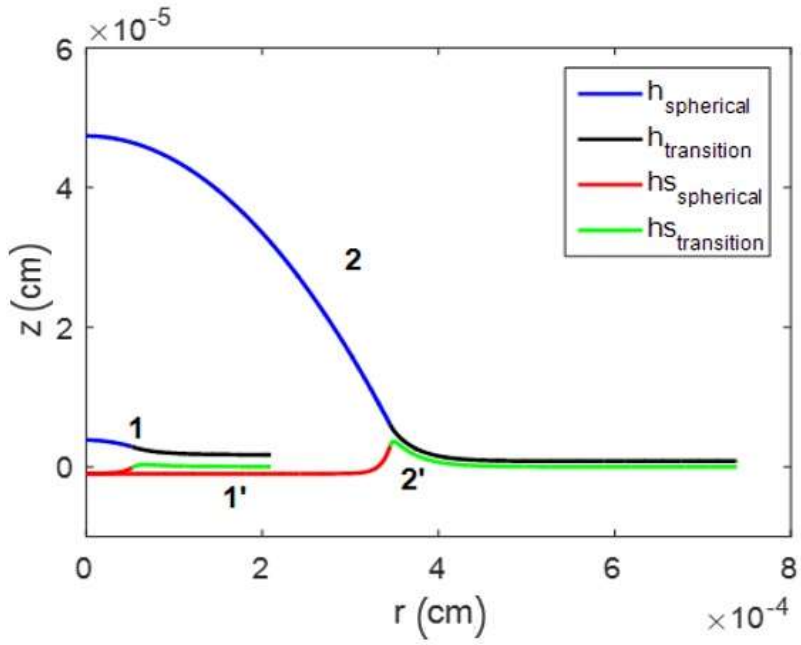

Figure 2. 5:Calculated profiles of the droplet and substrate deformation: $1, 1' -$ $a = 1 \times 10^{11}$ *dyne/cm3,* $2, 2' -$ $a = 1 \times 10^{12}$ *dyne/cm3 Source:(78)*

2.1.2.3(c) Effect of variation of elasticity coefficient, K

Elasticity coefficient controls the depth of deformation of the soft substrate. Here elasticity coefficient is changed according to $1 \times 10^{-13} \leq K \leq 1 \times 10^{-11}$ cm^3/dyne. The effect of decreasing the elasticity coefficient (i.e. $K \sim 0$) causes the outline of the droplet to approach the profile for non-deformable substrate which is apparent from Figure 2.6. It also shows that as K is increased (i.e. for a more elastic substrate) the equilibrium contact angle reduces marginally and the extent to which the soft substrate gets deformed increases (i.e. more deformation).

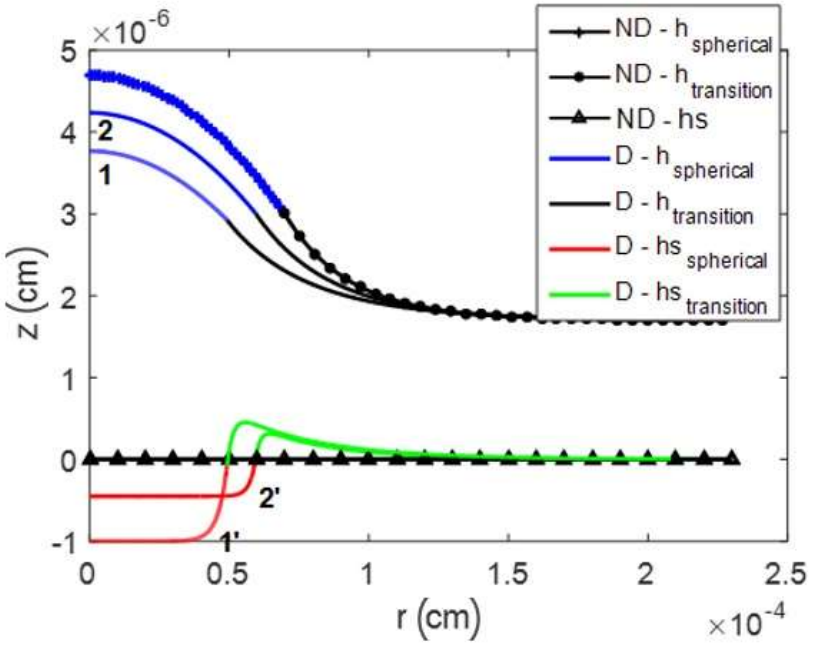

Figure 2. 6:Calculated profiles of the droplet and substrate deformation: $1, 1' -$ $K = 1 \times 10^{-11}$ *cm3/dyne,* $2, 2' -$ $K = 4.5 \times 10^{-12}$ *cm3/dyne, where "ND" stands for Non-Deformable substrate and "D" stands for Deformable substrate. Source:(78)*

2.1.2.3(d) Effect of variation of substrate surface tension, γ_s

Substrate surface tension is varied according to $0.001 \leq \gamma_s \leq 30$ dyne/cm. Increasing γ_s causes equilibrium contact angle to increase a little as displayed in Figure 2.7. It also shows that there is a smooth transition of the substrate deformation from the bulk droplet to the region of thin films. However, when γ_s tends to zero this smooth transition in the substrate deformation tends to transform into a sharp jump.

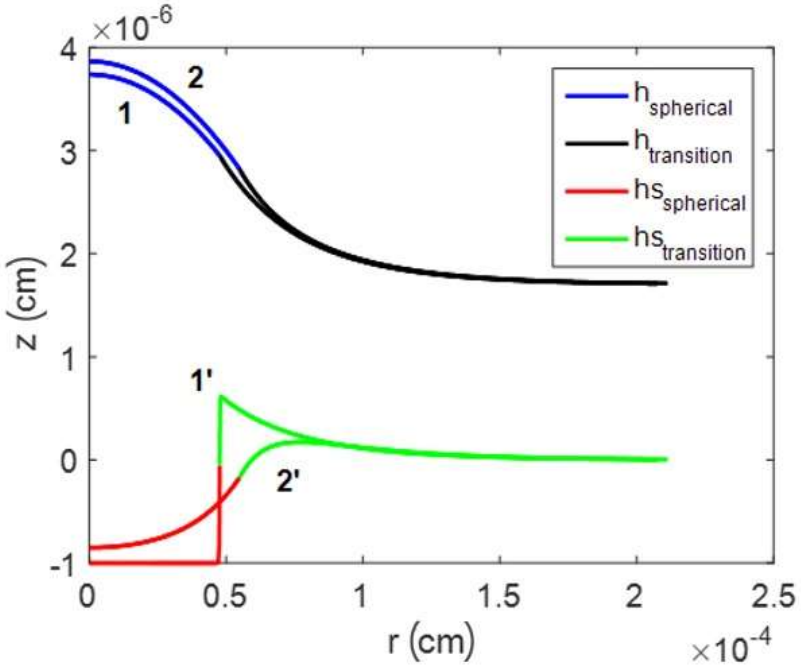

Figure 2. 7:Calculated profiles of the droplet and substrate deformation: $1, 1' - \gamma_s = 0.001$ *dyne/cm,* $2, 2' - \gamma_s = 30$ *dyne/cm. Source:(78)*

2.1.2.4 Equilibrium conditions of droplets on deformable substrates

As stated in the above section, excess free energy must remain at minimum in equilibrium conditions. Solely for this situation, the obtained shapes of the liquid droplet and deformed substrate are in actual for equilibrium. For a droplet to be at equilibrium on a deformable substrate, four essential conditions for (i) first variation of the free energy, (ii) second variation of free energy, (iii) transversality condition and (iv) Jacobi's sufficient condition, must always be satisfied(49,53). Solution obtained from Jacobi's condition should not disappear for a droplet on rigid/solid substrate (i.e., one dimensional problem. Altogether, these conditions give necessary and sufficient conditions of the minimum of the excess free energy. Unfortunately, the vital fourth condition is always neglected when deformation of soft solids under liquid droplets is considered. Under equilibrium conditions, simply if the Jacobi's sufficient condition is fulfilled, the estimated profiles of the fluid droplet and deformable substrate provide the minimum of free energy. To the best of our knowledge, it is for the first time the fourth condition is satisfied and the computed solution actually results in profiles for the droplet and the deformable substrate at equilibrium (49).
In Chapter 3, equilibrium conditions of droplets on deformable substrates are investigated. A simple model of the equilibrium droplet on the deformable substrate is considered, and it is shown that the deduced profiles of the equilibrium droplet and deformable substrate satisfy the Jacobi's condition, that is, really provide the minimum to the excess free energy of the system(49).

The validity of the Jacobi's condition for the deduced solutions of both droplet shape and profile of the deformable substrate undertaken in (49) , was checked for the first time. The latter means that any solution

of the same problem developed earlier or to be developed in the future should be checked for a validity of the Jacobi's condition for the deduced solution.

2.1.2.5 Hysteresis of Contact Angle of Sessile Droplets on Deformable Substrates

Apparently, there is only a single equilibrium contact angle, θ_e, on smooth homogeneous substrates. However, according to Kelvin's equation to reach this equilibrium contact angle the droplet should be at the equilibrium with oversaturated vapor(53). Therefore, experimentally only quasi equilibrium contact angles can be observed, which are referred to as hysteresis contact angles: static advancing contact angle $\theta_a > \theta_e$, and static receding contact angle $\theta_r < \theta_e$ (64).
Static advancing and receding contact angles are calculated in this using quasi-equilibrium states of a droplet on a soft substrate.
In Chapter 4 a theory of contact angle hysteresis of sessile liquid droplets on deformable substrate is developed in terms of disjoining pressure isotherm, which accounts for the action of surface forces in the vicinity of the contact line. Combined action of capillary pressure and surface forces, which act in the vicinity of the apparent three-phase contact line and substrate's elasticity determine both the liquid shape and the substrate deformation. A simplified s-shaped disjoining pressure isotherm is adopted, which allows direct calculations of static advancing/receding contact angles on deformable substrates and elasticity of the substrate is assumed to obey a simple Winkler's model for elastic surfaces(64,78).

2.1.2.6 Conclusions

The most recent advances are summarized in the area of static wetting of deformable substrates taking into consideration the effect of surface forces action coupled with elasticity of the substrate. Theoretical and experimental studies are reviewed in the area. Significant progress has been achieved in experimental investigations of deformations of soft solids due to recent advances in imaging techniques such as confocal microscopy and several theoretical models have been developed in an attempt to resolve the singularity caused by deformation of the substrates. The main conclusions are as follows: (i) any investigation of equilibrium of droplets on deformable substrates should be based on consideration of surface forces acting in the vicinity of the apparent three-phase contact line; (ii) excess free energy of the system droplet/deformable substrate should be considered and the equilibrium state corresponds to the minimum of the excess free energy; (iii) Any solution for the equilibrium profiles of the droplet and the deformable substrate should satisfy the Jacobi's sufficient condition.

2.2 Foam drainage and Interaction of liquid foams with porous substrates

2.2.1 Foam and the process of foam drainage

Foam is a two-phase colloidal system where gas cells surrounded by liquid as a result of forcing gas into the continuous liquid phase in the presence of surfactants and/or polymers (foaming agents). Foams can contain various liquid volume fraction according to their properties and the way of formation. Aqueous foams have a wide range of industrial and domestic applications such as acoustic thermal insulation, packaging solutions and constituents of structural foam materials(47) petroleum production and refining process(47) and food, cosmetic and medical products (47).

Foam products are also ideal for penetration and imbibition into porous media, such as gas and oil recovery and irrigation (7,47). It has been reported recently that foams are ideal products for the delivery of topical active agents such as antibacterial, skin protectants, antiviral agents and local anaesthetic agents and perform as ideal dug carriers for various dermatological applications(8,9,29,79–81).

The texture, nature and behaviour of liquid foams are characterised by several parameters such as bubble radius,R_b, liquid density, ρ, liquid viscosity, μ, surface tension, , the height of the foam and liquid volume fraction, φ (82–84).

The latter is defined as the volume of liquid in the foam divided by the total volume of the foam; it corresponds to approximately 0.05 for dry foams and up to 0.36 for wet foams. Liquid volume fraction higher than 0.36 is referred to as a bubbly liquid(85).

Foams are traditionally unstable systems where gas bubbles of polyhedral shape and different sizes and number of nearby bubbles are separated by the lamellae (thin films). The major processes taking place during foam collapse are i) drainage, ii) inter-bubble diffusion of gas (i.e. coarsening) and iii) rupture of lamellae (or burst of bubbles (i.e. coalescence))(86). Foams are created due the presence of surfactants/polymers which reduce the air/liquid interfacial tension and stabilise thin films against rupture(87,88).

Drainage is the process of flow of liquid in between gas bubbles through Plateau borders, nodes and films inside the foam structure. Free drainage occurs from the very beginning of foam formation where liquid drains out of a foam due to combined action of capillarity and/or gravity (31–34,89–91).

The drainage equations were introduced in references (35) and (33,36) based on continuity and pressure balance considerations. The drainage equation has been solved analytically for a multiplicity of cases such as forced drainage (33,34,38,39) and free drainage(32). Free drainage occurs from the very beginning of foam formation where liquid drains out of a foam due to the combined action of capillarity and gravity.

In the case of foam drainage and imbibition into porous substrate, there is a significant difference from the free drainage. The simultaneous action of both gravity and capillarity is the cause of drainage in both cases but during drainage/imbibition of foam placed on porous substrate the sucking action from the porous substrate considerably changes the process. It may in some cases result in the creation of free liquid layer at the foam/porous material interface. The liquid formed does not spontaneously get absorbed by the porous substrate and may stay for a prolong period during the proceeds. However, the existence of porous material in contact with the bottom of the foam leads to the simultaneous absorption of liquid through the unsaturated pores eventually leading to the decrease of the formed free liquid layer at the foam/substrate interface(19).

The interaction of foam with porous material is of high importance for biological and industrial applications where the substrate is porous (hair, textile, skin, rocks). These applications include firefighting, soil remediation, the production of cosmetics, pharmaceutical products and textiles (92–94) and extraction of oil and other non-aqueous fluids from porous material (rocks in wells) (95). Recently it has been reported in (8) (96) that foams can be applicable for use in drug delivery processes due to the improved wetting behaviour in comparison to other delivery methods (gels, creams and liquid lotions). Foam is less dense than other vehicle delivery systems and its properties can be adapted to meet the desired characteristics for a specific substrate on which it is applied to (10). The rate of drug delivery is highly connected with the stability of foam and the rate of drainage and collapse. The interaction between the foam and the porous substrate develops a new interconnected system where the rate of drainage is now also affected by the capillary suction and the characteristics of the porous material, ie average pore size, porosity, permeability and substrate thickness(19,40,94,97).

2.2.2 Foam drainage and imbibition into thick, porous substrate

Simultaneous drainage and imbibition of liquid from a foam into the porous substrate leads to the following differences as compared with the free drainage: (i) the presence of unsaturated pores inside the porous layer results in an imbibition of water from the Plateau channels into the pores, i.e. drainage/imbibition proceeds faster and (ii) this results in a drier foam layer in contact with a porous substrate, and close to the end of the drainage/imbibition process the liquid volume fraction will become lower as compared with the free drainage and below some final value. The final value can be characterised as follows: if the water content is above this final value then the pressure inside the Plateau channels is positive, that is, the liquid will flow from the Plateau channels to outside. If the final value of the water content is reached, then by further drainage the pressure inside the Plateau channels becomes smaller than the capillary pressure inside the pores of the porous substrate and the drainage stops. The previous consideration shows that the final equilibrium distribution of water content over the foam height is lower in the case of drainage/imbibition in contact with the porous substrate than in the case of a free drainage over a non-porous substrate.

The first model of foam drainage in contact with porous substrate was introduced only recently by Arjmandi-Tash et al.(19,98).

Considering the special features of the system's interaction the foam becomes gradually drier due to acceleration of drainage caused by the imbibition into the porous substrate.

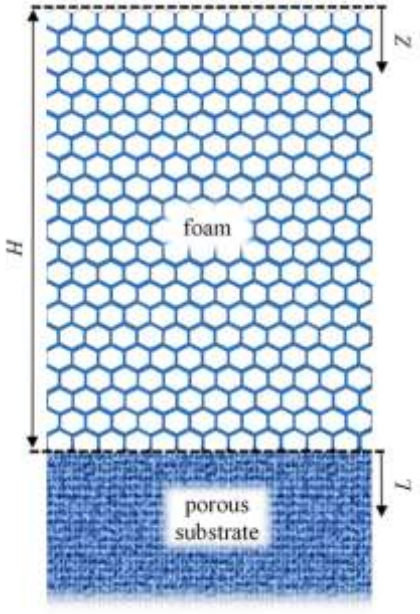

Figure 2. 8:Schematic diagram of a foam placed on a porous medium. Source: (97)

Below theoretical findings on drainage of foams placed on thick porous substrate are briefly reviewed. For many applications, particularly in pharmacy and cosmetics, the interaction of foam with substrate is of considerable importance as often the surfaces where foam is applied on are porous (skin, hair, textile materials). Recent investigations have confirmed that foams are an efficient alternative method of drug delivery on the skin of patients as was mentioned above. Lotions, creams, gels and ointment are the most common topical vehicle delivery systems that have been applied in dermatology; foams are delivery systems which grow in popularity. The density of foams is much lower than that of traditional vehicles and they spread out more easily. This reduces the requirement of applying pressure or prolonged period of contact with the sensitive diseased skin. In addition, drugs from foams absorb and penetrate more quickly as compared to other carriers.

The rate of drug delivery from foams can be controlled by the rate of foam drainage and collapse. Kinetics of topical drug delivery can be tailored by varying such foam characteristics as the bubbles size, liquid viscosity, initial liquid content and surface tension. In order to make a proper choice of foam characteristics, processes of drug delivery from foam should be considered in connection with the properties of substrate where the foam is applied to (skin or hair). Skin or bunch of hair have porous structure of their own, therefore an additional phenomenon, a capillary suction into porous substrate affects the foam drainage/imbibition.

Mathematical model of the process of simultaneous drainage and imbibition of liquid from a foam places on a porous substrate was developed in (19) which resulted in a system of two interconnected differential equations describing the flow of liquid inside both foam and the porous substrate.

There is a substantial difference in the drainage/imbibition of foam in the case of a free drainage (for example, foam placed on a solid substrate) and a drainage/imbibition of a foam placed on a porous substrate. In both cases the drainage is caused by the action of both gravity and the capillary forces. However, if foam is initially wet enough, then sooner or later the drainage (on a solid substrate) results in a formation of a free water layer under the foam and the water content in the foam layer immediately above the free water layer reaches the limiting value, which for 3D mono-disperse foam can be estimated as 0.36 corresponding to random packing limit for spherical particles. Sometimes the maximum liquid fraction is estimated as 0.26, what correspond to the minimum possible voids content at hexagonal packing of equal spheres. The latter value was accepted in(19).

The scenario is substantially different in the case of foam placed on a porous substrate: (i) the presence of unsaturated pores inside the porous layer results in an imbibition of water from the Plateau channels into the pores, i.e. drainage/imbibition proceeds faster and (ii) this results in a drier foam layer in contact with a porous substrate and close to the end of the drainage/imbibition process the liquid volume fraction will become lower as compared with the free drainage and below some final value. The final value can be characterised as follows: if the water content is above this final value then the pressure inside the Plateau channels is positive, that is, the liquid will flow from the Plateau channels to outside. If the final value of the water content is reached, then by further drainage the pressure inside the Plateau channels becomes smaller than the capillary pressure inside the pores of the porous substrate and the drainage stops. The previous consideration shows that the final equilibrium distribution of water content over the foam height is lower in the case of drainage/imbibition in contact with the porous substrate than in the case of a free drainage over a non-porous substrate.

The typical time evolution of the liquid volume fraction, φ, over the dimensionless foam height, ζ, and time evolution of the depth of imbibition into the porous medium, l, is shown in Figure 2.9.

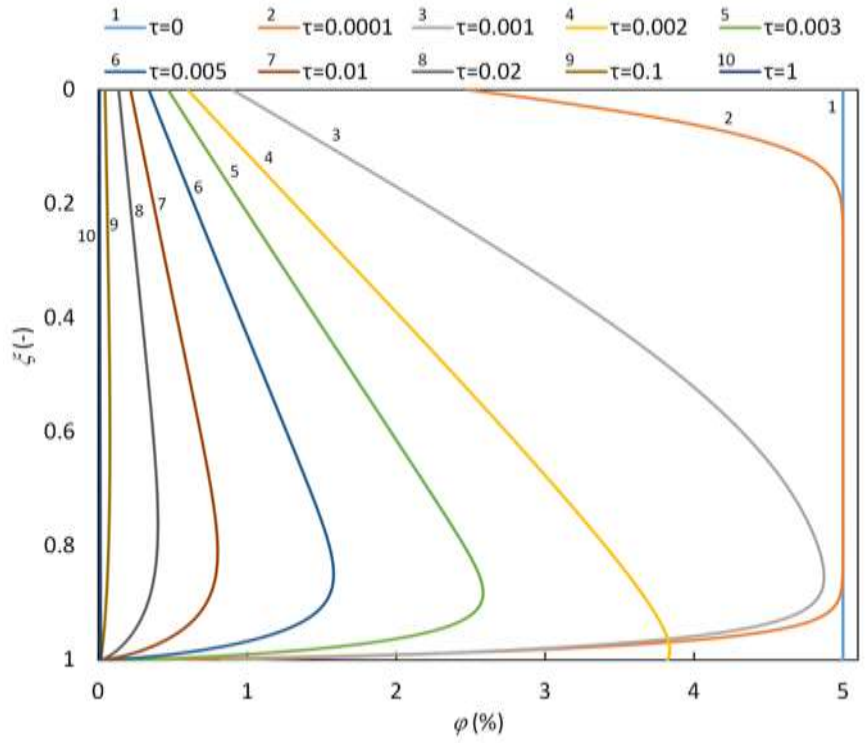

(a)

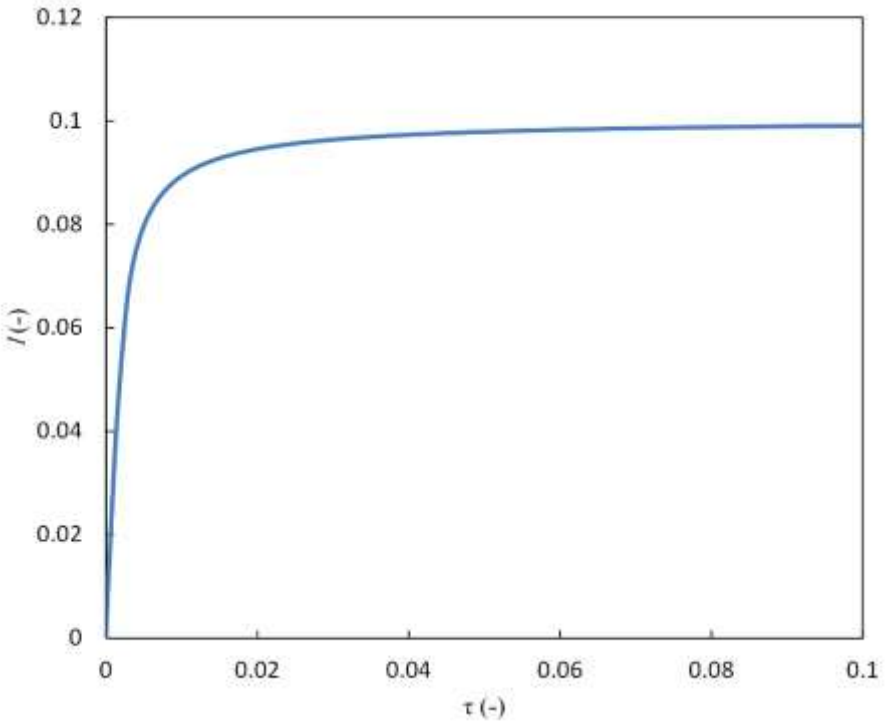

(b)

Figure 2. 9: Time evolution of a) liquid volume fraction over the foam height b) liquid imbibition into the porous medium at Bo=5.45, α=10, ε=0.03 and initial volume fraction of water is 5. Source: (97)

In the very beginning of the drainage/imbibition the liquid volume fraction decreases only at the top of the foam and near the foam/porous substrate interface, whereas in the middle part of the foam the initial value is retained. This is a common feature of foam drainage/imbibition process below. In contrast to the foam placed on a layer of liquid or on a non-porous substrate, the liquid volume fraction at the interface with

porous substrate decreases dramatically over a very short time due to imbibition into pores of the porous substrate. After initial considerable decrease in the liquid volume fraction near the interface the difference in the capillary pressure between foam and porous substrate decreases, whereas the penetration depth of the liquid into substrate increases and therefore, according to the modified Darcy's equation introduced for the system in (19) the imbibition becomes slower. At the same time there is a continuous supply of liquid to this region from the higher parts of the foam. That is why the further decrease in the liquid volume fractions slows down and in some cases after initial drop, the liquid volume fraction starts to increase and experiences a peak point (see τ=0.002 in Figure 2.9(a)). This process is controlled by Bond number, α, ε and initial liquid volume fraction. In addition, as is shown in Figure 2.9(b), in the beginning of the drainage the liquid penetrates into the porous substrate with a higher rate while after a short period of time the depth of liquid imbibition increases very gradually and it plateaus at a maximum value.

Figure 2.10 shows the time evolution of the liquid volume fraction at foam/porous substrate interface at various *Bo, α* and *ε* numbers, and with various initial liquid volume fractions. Based on the value of *Bo, α, ε* and initial liquid volume fraction *i*, there are three possible scenarios for the interaction of foam with a porous substrate: rapid imbibition, slow imbibition and intermediate imbibition regimes.

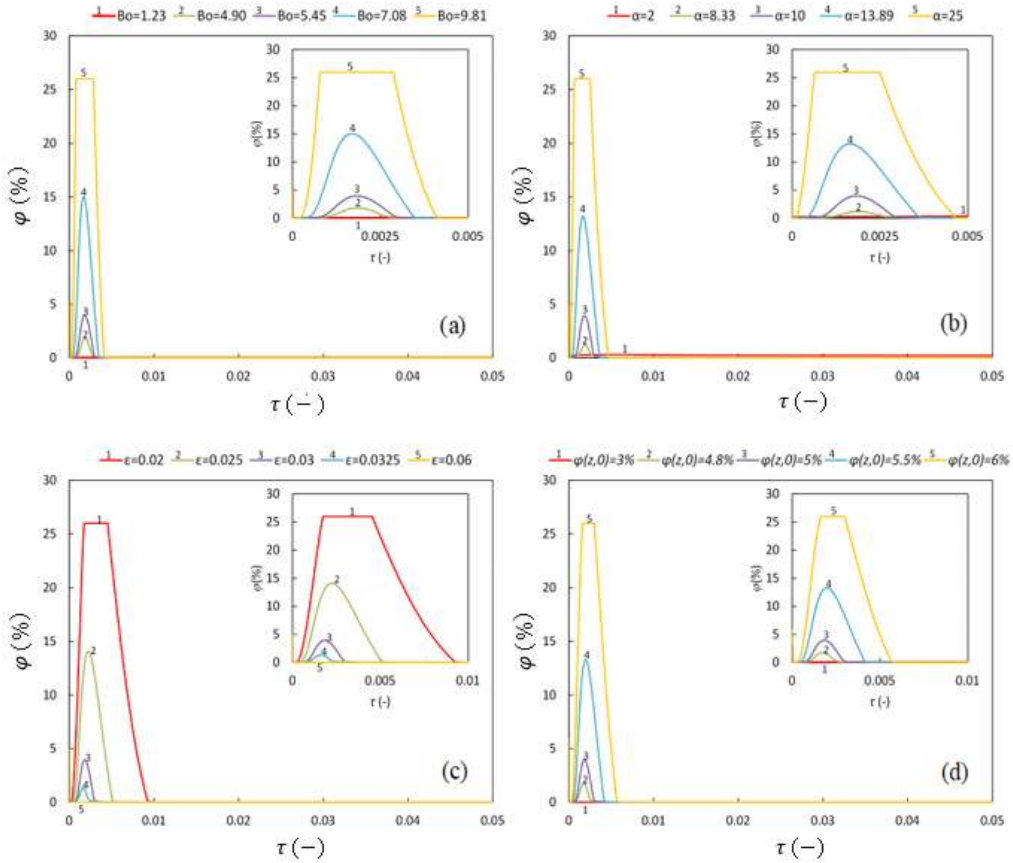

Figure 2. 10 :Time evolution of liquid volume fraction at foam/porous substrate interface at a) α=10, ε=0.03, φ_i =5% and various Bo; b) Bo=5.45, ε=0.03, φ_i =5% and various α; c) Bo=5.45, α=10, φ_i =5% and various ε; d) Bo=5.45, α=10, ε=0.03 and various φ_i. In all cases inserts present enlarged region of time scales from 0 to 0.005-0.01. Note, in Fig. 2.10 the first very fast stage when the liquid volume fraction at the foam/porous substrate interface decreases cannot be clearly shown but it is present in all cases considered. Source: (97)

The most interesting is the case of slow imbibition regime which occurs at high Bo, α and initial liquid volume fraction φ_i, and low ε values (e.g. Bo=9.81 in Figure 2.10(a), α=25 in Figure 2.10(b), ε=0.02 in Figure 2.10(c) and $\varphi(z, 0)$=6% in Figure 2.10(d)). This regime, when the liquid volume fraction at the foam/porous substrate interface can increase to a maximum limiting value and free liquid layer is formed over the porous substrate, is referred to as a slow imbibition.

The system is switched to a different regime at very low *Bo, α* and *φ*(z,0), and high porosity values, ε (e.g. *Bo* = 1.23 in Figure 2.10(a), *α* = 2 in Figure 2.10(b), *ε* = 0.06 in Figure 2.10(c) and φ(z,0) = 3% in Fig. 2.10(d)). These cases in which, the liquid drainage inside the foam occurs slower as compared with liquid penetration into the porous substrate and no free liquid is accumulated at the interface, is referred to as rapid imbibition regime. However, at intermediate values of the *Bo, α, ε* and initial liquid volume fraction φ_i (e.g. *Bo* = 4.90, 5.45 and 7.08 in Figure 2.10(a), *α* = 8.33, 10 and 13.89 in Figure 2.10(b), *ε* = 0.025, 0.03 and 0.0325 in Figure 2.10(c) and *φ(z,0)* = 4.8, 5 and 5.5% in Figure 2.10(d)), the rate of the imbibition into the porous substrate is comparable with the rate of drainage, and the system is referred to as an intermediate imbibition regime. Similar to the rapid imbibition regime, there is no free liquid formation at the foam/porous substrate interface in the case intermediate imbibition.

In Figure 2.11 the scenario of the slow imbibition is shown: initially the liquid volume fraction at the foam/porous substrate is lower than the critical value 0.26 until the moment $_m$; after that moment a free liquid film start forming at the foam/porous substrate interface. This free liquid film disappears at the moment $_M$.

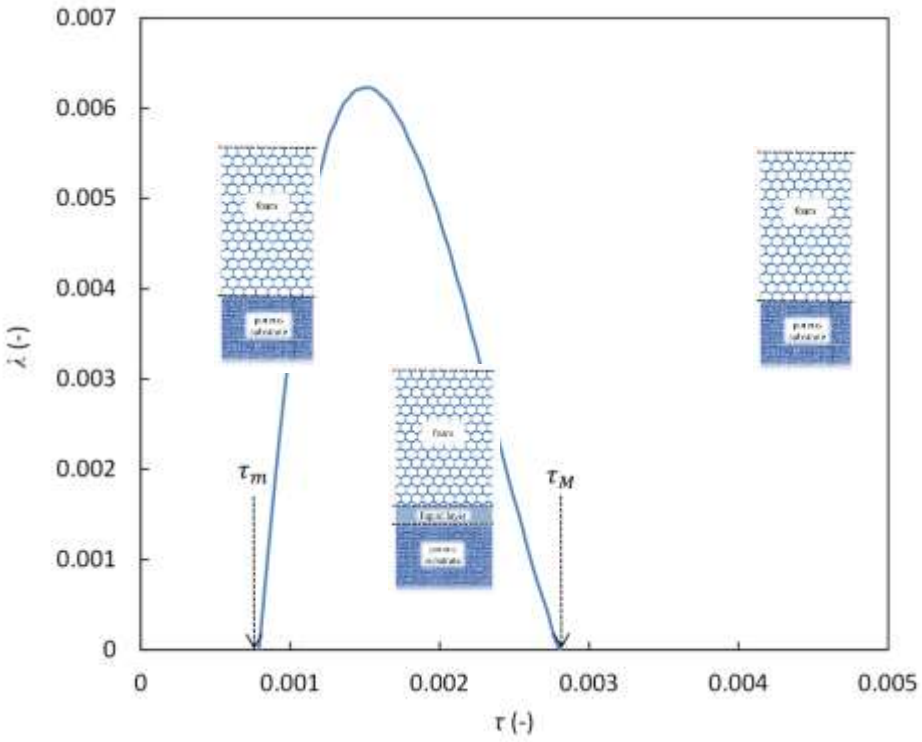

Figure 2. 11:Time evolution of the thickness of free liquid layer between foam and porous substrate at Bo=9.81, α=10, ε=0.03 and φi=5% Source:(97)

2.2.3 Foam drainage and imbibition into thin porous substrate

As in the case of thick porous substrates considered in the previous section, drainage is caused by a combination of a gravity/capillary forces and capillary suction applied by the pores from the porous substrate. Theory and calculations of foam drainage placed onto a porous media has been reviewed in the previous section and it was shown that, under certain conditions, a liquid layer can form at the foam-porous substrate

interface. Unfortunately, it is difficult to investigate experimentally the rate of penetration and the wetted volume inside a thick porous substrate in contact with foams. However, it is very straightforward to measure rate of penetration and wetted area in the case of contact of a foam with a thin porous layer. In Chapter 5 a theory of foam drainage (taking into account surface viscosity) placed on a completely wettable thin porous layer is developed: the rate of foam drainage and imbibition inside the porous layer and other characteristics of the process are predicted. This process is a model of drug delivery of foam placed on a skin or on a hair. The developed theory was verified in (40) against experimental measurements of foam drainage placed on thin porous substrates.

The effect of all model parameter on maximum liquid volume fraction at the foam/porous substrate interface was also investigated by N.Koursari, et al (40), as presented in Chapter 5 and the existence of three different drainage/imbibition regimes, (1) ‘fast imbibition regime’ (2) ‘intermediate imbibition’ (3) ‘fast imbibition regime’ was verified (40).

2.2.4 Conclusions

A description of foam and foam structure have been provided above and the process of foam drainage has been described. A theory of foam drainage placed on both a thick and a thin porous layer was developed: rate of drainage, wetted area inside the porous substrate (or radius of the wetted area inside the thin porous layer) and other characteristics of the process were predicted. One of the phenomena during application is a possibility of the build-up of a liquid layer on the foam/porous layer interface, which can be very useful and important for the application processes.

Nomenclature 2

A	–	Amplitude of the sinusoidal corrugation of the deformable substrate
a, b, c, d	–	Slopes of different regions of disjoining/conjoining pressure isotherm
α	–	α −film
β	–	β −film
D	–	Deformable substrate
$D(x)$	–	Jacobi condition
E	–	Young's Modulus
ϵ	–	Strain
F, F_{2D}	–	Excess free energy in three and two-dimensional cases
$F_{e,film}$, $F_{2De,film}$	–	Excess free energy of the equilibrium thin film on the deformed solid in three and two-dimensional cases
γ	–	Surface tension of the fluid
γ_s	–	Surface tension of the substrate
H	–	Apex of the droplet
H_a	–	Apex of the advancing droplet
H_r	–	Apex of the receding droplet
h	–	Film thickness, equilibrium liquid profile, droplet height
h_e	–	Stable equilibrium film thickness
h_s	–	Local deformation of the substrate
h_{se}	–	Local deformation of the substrate under the action of the ambient pressure
h_3	–	Thickness in the critical point for advancing droplet
h_4	–	Thickness in the critical point for receding droplet
K	–	Elasticity coefficient
k	–	Mean curvature of the solid
l	–	Characteristic length
λ	–	Wavelength of the sinusoidal corrugation of the deformable substrate
μ	–	Dynamic viscosity
ND	–	Non-deformable substrate
P_{air}	–	Pressure in the ambient air
P_e	–	Equilibrium excess pressure
P_a	–	Advancing pressure
P_r	–	Receding pressure
p	–	Vapor pressure
p_{sat}	–	Saturated vapor pressure
$\Pi(h)$	–	Disjoining/conjoining pressure isotherm
Q	–	Flow rate

R	–	Radius of curvature of the droplet
R_a	–	Radius of curvature of the advancing droplet
R_g	–	Gas constant
R_r	–	Radius of curvature of the receding droplet
r	–	Length along radial direction for three-dimensional case
T	–	Temperature
$t_0, t_1, t_2, t_3, t_4, t_5, t_6$	–	Parameters of disjoining/conjoining pressure isotherm
θ_e	–	Equilibrium contact angle
θ_a	–	Advancing contact angle
θ_r	–	Receding contact angle
$u(x)$	–	Solution of Jacobi's equation
V	–	Volume of the fluid
V_a	–	Volume of the advancing droplet
V_r	–	Volume of the receding droplet
v_m	–	Molar volume of the liquid
x	–	Length along radial direction for two-dimensional case
Y	–	Elastocapillary length
y	–	Uniform surface stress
$z = x - L_1$	–	Co-ordinate in the tangential direction

CHAPTER 3

Equilibrium Conditions of Droplets on Deformable Substrates

Overview

In this chapter equilibrium conditions of droplets on deformable substrates are presented.

The results of the study were published in *Langmuir* and are reused in this chapter with permission from corresponding author, Professor Victor M. Starov(v.m.starov@lboro.ac.uk).

Initially in this chapter equilibrium conditions of droplets on rigid substrates are discussed. A 2D droplet is considered for simplification and it is shown that all necessary conditions of equilibrium of liquid droplet on non-deformable substrate are satisfied. The research is then followed by investigation of equilibrium conditions of droplet on deformable substrate. The expression of the excess free energy of a liquid droplet on a deformable substrate is used and Winkler's model is adopted to account for the substrate's elasticity. Equations for equilibrium profiles are deduced based on consideration of the action of the Derjaguin's pressure in the vicinity of the TPCL and a simplified piece-wise linear disjoining/conjoining pressure isotherm is adopted for simplification. Jacobi's necessary condition of equilibrium is then investigated for the deduced profiles. Jacobi's expressions for the profiles of the droplet and the deformable substrate are deduced and it is proven for the first time that the derived profiles of the droplet and deformable substrate really correspond to the equilibrium.

3.1 Introduction

Young's equation is often used to describe equilibrium liquid droplets on a solid substrate(48). Young's equation reduces complete wettability, partial wettability and non-wettability cases to the determination of three interfacial tensions involved. However, Young's equation involves the balance of the horizontal forces leaving the vertical force unbalanced. The latter results in a vertical net force applied on the solid substrate(53), which could be possible on a rigid substrate. That is, in the case of a droplet deposited on a rigid substrate, the tranversality condition in the vicinity of the apparent three-phase contact line, provides the necessary boundary condition, i.e. $h' \to 0, x \to \infty$, and due to the substrates rigidity, there is no need to consider the unbalanced 'vertical' forces. However, it should be reconsidered in the case of deformable substrates.

In a more recent study for droplets depositing on solid substrates, Lubarda(99) derived Young's equation by applying an integral form of the equilibrium conditions. In this study the author proved that the singularity of the vertical component is eliminated by considering a small width near the triple line where capillary force is applied.

Since the initial works by Lester(25), Rusanov(56), Derjaguin et al.(100) Shanahan and de Gennes(101), wetting of deformable substrates has attracted the interest of several research groups(60). Derjaguin and co-workers(100) were the first to propose modelling of the force distribution on the soft substrate considering the action of the disjoining/conjoining pressure in a vicinity of the apparent three phase contact line. Consideration of disjoining/conjoining pressure action was undertaken later in (62) and (102).

Equilibrium condition of droplet on deformable substrates has recently been investigated theoretically and experimentally. Shanahan (103) showed that deformation occurs near the vicinity of the triple line owing both to adjacent heterogeneities and a net force applied. A number of experimental studies(20–22,65,67,104–108) were conducted to investigate the deformation of deformable substrates by liquid droplets near the three-phase contact line. However, in these works, the action of surface forces (disjoining/conjoining pressure) in the vicinity of the three-phase contact line, has been ignored.

The state of equilibrium demands equilibrium of liquid-vapor, liquid-solid and vapor-solid simultaneously and the latter one determines the presence of adsorbed liquid layers on the substrate. It was shown(20,53,62,63) that disjoining/conjoining pressure action in the vicinity of the apparent three-phase contact line results in a deformation of a deformable substrate. Unfortunately, the direct application of Young's equation leads (i) to deformation singularity at the apparent three-phase contact line(56–59) (ii) all the equilibrium properties (i.e. contact angle, droplet radius, etc.) of the system under consideration rely upon the selected artificial length parameter, which determines a width of zone near the contact line, where surface tension is applied(25,47,56,57,63,108) showed that surface forces (the disjoining/conjoining pressure), determine both profiles of the droplet and the deformable substrate combined with the action of capillarity, disjoining/conjoining pressure and elasticity of the deformable substrate determines an apparent contact angle on deformable substrates.

Under equilibrium conditions, the excess free energy should be at its minimum value. Only in this case the deduced profiles of the liquid and deformable substrate correspond to the equilibrium. For the equilibrium, the following four conditions should be satisfied:

1. The first variation of the free energy should be zero;

2. The second variation should be positive;

3. The transversality condition at the drop perimeter in the vicinity of the three-phase contact line should be satisfied(53).

4. Jacobi's sufficient condition should be satisfied. In the case of one-dimensional problem (a droplet on a rigid substrate) the solution of Jacobi's equation should not vanish at any position inside the area of investigation. In the case of deformable substrate, the Jacobi's condition is specified below.

Unfortunately, the important fourth condition of equilibrium is usually forgotten. Only if Jacobi's sufficient condition is satisfied, the deduced profiles of the droplet and deformable substrate provide the minimum of extra free energy at equilibrium. Below for the first time it is shown that the obtained solution results in equilibrium profiles for the droplet and the deformable substrate. If the fourth condition is satisfied then the solution provides the minimum for the excess free energy and equilibrium profiles; if this condition is not satisfied, the solution of equilibrium droplet and deformable substrate profiles does not correspond to the minimum of the excess free energy.

In all publications until now, the necessary condition of minimum of the excess free energy solutions have been checked in the case of equilibrium of droplets on deformable substrates. There has not been any attempt to check whether the Jacobi's condition is satisfied. One of the most fundamental principle is used in this research work, i.e. any profile should give a minimum value of the excess free energy. The properties and stability of liquid films on deformable substrates are deduced for the case of partial wetting. The action of disjoining/conjoining pressure is considered to act simultaneously with capillary pressure yielding the equilibrium liquid profile. The validity of the Jacobi's sufficient condition is verified for the first time.

3.2 Theory

Equilibrium liquid profiles on rigid substrates

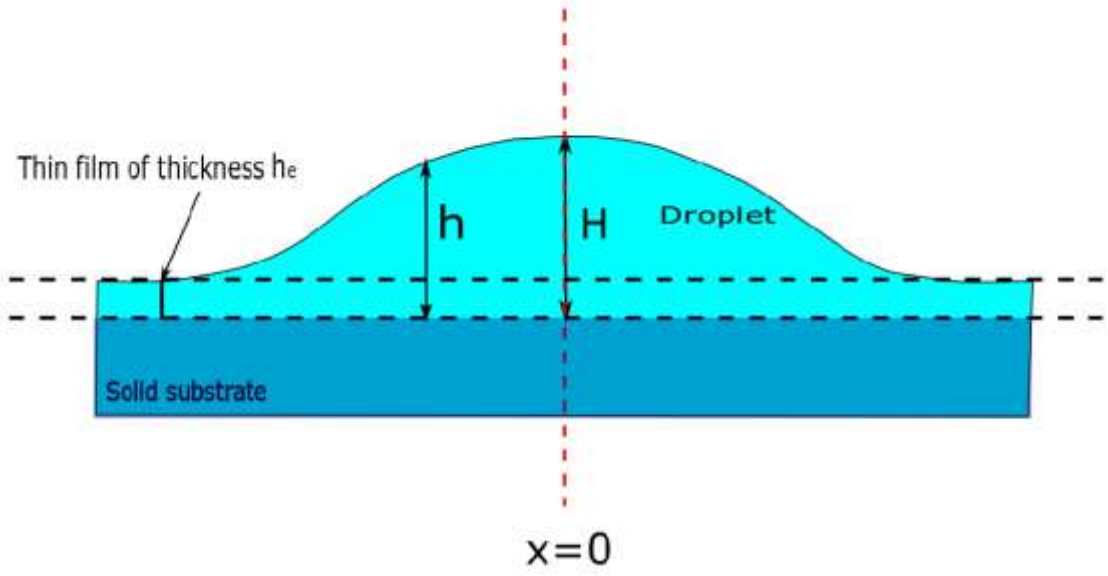

Figure 3. 1 : Schematic diagram of an equilibrium liquid droplet on a solid non-deformable substrate: the droplet is "sitting" at equilibrium on a flat liquid film of thickness h_e, which is at equilibrium with over-saturated vapor in the surrounding air (Partial wetting case).Source:(49)

To simplify all calculations only two-dimensional (2D) droplets are considered below. In the case of partial wetting, the simultaneous action of the disjoining/conjoining and capillary pressures leads to the existence of non-flat equilibrium droplets(53). The excess free energy, Φ , of a liquid droplet deposited on a non-deformable substrate can be expressed as (53).

$$\Phi = \gamma \cdot S + P_e \cdot V + \Phi_D - \Phi_{ref}, \tag{3.1}$$

where S, V, Φ_D and Φ_{ref} are excesses of the vapor-liquid interfacial area, the excess volume, the excess energy associated with the action of surface forces, and the excess free energy of a reference state respectively; γ is the liquid-vapor interfacial tension;

$$P_e = P_a - P_l, \tag{3.2}$$

where P_e is the excess pressure, P_a is the pressure in the ambient air and P_l the pressure inside the liquid, which is the state of a solid substrate covered by a stable equilibrium α-film(53). Gravity is neglected in Eq. 3.1 because the size of the droplet is assumed smaller than the capillary length. According to Eq. (3.2), $P_e < 0$, in the case of a droplet. P_e can be expressed through the vapour pressure according to Kelvin's equation:

$$P_e = \frac{R \cdot T}{v_m} \ln \frac{p_s}{p} < 0. \tag{3.3}$$

where, v_m is the molar volume of the liquid, T is the temperature in K, R is the gas constant, vapour pressure, p, which is higher than the saturated pressure p_s. According to Eq. 3.3 the droplets can be at equilibrium only with over saturated vapour.

In the case of a two-dimensional droplet, the excess free energy from Eq. (3.1) can be re-written as(53):

$$\Phi = \int \left\{ \gamma \left(\sqrt{1 + h'^2} - 1 \right) + P_e (h - h_e) + \int_h^\infty \Pi(h) dh - \int_{h_e}^\infty \Pi(h) dh \right\} dx \tag{3.4}$$

A schematic diagram of the droplet profile and the profile of the solid (non-deformable) substrate is shown in Figure 3.1.

A liquid profile, $h(x)$, for which the excess free energy, Φ, given by Eq. 3.4, has a minimum value, can describe an equilibrium liquid droplet deposited on a surface at the state of equilibrium(53)(60). The latter is valid only if the following conditions are satisfied: (a) Condition of existence of extremum (maximum or minimum), which means the first variation of Eq. 3.4 should vanish: $\delta\Phi = 0$. This results in Euler's-Lagrange equation, which in the case under consideration, is referred to as Derjaguin's equation (50):

$$\frac{\gamma(h'')}{(1 + h'^2)^{3/2}} + \Pi(h) = P_e. \tag{3.5}$$

The first term $\frac{\gamma(h'')}{(1+h'^2)^{3/2}}$ in Eq. 3.5 represents the action of capillary pressure and $\Pi(h)$ is the disjoining/conjoining pressure isotherm. b) The second condition is a necessary condition of minimum of the excess free energy Eq. 3.4: $\frac{\partial^2 f}{\partial h'^2} > 0$. This Legendre condition when applied to Eq. 3.4 results in:

$$\frac{\partial^2 f}{\partial h'^2} = \frac{\gamma}{(1 + h'^2)} > 0,$$

where,

$$f = \gamma \left(\sqrt{1 + h'^2} - 1 \right) + P_e (h - h_e) + \int_h^\infty \Pi(h) dh - \int_{h_e}^\infty \Pi(h) dh$$

Both the above conditions give only the necessary but not the sufficient condition of minimum of the excess free energy Eq. 3.1 or 3.4.

To have sufficient condition of minimum, it is necessary to have Jacobi's condition of minimum satisfied(50). This condition reads: solution of Jacobi's equation, $u(x)$, should not vanish at any position, x, inside the region of interest. Jacobi's equation according to (50):

$$\frac{d}{dx}\frac{\gamma u'}{(1+h'^2)^{3/2}} + \frac{d\Pi(h)}{dh}u = 0 \qquad (3.6)$$

The initial conditions for Eq. 3.6 are: $u(0) = 0, u'(0) \neq 0$. The solution of Eq. 3.6 with mentioned boundary conditions is as follows(53):

$$u = const \cdot h' \qquad (3.7)$$

According to Figure 3.1 (see (53)for details) condition $h'(x) < 0$ is satisfied in the case of equilibrium droplets and, hence, $u(x)$ does not change sign at any *x* from 0 to infinity. The latter means that solution of Eq. 3.5 really gives a stable equilibrium profile of liquid droplet on solid non-deformable substrate.

Equilibrium droplet on deformable substrate

In this section, conditions for existence of equilibrium droplets on deformable substrates are discussed. Below a two-dimensional (2D) droplet is considered, Figure 3.2, because the Jacobi's condition is much easier to check in this case. To get an analytical solution of the problem under consideration a number of simplifying assumptions are adopted below.

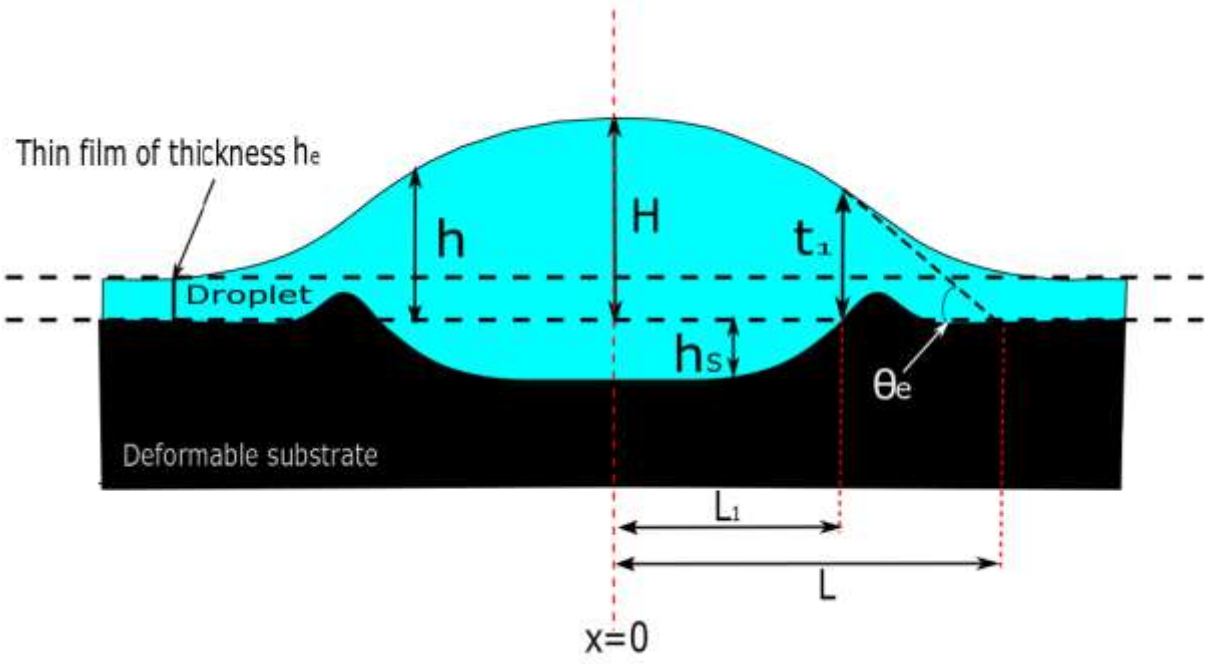

Figure 3. 2: Schematic diagram of droplet on a deformable substrate. $h(x)$ - the liquid profile, $h_s(x)$ - profile of the deformable substrate; L_1 - the distance from the centre of the droplet to the point where surface forces (disjoining/conjoining pressure) starts to act. Source:(49)

The excess free energy of a liquid droplet on a deformable substrate is expressed as follows:

$$\Phi - \Phi_{e,film} = \int_0^\infty f(h, h', h_s, h'_s)dx, \tag{3.8}$$

where $\Phi_{e,film}$ is the excess free energy of the equilibrium film (as in Eq. 3.1) and

$$f(h, h', h_s, h'_s) = \left\{ \begin{array}{c} \gamma\sqrt{1 + h'^2(x)} - \gamma + \gamma_s\sqrt{1 + h_s'^2(x)} - \gamma_s + \\ P_e(h - h_s) - P_e h_e + \frac{h_s^2}{2K} \\ -\frac{h_{se}^2}{2K} + \int_{h-h_s}^\infty \Pi(h)dh - \int_{h_e}^\infty \Pi(h)dh \end{array} \right\}, \tag{3.9}$$

where x is the tangential co-ordinate, γ and γ_s are liquid-vapour and solid-liquid interfacial tensions, $h(x)$ the profile of the droplet and $h_s(x)$ the profile of the deformed substrate; K is the elasticity coefficient of the deformable substrate. Winkler model of substrate elasticity is adopted in Eq.3.9 (47).

Firstly, equations for equilibrium profiles for profiles of both the droplet and the deformable substrate should be deduced. The corresponding equations for this are found in the same way as above in the case of the droplet on a solid substrate: that is, from the condition $\delta\Phi = 0$, where the excess free energy Φ is given now by Eq. 3.8. This procedure results in the following system of two differential equations:

$$\frac{\gamma h''}{(1 + h'^2)^{3/2}} + \Pi(h - h_s) = P_e,$$

$$\frac{\gamma_s h_s''}{(1 + h_s'^2)^{3/2}} - \Pi(h - h_s) - \frac{h_s}{K} = -P_e.$$

To simplify further the problem under consideration a low slope approximation is used below, that is, $h'^2 \ll 1$ and $h_s'^2 \ll 1$. After that, the two above equations become:

$$\gamma h'' + \Pi(h - h_s) = P_e, \tag{3.10}$$

$$\gamma_s h_s'' - \Pi(h - h_s) - \frac{h_s}{K} = -P_e. \tag{3.11}$$

A simplified, piece-wise linear disjoining/conjoining pressure isotherm is adopted below (Figure 3.3):

$$\Pi(h) = \begin{cases} a(t_0 - h), & 0 \le h \le t_1 \\ 0 \quad , & h > t_1 \end{cases} \tag{3.12}$$

The disjoining/conjoining pressure isotherm according to Eq. 3.12, has two regions: $0 \le h \le t_1$ and $h > t_1$. Symbol a corresponds to the slope of the linear part of the isotherm inside zone $0 \le h \le t_1$. Consequently, a can be expressed as: $a = \frac{P_1 - P_2}{t_1}$. The adopted shape of the disjoining/conjoining pressure isotherm, despite the simplifications, retains the main important properties of the real isotherm: (i) it has a short range of surface forces action, t_1, (ii) corresponds to partial wetting at the proper selection of parameters, (iii) corresponds to stable thin liquid films in the whole range of surface forces action. Reminder: (a) the equilibrium contact angle (on rigid non-deformable) substrate is expressed as(53) $\cos\theta = 1 - \frac{S}{\gamma}$, that is, if $S/\gamma < 1$, then the contact angle is in the range $0 < \quad < \pi/2$, which corresponds to the partial wetting; (b) the stability condition of flat thin films (53) read as $\frac{d\Pi}{dh} < 0$. In the case under consideration (Eq. 3.12): $\frac{d\Pi}{dh} = -a < 0$, that is, satisfied.

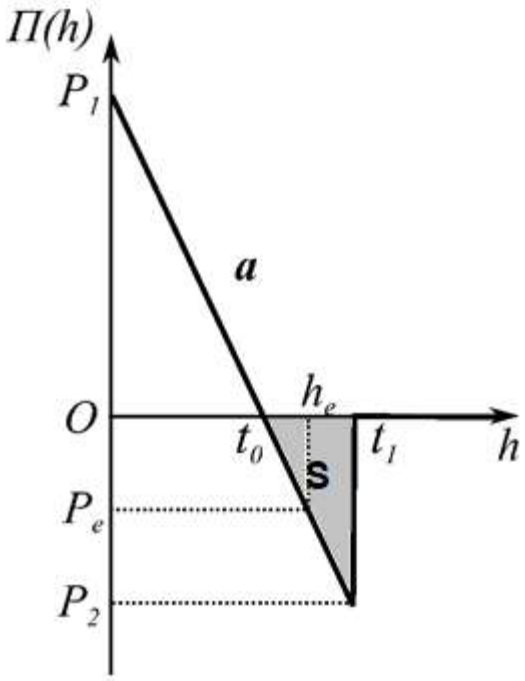

Figure 3. 3:Adopted piece-wise linear dependency of disjoining/conjoining pressure on the thickness h; a - is the slope of the linear part of the isotherm inside zone $0 \le h \le t_1$, P_e *- equilibrium excess pressure;* P_1 *and* P_2 *- parameters of the adopted isotherm. Source:(49)*

3.3 Results and Discussion

The physical properties used for the disjoining/conjoining pressure isotherm are summarised in Table 3.1.

Table 3. 1: Physical properties of the disjoining/conjoining pressure isotherm: Liquid-vapour interfacial tension, γ, Solid-liquid interfacial tension, γ_s,Disjoining/Conjoining pressure isotherm parameters P_1, P_2, P_e, t_0 and t_1,slope of Disjoining/cojoining pressure isotherm, a, and elasticity coefficient, K. Source: (49)

Physical Properties	**Value**
Liquid-vapour interfacial tension, γ	72 dyne/cm
Solid-liquid interfacial tension, γ_s	1 dyne/cm
P_1	1×10^7 dyne/cm^2
P_2	-1×10^7 dyne/cm^2
P_e	-1×10^5 dyne/cm^2
t_0	$\frac{P_1}{a} = 7 \times 10^{-7}$ cm
t_1	7×10^{-7} cm
a	$\frac{P_1 - P_2}{t_1} = 1 \times 10^{11}$ dyne/cm^3
K	$1 \times 10^{-12} - 1 \times 10^{-11}$ cm^3/dyne

The values of the physical properties mentioned in Table 3.1 were used for calculations below. These values were selected based on previously used and 1dyne=10^{-5}N (63). It is shown below that the dependency of the length L_1 on elasticity K is required for solution of Jacobi's equations.

Solution of Eqs. 3.10-3.11 is similar to (63) (see Appendix 3A). The solution of a system (3.10)-(3.11) results in the dependencies of both the L_1 and the apparent equilibrium contact angle, θ_e, (Figure 3.2) versus the elasticity coefficient, K, are shown in Figures 3.4 and 3.5, respectively.

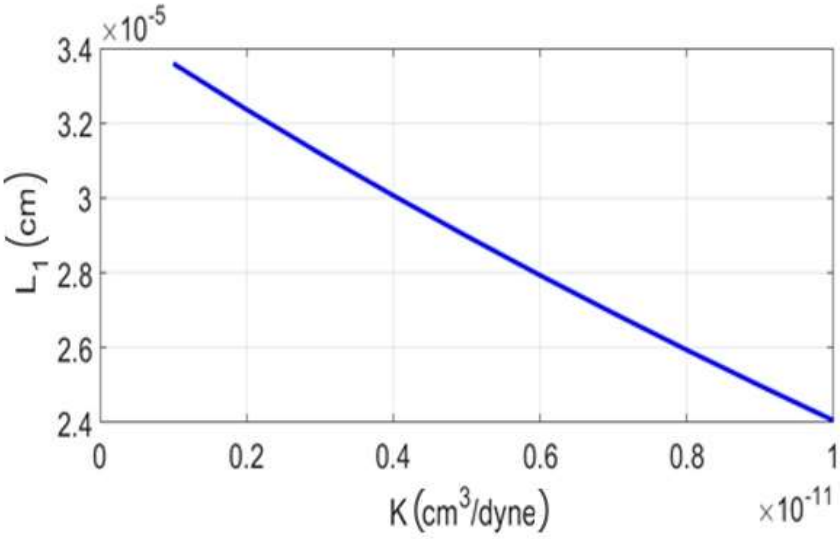

Figure 3. 4:Length of the circular part of the droplet (bulk of the liquid droplet), $L_1(cm)$ (see Fig. 3.2) versus elasticity coefficient $K(cm^3/dyne)$. Source:(49)

The dependency of $L_1(cm)$ on the elasticity coefficient was derived by considering all other physical properties of the disjoining/conjoining pressure isotherm mentioned in Table 3.1 as constants. $L_1(cm)$ is calculated from Eq. 3A.25 (please see Appendix 3A), for a range of values of the elasticity coefficient, $K(cm^3/dyne)$, as presented in Figure 3.4.

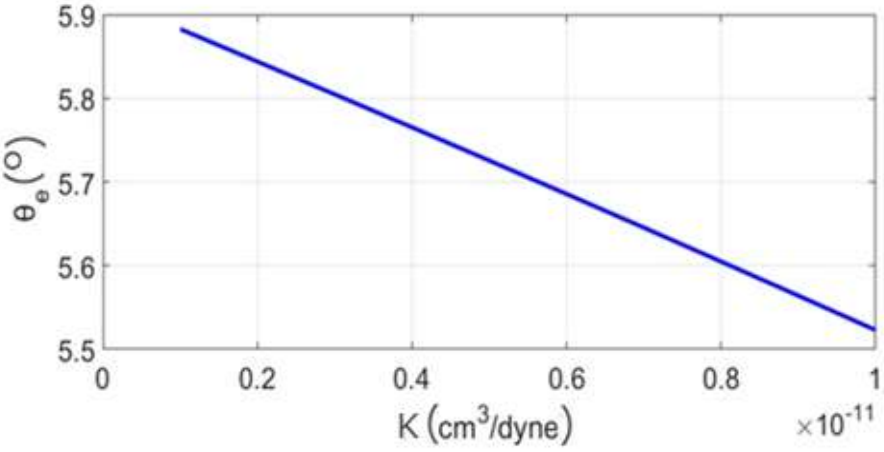

Figure 3. 5:Equilibrium contact angle, θ_e (^{o}), versus elasticity coefficient, $K(cm^3/dyne)$. Source:(49)

As shown in Figure 3.5, equilibrium contact angle decreases with $K(cm^3/dyne)$. Derivation of contact angle is presented in Appendix 3A.

According to Figure 3.5 the apparent equilibrium contact angle decreases with increase of the elasticity of the deformable substrate as expected.

It is easy to check that the second necessary condition for the existence of a minimum of the excess free energy of the system in the case of deformable substrate, $^2\Phi > 0$, is always satisfied (63) for excess free energy given by Eqs. 3.8-3.9.

The next step is checking that the Jacobi's sufficient condition is satisfied for the problem under investigation. According to (109), the four Jacobi equations for the four unknown functions $u_{ji}(x)$, where $i, j = 1,2$ in the case under consideration (Eqs. 3.8-3.9 at low slope approximation), are as follows:

$$\gamma u_{1i}'' + [\Pi'(h-h_s)u_{1i} - \Pi'(h-h_s)u_{2i}] = 0$$

$$\gamma u_{2i}'' - \left[\Pi'(h-h_s)u_{1i} - \Pi'(h-h_s)u_{2i} + \frac{u_{2i}}{K}\right] = 0$$

where $i = 1,2$. In the case of the simplified disjoining/conjoining isotherm (Figure 3.3) the latter system of differential equations simplifies as follows:

$$\gamma \cdot u_{1i}'' - (-a \cdot u_{1i} + a \cdot u_{2i}) = 0, \qquad (3.13)$$

$$\gamma_s \cdot u''_{2i} - \left(a \cdot u_{1i} - a u_{2i} + \frac{u_{2i}}{K}\right) = 0, \qquad (3.14)$$

where $i = 1,2$. Note, that Eqs. 3.13-3.14 are linear differential equations with respect to all unknown Jacobi's functions $u_{ji}(x)$, where $i, j = 1,2$. According to (109) these four Jacobi's functions should be subjected to the following initial conditions:

$$\left\{\begin{array}{c} u_{11}(0) = u_{12}(0) = u_{21}(0) = u_{22}(0) = 0 \\ u'_{11}(0) = 1\,,\; u'_{22}(0) = 1 \\ u'_{12}(0) = u'_{21}(0) = 0 \end{array}\right\} \qquad (3.15)$$

Because of linearity of Eqs. 3.13 and 3.14 and zero initial conditions for functions $u_{12}(x)$ and $u_{21}(x)$, these two functions are equal to zero identically. Hence, the only two unknown non-zero functions are $u_{11}(x)$ and $u_{22}(x)$. The Jacobi's condition is as follows(109): $D = \begin{vmatrix} u_{11} & u_{12} \\ u_{21} & u_{22} \end{vmatrix}$ should not change sign for all $x > 0$. Having in mind that $u_{12}(x) = u_{21}(x) = 0$, and taking into account that D should be positive (see below) the Jacobi's condition can be rewritten as:

$$D(x) = \begin{vmatrix} u_{11}(x) & 0 \\ 0 & u_{22}(x) \end{vmatrix} = u_{11}\, u_{22} > 0\,, \text{ at } x > 0. \qquad (3.16)$$

It is interesting to note that the deduced Jacobi's expressions for the profile of the droplet and the deformable substrate, $u_{11}(z)$ and $u_{22}(z)$ respectively, include only one value, L_1, which comes from the solution of the original problem (Eqs. 3.10-3.11).

It is shown (see Appendix 3A) that both $u_{11}(z)$ and $u_{22}(z)$ are positive for the region $x > L_1$. Hence, $D = u_{11}(z) \cdot u_{22}(z) > 0$ at $x > L_1$, as it is for the circular part of the liquid droplet (bulk of the liquid droplet) for $x < L_1$. The latter means that D is positive at all $x > 0$. That is, the Jacobi's condition is satisfied. Hence, the solution obtained for both liquid profile and the deformable substrate really provides the minimum to the excess free energy of the system. The results above prove that for the obtained solution for a droplet deposited on a deformable substrate, the excess free energy is at its minimum value and deduced solutions for the droplet profile and profile of the deformed substrate correspond to the equilibrium.

3.4 Conclusions

Equilibrium conditions for a droplet on a deformable substrate are investigated. Disjoining/conjoining pressure action is taken into account in the vicinity of the apparent three-phase contact line. The fundamental principle of a minimum value of excess free energy for both profiles of the droplet and the deformable substrate is considered. The equilibrium and stability of liquid droplets on deformable substrates are considered, under partial wetting conditions. For the first-time validity of the Jacobi's condition is verified and it is shown that this condition is satisfied for the obtained solution of the problem. A simplified linear pressure disjoining/conjoining pressure isotherm is adopted to obtain an analytical solution and low slope approximation is used for all calculations. Derived equations for both profiles of droplet and deformable substrate are sensitive to variations of the length of the circular (bulk part) region of the droplet. The two

Jacobi's equations deduced show that Jacobi's condition is fully satisfied for all the region of interest. Both Jacobi's equations are always increasingly positive for the bulk part of the droplet and for the transitional region where disjoining/conjoining pressure is predominant.

Nomenclature 3

a	–	Slope of disjoining /conjoining pressure isotherm defined in Eq. 3.12
Φ	–	Excess free energy
$\Phi_{e,film}$	–	Excess free energy of the equilibrium thin film on the deformed solid
Φ_D	–	Excess energy caused by surface forces action
Φ_{ref}	–	Excess free energy of a reference state
γ	–	Surface tension of the liquid/air interface
γ_s	–	Surface tension of the substrate/liquid interface
H	–	Apex of the droplet
h	–	Film thickness, equilibrium liquid profile, droplet height
h_e	–	Thickness of stable equilibrium flat film in front of the droplet
h_s	–	Profile of the deformed substrate
K	–	Elasticity coefficient
L_1	–	Length from the centre of the droplet to the point where surface forces (disjoining pressure) start to act
L	–	Effective length: Length from the centre of the droplet to the intersection of the profile with the initial non-deformable substrate
P_{air}	–	Pressure in the ambient air
P_e	–	Equilibrium excess pressure inside the droplet
p	–	Vapor pressure
p_{sat}	–	Saturated vapor pressure
$\Pi(h)$	–	Disjoining/conjoining pressure isotherm
R	–	Gas constant
S	–	Area of the liquid-air interface
S_s	–	Area of the solid-liquid interface
V	–	Excess volume
T	–	Temperature
t_0, t_1	–	Parameters of disjoining/conjoining pressure isotherm defined in Eq. (3.12)
θ_e	–	Equilibrium contact angle
v_m	–	Molar volume of the liquid
x	–	Co-ordinate in the tangential direction
$z = x - L_1$	–	Co-ordinate in the tangential direction

Appendix 3A

Solution of Eqs. (3.10)-(3.11)

In the case of the simplified isotherm of disjoining/conjoining pressure the governing Eqs. 3.10-3.11 can be rewritten as:

$$\gamma h'' + a(t_0 - h + h_s) = P_e, \tag{3A.1}$$

and

$$\gamma_s h_s'' - a(t_0 - h + h_s) - \frac{h_s}{K} = -P_e, \tag{3A.2}$$

with boundary conditions:

$$h'(0) = h_s'(0) = 0, \tag{3A.3}$$

$$h(x) \to h_e, h_s(x) \to 0, at\ x \to \infty. \tag{3A.4}$$

Bulk of the liquid droplet (circular region), $\boldsymbol{h - h_s > t_1}$.

For the bulk of the liquid droplet, i.e. region $h - h_s > t_1$, we obtain the two solutions

$$h_{sp}(x) = \frac{P_e x^2}{2\gamma} + H_e, \tag{3A.5}$$

and

$$h_{s,sp}(x) = KP_e + C_1\left(e^{\lambda_s x} + e^{-\lambda_s x}\right), \tag{3A.6}$$

where $\lambda_s = \sqrt{\frac{1}{K \cdot \gamma_s}}$, H_e is the apex height of the droplet and C_1 is an integration constant.

Using boundary condition $h_{sp}(L_1) - h_{s,sp}(L_1) = t_1$ results in:

$$\frac{P_e L_1^2}{2\gamma} + H_e - KP_e - C_1\left(e^{\lambda_s L_1} + e^{-\lambda_s L_1}\right) = t_1. \tag{3A.7}$$

Derivatives of found solutions at $x = L_1$ are as follows:

$$h'_{sp}(L_1) = \frac{P_e L_1}{\gamma};\ h'_{s,sp}(L_1) = \lambda_s C_1\left(e^{\lambda_s L_1} - e^{-\lambda_s L_1}\right). \quad \text{(3A.8)}$$

Transitional region, $h - h_s \leq t_1$

Equation for the droplet's profile:

$$h'' - \frac{a(h - h_s)}{\gamma} = \frac{P_e - at_0}{\gamma}. \quad \text{(3A.9)}$$

The substrate deformation profile can be simplified to:

$$h_s'' - h_s\left(\frac{1 + aK}{\gamma_s K}\right) + \frac{ah}{\gamma_s} = -\left(\frac{P_e - at_0}{\gamma_s}\right). \quad \text{(3A.10)}$$

The unknown solution is presented in the following form:

$$y(x) = h(x) + \alpha h_s(x), \quad \text{(3A.11)}$$

where $y(x)$ is a new unknown function which is a linear combination of both profiles, h_s, the deformed substrate, and h, the droplet; α is a constant to be determined.

Let us multiply Eq. (3A.10) by α and add the resulting equation to Eq. (3A.9), using (3A.11) the resulting equation is:

$$y'' - a\left(\frac{1}{\gamma} - \frac{\alpha}{\gamma_s}\right)y + h_s\left[a\alpha\left(\frac{1}{\gamma} - \frac{\alpha}{\gamma_s}\right) + \frac{a}{\gamma} - \frac{\alpha}{\gamma_s}\left(\frac{1 + aK}{K}\right)\right] = (P_e - at_0)\left(\frac{1}{\gamma} - \frac{\alpha}{\gamma_s}\right). \quad \text{(3A.12)}$$

The aim is to get an equation, which includes only one unknown function, $y(x)$. Hence, the constants in square brackets must be equal to zero, i.e.:

$$\alpha^2 + \left(-\frac{\gamma_s}{\gamma} + \frac{(1 + aK)}{aK}\right)\alpha - \frac{\gamma_s}{\gamma} = 0, \quad \text{(3A.13)}$$

which is a quadratic equation in α, which can be determined from the above equation and has two roots: where $\alpha_1 > 0$ and $\alpha_2 < 0$. Substitution of these values into Eq. 3A.12 results in two new unknown functions y_i, where $i = 1,2$:

$$y_i'' - a\left(\frac{1}{\gamma} - \frac{\alpha_i}{\gamma_s}\right) y_i = (P_e - at_0)\left(\frac{1}{\gamma} - \frac{\alpha_i}{\gamma_s}\right), i = 1,2. \qquad (3A.14)$$

Solution of Eqs. 3A.14 results in:

$$y_1 = h_e + C_2 e^{x\lambda_1} + C_3 e^{-x\lambda_1}$$

and

$$y_2 = h_e + C_4 e^{x\lambda_2} + C_5 e^{-x\lambda_2}.$$

The boundary conditions (3A.4) produce two integration constants which vanish; that is $C_2 = C_4 = 0$ and the equations become:

$$y_1 = h_e + C_3 e^{-x\lambda_1} \qquad (3A.15)$$

$$y_2 = h_e + C_5 e^{-x\lambda_2} \qquad (3A.16)$$

where $h_e = \frac{-(P_e - at_0)}{a}$, $\lambda_1 = \sqrt{a\left(\frac{1}{\gamma} - \frac{\alpha_1}{\gamma_s}\right)}$ and $\lambda_2 = \sqrt{a\left(\frac{1}{\gamma} - \frac{\alpha_2}{\gamma_s}\right)}$, $y_1 = h + \alpha_1 h_s$ and $y_2 = h + \alpha_2 h_s$. If we define $z = x - L_1$, and evaluating for $x = L_1$ for the circular part of the droplet (bulk of the liquid droplet) and $z = 0$ for the transitional region, then from Eq. 3A.15:

$$\begin{aligned} y_1(0) &= h_e + C_3 \\ &= h_{sp}(L_1) + \alpha_1 h_{s,sp}(L_1) \\ &= \frac{P_e L_1^2}{2\gamma} + H_e + \alpha_1\left[KP_e + C_1\left(e^{\lambda_s L_1} + e^{-\lambda_s L_1}\right)\right] \end{aligned} \qquad (3A.17)$$

Differentiation of Eq.3A.15 with respect to x and evaluating for $z = 0$ results in:

$$\begin{aligned} y'_1(0) &= -\lambda_1 C_3 \\ &= h'_{sp}(L_1) + \alpha_1 h'_{s,sp}(L_1) \\ &= \frac{P_e L_1}{\gamma} + \alpha_1\left[\lambda_s C_1\left(e^{\lambda_s L_1} - e^{-\lambda_s L_1}\right)\right] \end{aligned} \tag{3A.18}$$

Eq.3A.17 can be rewritten as:

$$C_3 = \frac{P_e L_1^2}{2\gamma} + H_e + \alpha_1\left[KP_e + C_1\left(e^{\lambda_s L_1} + e^{-\lambda_s L_1}\right)\right] - h_e \tag{3A.19}$$

Eq.3A.18 can be rewritten as:

$$-C_3 = \frac{1}{\lambda_1}\left\{\frac{P_e L_1}{\gamma} + \alpha_1\left[\lambda_s C_1\left(e^{\lambda_s L_1} - e^{-\lambda_s L_1}\right)\right]\right\} \tag{3A.20}$$

Evaluating Eq. 3A.16 for $z = 0$ results in:

$$\begin{aligned} y_2(0) &= h_e + C_5 \\ &= h_{sp}(L_1) + \alpha_2 h_{s,sp}(L_1) \\ &= \frac{P_e L_1^2}{2\gamma} + H_e + \alpha_2\left[KP_e + C_1\left(e^{\lambda_s L_1} + e^{-\lambda_s L_1}\right)\right], \end{aligned} \tag{3A.21}$$

which can be rewritten as:

$$C_5 = \frac{P_e L_1^2}{2\gamma} + H_e + \alpha_2\left[KP_e + C_1\left(e^{\lambda_s L_1} + e^{-\lambda_s L_1}\right)\right] - h_e \tag{3A.22}$$

Differentiation of Eq. 3A.16 and evaluating for $z = 0$ results in:

$$\begin{aligned} y'_{12}(0) = -\lambda_2 C_5 &= h'_{sp}(L_1) + \alpha_2 h'_{s,sp}(L_1) \\ &= \frac{P_e L_1}{\gamma} + \alpha_2\left[\lambda_s C_1\left(e^{\lambda_s L_1} - e^{-\lambda_s L_1}\right)\right], \end{aligned} \tag{3A.23}$$

which can be expressed as:

$$-C_5 = \frac{1}{\lambda_2}\left\{\frac{P_e L_1}{\gamma} + \alpha_2\left[\lambda_s C_1\left(e^{\lambda_s L_1} - e^{-\lambda_s L_1}\right)\right]\right\}. \qquad (3A.24)$$

Five Eqs. (3A.7), (3A.19), (3A.20), (3A.22) and (3A.24) include five unknown constants C_1, C_3, C_5, H_e *and* L_1 to be determined.

The solution of these five equations results in the following equation of only one unknown; that is L_1:

$$\left[-\frac{P_e L_1^2}{2\gamma} - \alpha_1 \cdot \frac{P_e L_1^2}{2\gamma} + \alpha_1 \cdot t_1 + h_e - \frac{P_e L_1}{\gamma \cdot \lambda_1} - \frac{\alpha_1 \cdot \lambda_s \cdot M}{\lambda_1} \cdot \frac{P_e L_1^2}{2\gamma} + \frac{\alpha_1 \cdot \lambda_s \cdot M \cdot K \cdot P_e}{\lambda_1} + \frac{\alpha_1 \cdot \lambda_s \cdot M \cdot t_1}{\lambda_1}\right] \cdot \frac{1}{\left(1 + \alpha_1 + \alpha_1 \cdot \lambda_s \cdot \frac{M}{\lambda_1}\right)} - \left[-\frac{P_e L_1^2}{2\gamma} - \alpha_2 \cdot \frac{P_e L_1^2}{2\gamma} + \alpha_2 \cdot t_1 + h_e - \frac{P_e L_1}{\gamma \cdot \lambda_2} - \frac{\alpha_2 \cdot \lambda_s \cdot M}{\lambda_2} \cdot \frac{P_e L_1^2}{2\gamma} + \frac{\alpha_2 \cdot \lambda_s \cdot M \cdot K \cdot P_e}{\lambda_2} + \frac{\alpha_2 \cdot \lambda_s \cdot M \cdot t_1}{\lambda_2}\right] \cdot \frac{1}{\left(1 + \alpha_2 + \alpha_2 \cdot \lambda_s \cdot \frac{M}{\lambda_2}\right)} = 0, \qquad (3A.25)$$

where,

$$M = \frac{\left(e^{\lambda_s L_1} - e^{-\lambda_s L_1}\right)}{\left(e^{\lambda_s L_1} + e^{-\lambda_s L_1}\right)}. \qquad (3A.26)$$

$L_1(cm)$ can then be calculated from Eq. 3A.25 for given values of the elasticity coefficient K (cm^3/dyne). This dependency is presented in Figure 3.4 in the main text.

As derived by Eq. 3A.25 and shown in Figure 3.4, for given values of all physical properties mentioned in Table 1 in main text, L_1 depends only on the elasticity coefficient, K.

Equilibrium contact angle

For the bulk of the liquid droplet, we have $h - h_s > t_1$. For this situation, from Figure 3.3, it can be seen that $\Pi(h - h_s) = 0$ which results in solution (3A.5).

The intersection of this profile with the initial non-deformable substrate defines the apparent three phase contact line with a macroscopic equilibrium contact angle (effective length) (see Figure 3.2 in the main text). If $x = L$ is this length, then:

$$h(L) = 0 \qquad (3A.27)$$

And

$$h'(L) = -\tan\theta_e \cong -\theta_e \qquad (3A.28)$$

It can then be deduced from Eq. 3A.5 and 3A.27 that

$$L = \sqrt{\frac{-2 \cdot \gamma H_e}{P_e}} \tag{3A.29}$$

Eqs. (3A.28)-(3A.29) result in the following expression for θ_e:

$$\theta_e = \sqrt{\frac{2 \cdot H_e(-P_e)}{\gamma}} \tag{3A.30}$$

It is important to note that θ_e is determined by both P_e, which is an independent variable and H_e (which depends on the elasticity coefficient $K(\mathrm{cm}^3/\mathrm{dyn})$)

The dependency between equilibrium contact angle, $\theta_e(^o)$, and elasticity coefficient, $K(\mathrm{cm}^3/\mathrm{dyn})$ is presented in Figure 3.5 in the main text.

Solution of Jacobi's equations (3.13) -(3.14)

$$\gamma \cdot u_{11}'' - (-a \cdot u_{11} + a \cdot u_{22}) = 0, \tag{3.13}$$

$$\gamma_s \cdot u_{22}'' - \left(a \cdot u_{11} - a u_{22} + \frac{u_{22}}{K}\right) = 0, \tag{3.14}$$

Bulk of the liquid droplet (circular region), $h - h_s > t_1$

For the bulk of the liquid droplet, i.e. the spherical region $h - h_s > t_1$, using boundary conditions given by Eq. 3.15, solution of Jacobi's Eq. 3.13 is expressed as:

$$u_{11,sp}(x) = x \tag{3A.31}$$

For the circular region of the liquid droplet, Eq. 3.14 reduces to:

$$\gamma_s \cdot u_{22,sp}'' - \frac{u_{22,sp}}{K} = 0 \tag{3A.32}$$

or

$$u''_{22,sp} - \lambda_s{}^2 \cdot u_{22,sp} = 0 \qquad \text{(3A.33)}$$

Where $\lambda_s = \sqrt{\frac{1}{K \cdot \gamma_s}}$.

The solutions of Eq.3A.33 can be expressed as:

$$u_{22,sp} = C_1 \cdot e^{\lambda_s \cdot x} + C_2 \cdot e^{-\lambda_s \cdot x}, \qquad \text{(3A.34)}$$

where C_1 and C_2 are integration constants.

Using boundary condition given by Eq. 3.15, integration constants can be derived and the solution of Jacobi's Eq. 3.15 is now written as:

$$u_{22,sp}(x) = \frac{1}{\lambda_s} \cdot sinh\,(\lambda_s \cdot x), \qquad \text{(3A.32)}$$

According to Eqs. 3A.31-3A.32: $D(x) = u_{11,sp} \cdot\ u_{22,sp} = x\frac{1}{\lambda_s} \cdot sin\,h(\lambda_s \cdot x) > 0$ at $0 < x < L_1$.

Transitional Region, $h \leq t_1$

For simplification, z coordinates will be used for the transitional region, i.e $0 \leq h - h_s \leq t_1$, where $z = x - L_1$.

For this region, Jacobi's Eq. 3.13 and 3.14 are expressed as:

$$\gamma \cdot u''_{11} - (-a \cdot u_{11} + a \cdot u_{22}) = 0 \qquad \text{(3A.33)}$$

$$\gamma_s \cdot u''_{22} - \left(a \cdot u_{11} - a \cdot + \frac{u_{22}}{K}\right) = 0 \qquad \text{(3A.34)}$$

To deduce the solution of the system of Eqs. 3A.33-3A.34, the unknown solution is presented in the following form*:*

$$y(z) = u_{11}(z) + \alpha u_{22}(z), \qquad \text{(3A.35)}$$

where $y(z)$ is a new unknown function, which is a linear combination of both $u_{11}(z)$ and $u_{22}(z)$; α is a constant to be determined.

Addition of (3A. 33) and $\alpha \cdot$ (3A. 34) results in:

$$y'' + \left(\frac{a}{\gamma} - \frac{a \cdot \alpha}{\gamma_s}\right) \cdot y + \left[-\frac{a}{\gamma} + \frac{a \cdot \alpha}{\gamma_s} - \frac{\alpha}{\gamma_s \cdot K} - \frac{a \cdot \alpha}{\gamma} + \frac{\alpha \cdot \alpha^2}{\gamma_s}\right] \cdot u_{22} = 0 \quad \text{(3A.36)}$$

The aim is to get equation, which includes only one unknown function, *y(x).* Hence, the constants in square brackets must be equal to zero, i.e.:

$$\alpha^2 + \left(-\varepsilon + 1 - \frac{1}{a \cdot K}\right) \cdot \alpha - \varepsilon = 0. \quad \text{(3A.37)}$$

Eq. 3A.37 gives two values of α as used earlier,

$$\alpha_{1,2} = \frac{-\left(-\varepsilon + 1 - \frac{1}{a \cdot K}\right) \mp \sqrt{\left(-\varepsilon + 1 - \frac{1}{a \cdot K}\right)^2 + 4 \cdot \varepsilon}}{2} \quad \text{(3A.38)}$$

where $\alpha_1 > 0$ *and* $\alpha_2 < 0$.

After that Eq. 3A.36 transforms into two equations with two unknown functions y_1 and y_2 :

$$y_1'' + \frac{a}{\gamma_s}(\varepsilon - a_1) \cdot y_1 = 0 \quad \text{(3A.39)}$$

$$y_2'' + \frac{a}{\gamma_s}(\varepsilon - a_2) \cdot y_2 = 0 \quad \text{(3A.40)}$$

where $\varepsilon = \frac{\gamma_s}{\gamma}$, *and* $(\varepsilon - a_1) < 0$, $(\varepsilon - a_2) > 0$.

The solutions of Eqs. 3A.39 and 3A.40 are as follows:

$$y_1 = C_1 \cdot e^{\lambda_1 \cdot z} + C_2 \cdot e^{-\lambda_1 \cdot z} \quad \text{(3A.41)}$$

$$y_2 = C_3 \cdot sin\,(\lambda_2 \cdot z) + C_4 \cdot cos\,(\lambda_2 \cdot z), \quad \text{(3A.42)}$$

where,

$$\lambda_1 = \sqrt{-\frac{a}{\gamma_s}(\varepsilon - \alpha_1)} \tag{3A.43}$$

And

$$\lambda_2 = \sqrt{\frac{a}{\gamma_s}(\varepsilon - \alpha_2)} \tag{3A.44}$$

To find constants $C_1, C_2, C_3\ and\ C_4$, the following Boundary conditions are used:

$$\begin{Bmatrix} u_{11}(0) = u_{11,sp}(L_1) = L_1 \\ \frac{du_{11}(0)}{dx} = \frac{du_{11,sp}(L_1)}{dx} = 1 \\ u_{22}(0) = u_{22,sp}(L_1) = \frac{1}{\lambda_s} \cdot sinh(\lambda_s \cdot L_1) \\ \frac{du_{22}(0)}{dx} = \frac{du_{22,sp}(L_1)}{dx} = cosh(\lambda_s \cdot L_1) \end{Bmatrix} \tag{3A.45}$$

Based on Eq. 3A.35, the following expressions for Jacobi's equations, $u_{11}(z)$ and $u_{22}(z)$, are deduced which correspond to the transitional region of the droplet:

$$\begin{aligned} u_{11}(z) = {} & \frac{1}{(\alpha_2 - \alpha_1)} \\ & \cdot \Bigg\{ \alpha_2 \\ & \cdot \Bigg(\Bigg(\frac{1 + cosh\,(\lambda_s \cdot L_1) \cdot \alpha_1}{2 \cdot \lambda_1} + \frac{L_1}{2} \\ & + \frac{\alpha_1 \cdot sinh(\lambda_s \cdot L_1)}{2 \cdot \lambda_s} \Bigg) \cdot e^{\lambda_1 z} \\ & + \Bigg(\frac{L_1}{2} + \frac{\alpha_1 \cdot sinh(\lambda_s \cdot L_1)}{2 \cdot \lambda_s} \\ & - \frac{1 + cosh\,(\lambda_s \cdot L_1) \cdot \alpha_1}{2 \cdot \lambda_1} \Bigg) \cdot e^{-\lambda_1 \cdot z} \Bigg) - \alpha_1 \\ & \cdot \Bigg(\frac{1 + \alpha_2 \cdot cosh(\lambda_s \cdot L_1)}{\lambda_2} \cdot si\,n(\lambda_2 \cdot z) \\ & + \Bigg(L_1 + \frac{\alpha_2 \cdot sinh(\lambda_s \cdot L_1)}{\lambda_s} \Bigg) \cdot co\,s(\lambda_2 \cdot z) \Bigg) \Bigg\} \end{aligned} \tag{3A.46}$$

$$u_{22}(z) = \frac{1}{(\alpha_1 - \alpha_2)} \cdot \left\{ \left(\left(\frac{1 + cosh\,(\lambda_s \cdot L_1) \cdot \alpha_1}{2 \cdot \lambda_1} + \frac{L_1}{2} + \frac{\alpha_1 \cdot sinh(\lambda_s \cdot L_1)}{2 \cdot \lambda_s} \right) \cdot e^{\lambda_1 \cdot z} + \left(\frac{L_1}{2} + \frac{\alpha_1 \cdot sinh(\lambda_s \cdot L_1)}{2 \cdot \lambda_s} - \frac{1 + cosh\,(\lambda_s \cdot L_1) \cdot \alpha_1}{2 \cdot \lambda_1} \right) \cdot e^{-\lambda_1 \cdot z} \right) - \left(\frac{1 + \alpha_2 \cdot cosh(\lambda_s \cdot L_1)}{\lambda_2} \cdot sin\,(\lambda_2 \cdot z) + \left(L_1 + \frac{\alpha_2 \cdot sinh(\lambda_s \cdot L_1)}{\lambda_s} \right) \cdot cos\,(\lambda_2 \cdot z) \right) \right\} \quad \text{(3A.47)}$$

Results

To investigate deduced Jacobi's functions according to Equations 3A.46 and 3A47, the properties of the disjoining/ conjoining pressure isotherm presented in Table 3.1 (please see main text) are used. The expressions of the two functions are computed as functions of $z(cm)$ and a wide range of elasticity coefficient K. The length of the spherical region, L_1, used in Jacobi's equations 3A.46 and 3A.47 is calculated using the same disjoining/ conjoining pressure isotherm (please see Figure 3.3) and low slope approximation, $h'^2 \ll 1$ and $h_s'^2 \ll 1$. The examples of calculated dependences are presented in Figures. 3A.1-3A.2.

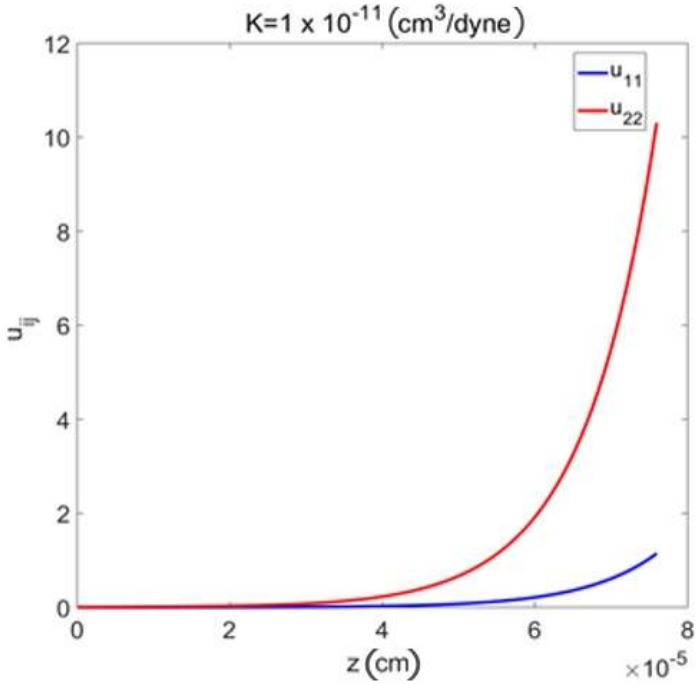

Figure 3A. 1: Jacobi's functions $u_{11}(z)$ and $u_{22}(z)$ versus the length of the transition region $z(cm)$, for $K = 1 \times 10^{-11}$ cm³/dyne. Source:(49)

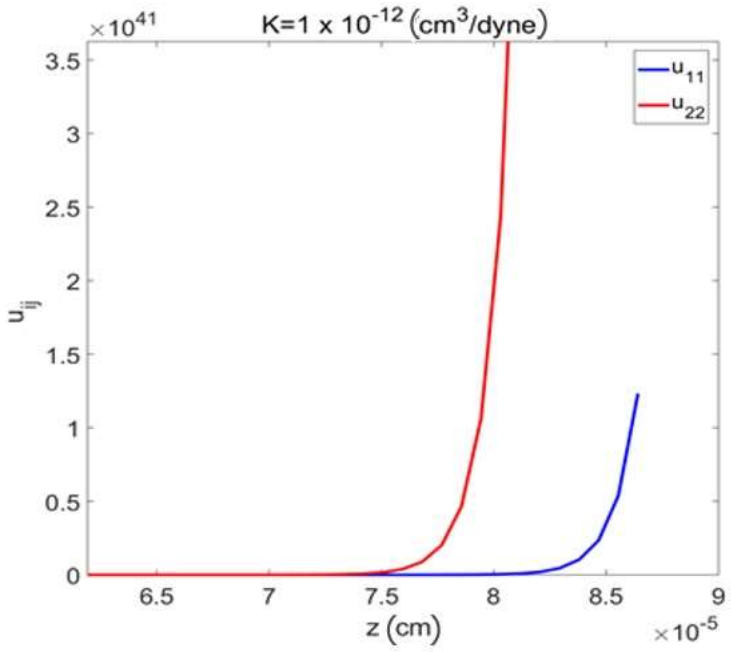

Figure 3A. 2: Jacobi's functions $u_{11}(z)$ and $u_{22}(z)$ versus the length of the transition region $z(cm)$, for $K = 1 \times 10^{-12}$ cm³/dyne. Source:(49)

As shown in Figures 3A.1 and 3A.2, both $u_{11}(z)$ and $u_{22}(z)$ are positive for the region of interest, $x > L_1$ and for all region $0 \leq z < +\infty$. All values of elasticity coefficient investigated lead to a similar increasing behaviour with always positive values for both $u_{11}(z)$ and $u_{22}(z)$.

It is shown that $D = u_{11}(z) \cdot u_{22}(z)$ at $x > L_1$. The latter means that D is positive at all $x > 0$. That is, the Jacobi's condition is satisfied.

CHAPTER 4

Hysteresis of Contact Angle of Sessile Droplets on Deformable Substrates: Influence of Disjoining Pressure

Overview

In the previous chapter equilibrium conditions of droplets on rigid and deformable substrates were investigated. In this chapter static hysteresis of contact angle of droplets on deformable substrates will be presented and advancing and receding contact angles will be theoretically predicted. The results of investigations were published in Colloids and Surfaces A: Physicochemical and Engineering Aspects, and reused below with permission from corresponding author, Professor Victor M. Starov(v.m.starov@lboro.ac.uk)

In this Chapter equilibrium contact angle of droplet on deformable substrate is initially theoretically discussed as a basis for introduction to the phenomenon of hysteresis. In the next section a theoretical model for hysteresis of contact angle for droplet on deformable substrate is derived and advancing and receding contact angles are evaluated. Advancing contact angle is reached when the excess pressure P_e, reaches a critical value P_a, while for higher pressures$P_r > P_e$ receding contact angles are formed. Model derivation is simplified by the adoption of a piecewise linear disjoining pressure isotherm.

4.1 Introduction

Static hysteresis of contact angle of droplets on solid substrates is usually assumed to be affected by roughness and/ or chemical heterogeneity of the substrate. It is considered in this case that at each point on the surface the equilibrium value of the contact angle is established depending only on the local properties of the substrate. As a result, a whole series of local thermodynamic equilibrium states can be realized, corresponding to a certain interval of contact angles. The maximum possible value corresponds to static advancing contact angle (abbreviated as θ_a) and the minimum value corresponds to static receding contact angle (abbreviated as θ_r).

However, roughness and chemical heterogeneity of the substrate are not the only reason behind contact angle hysteresis. Hysteresis has also been observed in the cases of smooth homogenous substrates such as free liquid films that are not at all rough and are chemically homogeneous. Recently there have been a number of publications that support the existence of contact angle hysteresis on smooth and homogeneous rigid substrates (75,76,110).
In the case of complex liquid-fluid systems such as microemulsions(111), monolayers of biologically important surfactants (phospholipid monolayers)(112,113) or self-assembled monolayers of proteins , the characteristics of phase behaviour are determined by interfacial layers and their stability. In a similar way, for the case of liquid-soft solid systems, their properties and stability are related to the forces acting on the thin films that separate the phases of the system.

Disjoining pressure is a manifestation of the surface forces action in the free thin liquid films and layers(53).It acts in the vicinity of the apparent three phase contact line. Earlier theories for the contact angle hysteresis

of menisci and droplet on smooth homogeneous solid substrate were developed using S-shaped disjoining pressure isotherm(53,75,76,110). Contact angle hysteresis has been proven to be directly related to the Derjaguin isotherm for free liquid films and layers(114).

According to Kelvin's equation, a droplet can be at equilibrium with oversaturated vapour only and to reach the equilibrium the oversaturation should be kept for a prolong period of time(53,63). Consequently, it is still difficult, if possible, to achieve the equilibrium at all in the case of pure liquids. According to a regular procedure of deposition of droplets on any surface, after the deposition the droplet reaches the static advancing contact angle. It is usually believed that this angle is close enough to the equilibrium contact angle. It was shown earlier(76) that this is not true, at least in the case of smooth homogeneous non-deformable substrates.

The consideration of equilibrium contact angles on deformable substrate is similar to that for droplets on solid, smooth and homogeneous substrate in Ref.(111) but with introduction of elasticity in the substrate(115). However, as it was mentioned above, formation of equilibrium droplets on non-deformable or deformable substrates has only theoretical interest because experimentally it is difficult, if possible at all, to investigate equilibrium droplets.

Only static advancing or static receding contact angles are usually experimentally investigated. It is the reason why both static advancing and static receding contact angles on deformable substrates are considered below.

In the next section, equilibrium of droplets on a deformable substrate is discussed which is then extended to introduce the theory of hysteresis of contact angle on deformable substrates. Herein, the static advancing contact angle for droplet on deformable substrate and the static receding contact angle are investigated and compared to those on non-deformable substrate(76).The influence of surface forces and disjoining pressure is considered.

4.2 Theory

Equilibrium contact angle of droplet on deformable substrates and the surface forces action

This section deals with the theory of equilibrium of droplets on deformable substrates. It forms the basis for introduction of hysteresis to the problem below. Apparently, there is only a single equilibrium contact angle, θ_e, on smooth homogeneous substrates. However, according to Kelvin's equation, to reach this equilibrium contact angle the droplet should be at the equilibrium with oversaturated vapour(53). Therefore, experimentally only non-equilibrium contact angles can be observed, which are referred to as hysteresis contact angles: static advancing contact angle, $\theta_a > \theta_e$, and static receding contact angle, $\theta_r < \theta_e$.

That is, consideration of equilibrium contact angles presented below should be considered from this point of view. A simple Winkler's model for the deformable solid is used below. According to Winkler's model there is a linear relationship between the local deformation and the applied local stress(73,77). According to this model, deformation of the deformable substrate, h_s, is local and is directly proportional to the applied pressure, P:

$$h_s = -KP, \qquad (4.1)$$

where, K is the elasticity coefficient, h_s is the local deformation of the substrate due to the applied pressure, P, from above.

Let P_{air} be the pressure in the ambient air. Under the action of the pressure from the ambient air the solid deformation is:

$$h_{se} = -KP_{air}. \tag{4.2}$$

The deformed solid substrate is covered by the thin equilibrium liquid film, which is calculated according to combination of the well-known Kelvin's equation and disjoining pressure isotherm(53):

$$\Pi(h_e) = P_e = \frac{R_g T}{\nu_m} \ln \frac{p_{sat}}{p}, \tag{4.3}$$

where ν_m is the molar volume of the liquid; T is the temperature in K; R_g is the gas constant; vapour pressure, p, is higher than the saturated pressure p_{sat}; P_e is the equilibrium excess pressure in the liquid. Reminder, at the equilibrium state, the droplet must be at equilibrium with oversaturated vapour only, according the Kelvin's Eq. 4.3. The excess free energy of the equilibrium thin film on the deformed solid per unit area is given by:

$$\frac{F_{e,film}}{S_{film}} = \gamma + \gamma_s + P_e h_e + \frac{h_{se}^2}{2K} + \int_{h_e}^{\infty} \Pi(h) dh, \tag{4.4}$$

where, $P_e = P_{air} - P_{liquid}$; γ and γ_s are liquid-vapour and solid-liquid interfacial tensions. This free energy should be subtracted from the free energy of the droplet on the deformable substrate, otherwise the excess free energy of the droplet is infinite. Hence, the excess free energy of the droplet on a deformable solid substrate is as follows:

$$F - F_{e,film} = \gamma \Delta S + \gamma_s \Delta S_s + \Delta V + F_{surface\ forces} + F_{deformation}, \tag{4.5}$$

where Δ means "as compared with a flat equilibrium film".

Eq. 4.5 can be rewritten as:

$$F - F_{e,film} = \int_0^{\infty} f(h, h', h_s, h'_s) dx, \tag{4.6}$$

where

$$f(h,h',h_s,h'_s)=\begin{bmatrix}\gamma\left(\sqrt{1+h'^2(x)}-1\right)+\gamma_s\left(\sqrt{1+h_s'^2(x)}-1\right)+\\ P_e(h-h_s)-P_eh_e+\frac{h_s^2}{2K}-\frac{h_{se}^2}{2K}\\ +\int_{h-h_s}^{\infty}\Pi(h)dh-\int_{h_e}^{\infty}\Pi(h)dh\end{bmatrix}. \quad (4.7)$$

In above equations x is the length along the tangential direction. The expression under the integral in Eq. 4.6 tends to zero as x tends to infinity.

Under equilibrium conditions the excess free energy (Eq. 4.6) should reach the minimum value. To satisfy this condition the first variation of the excess free energy should vanish, which results in two Euler equations for profiles of both the droplet and deformable substrate:

$$\frac{d}{dx}\left(\frac{\partial f}{\partial h'}\right)-\frac{\partial f}{\partial h}=0, \quad (4.8)$$

$$\frac{d}{dx}\left(\frac{\partial f}{\partial h_s'}\right)-\frac{\partial f}{\partial h_s}=0. \quad (4.9)$$

Therefore, profile of the droplet, $h(x)$, and profile of the substrate, $h_s(x)$, satisfy the following set of equations according to Ref. (63) with a simplifying assumption that the substrate surface tension, γ_s, is neglected gives:

$$\gamma\left(\frac{h''}{(1+h'^2)^{3/2}}\right)+\Pi(h-h_s)=P_e, \quad (4.10)$$

$$\Pi(h-h_s)+\frac{h_s}{K}=P_e. \quad (4.11)$$

Variable h and its derivatives, h' and h'' are all functions of x coordinate. Eq. 4.10 is substantially different from the usual capillary equation for the droplet profile on a rigid substrate(53) because now the disjoining pressure term, $\Pi(h-h_s)$, in Eq. 4.10 depends on the profile of the deformable substrate, $h_s(x)$, which is determined by the Eq. 4.11 . Note, the value of P_e, is determined by the value of the oversaturated pressure in the ambient air.

Theory and model for hysteresis of contact angle on deformable substrate

In this section, non-equilibrium (quasi-equilibrium) states of a droplet on a soft substrate are considered for calculation of static advancing/receding contact angles. In this case, the droplet volume is imposed externally and can be varied externally (pumping the liquid in or out). The droplet will instantaneously start moving microscopically if $P \neq P_e$, because in this scenario excess pressure is different from its value at equilibrium(76). If the pressure inside the droplet is increased, then the droplet will start to move. All process can be subdivided into “slow microscopic” and “fast macroscopic” processes. Change of the drop curvature

over the main spherical part of the droplet is a "fast macroscopic" process, flow in a relatively thick β-films is also a "macroscopic" process, because the relative viscous resistance in these films is much smaller as compared with the flow in thin α-films(50). Hence, the idea is as follows until the flow takes place in relatively thin α-films(53), then the droplet is at quasi-equilibrium state and slow microscopic motion. As soon as the flow jump wise occupies the zone of relatively thick β-films, then the droplet starts the macroscopic motion.

Note, the thickness of β-films is almost one order of magnitude bigger than the thickness of α-films. Under the applied pressure difference, $\Delta p = P - P_e$, the flow rate, Q, in the film of thickness h is $Q = \frac{\Delta p}{6\mu l} h^3$, where $l \sim \sqrt{H h_e}$ is the characteristic length of the transition zone between the bulk droplet and the thin films in front(53), is the dynamic viscosity. That means, the flow inside β-films is 3 orders of magnitude faster than in α-films. It is the reason why the flow located inside α-films is referred to as "microscopic flow", while the flow inside β-films is referred to as "macroscopic flow".

In advancing droplet, the transition from microscopic to macroscopic motion occurs when the excess pressure reaches the critical value P_a and correspondingly the macroscopic contact angle reaches the critical value θ_a (53,76). At that point, which is analytically described below (also depicted in Figure 4.1), the surface of the droplet becomes more steep until it reaches a 'dangerous point', h_3 , (53)where the sloped becomes vertical. Therefore, droplet does not move macroscopically until $P = P_a$ and the advancing contact angle, θ_a, is reached. After that the flow jump-wisely transferred from thin α-films to much thicker β-films and becomes much faster, i.e., macroscopic.

At higher pressures, $P_r > P_e$, receding contact angle is formed. In the case of receding droplet the transition from microscopic to macroscopic motion occurs when the excess pressure reaches the critical value P_r and correspondingly macroscopic contact angle reaches a critical value θ_r (53,76).As shown in Figure 4.2, the droplet surface becomes more and more flat and after a critical pressure, P_r, is reached the droplet will start to slide fast along a thick β-film and leaving the β-film behind. 'Dangerous' point is marked h_4 (53)in Figure 4.2**.**

It is assumed that the droplet profile everywhere except for a narrow flow zone can be described by Eqs. 4.10-4.11 where the equilibrium excess pressure, P_e, should be replaced by a non-equilibrium pressure, P (Figure 4.1 and Figure 4.2). For advancing droplets, due to decrease in pressure, microscopically the slope grows and tends to infinity at some critical point (marked in Figure 4.1) when P_a is reached. Apex, H_a, and the radius, R_a, of the advancing droplet are shown in Figure 4.1. It is assumed below according to (53,75,76) that Eqs. 4.10-4.11 can be used to describe a quasi-equilibrium part of the droplet (Figure 4.1) even in the case of droplet on a soft substrate. Subsequently, P_e is replaced by P_a in all equations from the previous section. Similarly, when the pressure in the droplet increases, microscopically the slop of the droplet decreases and becomes flat in the end (a zero slope) at P_r at some critical point (marked in Figure 4.2). Droplet is in this case receding where apex, H_r, and the radius, R_r, of the receding droplet are shown in Figure 4.2.

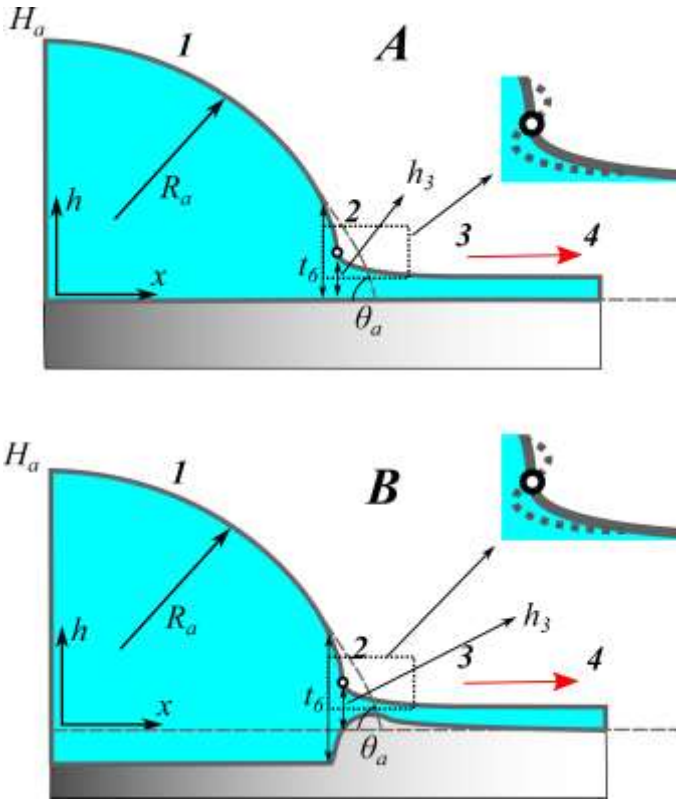

Figure 4. 1: Schematic of a droplet on a solid non-deformable substrate (A) and soft/deformable substrate (B) at the moment before advancing begins. 1- quasi-equilibrium part of the droplet; 2- inflection point, where the slope becomes vertical; 3- flow zone; 4- equilibrium thin liquid film in front; $\boldsymbol{h_3}$ *is the thickness at the critical point. Close to the marked point a dashed line shows the profile of the transition zone just after the contact angle reaches the critical value* $\boldsymbol{\theta_a}$ *and advancing starts as a caterpillar motion (see explanations in the text) Source:(64)*

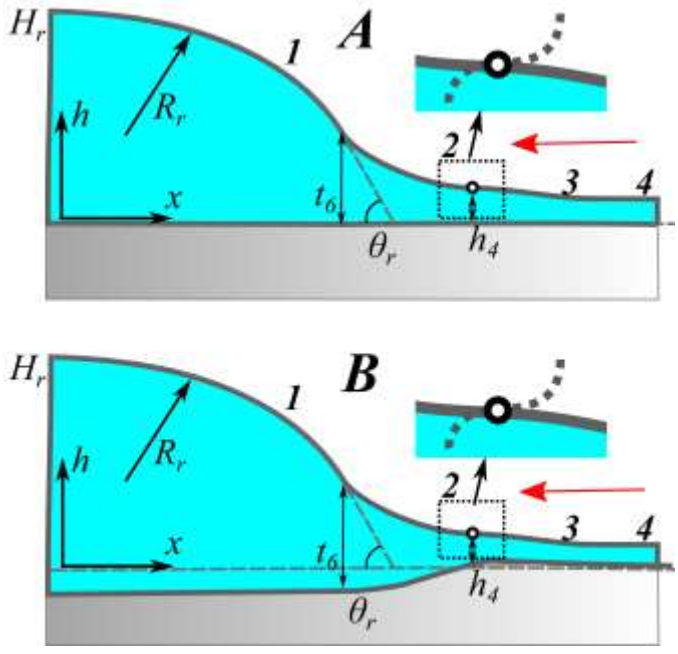

Figure 4. 2:Schematic of a droplet on a solid non-deformable substrate (A) and soft/deformable substrate (B) at the moment before receding begins. 1- quasi-equilibrium part of the droplet; 2- inflection point, where the slope becomes vertical; 3- flow zone; 4- equilibrium thin liquid film in front; h_4 *is the thickness at the critical point. Close to the marked point a dashed line shows the profile of the transition zone just after the contact angle reaches the critical value* θ_r *and receding starts (see explanations in the text). Source:(64)*

Earlier, the theory of advancing and receding contact angles was developed in the case of smooth homogeneous non-deformable substrates (76). It was shown in (76) that there exist "dangerous" points on the profiles of the advancing and receding droplets, which are inflection points with a thickness h_3 (Figure 4.1A), in case of advancing droplet and thickness h_4 (Figure 4.2A), in case of receding droplets. At some critical pressure, P_a, the slope becomes infinite at the critical point (Figure 4.1), the droplet cannot remain in the state of slow "microscopic" motion and starts "macroscopic" motion. That means, for the case of advancing droplets, "dangerous" point, h_3, is the moment when advancing starts, should be satisfied two the following conditions:

$$h'' = 0, \qquad h' = -\infty, \qquad at \;\; h = h_3. \tag{4.12}$$

Similarly, the slope decreases with increase in excess pressure in the case of receding around a critical point (Figure 4.2). At some critical pressure, P_r, the slope becomes zero at the critical point, the droplet cannot remain in the state of slow "microscopic" motion and starts "macroscopic" motion. That means that the "dangerous" point, h_4, is the moment when receding starts, should be satisfied two the following conditions:

$$h'' = 0, \qquad h' = 0, \qquad at \;\; h = h_4. \tag{4.13}$$

Even under simplifying assumptions adopted above, the system of Eqs. 4.10 and 4.11 is coupled and can be solved numerically only. It is the reason why a simplified disjoining pressure isotherm (piecewise linear function of h) is adopted below (see Figure 4.3) to simplify the system of Eqs. 4.10-4.11 further and to obtain an analytical solution:

$$\Pi(h) = \begin{cases} a(t_0 - h) & 0 \le h \le t_1 \\ b(h - t_2) & t_1 \le h \le t_3 \\ c(t_4 - h) & t_3 \le h \le t_5, \\ d(h - t_6) & t_5 \le h \le t_6 \\ 0 & h > t_6 \end{cases} \tag{4.14}$$

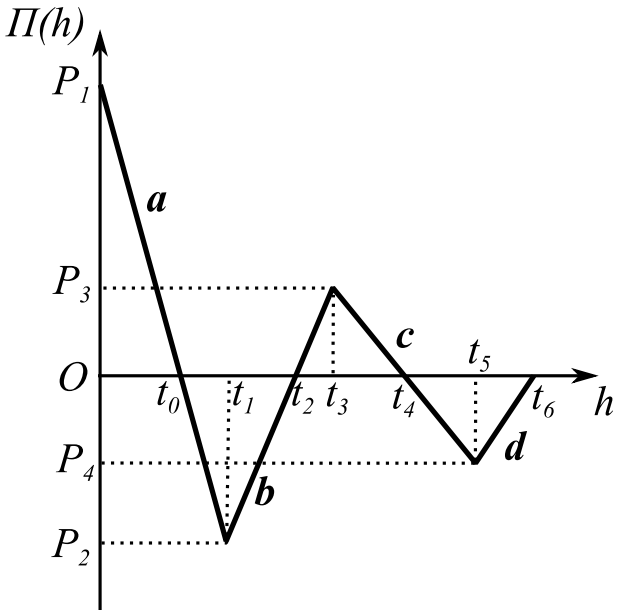

Figure 4. 3:Simplified disjoining pressure isotherms adopted for calculations below. Part a is referred to as thin α-films, Part c is referred to as thick β-films. Source:(64)

Disjoining pressure isotherm has four regions namely, $0 \leq h \leq t_1$, $t_1 \leq h \leq t_3$, $t_3 \leq h \leq t_5$ and $t_5 \leq h \leq t_6$. Schematic plot of the adopted disjoining pressure isotherm is presented in Figure 4.3. Symbols a, b, c and d are used below for slope of linear parts of isotherms inside corresponding zones. Hence, a is the slope of the linear function in the region $h_e \leq h \leq t_1$ given by:

$$a = \frac{P_1 - P_2}{t_1} = \frac{P_1 - P_e}{h_e}, \tag{4.15}$$

b is the slope of the linear function in the region $t_1 \leq h \leq t_3$ given by:

$$b = \frac{P_3 - P_2}{t_3 - t_1}, \tag{4.16}$$

and c is the slope of the linear function in the region $t_3 \leq h \leq t_5$ given by:

$$c = \frac{P_3}{t_4 - t_3}. \tag{4.17}$$

and d is the slope of the linear function in the region $t_5 \leq h \leq t_6$ given by:

$$d = \frac{P_4}{t_5 - t_6}. \tag{4.18}$$

The selected piecewise linear dependency of the disjoining pressure isotherm $\Pi(h)$ on h (see Eq. 4.14) captures the essential properties of the disjoining pressure isotherm: (i) it satisfies the stability condition, $\Pi'(h) < 0$ when $0 \le h \le t_1$ (α-films (53) and $t_3 < h < t_5$ (β-films(53)); (ii) it corresponds to the partial wetting case at the proper selection of the parameters; (iii) the influence of surface forces is short ranged and radius of their influence is t_6. All parameters of disjoining pressure presented in Fig. 4.3 are selected below to mimic, as much as possible, the isotherm used in (76) for calculation of advancing/receding contact angles on smooth non-deformable substrate.

In order to solve the system of Eqs. 4.10 and 4.11 subtract them, which results in:

$$\gamma\left(\frac{h''}{(1+h'^2)^{3/2}}\right) - \frac{h_s}{K} = 0. \qquad (4.19)$$

Eq. 4.19 must be solved for four different transition regions where disjoining pressure is applicable, i.e., from h_e to t_6. According to Eq. 4.19 the condition $h'' = 0$ is satisfied when $h_s = 0$ (at $h = h_3 \ and \ P = P_a$ (for advancing droplet) and at $h = h_4$ and $P = P_r$ (for receding droplet). The "dangerous points" are located on the disjoining pressure isotherm in the region b for advancing and region c for receding droplet (see Figure 4.3). Hence, it is possible to conclude:

$$h_3 = t_2 + \frac{P_a}{b} \quad \text{and} \quad h_4 = t_4 - \frac{P_r}{c}. \qquad (4.20)$$

Detailed derivation for advancing droplets are presented in Appendix. Derivation for receding droplets is not included to avoid repetitions.

4.3 Results and Discussion

The following table gives the physical properties used below for the disjoining pressure isotherm shown in Figure 4.3 for calculation of advancing/receding contact angles. The units used in this work allow a more suitable graphical representation of the results and are easily comparable with results presented in (76,115).

Table 4. 1: Disjoining pressure isotherm properties: Surface tension, γ, Disjoining/Conjoining pressure isotherm parameters, P_1, P_2, P_3, P_4, t_0, t_1, t_2, t_3, t_4, t_5 and t_6, slopes of the disjoining/conjoining pressure isotherm for different regions, a , b ,c and d ,elasticity coefficient, K , and volume of advancing droplet V_a, for calculations of advancing/receding contact angles. Source:(64)

Physical Properties	**Isotherm**
Surface tension, γ	72.00dyne/cm
P_1	1.300×10^{13} dyne/cm^2
P_2	-4.450×10^{8} dyne/cm^2
P_3	2.800×10^{7} dyne/cm^2
P_4	-6.500×10^{4} dyne/cm^2
t_0	$\frac{P_1}{a} = 2.299 \times 10^{-8}$ cm
t_1	2.300×10^{-8} cm
t_2	$t_3 - \frac{P_3}{b} = 2.083 \times 10^{-7}$ cm
t_3	2.200×10^{-7} cm
t_4	3.000×10^{-6} cm
t_5	3.007×10^{-6} cm
t_6	2.000×10^{-5} cm
a	$\frac{P_1 - P_2}{t_1} = 5.652 \times 10^{20}$ dyne/cm^3
b	$\frac{P_3 - P_2}{t_3 - t_1} = 2.401 \times 10^{15}$ dyne/cm^3
c	$\frac{P_3}{t_4 - t_3} = 1.007 \times 10^{13}$ dyne/cm^3
d	$\frac{P_4}{t_5 - t_6} = 3.825 \times 10^{9}$ dyne/cm^3
K	2.000×10^{-16} cm^3/dyne, i.e., $bK < 1$
V_a	1.000×10^{-2} cm^2

The values of the disjoining pressure isotherm mentioned in Table 4.1 are selected values to match the disjoining pressure isotherm used in Ref (76) and 1dyne=10^{-5}N. These specific values are used so that the results can be compared with those in Ref. (76)for non-deformable substrates.

To begin with, volume of the advancing droplet is varied to investigate its effect on advancing contact angle for a non-deformable ($K = 0$ cm^3/dyne) and deformable substrate ($K = 2.000 \times 10^{-16}$ cm^3/dyne).The higher the initial volume of the droplet, V_a, the lower the value of θ_a. The highest values of θ_a are found for droplets with small size, i.e. with a high excess pressure (γ/R_a). The trend of θ_a variation with V_a is in agreement with the results presented for advancing droplet on solid non-deformable substrate(76), i.e. a decreasing function. At $V_a \approx 5 \times 10^{-9}$cm^2 and $K = 0$ cm^3/dyne the current model predicts $\theta_a \approx 57.78^o$ whereas from Ref (76) gives $\theta_a \approx 57.43^o$, which are in a very good agreement. Effect of increasing the elasticity of the substrate, i.e. $K = 2 \times 10^{-16}$ cm^3/dyne, results in overall decrease in the values of θ_a (see

the broken line in Figure 4.4). This shows that on a deformable substrate static advancing contact angle decreases as compared with a non-deformable substrate.

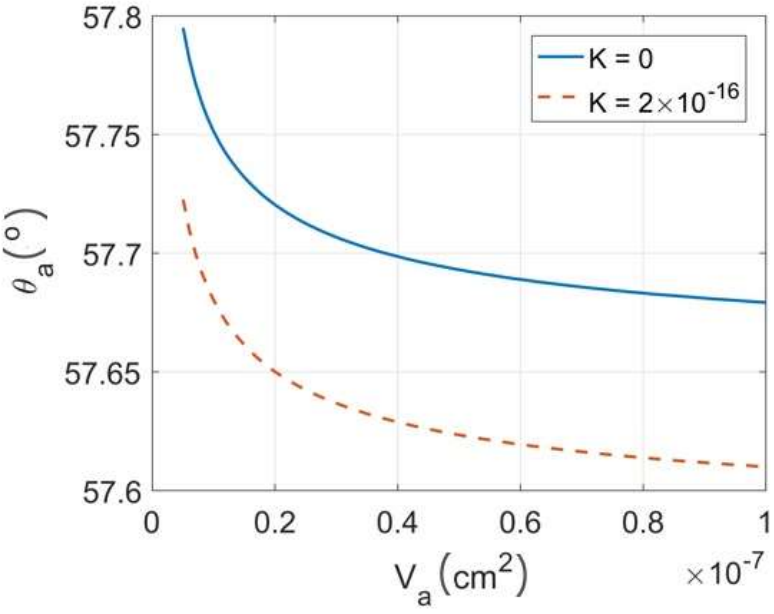

Figure 4. 4: Effect of variation of droplet volume on static advancing contact angle. Source:(64)

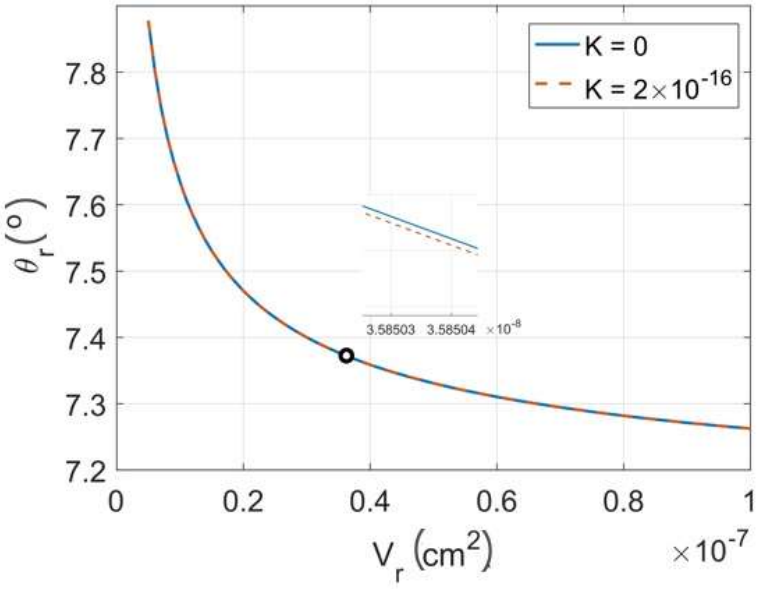

Figure 4. 5: Effect of variation of droplet volume on apparent receding contact angle. Source:(64)

Volume of the receding droplet is varied to investigate its effect on receding contact angle for a non-deformable ($K = 0$ cm^3/dyn) and deformable substrate ($K = 2 \times 10^{-16}$ cm^3/dyn), see Figure 4.5. The higher the initial volume of the droplet, V_r, the lower the value of θ_r. Highest values of θ_r are observed for droplets with small size, i.e. with a high excess pressure (γ/R_r). The trend of θ_r variation with V_r is a decreasing function and is in agreement with the results presented for advancing droplet on solid substrate (76). At $V_a \approx 5 \times 10^{-9}$cm^2 and $K = 0$ cm^3/dyn, model predicts $\theta_r \approx 7.88^o$ whereas from Ref. (76)estimates $\theta_r \approx 8.8^o$. The difference is primarily due to the use of approximate values for piece-wise linear disjoining pressure isotherm. Effect of increasing the elasticity of the substrate, i.e. $K = 2 \times 10^{-16}$ cm^3/dyn, results in a very slight overall decrease in the values of θ_r (see red dotted line zoomed region in Figure 4.5) as compared with as corresponding non-deformable substrate. Therefore, it can be assumed that with a more deformable substrate apparent static receding contact angle is expected to decrease, but the decrease is very small at least according to the model used for deformable substrate.

As calculated and shown in Figures 4.4 and 4.5, contact angle hysteresis on deformable substrates is lower than that on non-deformable substrates. A decreasing trend of hysteresis with increasing substrate elasticity has been observed experimentally using various experimental techniques(116,117).

4.4 Conclusions

Advancing and receding contact angles on smooth and homogeneous deformable substrate are theoretically investigated. Disjoining pressure action is taken into account in the vicinity of the three-phase contact line and Winkler's model is used to account for the elasticity of the deformable substrate. It is demonstrated that advancing and receding contact angle of a droplet on smooth, homogeneous deformable substrate depend upon the droplet volume, and elasticity of the substrate. For deformable substrate calculated advancing contact angle is lower than advancing contact angle on the corresponding non-deformable substrate. Increase in volume of the droplet causes the advancing contact angle to reduce. For deformable substrate, estimated receding contact angle is less than receding contact angle on a non-deformable substrate, but the decrease is very small. Both advancing and receding contact angles decrease with increasing substrate elasticity. Hysteresis of contact angle was proven to be lower for deformable substrates than that for non-deformable, which has been previously proven experimentally on various polymer substrates (116,117).

Nomenclature 4

a, b, c, d	–	Slopes of different regions of disjoining/conjoining pressure isotherm defined in Figure 4.3
α	–	α −film
β	–	β −film
F		Excess free energy
$F_{e,film}$	–	Excess free energy of the equilibrium thin film on the deformed solid
γ	–	Surface tension of the fluid
γ_s	–	Surface tension of the substrate
H	–	Apex of the droplet
H_a	–	Apex of the advancing droplet
H_r	–	Apex of the receding droplet
h	–	Film thickness, equilibrium liquid profile, droplet height
h_e	–	Stable equilibrium film thickness
h_s	–	Local deformation of the substrate
h_{se}	–	Local deformation of the substrate under the action of the ambient pressure
h_3	–	Thickness in the critical point for advancing droplet

h_4 – Thickness in the critical point for receding droplet
K – Elasticity coefficient
l – Characteristic length
μ – Dynamic viscosity
P – Non-equilibrium pressure, applied pressure from a droplet to its substrate
P_{air} – Pressure in the ambient air
P_e – Equilibrium excess pressure
P_a – Advancing pressure
P_r – Receding pressure
p – Vapour pressure
p_{sat} – Saturated vapour pressure
$\Pi(h)$ – Disjoining pressure isotherm
Q – Flow rate
R – Radius of curvature of the droplet
R_a – Radius of curvature of the advancing droplet
R_g – Gas constant
R_r – Radius of curvature of the receding droplet
S – Area of the liquid-air interface
S_s – Area of the solid-liquid interface
T – Temperature
$t_0, t_1, t_2, t_3, t_4, t_5, t_6$ – Parameters of disjoining/conjoining pressure isotherm defined in Figure 4.3
θ_e – Equilibrium contact angle
θ_a – Advancing contact angle
θ_r – Receding contact angle
V – Volume of the fluid
V_a – Volume of the advancing droplet
V_r – Volume of the receding droplet
v_m – Molar volume of the liquid
x – Co-ordinate in the tangential direction

Appendix 4A

For advancing contact angle

To avoid repetition, detailed derivation for the disjoining pressure isotherm (Figure 4.3) is presented below. Governing equations from Eqs. 4.10 and 4.11 can be rewritten now as:

$$\gamma\left(\frac{h''}{(1+h'^2)^{3/2}}\right)+\Pi(h-h_s)=P_a, \tag{4A.1}$$

$$\Pi(h-h_s)+\frac{h_s}{K}=P_a. \tag{4A.2}$$

For the bulk of the liquid droplet, i.e. the spherical region, we have, $h > t_6$. For this condition, from Figure 4.3 it can be seen that $\Pi(h)=0$ which changes Eq. 4A.1 into,

$$\gamma\left(\frac{h''}{(1+h'^2)^{3/2}}\right)=P_a, \tag{4A.3}$$

which can be integrated once to give,

$$\frac{\gamma}{\sqrt{1+h'^2}}=\gamma+P_a(H_a-h), \tag{4A.4}$$

where H_a is the height of the droplet at the origin, $x=0$. The solution of the differential equation in Eq. 4A.4 is,

$$h(x)=\frac{\gamma}{P_a}\left[1+\frac{P_aH_a}{\gamma}-\sqrt{1-\left(\frac{P_ax}{\gamma}\right)^2}\right]. \tag{4A.5}$$

The intersection of this profile with the substrate describes the three-phase contact line which consequently determines macroscopic advancing contact angle $h'(0)=-\tan\theta_a$. Using this condition and Eq. 4A.4 is used to estimate θ_a,

$$\theta_a=\cos^{-1}\left(\frac{P_aH_a}{\gamma}+1\right) \tag{4A.6}$$

For the bulk of the liquid droplet, i.e. the spherical region we have, $h-h_s > t_6$. For this condition, from Eq. 4.14 it can be seen that $\Pi(h)=0$ which changes Eq. 4A.2 into:

$$h_s = KP_a. \tag{4A.7}$$

From Eqs. 4.14 and 4A.2, h_s is evaluated for the different regions of the disjoining pressure isotherm,

$$h_s = \frac{K(P_a + bt_2 - bh)}{1 - bK} \quad \text{for} \quad t_1 \le h \le t_3, \tag{4A.8}$$

and

$$h_s = \frac{K(P_a - ct_4 + ch)}{1 + cK} \quad \text{for} \quad t_3 \le h \le t_5. \tag{4A.9}$$

and

$$h_s = \frac{K(P_a + dt_6 - dh)}{1 - dK} \quad \text{for} \quad t_5 \le h \le t_6. \tag{4A.10}$$

It is necessary to note here that regions of interest for the advancing contact angle are reduced to three regions: $t_1 \le h \le t_3$, $t_3 \le h \le t_5$ and $t_5 \le h \le t_6$. In a similar method of solution, integrate Eq. 4.19 with respect to h for the disjoining pressure isotherm region $t_1 \le h \le t_3$ results in,

$$\frac{1}{\sqrt{1 + h'^2}} = C_{2,a} + \frac{b}{2\gamma(1 - bK)} h^2 - \frac{(P_a + bt_2)}{\gamma(1 - bK)} h, \tag{4A.11}$$

where $C_{2,a}$ is the integration constant. For the disjoining pressure isotherm region $t_3 \le h \le t_5$ integrate Eq. 4.19 with respect to h,

$$\frac{1}{\sqrt{1 + h'^2}} = C_{3,a} - \frac{c}{2\gamma(1 + cK)} h^2 - \frac{(P_a - ct_4)}{\gamma(1 + cK)} h, \tag{4A.12}$$

where $C_{3,a}$ is the integration constant. For the disjoining pressure isotherm region $t_5 \le h \le t_6$ integrate Eq. 4.19 with respect to h,

$$\frac{1}{\sqrt{1 + h'^2}} = C_{4,a} + \frac{d}{2\gamma(1 - dK)} h^2 - \frac{(P_a + dt_6)}{\gamma(1 - dK)} h, \tag{4A.13}$$

where $C_{4,a}$ is the integration constant. Let $x = L_{6,a}$ be the position, where the total thickness of the liquid film is equal to the radius of disjoining pressure action, that is at $x = L_{6,a}$, $h(L_{6,a}) - h_s(L_{6,a}) = t_6$. Then from Eq. 4A.7 and this boundary condition:

$$h(L_{6,a}) = t_6 + KP_a. \tag{4A.14}$$

From Eq. 4A.5 $h(L_{6,a})$ is equal to:

$$h(L_{6,a}) = \frac{\gamma}{P_a}\left[1 + \frac{P_a H_a}{\gamma} - \sqrt{1 - \left(\frac{P_a L_{6,a}}{\gamma}\right)^2}\right]. \tag{4A.15}$$

According to equations 4A.14 and 4A.15 the thickness of both sides must be equal. This allows determining:

$$L_{6,a} = \sqrt{\left(\frac{\gamma}{P_a}\right)^2 - \left(t_6 + KP_a - \frac{\gamma}{P_a} - H_a\right)^2}. \tag{4A.16}$$

Let $x = L_a$ be the position, where the spherical profile intersects initial non-deformed surface, hence, at $x = L_a$, $h(L_a) = 0$. For this condition evaluate for L_a gives:

$$L_a = \sqrt{\left(\frac{\gamma}{P_a}\right)^2 - \left(\frac{\gamma}{P_a} + H_a\right)^2}. \tag{4A.17}$$

Boundary conditions are,

$$\begin{aligned} &\text{At } h = h_3, && h' = -\infty, \text{ from Ref. (76)},\\ &\text{At } h = t_3, && h'_c = h'_b \text{ and } h_c = h_b,\\ &\text{At } h = t_5, && h'_c = h'_d \text{ and } h_c = h_d. \end{aligned}$$

Where subscripts only point to different regions on the disjoining pressure isotherm plotted in Figure 4.3. Using the above boundary conditions, unknowns $L_{4,a}$, L_a, $C_{2,a}$, $C_{3,a}$ and $C_{4,a}$ can be evaluated. Volume of the advancing droplet, V_a, is fixed. Therefore,

$$V_a = 2\left\{L_a\left(H_a + \frac{\gamma}{P_a} - KP_a\right)\right.$$
$$\left. - \frac{1}{2}\left[-L_a\sqrt{\left(\frac{\gamma}{P_a}\right)^2 - L_a^2} + \left(\frac{\gamma}{P_a}\right)^2 \sin^{-1}\left(\frac{L_a P_a}{\gamma}\right)\right]\right\} \quad \text{(4A.18)}$$

CHAPTER 5

Foam drainage placed on a thin porous layer

Overview

In chapters 3 and 4 wetting phenomena (equilibrium conditions and static hysteresis of contact angle) of droplets on deformable substrates were theoretically investigated. Below the research is focused in investigating the process of foam drainage and imbibition of foam placed on thin porous layer both theoretically and experimentally. In this study a theory of foam drainage (taking into account surface viscosity) placed on a completely wettable thin porous layer is developed and the kinetics of foam drainage and imbibition inside the porous layer and other characteristics of the process are predicted and compared with experimental observations. The results of investigations were published in Soft Matter, and reused in this chapter with permission from corresponding author, Professor Victor M. Starov(v.m.starov@lboro.ac.uk).

Following a recently developed theory of foam drainage placed on a thick porous substrate presented in(19), in this Chapter , section 5.2 is devoted in developing a modified theory to the case of the foam drainage placed on a thin porous layer for foam produced from a Newtonian surfactant in a column of height H placed on a thin porous substrate. The flow of liquid is assumed to occur only inside Plateau borders and flow through films and nodes is neglected. The theoretical model derived is able to describe drainage kinetics and the action of surface viscosity is taken into consideration. Boundary conditions of the foam/porous layer interface are discussed in section 5.2.3 and the equilibrium profile of the liquid content is presented in 5.2.4 in the case when gravity and capillarity forces equilibrate at the foam/porous layer interface. Experimental procedure is described in section 5.3 and Section 5.4 presents a comparison between experimental measurements and model predictions.

5.1 Introduction

Foams are a special type of colloidal dispersion consisting of both liquids and bubbles stabilised by surfactants and/or polymers(118–122). Foams have a wide range of domestic and industrial applications as intermediate or final products. The list of possible applications is inexhaustible and includes oil recovery and refining process (122), food, pharmacy, and personal care products, acoustic thermal insulation, packaging solutions and constituents of structural foam materials(123). The foam structure was initially described by Joseph Plateau in 1873 (124). Gas bubbles are separated by thin liquid films titled lamella. The three lamella meet at 120^{o} angles, and the border between three bubbles is referred to as Plateau border(122). Surfactants/polymers (foaming agents) are incorporated into foams to reduce surface tension, increase interfacial area and increase the stability of the liquid films between bubbles. The stability of foams is determined by both bulk and interfacial properties, i.e. gravity and capillarity, as well as elasticity of the interfaces, liquid viscosity and density, and surface forces in thin films(122).

Foam structure has been previously sufficiently investigated and researchers have recently shown increasing interest in liquid flow dynamics in foams(125–133). The liquid flow between the gas bubbles, driven by capillarity and gravity forces, is known as drainage and it goes through both Plateau borders and nods. As liquid drains due to the applied local forces, i.e. gravity and capillarity within the foam, it causes alterations in the local liquid volume fraction. When these forces counter-balance each other, the steady-state is reached. Usually flow inside Plateau borders is assumed to be predominant(85,125) for sufficiently dry foams (the liquid volume fraction below ~0.12), while flow through nodes dominates for a sufficiently wet foams (the

liquid volume fraction above ~0.12) and flow in thin films can be usually ignored. Below in our experiments the initial liquid volume fraction was selected as 0.08, that is below the critical value, that is, we consider an approximation then the drainage is supposed to be dominated by the flow inside Plateau borders. That is, the liquid volume fraction is low enough, and, hence, the flow in the nods is not taken into account. This applies for most part of the foam investigated in our experiments during drainage except for a small region at the bottom of the foam in cases we have formation of a free liquid layer between the foam and the porous layer.

Usually two different scenarios for boundary condition at liquid-air interface are used: (i) Poiseuille flow (non-slip condition) which states that the fluid velocity at the wall of Plateau borders is equal to zero and implies a strong viscous dissipations(134) or (ii) a plug flow (free slip condition) where there is no hydrodynamic resistance to the flow in Plateau borders(125). Below the following assumptions are adopted: (a) the main part of the liquid volume is located inside Plateau borders and dry foam approximation is used for the drainage equations; (b) surface viscosity is taken into account, which results in an "effective slip" at the liquid-air interface.

Studies of drainage are of a great industrial interest and multiple theories have been developed over the last decades to describe the drainage (123,135). Drainage equations have been solved for various situations. Examples include free drainage(31,32,90), wetting of a dry foam(37,136), forced drainage (33,34,137)and pulse drainage (33,123). Foams are ideal products for the delivery of topical active agents such as corticosteroids, antibacterial, local anaesthetic agents, skin protectants and antiviral agents entailing effective, elegant and appealing vehicles for dermatological applications(8). Foams are more easily applicable than conventional products such as gels and creams, they have enhanced spreading behaviour and increasing patient compliance for several conditions such as psoriasis, eczema and atopic dermatitis(9,10,28,29,138). Foams for pharmaceutical and topical use are in general produced with the 'sudden pressure reduction' method(79). Pressurised foams are also efficient dispersal systems for the delivery of pharmaceutical active components incorporated into nanoparticles. In this case, foam collapse on a topical substrate causing the active agents to concentrate braking down nanoparticles and leading to a potential drug release(80,81).

The kinetics of topical drug delivery can be altered by changing the physical properties of the foam. That is why there is an increasing interest in liquid drainage of foams on porous media(19,98,139). The desired properties depend upon the porous material, which the foam was being applied to.

Below drainage of foams placed on thin porous substrate is investigated. In this case drainage process is a combination of a drainage caused by gravity/capillary action inside foam and a capillary suction applied by the pores from the porous substrate. Theory and calculations of foam drainage placed on a "thick" porous substrate (with non-slip boundary conditions on the liquid-air interfaces) has been for the first time investigated in (98)and it was shown that, under certain conditions, a free liquid layer can form at the foam/porous substrate interface (19). Unfortunately, it is difficult to investigate experimentally the rate of penetration and the wetted volume inside a thick porous substrate in contact with foams. However, it is very straightforward to measure rate of penetration and wetted area in the case of contact of a foam with a thin porous layer. The latter case is investigated below.

The aim of the present study is to develop a theory of foam drainage placed on a thin porous substrate taking into account the presence of surface viscosity on the liquid-air interfaces and decrease of the foam height in the course of drainage/imbibition. This process is a model of drug delivery of foam placed on a skin or on a hair. The developed theory is compared with experimental measurements of foam drainage placed on thin porous substrates.

5.2 Theory

A theory of the foam drainage placed on a thick porous substrate was presented in (19). In this study non-slip boundary condition on the liquid-air interface was adopted and it was shown that the movement of the top boundary of the foam can be neglected using non-slip boundary condition at the liquid/air interface and imbibition into a thick porous substrate. Herein, the theory is modified below to the case of the foam drainage placed on a thin porous layer (Fig. 5.1) and surface viscosity taken into account. Description of the flow inside the thin porous layer is similar to that of presented earlier in (139).

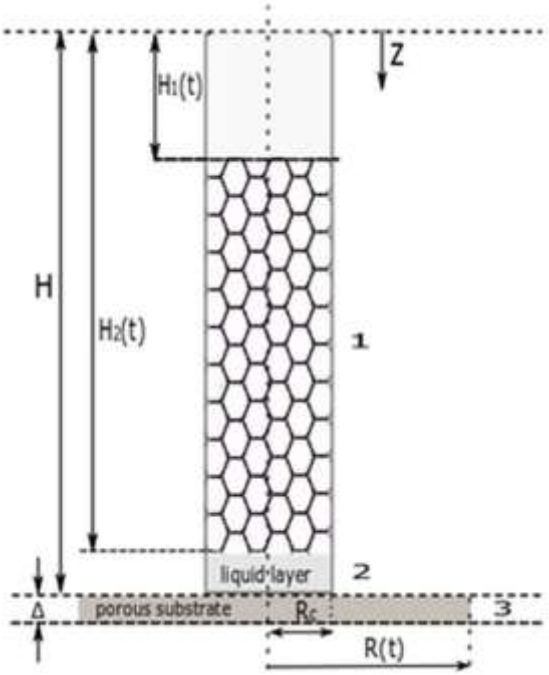

Figure 5. 1:Schematic presentation of the foam placed on a thin porous substrate. 1 – foam; 2 – possible layer of the liquid at the foam/porous substrate interface; 3 – porous layer of thickness ; R(t) is the radius of the wetted area inside the porous layer. Source:(40)

5.2.1 Flow inside foam

Let us consider foam produced from a Newtonian surfactant solution in a column of height *H* placed on a thin porous layer (Figure 5.1). All bubbles are supposed to be of a uniform size with no change duration the experiments. Liquid drainage inside the foam occurs in the vertical direction along the co-ordinate axis z, directed downward, with $z = 0$ at the top of the column. Time evolutions of the foam height and possible free liquid layer under the foam are $H - H_1$ and $H - H_2$, respectively (Figure 5.1). The flow is assumed to occur inside the Plateau borders only and the contribution of the liquid flow in the films and nodes is neglected. In this case the drainage kinetics can be described by the following equation (19,98,140–143):

$$\frac{d\varphi}{dt} + \frac{dQ}{dz} = 0, \tag{5.1}$$

where

$$Q = \left(\frac{C_1^{\frac{1}{2}} \rho g}{\mu\beta} R_b^2 \frac{\varphi^2}{(1-\varphi)^{\frac{1}{3}}} - \frac{C_2 \gamma}{2\mu\beta} R_b \frac{\varphi^{\frac{1}{2}} \left(1 - \frac{\varphi}{3}\right)}{(1-\varphi)} \frac{d\varphi}{dz} \right) \tag{5.2}$$

$$\frac{1}{\beta} = \left(c \frac{1}{3^{\frac{3}{2}} 5} \frac{1}{n_p^{\frac{1}{2}} \delta^{\frac{3}{2}} \pi^{\frac{1}{2}}} \right) = \left(a \frac{1}{3^{\frac{3}{2}} 5} \frac{1}{n_p^{\frac{1}{2}} \delta^{\frac{3}{2}} \pi^{\frac{1}{2}}} \right) \left(1 + B \sqrt{\frac{}{(1- \quad)^{2/3}}} \right) \tag{5.3}$$

$$= \frac{1}{_0} \left(1 + B \sqrt{\frac{}{(1- \quad)^{2/3}}} \right)$$

and $R_{pb} = R_b \sqrt{\frac{C_1}{C_2^2}} \sqrt{\frac{}{(1- \quad)^{2/3}}}$; $c = a + b \left(\frac{R_{pb}}{_s} \right) = a \left(1 + \frac{b \quad R_b}{a \quad _s} \sqrt{\frac{C_1}{C_2^2}} \sqrt{\frac{}{(1- \quad)^{2/3}}} \right) = a \left(1 + B \sqrt{\frac{}{(1- \quad)^{2/3}}} \right)$

where $B = \frac{b \quad R_b}{a \quad _s} \sqrt{\frac{C_1}{C_2^2}}$ and $\frac{1}{_0} = \left(a \frac{1}{3^{\frac{3}{2}} 5} \frac{1}{n_p^{\frac{1}{2}} \delta^{\frac{3}{2}} \pi^{\frac{1}{2}}} \right)$.

In the above equations, φ is the liquid volume fraction; μ is the dynamic viscosity of the liquid; $_s$ is the surface viscosity; γ is the liquid-air interfacial tension; R_b is the radius of bubbles; R_{pb} is the radius of Plateau border; ρ and g are the liquid density and the gravity acceleration, respectively; n_p is the number of Plateau borders per bubble; $_0$ is a coefficient (142,143); $C_2^2 \sim 0.161$; c is the velocity coefficient, $c = a + b \left(\frac{R_{pb} \mu}{_s} \right), a = 0.5169;\ b = 0.5442$ (142), for foams produced from Newtonian solutions; C_1 is a geometrical coefficient expressed as $C_1 = \frac{4\pi}{(3 n_p \delta)} \sim 0.378 - 0.972$ for a foam with structures between bcc (body-centred cubic) and fcc (face-centred cubic) and bubbles of the same size ($\delta = 0.718 - 1.108$, $n_p = 6 - 10$). The action of the surface viscosity is taken into account in Eq. 5.3 according to Ref. (142).

Let us introduce the following dimensionless variable and co-ordinate: $\zeta \to \frac{z}{z_0}$, $\tau \to \frac{t}{t_0}$ where

$$z_0 = \sqrt{\frac{\gamma}{\rho g}}, \qquad t_0 = \frac{2 \quad _0 \mu}{C_2 \rho g R_b} \tag{5.4}$$

Substitution of these variables into Eq. 5.1 results in

$$\frac{d\varphi}{d\tau}+\frac{d}{d\zeta}\left(2\sqrt{Bo}\,\frac{\varphi^{2}\left(1+B\sqrt{\overline{(1-\quad)^{2/3}}}\right)}{(1-\varphi)^{\frac{1}{3}}}-\frac{\varphi^{\frac{1}{2}}\left(1-\frac{\varphi}{3}\right)\left(1+B\sqrt{\overline{(1-\quad)^{2/3}}}\right)}{(1-\varphi)}\frac{d\varphi}{d\zeta}\right)=0, \tag{5.5}$$

where

$$Bo=\frac{\Delta P_{grav}}{\Delta P_{cap}}=\frac{\rho g\frac{C_1^{\frac{1}{2}}}{C_2}R_b}{\frac{\gamma}{\frac{C_1^{\frac{1}{2}}}{C_2}R_b}}=\frac{C_1}{C_2^2}\frac{\rho g R_b^2}{\gamma} \tag{5.6}$$

is a corresponding Bond number.

For a fresh foam produced in the foam column, the initial liquid volume fraction profile is assumed to be uniform and, that is, $\varphi(\zeta,\tau=0)=\varphi_i$, where φ_i is initial liquid volume fraction.

Assuming that the liquid films between bubbles in foam are flat, i.e. $R_b \gg R_{pb}$, (see Figure 5.2) the pressure in all bubbles is identical (98) and equals to:

$$P_b = P_a+\frac{4\gamma}{R_b} \tag{5.7}$$

where P_a is the atmospheric pressure.

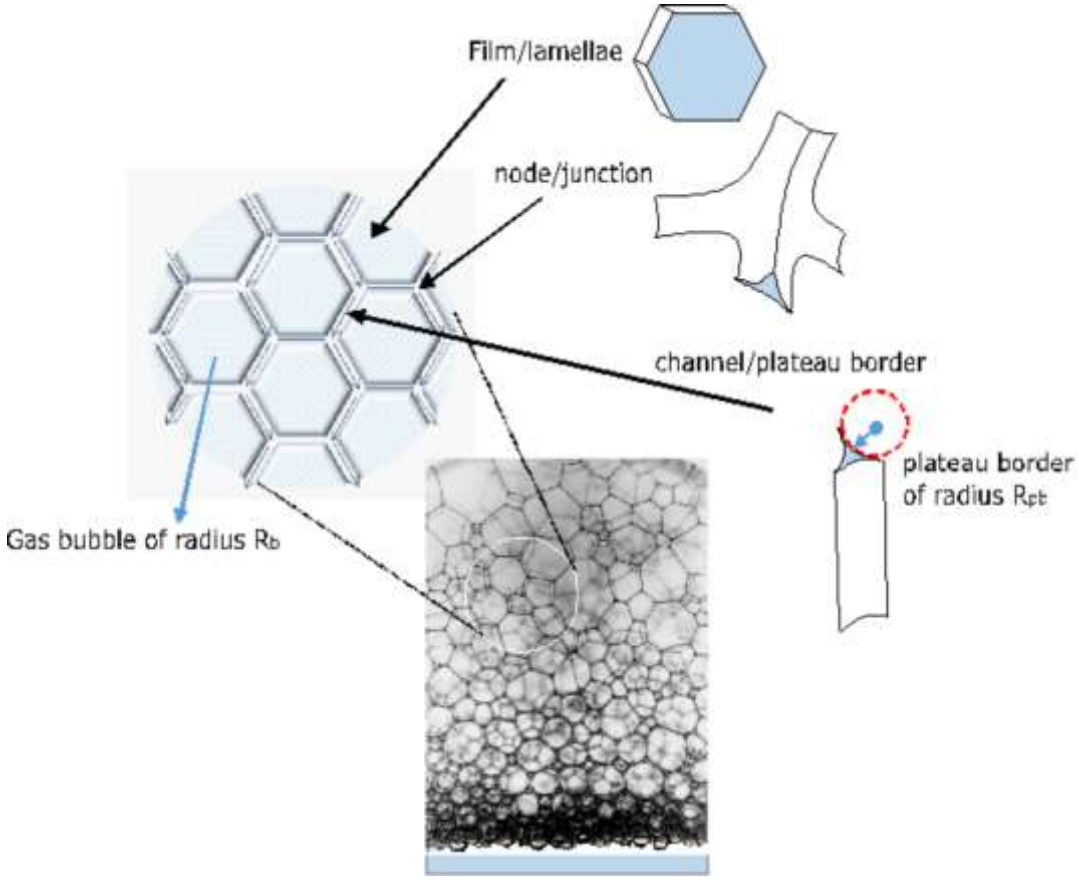

Figure 5. 2 :Schematic representation of a generalized foam system formed of gas bubbles with average radius of R_b in a continuous liquid phase. The connection of three lamellae is referred to as Plateau border (concave triangles) of radius R_{pb}, being the radius of curvature of the sides. Source:(40)

$$P_c = \frac{\gamma}{R_{pb}}, \tag{5.8}$$

where P_c is the capillary pressure and γ the liquid-air interfacial tension.

According to (37):

$$C_2^2 R_{pb}^2 = C_1 R_b^2 \frac{\varphi}{(1-\varphi)^{\frac{2}{3}}} \tag{5.9}$$

From Eqs. 5.7-5.9 the pressure in the Plateau border is

$$P_{pb}(z,t) = P_b - P_c = P_a + \frac{\gamma}{R_b}\left(4 - \frac{C_2}{C_1^{\frac{1}{2}}}\frac{\left(1-\varphi(z,t)\right)^{\frac{1}{3}}}{\varphi(z,t)^{\frac{1}{2}}}\right). \tag{5.10}$$

Let us introduce P_{pm}as the mean capillary pressure inside capillaries inside the porous layer, which can be estimated by $P_{pm} \sim \frac{n\gamma}{R_{pm}}$, where R_{pm} is radius of pores, $n = 1$ in the case of porous media built by cylinders (for example, hair) and $n = 2$ in the case of two-dimensional geometry. Accordingly, the pressure difference, which results in the liquid flow from the Plateau borders into the porous layer at the foam/porous layer interface, is:

$$\Delta P = P_{pb} - P_{pm} = \frac{\gamma}{R_b}\left(4 - \frac{C_2}{C_1^{\frac{1}{2}}}\frac{\left(1-\varphi(z=H_2,t)\right)^{\frac{1}{3}}}{\varphi(z=H_2,t)^{\frac{1}{2}}}\right) + \frac{n\gamma}{R_{pm}}. \qquad (5.11)$$

If $\Delta P > 0$, then liquid from the Plateau border will penetrate the porous layer. However, if $\Delta P < 0$, then penetration will stop. Let us introduce the final liquid content, φ_f, as the liquid volume fraction at the foam/porous layer interface at which the pressure inside the Plateau channels and the pressure inside the porous layer equilibrate. The consideration above and Eq. 5.11 determine the end of the drainage process and the final liquid content at the foam/porous substrate interface, φ_f , when $\Delta P = 0$:

$$\frac{\gamma}{R_b}\left(4 - \frac{C_2}{C_1^{\frac{1}{2}}}\frac{\left(1-\varphi(H_2,t)\right)^{\frac{1}{3}}}{\varphi(H_2,t)^{\frac{1}{2}}}\right) + \frac{n\gamma}{R_{pm}} = 0. \qquad (5.12)$$

Hence,

$$\frac{\varphi_f}{(1-\varphi_f)^{\frac{2}{3}}} = \frac{\left(\frac{C_2^2}{16C_1}\right)}{\left(1+\frac{nR_b}{4R_{pm}}\right)^2} \qquad (5.13)$$

If we introduce α as a ratio of capillary pressure in the porous layer to capillary pressure in the bubbles:

$$\alpha = \frac{\Delta P_{capin\ substrate}}{\Delta P_{capin\ bubbles}} = \frac{\frac{n\gamma}{R_{pm}}}{\frac{4\gamma}{R_b}} = \frac{nR_b}{4R_{pm}} \qquad (5.14)$$

and taking into account that $\varphi_f << 1$ then, Eq. 5.13 can be rewritten as:

$$\varphi_f = \frac{\left(\frac{C_2^2}{16C_1}\right)}{(1+\alpha)^2} \qquad (5.15)$$

According to the definition $\varphi_f = \frac{\left(\frac{C_2^2}{16C_1}\right)}{\left(1+\frac{2R_b}{4R_{pm}}\right)^2} < \varphi_{max}$ or $\left[\frac{\left(\frac{C_2^2}{16C_1}\right)}{\varphi_{max}}\right]^{-\frac{1}{2}} < \left(1+\frac{2R_b}{4R_{pm}}\right)$. Estimations show that at $C_2^2 \sim 0.161$, $C_1 = \frac{4\pi}{(3n_p\delta)} \sim 0.378 - 0.972$, and $\varphi_{max} = 0.26 : \left[\frac{\left(\frac{C_2^2}{16C_1}\right)}{\varphi_{max}}\right]^{-\frac{1}{2}} \sim 0.2 - 0.32$. The latter means that $\varphi_f < \varphi_{max}$ at any size of pores and foam bubbles. Hence, it cannot be the liquid film in the end of the drainage process (see below).

Eq. 5.15 and the previous consideration shows that the drainage of foam placed on the porous substrates is substantially different from that in the case of free drainage or drainage of foam placed on a non-porous substrate: in the case of porous substrate the final concentration at the foam/porous substrate interface is much lower as compared with the case of free drainage, when this concentration reaches the maximum possible concentration.

5.2.2 Liquid imbibition into porous layer

It is assumed below, according to (139), that the porous layer is completely wettable by the liquid and thin enough and the time for its saturation in the vertical direction can be neglected relative to other time scales of the process (see (139) for more detailed definition of "thin" porous layer).

The liquid flow inside the porous layer in the radial direction obeys the Darcy's law:

$$\frac{1}{r}\frac{d}{dr}(rv) = 0, \qquad v = \frac{K_p}{\mu}\left|\frac{dp}{dr}\right|. \qquad (5.16)$$

Solution of the latter equations is

$$p = -\left(\frac{\mu}{K_p}\right)\ln(r) + E, \quad v = \frac{F}{r} \qquad (5.17)$$

where E and F are integration constants, which should be determined using the boundary conditions for the pressure at the column edge, $r = R_c$, and at the circular edge of the wetted region inside the porous layer, $r = R(t)$ (139).

The boundary condition at the circular edge of the wetted region inside the porous layer is expressed as:

$$P = P_a - P_{pm}, \;\; r = R(t), \tag{5.18}$$

where $P_{pm} \approx \frac{n\gamma}{R_{pm}}$ is the capillary pressure inside the pores of the porous layer, and R_{pm} is a characteristic scale of the pore radii inside the porous layer.

The other boundary condition is written as:

$$P = P_a + \frac{\gamma}{R_b}\left(4 - \frac{C_2}{C_1^{\frac{1}{2}}}\frac{\left(1-\varphi(H_2,t)\right)^{\frac{1}{3}}}{\varphi(H_2,t)^{\frac{1}{2}}}\right), \quad r = R_c. \tag{5.19}$$

Using the latter two boundary conditions, both integration constants, *E* and *F*, can be determined, which gives the following expression for the radial velocity according to Eq. 5.17:

$$v = \frac{K_p}{\mu}\frac{\Delta P}{r\ln\left(\frac{R}{R_c}\right)}, \tag{5.20}$$

where ΔP is given by Eq. 5.11.

The velocity at the circular edge of the wetted region inside the porous layer is:

$$\varepsilon\frac{dR}{dt} = v|_{r=R} \tag{5.21}$$

where ε is the porosity of porous layer. Combination of the latter two equations gives the evolution equation for $R(t)$:

$$\frac{dR}{dt} = \frac{K_p}{\varepsilon\mu}\frac{\Delta P}{R\ln\left(\frac{R}{R_c}\right)} \tag{5.22}$$

Let us introduce the following dimensionless variables: $l \to \frac{R}{R_0}$, $\tau \to \frac{t}{t_0}$ where t_0 is defined by Eq. 5.4 and R_0 is the characteristic radius of wetted area of the porous layer, which is defined as:

$$R_0 = \sqrt{\frac{4\gamma K_p t_0}{\mu R_b \varepsilon}(1+\alpha)} \tag{5.23}$$

Now Eq. 5.22 can be rewritten as:

$$\frac{dl}{d\tau} = \frac{1}{l \ln \frac{l}{l_c}} \left(1 - \frac{\sqrt[3]{\frac{\left(1 - \varphi\left(\zeta = \frac{H_2}{z_0}, \tau\right)\right)}{(1 - \varphi_f)}}}{\sqrt{\frac{\varphi\left(\zeta = \frac{H_2}{z_0}, \tau\right)}{\varphi_f}}} \right) \tag{5.24}$$

where $l_c = R_c/R_o$

with initial condition $l(0) = l_c$

ζ_Δ

5.2.3 Boundary conditions at the foam/porous layer interface

No free liquid layer formation

In our previous publication(19), it was assumed that the height of the foam remains constant during the contact with the vertical porous substrate and it was possible to neglected the small changes in the foam height which occurs due to the drainage of the foam. The latter was a consequence of the assumption of non-slip boundary conditions on the surfaces of Plateau borders and because penetration of the liquid into the vertical thick porous medium was small enough. Situation is different in the case under consideration. That is, below the changes of the foam height due to the liquid drainage from the foam into the porous layer is taken into account. Let us consider a mass conservation law of liquid within the column and porous layer, in the case when the free liquid layer does not form at the foam/porous layer interface:

$$\pi R_c^2 \left(\int_{H_1(t)}^{H_2} \varphi(z,t) dz \right) + \varepsilon \Delta \pi R^2(t) = V_0 = \pi R_c^2 \varphi_i \big(H_2 - H_1(0)\big) \tag{5.25}$$

Differentiating Eq. (5.25) with time results in:

$$\pi R_c^2 \left(\int_{H_1(t)}^{H_2} \frac{d}{dt} \varphi(z,t) dz - \varphi(H_1(t),t) \frac{dH_1(t)}{dt} \right) + 2\varepsilon \Delta \pi R(t) \frac{dR(t)}{dt} = 0 \tag{5.26}$$

Using Eqs. 5.1 and 5.2 the latter equation can be rewritten as:

$$\pi R_c^2\left(Q\big(H_1(t)\big) - Q(H_2) - \varphi(H_1(t),t)\frac{dH_1(t)}{dt}\right) + 2\varepsilon\Delta\pi R(t)\frac{dR(t)}{dt} = 0 \qquad (5.27)$$

In the case of no free liquid layer at the foam/porous layer interface, the bottom of the foam remains directly in contact with the porous layer and its position does not move during the drainage. Therefore, only the top of the foam can move because of the drainage. At the top of the foam there is no accumulation/source of liquid and, hence, $Q_f(H_1,t) = 0$. Let us introduce the flux of the liquid at the foam/porous layer interface as:

$$Q_f(H_2,t) = \pi R_c^2 Q(H_2,t)) = \pi R_c^2\left(\frac{C_1^{\frac{1}{2}}\rho g}{\mu\beta}R_b^2\frac{\varphi^2(H_2,t)}{(1-\varphi(H_2,t)^{\frac{1}{3}}} - \frac{C_2\gamma}{2\mu\beta}R_b\frac{\frac{\varphi^{\frac{1}{2}}(H_2,t)(1-\varphi(H_2,t)}{3}}{\big(1-\varphi(H_2,t)\big)}\frac{d\varphi(H_2,t)}{dz}\right) \qquad (5.28)$$

and the flux of the liquid inside the porous layer as:

$$Q_{pm}(t) = \frac{2\pi\Delta K_p}{\mu}\frac{\left(\frac{\gamma}{R_b}\left(4 - \frac{C_2}{C_1^{\frac{1}{2}}}\frac{\big(1-\varphi(H_2,t)\big)^{\frac{1}{3}}}{\varphi(H_2,t)^{\frac{1}{2}}}\right) + \frac{n\gamma}{R_{pm}}\right)}{\ln\frac{R}{R_c}} \qquad (5.29)$$

Hence, Eq. 5.27 can be rewritten as:

$$\frac{dH_1(t)}{dt} = \frac{1}{\pi R_c^2\varphi(H_1(t),t)}\Big(Q_{pm}(t) - Q_f(H_2,t)\Big) \qquad (5.30)$$

Using dimensionless variables and co-ordinate as before: $\zeta \to \frac{Z}{Z_0}, l \to \frac{R}{R_0}, \tau \to \frac{t}{t_0}$, Eq. 5.30 can be rewritten as:

$$\frac{d\zeta_1(\tau)}{d\tau} = \frac{1}{\varphi(\zeta_1(\tau),\tau)}\left[\left(\frac{2\varepsilon\zeta_\Delta}{l_c^2}\left(\frac{1}{\ln\frac{l}{l_c}}\left(1-\frac{\sqrt[3]{\frac{(1-\varphi(\zeta_2,\tau))}{(1-\varphi_f)}}}{\sqrt{\frac{\varphi(\zeta_2,\tau)}{\varphi_f}}}\right)\right)\right) - \left(2\sqrt{Bo}\,\frac{\varphi(\zeta_2,\tau)^2\left(1+B\sqrt{\frac{(\zeta_2,\tau)}{(1-\ (\zeta_2,\tau))^{2/3}}}\right)}{(1-\varphi(\zeta_2,\tau))^{\frac{1}{3}}} - \frac{\varphi(\zeta_2,\tau)^{\frac{1}{2}}\left(1-\frac{\varphi(\zeta_2,\tau)}{3}\right)\left(1+B\sqrt{\frac{(\zeta_2,\tau)}{(1-\ (\zeta_2,\tau))^{2/3}}}\right)}{(1-\varphi(\zeta_2,\tau))}\frac{d\varphi(\zeta_2,\tau)}{d\zeta}\right)\right], \quad (5.31)$$

where $\zeta_\Delta = \Delta/z_0$.

Let us consider a mass conservation law of the gas phase within the foam in the case, when there is no bubble rupture at the top of the foam i.e. $\varphi(H_1,t) > \varphi_{cr}$ (φ_{cr} is a critical liquid volume fraction below which the coalescence/bubble burst begins) and $Q(H_1,t) = 0$:

$$\pi R_c^2\left(\int_{H_1(t)}^{H_2}[1-\varphi(z,t)]dz\right) = cons \quad (5.32)$$

Differentiating Eq. 5.32 with time leads to the following expressions for the rate of the moving top boundary of the foam:

$$\frac{dH_1(t)}{dt} = \frac{1}{\pi R_c^2\left(1-\varphi(H_1(t),t)\right)}Q_f(H_2,t) \quad (5.33)$$

and in dimensionless form:

$$\frac{d\zeta_1(\tau)}{d\tau} = \frac{1}{1-\varphi(\zeta_1(\tau),\tau)}\left(2\sqrt{Bo}\,\frac{\varphi(\zeta_2,\tau)^2\left(1+B\sqrt{\frac{(\zeta_2,\tau)}{(1-\ (\zeta_2,\tau))^{2/3}}}\right)}{\left(1-\varphi(\zeta_2,\tau)\right)^{\frac{1}{3}}} - \frac{\varphi(\zeta_2,\tau)^{\frac{1}{2}}\left(1-\frac{\varphi(\zeta_2,\tau)}{3}\right)\left(1+B\sqrt{\frac{(\zeta_2,\tau)}{(1-\ (\zeta_2,\tau))^{2/3}}}\right)}{(1-\varphi(\zeta_2,\tau))}\frac{d\varphi(\zeta_2,\tau)}{d\zeta}\right) \quad (5.34)$$

Comparison of Eqs. 5.30 and 5.33 results in the following expression for the boundary condition at the foam/porous layer interface in the case, when the free liquid layer does not form:

$$Q_f(H_2,t) = (1-\varphi(H_1(t),t))Q_{pm}(t) \quad (5.35)$$

and in dimensionless form:

$$2\sqrt{Bo}\,\frac{\varphi(\zeta_2,\tau)^2\left(1+B\sqrt{\frac{(\zeta_2,\tau)}{(1-\ (\zeta_2,\tau))^{2/3}}}\right)}{(1-\varphi(\zeta_2,\tau))^{\frac{1}{3}}} - \frac{\varphi(\zeta_2,\tau)^{\frac{1}{2}}\left(1-\frac{\varphi(\zeta_2,\tau)}{3}\right)\left(1+B\sqrt{\frac{(\zeta_2,\tau)}{(1-\ (\zeta_2,\tau))^{2/3}}}\right)}{\left(1-\varphi(\zeta_2,\tau)\right)}\frac{d\varphi(\zeta_2,\tau)}{d\zeta} = \left(1-\varphi(\zeta_1(\tau),\tau)\right)\frac{2\varepsilon\zeta_\Delta}{l_c^2}\left(\frac{1}{\ln\frac{l}{l_c}}\left(1-\frac{\sqrt[3]{\frac{\left(1-\varphi(\zeta_2,\tau)\right)}{\left(1-\phi_f\right)}}}{\sqrt{\frac{\varphi(\zeta_2,\tau)}{\varphi_f}}}\right)\right) \quad (5.36)$$

Note, in the above equations we supposed that the liquid volume fraction at $z = H_1$ is higher than φ_{cr}, there is no bubble collapsing/coalescence at the top of the foam and the top boundary condition is zero liquid flux, i.e $Q_f(H_1(t),t) = 0$. According to our experimental results the latter boundary condition on the top of the foam is always satisfied.

The suggested system of Eqs. 5.5, 5.24 with boundary condition 5.36 at foam/porous layer interface is valid only when no free liquid layer is formed at foam/porous layer interface, i.e. if $\varphi(H_2,t) < \varphi_{max}$. In this case porous layer sucks all liquid coming from the foam and the top boundary of the foam moves downward due to liquid drainage inside the foam according to Eqs. 5.31 or 5.34. This case was referred to a fast or intermediate imbibition of the liquid into the porous layer (19,98).

Accumulation of a free liquid layer at the foam/porous substrate interface

If the liquid volume fraction at foam/porous layer interface reaches the maximum value, φ_{max}, at the moment $t = t_m$, the accumulation of a free liquid layer starts and a free liquid layer is formed in between the porous layer and the foam. It was shown above (see Eq. 5.15) that the final value of the liquid contents at the foam/porous layer interface, φ_f, is always less than the maximum possible value of the liquid contents, φ_{max}. The latter means that the presence of the free liquid layer in between the foam and the porous layer continues until the moment $t = t_M$, when porous layer sucks the liquid above from the free liquid layer and again all liquid coming from the foam goes directly into the porous layer. Therefore, the boundary condition at the bottom of the foam is constant liquid volume fraction at $t_m < t < t_M$:

$$\varphi(H_2,t) = \varphi_{max} \tag{5.37}$$

and in dimensionless form at $\tau_m < \tau < \tau_M$:

$$\varphi(\zeta_2,\tau) = \varphi_{max} \tag{5.38}$$

where $\varphi_{max} = 0.26$, $\tau_m = \frac{t_m}{t_0}$ and $\tau_M = \frac{t_M}{t_0}$. The boundary condition 5.37 or 5.38 is valid until the moment t_M and afterwards the conditions 5.35 and 5.36 are again satisfied.

In the case of liquid accumulation at foam/porous layer interface, it is necessary to find the thickness of the liquid film in between the foam and the porous layer. For this purpose, let us consider a mass conservation law of liquid within the foam and the porous layer:

$$\pi R_c^2 = \left(\int_{H_1(t)}^{H_2(t)} \phi(z,t)dz + H - H_2(t) \right) + \varepsilon \Delta \pi R^2(t) = cons. \tag{5.39}$$

It is assumed on this stage again that the liquid volume fraction at the top of the foam is higher than critical liquid volume fraction, $\varphi(H_1,t) > \varphi_{cr}$, and, hence, $Q_f(H_1(t),t) = 0$.

Differentiating Eq. 5.39 with time results in:

$$\pi R_c^2 \left(\int_{H_1(t)}^{H_2(t)} \frac{d\varphi(z,t)}{dt} dz + \varphi_{max} \frac{dH_2(t)}{dt} - \varphi(H_1(t),t) \frac{dH_1(t)}{dt} - \frac{dH_2(t)}{dt} \right) + 2\varepsilon\Delta\pi R(t) \frac{dR(t)}{dt} = 0 \quad (5.40)$$

Substituting Eq. 5.1 leads to the following equation:

$$\left(1 - R_{0_{max}}\right)\pi R_c^2 \frac{dH_2(t)}{dt} + \varphi(H_1(t),t)\pi R_c^2 \frac{dH_1(t)}{dt} = Q_{pm}(t) - Q_f(H_2(t),t) \quad (5.41)$$

On the other hand, differentiation of a mass conservation law of the gas phase within the foam (see Eq. 5.32), where now $H_2(t)$ is not constant any more) in the case of liquid accumulation, results in Eqs. 5.41 and 5.42 (see below), which is a system of two linear equations in respect of two unknown $\frac{dH_1(t)}{dt}$ and $\frac{dH_2(t)}{dt}$. Solution of this system results in a system of two differential equations for the rate of moving boundaries at the bottom and the top of the foam:

$$(1 - \varphi_{max})\pi R_c^2 \frac{dH_2(t)}{dt} - \left(1 - \varphi(H_1(t),t)\right)\pi R_c^2 \frac{dH_1(t)}{dt} = -Q_f(H_2(t),t) \quad (5.42)$$

$$\frac{dH_2(t)}{dt} = -\frac{Q_f(H_2(t),t) - \left(1 - \varphi(H_1(t),t)\right)Q_{pm}(t)}{(1 - \varphi_{max})\pi R_c^2} \quad (5.43)$$

$$\frac{dH_1(t)}{dt} = \frac{Q_{pm}(t)}{\pi R_c^2} \quad (5.44)$$

In dimensionless forms:

$$\frac{d\zeta_2(\tau)}{d\tau} = -\frac{1}{(1-\varphi_{max})}\left(2\sqrt{Bo}\,\frac{\varphi(\zeta_2,\tau)^2\left(1+B\sqrt{\frac{(\zeta_2,\tau)}{(1-\ (\zeta_2,\tau))^{2/3}}}\right)}{\left(1-\phi(\zeta_2,\tau)\right)^{\frac{1}{3}}}\right.$$
$$\left. -\frac{\varphi(\zeta_2,\tau)^{\frac{1}{2}}\left(1-\frac{\varphi(\zeta_2,\tau)}{3}\right)\left(1+B\sqrt{\frac{(\zeta_2,\tau)}{(1-\ (\zeta_2,\tau))^{2/3}}}\right)}{\left(1-\varphi(\zeta_2,\tau)\right)}\frac{d\varphi(\zeta_2,\tau)}{d\zeta}\right. \qquad (5.45)$$
$$\left. -\left(1-\varphi(\zeta_1(\tau),\tau)\right)\frac{2\varepsilon\zeta_\Delta}{l_c^2}\left(\frac{1}{\ln\frac{l}{l_c}}\left(1-\frac{\sqrt[3]{\frac{1-\varphi(\zeta_2,\tau)}{(1-\varphi_f)}}}{\sqrt{\frac{\varphi(\zeta_2,\tau)}{\varphi_f}}}\right)\right)\right.$$

$$\frac{d\zeta_1(\tau)}{d\tau} = \frac{2\varepsilon\zeta_\Delta}{l_c^2}\left(\frac{1}{\ln\frac{l}{l_c}}\left(1-\frac{\sqrt[3]{\frac{1-\varphi(\zeta_2,\tau)}{(1-\varphi_f)}}}{\sqrt{\frac{\varphi(\zeta_2,\tau)}{\phi_f}}}\right)\right) \qquad (5.46)$$

According to Eq. 5.43 the thickness of the free liquid layer is therefore calculated as:

$$\frac{d(H-H_2(t))}{dt} = \frac{Q_f(H_2(t),t)-\left(1-\varphi(H_1(t),t)\right)Q_{pm}(t)}{(1-\varphi_{max})\pi R_c^2} \qquad (5.47)$$

or in dimensionless form:

$$\frac{d(\zeta_H-\zeta_2(\tau))}{d\tau}=\frac{1}{(1-\varphi_{max})}\left(2\sqrt{Bo}\frac{\varphi(\zeta_2,\tau)^2\left(1+B\sqrt{\frac{(\zeta_2,\tau)}{(1-\ (\zeta_2,\tau))^{2/3}}}\right)}{\left(1-\varphi(\zeta_2,\tau)\right)^{\frac{1}{3}}}\right.$$
$$-\frac{\varphi(\zeta_2,\tau)^{\frac{1}{2}}\left(1-\frac{\varphi(\zeta_2,\tau)}{3}\right)\left(1+B\sqrt{\frac{(\zeta_2,\tau)}{(1-\ (\zeta_2,\tau))^{2/3}}}\right)}{\left(1-\varphi(\zeta_2,\tau)\right)}\frac{d\varphi(\zeta_2,\tau)}{d\zeta} \qquad (5.48)$$
$$\left.-\left(1-\varphi(\zeta_1(\tau),\tau)\right)\frac{2\varepsilon\zeta_\Delta}{l_c^2}\left(\frac{1}{\ln\frac{l}{l_c}}\left(1-\frac{\sqrt[3]{\frac{1-\varphi(\zeta_2,\tau)}{(1-\varphi_f)}}}{\sqrt{\frac{\varphi(\zeta_2,\tau)}{\phi_f}}}\right)\right)\right),$$

where $\zeta_H=\frac{H}{z_0}$. It is assumed in Eq. 5.47 that the thickness of the free liquid layer, $H-H_2(t)$,is so small and the pressure inside the film remains constant and it can be calculated according to Eq. 5.10.

In the case of liquid layer formation at the foam-porous substrate interface, the liquid volume fraction close to the above interface is out of the range of application of non-wet foam approximation. However, our calculations show (as well as calculations presented earlier in (19) that the region where the liquid volume fraction is above the initial volume fraction is very narrow, which allows us to assume the approximation used (flow in Plateau borders only) still can be used in the whole foam.

5.2.4 Equilibrium profile of liquid content

The equilibrium profile of the liquid content inside the foam is reached when the gravity and capillary gradient forces equilibrate each other inside the foam and the pressure at the foam/porous layer interface reaches the equilibrium value according to Eq. 5.13. The equilibrium profile can be found by assuming zero liquid flux across the whole foam height.

Integration of Eq. (5.1) in this case using the final liquid content, φ_f,described in Eq. 5.13 at the bottom of the foam ($\varphi(H_2(t),t)=\varphi_f$ results in:

$$\left(1-\varphi_e(z)\right)^{\frac{1}{3}}\varphi_e^{\frac{-1}{2}}(z)=\left(1-\varphi_f\right)^{\frac{1}{3}}\varphi_f^{\frac{-1}{2}}+\frac{C_1^{\frac{1}{2}}\rho g R_b}{C_2\gamma}(H_{2e}-z_e) \qquad (5.49)$$

Eq. 5.49 can be rewritten in the following dimensionless form:

$$\left(1-\varphi_e(\zeta)\right)^{\frac{1}{3}}\varphi_e^{\frac{-1}{2}}(\zeta)=(1-\varphi_f)^{\frac{1}{3}}\varphi_f^{\frac{-1}{2}}+\sqrt{Bo}(\zeta_{2e}-\zeta_e) \qquad (5.50)$$

The above equation determines the equilibrium liquid volume fraction at different heights of the foam. If $\zeta=\zeta_{1e}$ is substituted in the above equation, where ζ_{1e} is the dimensionless position of the top of the foam at equilibrium, then the equilibrium liquid volume fraction at the top of the foam can be deduced. The latter is a function of the foam height at equilibrium, $\zeta_{2e}-\zeta_{1e}$ and can be calculated from Eq. 5.50 as

$$\left(1-\varphi_e(\zeta_{1e})\right)^{\frac{1}{3}}\varphi_e^{\frac{-1}{2}}(\zeta_{1e})=(1-\varphi_f)^{\frac{1}{3}}\varphi_f^{\frac{-1}{2}}+\sqrt{Bo}(\zeta_{2e}-\zeta_{1e}) \qquad (5.51)$$

The equilibrium profile of liquid volume fraction at different height of the foam (according to Eq. (5.50)) is schematically illustrated in Figure 5.3.

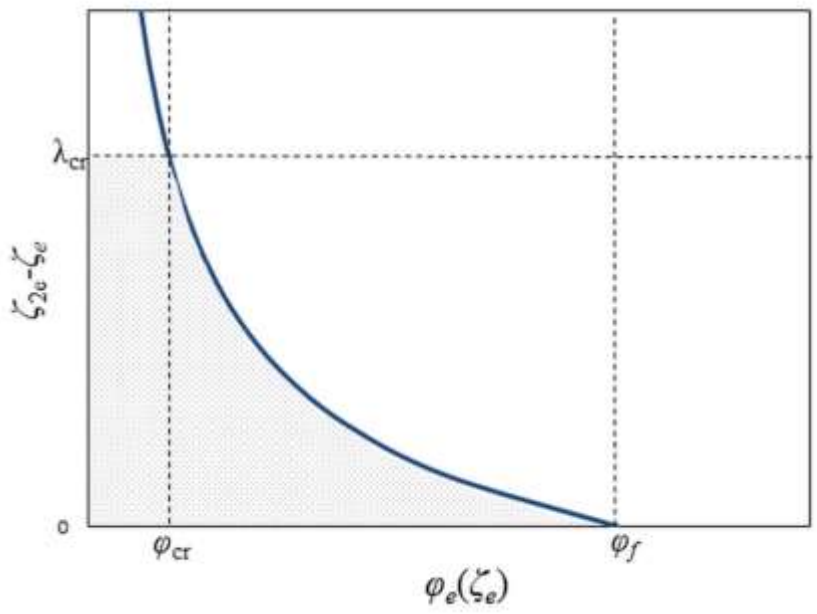

Figure 5. 3:The equilibrium profile of liquid volume fraction at different heights of the foam. Here we assume that $\varphi_{cr}<\varphi_f$. Source:(40)

As shown in Figure 5.3, $\varphi_e(\zeta_e)$ is equal to φ_f at the bottom of the foam, $\zeta_e=\zeta_{2e}$, and at higher heights of the foam the equilibrium liquid volume fraction decreases and becomes lower than φ_f.

According to Ref. (144) when a foam is in contact with porous layer the liquid volume faction decreases more rapidly at the top and bottom of the foam than in the middle parts at the initial stages of drainage. Note, in all previous consideration as well as in Eq. 5.50 it was assumed that the liquid volume fraction, everywhere within the foam is higher than φ_{cr}, and there is no bubble collapsing/coalescence. In Ref. (145) a narrow field of liquid fraction ranging from 0.0005 to 0.0007 was found as the critical liquid volume fraction in foam stabilised by mixture of surfactants. Based on the values of $\mathcal{M}_{cr}$ and φ_f, there are two possibilities for

the boundary conditions at the top and bottom of the foam: (i) if $\varphi_{cr} > \varphi_f$, during the process both liquid volume fractions at the bottom and top of the foam drop to the value of φ_{cr} and therefore, bubbles coalesce at the bottom and they collapse at the top of the foam. As a result, a big bubble form at the bottom of the foam column and the height of the foam decreases from the top not only because of the drainage but also due to bubbles rupture. According to Eqs. 5.14 and 5.15, it happens more likely for the foams with bigger bubble sizes in contact with layers with smaller pores sizes, i.e. higher values of α and lower values of φ_f: using estimation φ_{cr}~0.0005 and Eq. 5.15 we conclude $10.65\ R_{pm} < R_b$. Hence, in this case the foam is almost completely consumed by the porous layer. (ii) if $\varphi_{cr} < \varphi_f$, or $10.65\ R_{pm} > R_b$ the liquid volume fraction at the bottom of the foam remains always higher than φ_{cr} and therefore, there is no bubble coalesce at the bottom of the foam. Substituting $\varphi_e(\zeta_{1e}) = \varphi_{cr}$ in Eq. 5.50 allows determining a critical foam height, λ_{cr}. This critical foam height is shown in Figure 5.3 where $\varphi_e(\zeta_e) = \varphi_e(\zeta_{1e}) = \varphi_{cr}$. If the initial foam height, $\zeta_2(\tau = 0) - \zeta_1(\tau = 0) = \zeta_{2i} - \zeta_{1i}$ is less than λ_{cr}then over duration of the whole process the liquid volume fraction at the top of the foam also remains above the φ_{cr} and there will be no bubble rupture at the top of the foam. However, if $\zeta_{2i} - \zeta_{1i}$ is bigger than λ_{cr} then two possibilities can be predicted: (1) over duration of the whole drainage process the liquid volume fraction at the top of the foam remains above the φ_{cr}. Consideration of this stage is identical to the previous case; (2) at some moment $_{cr}$, $\varphi(\zeta_1, \tau_{cr}) = \varphi_{cr}$. After that moment the top boundary of the foam decreases not only because of the drainage and liquid penetration into the porous layer but also due to the bubble collapse. Therefore, the foam height will decrease from the top boundary while $\varphi(\zeta_1, \tau) = \varphi_{cr}$. The reduction of foam height continues until the time when it reaches equilibrium. According to Eq. 5.50 and Figure 5.3, the final height of the foam in this case is fixed and equal to the critical foam height, $\zeta_{2e} - \zeta_{1e} = \lambda_{cr}$. Considering the amount of the gas phase within the foam at initial and final state of the process, it is possible to predict which of the two above mentioned possibilities will occur. If the initial amount of the gas phase within the foam is higher than the final gas content at equilibrium, then during the drainage the liquid volume fraction at the top of the foam drops to the value of φ_{cr} (i.e. the second possibility occurs) and there is bubble rupture at the top of the foam:

$$\pi R_c^2 (1 - \varphi_i)(H_{2i} - H_{1i}) > \pi R_c^2 \int_{H_{1e}}^{H_{2e}} 1 - \varphi_e(z) dz, \qquad (5.52)$$

where $_i$ is the initial liquid volume fraction. Making the above equation dimensionless and using $\zeta_{2e} = \zeta_{1e} + \lambda_{cr}$ leads to the following condition for the bubble rupture at the top of the foam:

$$\varphi_i < 1 - \frac{\left(\lambda_{cr} - \int_0^{\lambda_{cr}} \varphi_e(\zeta_{2e} - \zeta) d\zeta\right)}{(\zeta_{2i} - \zeta_{1i})} = \varphi_t, \qquad (5.53)$$

A comparison between the values of $\varphi_i$and φ_t(Liquid volume fraction at foam/ porous layer interface) for each foaming solution can predict the state of the top of the foam during the drainage. The integral in Eq. 5.53 (to find the values of φ_t) can be calculated numerically using Eq. (5.50) for different values of B_o number and it is identical to the shaded area in Figure. 5.3. Therefore, in the case in which $\varphi_{cr} < \varphi_f$ and the initial foam height, $\zeta_{2i} - \zeta_{1i}$, is bigger than λ_{cr} the bubbles rupture at the top of the foam only if the condition specified in Eq. 5.53 is satisfied for the value of initial liquid volume fraction. Otherwise the liquid volume

fraction everywhere within the foam remains above the φ_{cr} and there is no bubble rupture/coalescence within the foam.

5.3 Experimental procedure

The surfactant used for preparation of foaming solution was sodium dodecyl sulphate (SDS) purchased from Sigma-Aldrich, without additional purification. SDS is an anionic surfactant. The surfactant concentrations used were above critical micelle concentration (CMC) i.e SDS 4 CMC. Ultra-pure water was produced by Millipore Q.

The foam drainage experiments were carried out in a glass tube, 9cm long with a 2.5cm outer diameter and 2.1cm inner diameter. The porous substrate used was filter paper, positioned at the bottom of the column and attached to it (Figure 5.1). The vertical glass column was initially glued to a flat filter paper to prevent any leaking of liquid or foam from the bottom of the column. The filter paper was placed onto a glass mat to prevent dripping and leaking of liquid (Figure 5.4).

The glass tube was positioned vertically and held by a scaled clamp stand. Two Pike Allied Vision Technologies Cameras: camera 1, Sony TV Lens 1:1.8 16mm focusing on the top of the column measuring the spreading area on the substrate and camera 2 on the right-hand side of the foam monitoring the foam height alterations (Figure 5.4) were used for capturing images of the experiment at regular time intervals. To prevent loss of foam due to evaporation parafilm was applied to the top of the foam column.

A plastic squeeze bottle containing the surfactant solution is compressed manually generating the foam due to inserted air from the attached nozzle. The foam of uniform liquid volume fraction was then injected into the foam column to an initial height of 4cm. The initial liquid volume fraction was constant throughout the foam body due to the procedure used and the small initial foam height generated. Experiments run for 7-10min depending on the stability of the foam. The images captured by the two cameras were analyzed by ImageJ and three quantities were measured: (a) wetting radius, R(t), (b) foam height, $H - H_1(t)$, and (c) free liquid layer thickness at the bottom of the foam (if any), $H - H_2(t)$, (see Fig. 1). For the investigated surfactant solution, experiments were repeated at least 2-3 times. The variation of the experimental data was quantified by standard deviation and presented in Figures. 5.5-5.7 in section 5.4 below.

Permeability (see table 5.1) of the filter paper was measured according to procedure presented in Ref.(139,141) by placing a strip of each grade in water and measuring the change in height. The dependency between height squared against time was plotted with the gradient representing permeability. Porosity was calculated by placing the glass tube vertically on each filter paper and filled with water to a specified height. The volume of water was then divided by the wetted area to give a value for porosity (see Table 5.1).

Table 5. 1: Filter Paper Properties, Filter paper thickness Δ, average pore radius R_{pm}, porosity ε , and permeability K_p. Average pore size values obtained from Whatman filter paper guide (P&R Labpak Limited, 2017) and from Camlab website (146). Source:(40)

Thickness $\Delta\ (m)$	2.2 x 10^{-4}
Average pore radius $R_{pm}(m)$	5.5 x 10^{-6}
Porosity ε	0.605
Permeability $K_p\ (m^2)$	3.5 x 10^{-13}

The initial volume fractions of foams (see Table 5.2) were found by weighing a known volume of foam and dividing this weight by the volume of the foam and the liquid density, that is, $_i = \frac{M_i}{V_i}$, where M_i and V_i are initial weight and volume of the foam respectively; is the liquid density.

Table 5. 2:Initial liquid volume fractions of generated foam and parameters average bubble radius R_b, surface viscosity, μ_s, viscosity, μ ,and density, ρ, for the investigated surfactant solution. * Obtained from Ref.(147). Source:(40)*

Foam Solution	initial liquid volume fraction $_i(\%)$	average bubble radius $R_b(m)$	surface viscosity* $\mu_s\ (Pa \cdot s.m)$	viscosity $\mu\ (Pa \cdot s)$	density $\rho\ (kg/m^3)$
SDS – 4 CMC	8	0.0007	1.45 0.03 $x\ 10^{-6}$	8.9 $\times\ 10^{-4}$	1000

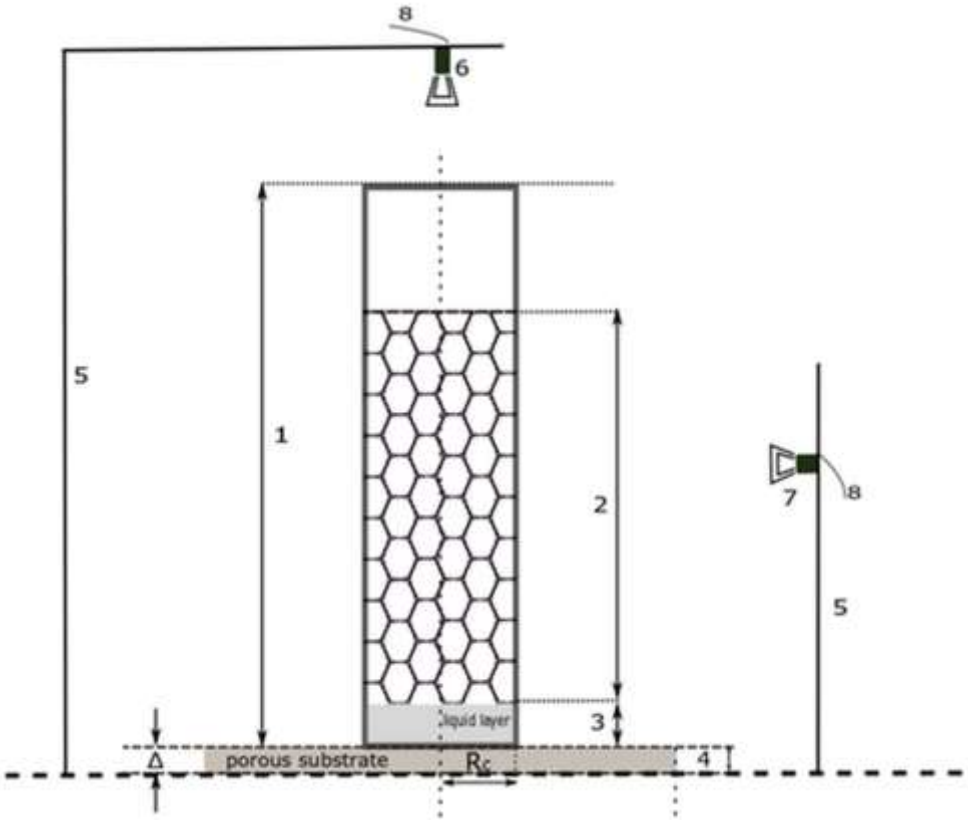

Figure 5. 4:Experimental set-up; (1) foam column of radius R_c (2) Foam (3) formed free liquid layer (if any), (4) thin porous substrate of thickness Δ, (5) clamp, (6) digital camera 1, (7) digital camera 2, (8) interface to PC. Source:(40)

5.4 Results and discussion

The imbibition into the porous substrate is characterised through measurements of wetted radius, $R(t)$, with initial value equal to the radius of the foam column $R(0) = R_c$ (see Figure 5.1). A comparison between experimental measurements and predictions according to the above theoretical results of foam height, accumulated free liquid layer (if any) at the foam/porous layer interface and wetted area inside the porous substrate versus time are shown below.

The model of foam drainage described by dimensionless Eq. (5.5) and liquid imbibition into porous layer is described by Eq. (5.24) have been solved using COMSOL software, finite element method on one dimensional regular grid with maximum element size equals to 0.005 of the initial foam height. A backward differentiation formula was used to solve time-dependent variables and time stepping was free taken by the solver with initial step size of 10^{-20} s. Relative tolerance was set to 10^{-8}, whereas absolute tolerance was set to 10^{-10}. The boundary conditions at the top and bottom of the foam and their locations were imposed and updated as described in section 5.2. The derived equations for foam drainage and liquid imbibition into porous layer were solved using the boundary conditions to obtain the evolution of liquid volume fraction inside the foam. The values of initial parameters, K_p , Δ, R_b, ε, μ, ρ, average pore size and initial liquid volume fraction, φ_i, based on the experimental

data have been incorporated in the simulations (Table 5.2). The calculated values of t_0, z_0, R_0, Bo, α, and l_c, are shown in Table 5.3.

Table 5. 3:. Calculated parameters:characteristic time, t_0,characteristic length, z_0,characteristic radious, R_0, Bond number,Bo,ratio of capillary pressure in the porous layer to capillary pressure in the bubbles, α,and dimenssionless radious of the column, l_c , for the investigated surfactant solution. Source: (40)

	t_0(min)	$z_0(m)$	$R_0(m)$	Bo	α	l_c
SDS 4cmc	0.1988	0.0018994	0.0012	0.3655	68.182	10.028

5.4.1 Foam height comparison

We found a reasonable agreement between the theoretical predictions and experimental measurement of time evolution of both the foam height, $H - H_1(t)$, and the wetted area (shown in Figures. 5.5 and 5.6). Comparison between the predicted and experimental time evolution of the height of the foam, for the solution systems is presented in Figure 5.5. For the investigated system, theoretical predictions show a reasonable agreement with experimentally obtained results. The initial foam height was between 4cm-4.2cm, for all performed experiments.

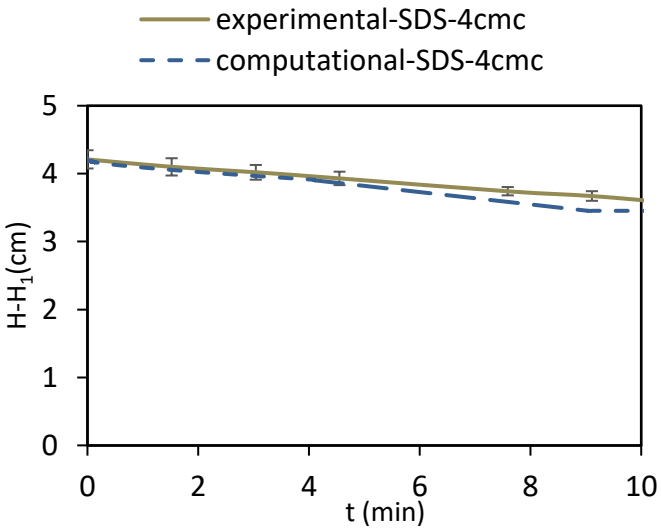

Figure 5. 5:Comparison of the experimentally obtained time evolution of the height of the foam, $H - H_1(t)$, with simulation results for SDS 4cmc solutions. Experimental line is the best fit only to guide the eye. Source:(40)

5.4.2 Wetted area

At $\Delta P > 0$ (see Eq.5.11) drained liquid from the foam penetrates into the porous layer and spreads inside the porous layer with an increasing radius, $R(t)$, of the wetted area as described by Eq. 5.22 or in dimensionless form by Eq. 5.24. Wetted area, $A(t)$, was bounded by a circle with radius $R(t)$.

Experimentally measured time evolution of wetted area inside porous layer for the surfactant solution is in a reasonable agreement with the theoretical prediction (see Figure 5.6).

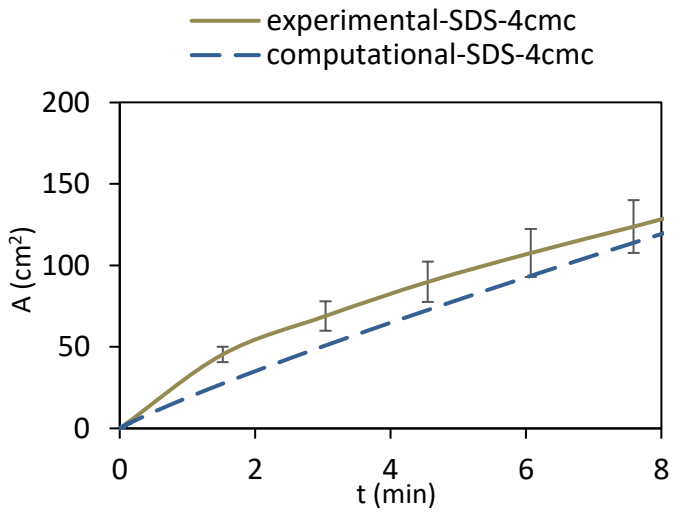

Figure 5. 6:Comparison of the experimentally obtained wetted area $A\ (t)$, with simulation results for SDS 4cmc solution. Experimental line is the best fit only to guide the eye. Source:(40)

Imbibition proceeds until φ_f is reached (when $\Delta P = 0$) (see Eq. 5.12), when the drainage/imbibition process is completed, and there is no further liquid penetration into the porous substrate. Spreading area, $A(t)$, gradually increases until φ_f is reached. In the experiment presented Fig. 5.6 the final low concentration φ_f was not reached during our experiment.

5.4.3 Free liquid layer

When liquid volume fraction at the foam/porous substrate interface reaches the maximum value, $\varphi_{\max}$, a free liquid layer starts to accumulate on the interface. The accumulation is accompanied by the simultaneous imbibition into the porous layer, which in the end dominates resulting in the gradual penetration of the created liquid from the free liquid layer into the porous substrate and final disappearance of the free liquid layer. The time evolution of the thickness of the formed free liquid layer is presented in Figure 5.7 for the investigated system SDS 4cmc solutions.

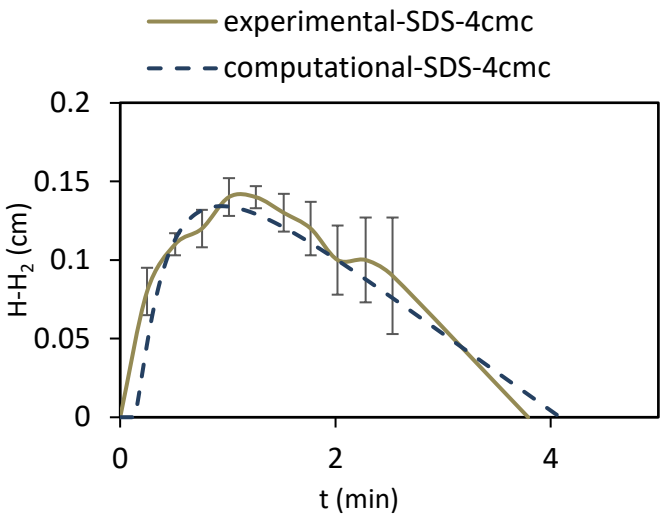

Figure 5. 7:Comparison of the experimentally obtained free liquid layer thickness, $H - H_2(t)$, with simulation result for SDS 4cmc solution. Experimental line is the best fit only to guide the eye. Source:(40)

In the case of no free liquid layer accumulation, there is no movement of the foam/porous substrate interface and the drainage/imbibition process is described by Eqs. 5.5, 5.24 and 5.36 under the assumptions that the liquid volume fraction at the top of the foam is higher than φ_{cr}, that is, no bubble collapsing/coalescence happens at the top of the foam and the top boundary condition is zero liquid flux, i.e $Q_f(H_1(t), t) = 0$. In this case, the porous material simultaneously absorbs all drained liquid flown to the foam/substrate interface and the liquid fraction at the foam/porous layer interface does not reach the maximum value φ_{max} and the free liquid layer does not form (fast imbibition according to(19,98). However, If liquid volume fraction at the foam/porous layer interface increases and reaches the maximum limiting value, φ_{max}, liquid will accumulate at the lower parts of the foam and the process is described by Eq. 5.47, which is referred to as slow imbibition.

For the investigated systems, calculated maximum liquid height shows reasonable agreement with experimental data (Figure 5.7). Figure 5.7 show that there is a very good agreement of (i) the predicted moment when the free liquid layer starts to form, (ii) the maximum thickness of the free liquid layer (iii) the dynamics of the free liquid layer accumulation until the maximum value is reached, (iv) reasonable qualitative agreement during the last stage, when the free liquid layer gradually disappears.

5.4.4 Effect of model parameters

For all investigated system liquid volume fraction at the top of the foam and at the foam/porous substrate interface initially decreases, while the value of liquid volume fraction in the central part of the foam body remains approximately constant.

After the end of the initial stage, the accumulation or not accumulation of a free liquid layer at the foam/porous substrate interface is determined by time evolutions of liquid volume fraction at the bottom boundary of the foam, $\varphi(\zeta = 1, \tau)$, with maximum value refereed below as $\varphi_{interface}$ and depends on

dimensionless parameters Bo, φ_i, α , ζ_Δ, l_c, ζ_H and ε . The existence of different regimes is investigated and the relationship between the maximum liquid volume fraction at the foam/substrate boundary, $_{interface}$ is described by Eq. 5.54. This equation was derived via multiple regression analysis between various simulations. The effect of each dimensionless parameter on $\varphi_{interface}$ and their relationship has been obtained. At the very beginning of the drainage/imbibition process the liquid volume fraction at the foam/substrate interface, $\varphi(\zeta = 1, \tau)$, drops from its initial value, φ_i, to approximately final liquid volume fraction, as initially drained liquid is instantly absorbed by the unsaturated pores of the substrate and depending on the drainage/imbibition process the following three different scenarios are possible:

1) Liquid volume fraction, $\varphi(\zeta = 1, \tau)$, can increase and in certain cases reach the value of maximum liquid volume fraction,φ_{max}. In this case, the rate of foam drainage is higher than the rate of imbibition and a free liquid layer is formed at the foam/porous substrate interface. This case is referred to as 'slow imbibition' regime (19)and is observed for higher values of Bo, φ_i, l_c , a and ζ_H and lower values of ζ_Δ, and ε (Eq.5.54). This case corresponds to our experimental conditions presented in Figure 5.7.
2) There is a case where liquid volume fraction at the foam/porous substrate, $\varphi(\zeta = 1, \tau)$, interface continuously decreases until it finally reaches the final liquid volume fraction. Here, liquid imbibition into the porous substrate occurs faster than foam drainage and therefore, there is no free liquid layer accumulation. This regime is referred to as 'rapid imbibition' regime(19). As observed via multiple regression analysis, 'rapid imbibition' regime is observed for low values of Bo, φ_i, l_c , a and ζ_H and higher values of ζ_Δ,and ε (Eq.5.54).
3) In between the above-mentioned cases there is an intermediate regime where liquid volume fraction, experiences a pick point in between φ_i and φ_{max}. In this case imbibition occurs almost in parallel with foam drainage with comparable rates. This regime is referred to as 'intermediate imbibition'(19). After the initial rapid decrease, liquid volume fraction at the foam/porous substrate interface will gradually increase, reaching a maximum value always lower than φ_{max} until it finally decreases to the final liquid volume fraction. It is important to note that at this regime there is no free liquid layer formation at the foam/porous substrate interface.

$$\varphi_{interface} = \frac{6.050622\ {\varphi_i}^{2.264} Bo^{0.2291} {l_c}^{0.2201} {\zeta_H}^{0.2615} a^{0.0882}}{{\zeta_\Delta}^{0.3824} \varepsilon^{0.1796}} \qquad (5.54)$$

The whole process of drainage/imbibition is very sensitive to the initial liquid volume fraction in the foam: a small increase of initial volume fraction can cause a shift from fast to slow regime.

In a slow imbibition regime, the effect of dimensionless parameters Bo, φ_i, α , ζ_Δ, l_c, ζ_H and ε on the dimensionless time required for the free liquid layer to disappear and completely be absorbed by the porous substrate, i.e $\tau_t = \tau_M - \tau_m$ (19) has been investigated via multiple regression analysis. In all cases investigate we found that that the time required for free liquid layer to start forming, τ_m was much smaller as compared with τ_M. After $\tau_t \approx \tau_M$ all drained liquid is absorbed by the porous substrate until the liquid volume fraction drops to final liquid volume fraction. Note that τ_t can be calculated only for the case of 'slow imbibition' regime where free liquid layer forms at the

foam/porous material interface. The effect of each dimensionless parameters and their combined effect on the total dimensionless time,τ_t, is expressed below by Eq. 5.55. The results show an increasing trend of the dependant parameter, τ_t as Bo, l_c, φ_i, ζ_H increase while the process is delayed when the porosity, ε, and the substrate thickness, ζ_Δ , increase.

$$\tau_t = \frac{{\varphi_i}^{1.9901} Bo^{0.2628} {l_c}^{2.0540} {\zeta_H}^{1.4644}}{2.76312 {\zeta_\Delta}^{1.4371} \varepsilon^{1.3128} \alpha^{0.0024}} \tag{5.55}$$

5.5 Conclusions

A theory of foam drainage placed on a thin porous layer is developed: rate of drainage and imbibition inside the porous layer and other characteristics of the process are theoretically predicted. The theory predictions are compared with experimental observations of the foam drainage placed on thin porous layers. Comparison showed a reasonably good agreement between the theory predictions and experimental observations. One of the phenomena during application is a possibility of the build-up of a free liquid layer on the foam/porous layer interface, which can be important for the application processes. Conditions and duration of a free liquid layer formation have been theoretically predicted and compared with experimental observations. According to the derived mathematical model, the kinetics of drainage/imbibition process and the possibility of free liquid layer formation is determined by seven dimensionless parameters, Bo, φ_i, l_c, ζ_H, ζ_Δ, a and ε. The existence of three different imbibition regimes, referred to as ‘rapid’, ‘intermediate’ and ‘slow’ regime depends on the values of the above-mentioned dimensionless parameters.

Nomenclature 5

Δ	Thickness of porous layer
$R(t)$	Radius of the wetted area inside the porous layer
R_c	Radius of column
R_b	Bubble radius
R_{pb}	Plateau border radius
R_{pm}	Pore radius of porous media
φ	Liquid volume fraction
φ_i	Initial liquid volume fraction
φ_f	Final Liquid volume fraction at foam/ porous layer interface
φ_{cr}	Critical liquid volume fraction
φ_{max}	Maximum liquid volume fraction
$\varphi_{interface}$	Maximum liquid volume fraction at the foam/porous substrate interface
μ	Dynamic viscosity of liquid
μ_s	Surface viscosity of liquid
γ	Liquid-air interfacial tension
ρ	Liquid density
g	Gravity acceleration
n_p	Number of Plateau borders per bubble
C_2^2	0.161 (constant)
A	Spreading area, cm^2
c	Velocity coefficient
C_1	Geometrical coefficient, $\sim 0.378 - 0.972$ for foam with structures between bcc and fcc and bubbles of same size.
ζ	The dimensionless vertical coordinate
ζ_H	The dimensionless height of the column
ζ_{1e}	The dimensionless position of the top of the foam at equilibrium
ζ_Δ	Δ/z_0
τ	The dimensionless time
τ_t	Dimensionless time required for completion of imbibition process

l	The dimensionless radius of the absorbed area into the porous area
l_c	The dimensionless radius of the column
Bo	Bond number
P_b	Pressure inside bubbles
P_a	Atmospheric pressure
P_c	Capillary pressure
P_{pm}	Mean capillary pressure inside capillaries in the porous layer.
τ_{max},	Maximum dimensionless time required for completion of drainage/imbibition process
α	Ratio of capillary pressure in porous layer to capillary pressure in the bubbles
β	Coefficient in Eq. 5.2
v	Velocity at circular edge of the wetted region inside the porous layer
ε	Porosity of porous layer
Q	Total volumetric flux through the Plateau borders
Q_f	Flux of the liquid at foam/porous layer interface
Q_{pm}	Flux of the liquid inside the porous layer
λ_{cr}	Critical foam height

CHAPTER 6

Drying of Foam under Microgravity Conditions

Overview

In the previous Chapter the process of foam drainage/imbibition into porous layer was theoretically and experimentally investigated taking into consideration the effect of surface viscosity. In this chapter a new method of foam drying under microgravity conditions is presented. The results of the investigation were published earlier in Microgravity Science and Technology and reused below with permission (Corresponding author: Nektaria Koursari).

In Section 6.2 the derivation of a theoretical model is presented for foam produced from a Newtonian surfactant solution in a column of length *H* attached to a thin porous layer. Liquid flow inside the foam, is caused by a capillary suction only applied by the pores of the porous layer and occurs in the horizontally along the co-ordinate axis z. Experimental procedure is described in section 6.3 and Results section 6.4 presents a comparison between experimental and simulations results of time evolutions of spreading radius.

6.1 Introduction

Foam is a colloidal dispersion where gas bubbles are dispersed in a continuous liquid phase. The bubbles, referred to as the dispersed phase, are polyhedral and are separated by thin films called lamella. The border where lamella (soap films) meet between three gas bubbles is referred to as Plateau border (channel), which join by a factor of four in regions called nodes (vertices)(148). Foam bubbles are characterised by their bubble radius. Bubble radius and other characteristic parameters, i.e. interface elasticity, liquid density and viscosity, liquid volume fraction, gravity and capillarity determine the foam stability and the properties of the foam(122). The liquid volume fraction, φ, varies between ~1% and ~35%, while most of the liquid is concentrated in the Plateau borders at reasonably low liquid volume fraction below ~12%, which is considered below. In this case most of the liquid in foams is accumulated inside the Plateau borders. However, the suggested method of drying foam at microgravity conditions is applicable at any liquid volume fraction below ~35%.

The term ‘foam stability’ refers to the stability of the foam films between gas bubbles which can be controlled by the addition of foaming agents, i.e. surfactants, polymers or proteins that form mono- or multi-layers at the lamella/air interface, reducing the surface tension of the multiphase system (149). Foam have a variety of industrial and domestic applications and are closely related to the production of a number of well-known products, i.e. shaving foams, firefighting foams, personal care products, medical products, structural material and processes such as floatation and mineral separation(149). In hydrocarbon industry foams are also utilised at all stages in the oil recovery process including well drilling and oil well production(43).

For liquid foams under terrestrial conditions the liquid flows through Plateau regions due to effect of gravity and capillarity forces. The action of gravity and capillarity result in the alteration of the local

liquid volume fraction inside the foam body. When gravity and capillarity equilibrate, then steady state is reached(40) The liquid flow though Plateau borders, films and nodes is referred to as foam drainage. Gravitational drainage causes the liquid to drain out of the foam body to the lower layers following the gravity direction(89). The drainage equations were introduced in (33,35) based on continuity and pressure balance considerations taking into account flow inside Plateau borders only. We include all liquid into Plateau borders, that is the whole liquid is concentrated inside the PBs, as the initial liquid fractions used were below the limiting value (of 0.12). The assumption of rigid interfaces has been adopted due the relatively low value of calculated Boussinesq number for given values of liquid viscosity, μ, radius of plateau border, R_{pb} and surface viscosity. i.e $Bousinesq = \frac{\mu \cdot R_{pb}}{\mu_s} \sim 2.2\ x\ 10^{-2} \ll 1$.

The drainage equation has been solved analytically for a multiplicity of cases including forced drainage (33) , gravity free drainage(136) and free drainage(134).

However, gravitational drainage is not always desirable for several applications such as the fabrication of metallic foams (42,150) oil recovery techniques(43) floatation and pumping(44). Gravity affects the foam formation, its evolution and stability by causing flow of liquid from higher to lower layers of the foam, while microgravity conditions allow the exclusive investigation of capillary flows only. Therefore, investigating the behaviour of wet foams under microgravity conditions allows overcoming the instability barriers imposed when gravity forces are present(41).

Microgravity is not only desirable for the investigation of capillary drainage but also for several research studies leading to optimisation of terrestrial processes and product quality improvement. In fluid-science experiments effects such as convection, sedimentation, stratification and fluid static pressure can be eliminated under microgravity conditions and therefore allows the investigation of fluid-dynamic effects normally affected by gravitation(151). Other applications of microgravity investigations include frontal displacement of fluids(152) where instability of the interface could lead to the creation of gas 'fingers' penetrating the bulk fluid, capillary driven filtration in porous media(153), Soret Coefficients of Organic Solutions measured in the Microgravity (154), thermodiffusion microgravity measurements of ternary mixtures(155) measurements of thermo- and diffusio-phoretic velocities of aerosol particles (particle motion), which play a significant role in the scavenging of aerosols due to crystal growth or evaporation(156). Microgravity conditions also benefit the investigation of bubble dynamics during degassing of liquids for applications heat pumps, heat exchangers, cooling systems, food technology and human physiology(157) and microgravity investigations of drainage in porous media(158).

Recently, microgravity experiments have been performed (41), in parabolic flights which allow 20s in microgravity established at the top of the parabolic trajectory and the so-called 'capillary imbibition or capillary wetting'' was investigated. S.J.Cox, D.Weaire and G.Verbist, 2004 complemented on the latter experimental study by modifying the standard drainage models for the microgravity case. The authors considered two equations based upon i) Poiseuille flow through Plateau borders and ii) assuming plug flow in the Plateau borders and proved that the liquid move upwards into the foam body(159). Experiments and simulations studying liquid flow into the foam body were also performed by A.Saint-Jalmes et.al ,2006, where three parabolic flight campaigns were performed under the supervision of European Space Agency (ESA). The purpose of the campaigns was to gain information

and understanding of the foam structure, stability, rheology, the liquid distribution and the way the liquid propagates between the different structure layers in microgravity conditions (160).

Among the most well-known microgravity related research tasks are RADIOUS (research associations for the development of industrial use of space), dedicated to the environment and energy, C-CORE (Consortium of Industrial Research in the use of space) focusing in fluid physics experiments and MIRROR (Microgravity, Industry Related research for oil recovery) focusing on the study of diffusion coefficient of crude oil, foam stability in microgravity and capillary flow in porous media. In the case of oil industry related subjects, foams could be desirable or undesirable depending upon their intensive use(43)**.** As part of the latter programme, foam stability experiments were performed aiming to provide information for the development of the oil recovery techniques often challenged by the effect of gravity (43).

Recently, foams have been characterised as ideal products for the delivery of topical active agents such as skin protectants, corticosteroids and local anaesthetics ideal for dermatological application(161). The kinetics of topical drug delivery depend upon the foam properties, the porous material and the interaction of the foam/thin porous layer system. Due to the increasing interest in liquid drainage of foams on porous material (19,162) a theory of foam drainage placed on thin porous substrate was recently developed under terrestrial gravity conditions (40). In this study drainage process was considered as a combination of drainage caused by gravity/capillary action and a capillary suction applied by the pores from the porous substrate. The rate of drainage, radius of the wetted area inside the porous material and other characteristics of the process were theoretically predicted and compared with experimental observations on various foam-thin substrates systems.

Below the previously developed theory of foam drainage on thin porous material (40) has been adapted and modified to be applied to foams drying on porous material in the absence of gravitational field. Experimental observations are compared with theoretical predictions for surfactant solutions Triton-X-100 50CMC and 20CMC on four types of filter papers, i.e. grade 1,3,5 and 601.

The experiments were conducted in the laboratory while the effect of gravity was eliminated by using a foam column placed horizontally, attached to one end on a thin porous substrate (Fig.6.1).

6.2 Theory

1. Let us consider foam produced from a Newtonian surfactant solution in a column of length H attached to a thin porous layer (Figure 6.1). All bubbles are supposed to be of a uniform size and do not change size over duration of the experiments. Liquid flow inside the foam, caused by a capillary suction applied by the pores of the porous layer, occurs in the horizontal direction along the co-ordinate axis z directed horizontally, with $z = 0$ at the left-hand side of the column.

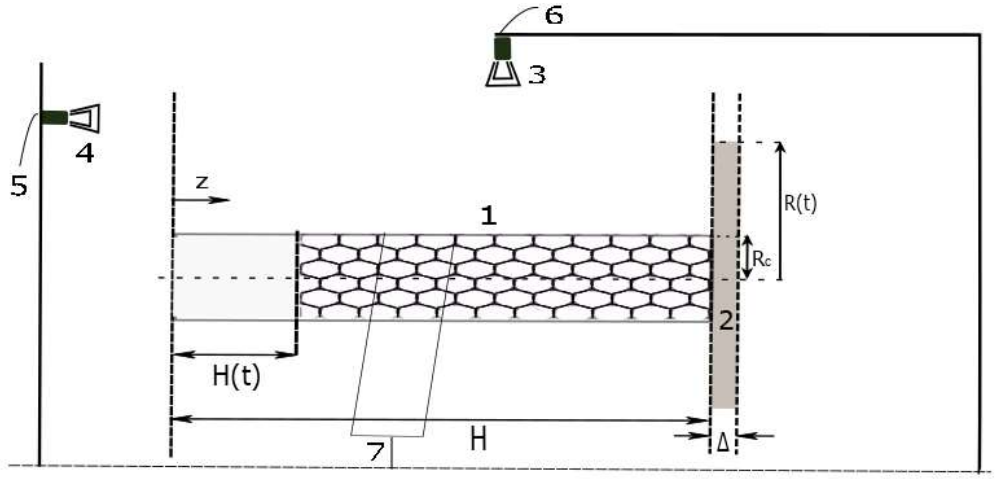

Figure 6. 1: Schematic presentation of the foam in horizontal position attached on one-side to a thin porous substrate. 1 – foam; 2 – porous layer of thickness ; R(t) is the radius of the wetted area inside the porous layer 3- digital camera 1 4- digital camera 2, 5- interface to PC from camera 1 6- interface to PC from camera 2, 7- clamp. Source:(163)

The flow inside the foam is assumed to occur inside the Plateau regions only and the contribution of the liquid flow in the films and nodes is neglected. In this case the drainage kinetics can be described by the following equation(19,98,140–143):

$$\frac{d\varphi}{dt} + \frac{dQ}{dz} = 0, \tag{6.1}$$

where Q is the flow rate expressed as:

$$Q = \left(\frac{C_1^{\frac{1}{2}} \rho g}{\mu\beta} R_b^2 \frac{\varphi^2}{(1-\varphi)^{\frac{1}{3}}} - \frac{C\gamma}{2\mu\beta} R_b \frac{\varphi^{\frac{1}{2}}\left(1-\frac{\varphi}{3}\right)}{(1-\varphi)} \frac{d\varphi}{dz} \right) \tag{6.2}$$

Under microgravity conditions, $g = 0$, and Eq. 6.2 can be rewritten as:

$$Q = \left(-\frac{C\gamma}{2\mu\beta} R_b \frac{\varphi^{\frac{1}{2}}\left(1-\frac{\varphi}{3}\right)}{(1-\varphi)} \frac{d\varphi}{dz} \right) \tag{6.3}$$

and

$$\frac{1}{\beta} = \left(c \frac{1}{3^{\frac{3}{2}} 5} \frac{1}{n_p^{\frac{1}{2}} \delta^{\frac{3}{2}} \pi^{\frac{1}{2}}} \right) \tag{6.4}$$

Substituting Eq. 6.3 into 6.1 results in:

$$\frac{\partial \varphi}{\partial \mathrm{t}} + \frac{\partial \left(-\frac{C\gamma}{2\mu\beta} R_b \frac{\varphi^{\frac{1}{2}} \left(1 - \frac{\varphi}{3}\right)}{(1-\varphi)} \frac{d\varphi}{dz} \right)}{\partial z} = 0 \tag{6.5}$$

In the above equations, φ is the liquid volume fraction; μ is the dynamic viscosity of the liquid; γ is the liquid-air interfacial tension; R_b is the radius of bubbles; ρ and g are the liquid density and the gravity acceleration, respectively; n_p is the number of Plateau borders per bubble; is a coefficient(143); $C^2 = \sqrt{3} - \pi/2 \sim 0.161$; $c = 0.5169$ is the velocity coefficient (142) foams produced from Newtonian solutions; C_1 is a geometrical coefficient expressed as $C_1 = \frac{4\pi}{(3 n_p \delta)} \sim 0.378 - 0.972$ for a foam with structures between bcc (body-centred cubic) and fcc (face-centred cubic) and bubbles of the same size ($\delta = 0.718 - 1.108$, $\mathrm{n_p} = 6 - 10$)(164).The non-slip boundary condition on the liquid-air interface of Plateau borders are adopted below. For this purpose the Triton -100 surfactant was selected, which has a relatively high surface viscosity.

Let us introduce the following dimensionless variable and co-ordinate: $\zeta \to \frac{z}{z_0}$, $\tau \to \frac{t}{t_0}$, where z_0 and t_0 the characteristic scale and time respectively.

Non-dimensonalisation of Eq. 6.5 results in:

$$\frac{\partial \varphi}{\partial \tau} + \frac{\partial \left(-\frac{t_0}{{z_0}^2} \cdot \frac{C \cdot \gamma}{2 \cdot \mu \cdot \beta} \cdot R_b \frac{\varphi^{\frac{1}{2}} \left(1 - \frac{\varphi}{3}\right)}{(1-\varphi)} \cdot \frac{d\varphi}{d\zeta} \right)}{\partial \zeta} = 0 \tag{6.6}$$

If $z_0 = H$ [m] is the characteristic scale, then from Eq. 6.6 considering Eq. 6.7 :

$$\frac{t_0}{{z_0}^2} \cdot \frac{C \cdot \gamma}{2 \cdot \mu \cdot \beta} \cdot R_b = 1 \qquad (6.7)$$

The expression of the characteristic time is as follows:

$$t_0 = \frac{{z_0}^2 \cdot 2 \cdot \mu \cdot \beta}{C \cdot \gamma \cdot R_b} = \frac{H^2 \cdot 2 \cdot \mu \cdot \beta}{C \cdot \gamma \cdot R_b} \qquad (6.8)$$

Substitution of t_0 into Eq. 6.6 results in:

$$\frac{d\varphi}{d\tau} + \frac{d}{d\zeta}\left(\frac{-\varphi^{\frac{1}{2}}\left(1 - \frac{\varphi}{3}\right)}{(1-\varphi)}\frac{d\varphi}{d\zeta}\right) = 0, \qquad (6.9)$$

Assuming that the liquid films between bubbles in foam are flat, i.e. $R_b \gg R_{pb}$, (see Figure 6.2) the pressure in all bubbles is identical(19,98) and equals to:

$$P_b = \frac{4\gamma}{R_b} \qquad (6.10)$$

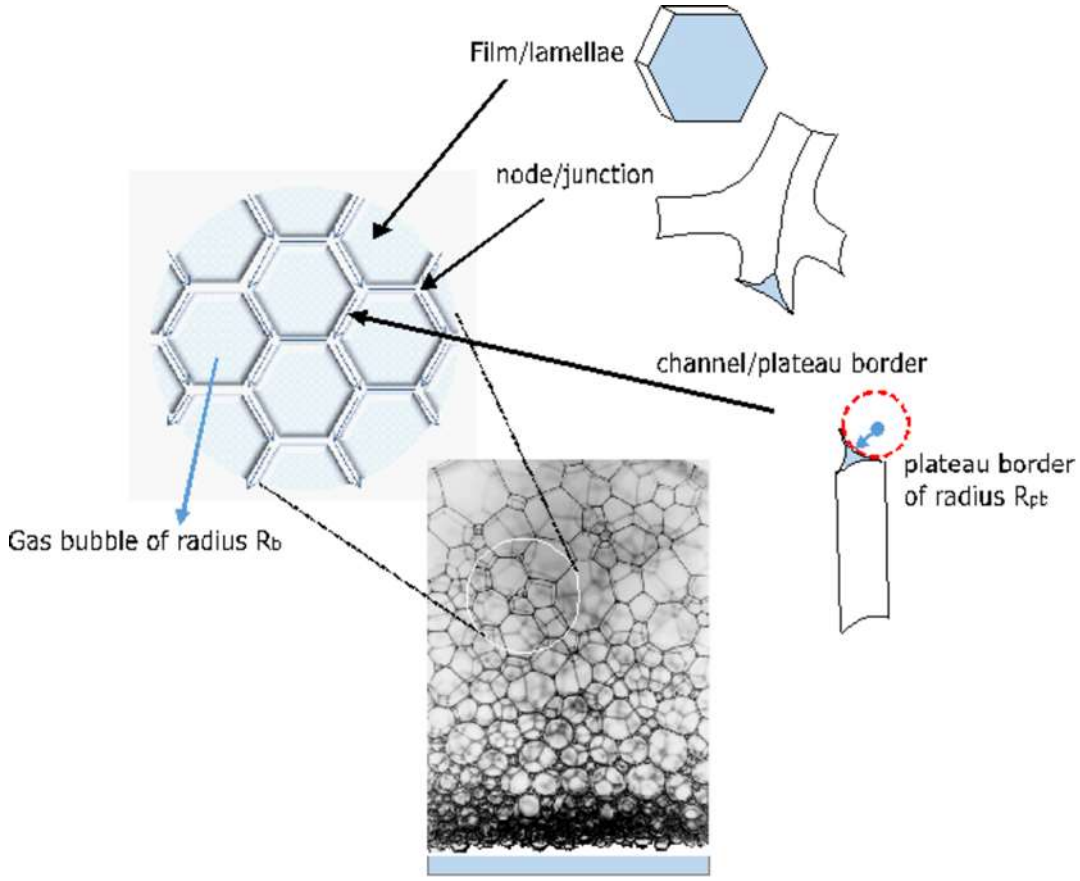

Figure 6. 2:Schematic presentation of a generalised, homogenous foam system formed of identical gas bubbles of radius R_b in a continuous liquid phase and liquid filled channels and nodes. The connection of three lamellae is referred to as Plateau border (concave triangles) of radius R_{pb}, being the radius of curvature of the sides. Source:.(163)

$$P_b = \frac{4\gamma}{R_b}$$

$$P_c = \frac{\gamma}{R_{pb}} \qquad (6.11)$$

where P_c is the capillary pressure and γ the liquid-air interfacial tension.

According to(164):

$$C^2 R_{pb}^2 = C_1 R_b^2 \frac{\varphi}{(1-\varphi)^{\frac{2}{3}}} \qquad (6.12)$$

From Eqs. (6.10-6.12) the pressure in the Plateau border is:

$$P_{pb}(z,t) = P_b - P_c = \frac{\gamma}{R_b}\left(4 - \frac{C}{C_1^{\frac{1}{2}}}\frac{\left(1-\varphi(z,t)\right)^{\frac{1}{3}}}{\varphi(z,t)^{\frac{1}{2}}}\right). \quad (6.13)$$

Let us introduce P_{pm} as the mean capillary pressure inside capillaries inside the porous layer, which can be estimated by $P_{pm} \sim \frac{n\gamma}{R_{pm}}$, where R_{pm} is radius of pores, $n = 1$ in the case of porous media built by cylinders (for example hair) and $n = 2$ in the case of two-dimensional geometry. Accordingly, the pressure difference, which results in the liquid flow from the Plateau channel into the porous layer at the foam/porous layer interface, is:

$$\Delta P = P_{pb} - P_{pm} = \frac{\gamma}{R_b}\left(4 - \frac{C}{C_1^{\frac{1}{2}}}\frac{\left(1-\varphi(z=H,t)\right)^{\frac{1}{3}}}{\varphi(z=H,t)^{\frac{1}{2}}}\right) + \frac{n\gamma}{R_{pm}}. \quad (6.14)$$

If $\Delta P > 0$, then liquid from the Plateau border will penetrate the porous layer. However, if $\Delta P < 0$, then penetration will stop. Let us introduce the final liquid content, φ_f, as the liquid volume fraction at the foam/porous layer interface at which the pressure inside the Plateau channels and the pressure inside the porous layer equilibrate. The consideration above and Eq. (6.11) determine the end of the drainage process and the final liquid content at the foam/porous substrate interface, φ_f , when $\Delta P = 0$:

$$\frac{\gamma}{R_b}\left(4 - \frac{C}{C_1^{\frac{1}{2}}}\frac{\left(1-\varphi(z=H,t)\right)^{\frac{1}{3}}}{\varphi(z=H,t)^{\frac{1}{2}}}\right) + \frac{n\gamma}{R_{pm}} = 0. \quad (6.15)$$

Hence,

$$\frac{\varphi_f}{(1-\varphi_f)^{\frac{2}{3}}} = \frac{\left(\frac{C^2}{16C_1}\right)}{\left(1+\frac{nR_b}{4R_{pm}}\right)^2} \quad (6.16)$$

If we introduce α as a ratio of capillary pressure in the porous layer to capillary pressure in the bubbles:

$$\alpha = \frac{\Delta P_{capin\ substrate}}{\Delta P_{capin\ bubbles}} = \frac{\frac{n\gamma}{R_{pm}}}{\frac{4\gamma}{R_b}} = \frac{nR_b}{4R_{pm}} \qquad (6.17)$$

and taking into account that $\varphi_f << 1$ then, Eq. 6.16 can be rewritten as:

$$\varphi_f = \frac{\left(\frac{C^2}{16C_1}\right)}{(1+\alpha)^2} \qquad (6.18)$$

According to the definition $\varphi_f = \frac{\left(\frac{C^2}{16C_1}\right)}{\left(1+\frac{2R_b}{4R_{pm}}\right)^2} < \varphi_{max}$ or $\left[\frac{\left(\frac{C^2}{16C_1}\right)}{\varphi_{max}}\right]^{-\frac{1}{2}} < \left(1+\frac{2R_b}{4R_{pm}}\right)$. Estimations show that at $C^2 \sim 0.161$, $C_1 = \frac{4\pi}{(3n_p\delta)} \sim 0.378 - 0.972$, and $\varphi_{max} = 0.26 : \left[\frac{\left(\frac{C^2}{16C_1}\right)}{\varphi_{max}}\right]^{-\frac{1}{2}} \sim 0.2 - 0.32$. The latter means that $\varphi_f < \varphi_{max}$ at any size of pores and foam bubbles.

Eq. 6.18 shows that it is possible to control the final liquid contents inside the foam simply varying the parameter , which is determined by the average pore radius inside the porous layer.

Eq.6.16 allows calculating the final radius, of the wetted area inside the porous layer, R_f. The final volume fraction is equal to $_f$ and the volume of liquid inside the foam $V_f = \pi \cdot H \cdot R_c^2 \cdot \varphi_f$ according to the mass conservation law: $V_f + \pi \cdot \cdot \cdot R_f^2 = V_i$, where the initial liquid volume inside the foam is: $V_i = \pi \cdot H \cdot R_c^2 \cdot \varphi_i$ Substitution of expressions for initial and final volume we arrive to:

$$l_f = \sqrt{\frac{i - f}{\cdot / H}} \qquad (6.19)$$

The suggested method allows (i) to vary final values of the liquid contents inside the foam, φ_f by varying porosity, thickness and capillary pressure inside the porous substrate; (ii) it is possible to stop imbibition into the porous layer at any moment simply by removing the porous layer. It will allow to reach any pre-scribed value of the remaining liquid inside the foam in between $_i$ and φ_f .

Eq. 6.18 and the previous consideration shows that the drainage of foam placed on the porous substrates is substantially different from that in the case of free drainage or drainage of foam placed on a non-porous substrate: in the case of drainage of foam placed on porous substrate the final liquid volume

fraction at the foam/porous substrate interface is much lower as compared with the case of free drainage, when this volume fraction reaches the maximum possible value.

2. Liquid imbibition into porous layer

It is assumed below, according to(139), that the porous layer is thin enough and the time for its saturation in the vertical direction can be neglected relative to other time scales of the process.

The liquid flow inside the porous layer in the radial direction obeys the Darcy's law:

$$\frac{1}{r}\frac{d}{dr}(rv) = 0, \qquad v = \frac{K_p}{\mu}\left|\frac{dp}{dr}\right|. \tag{6.20}$$

Solution of the latter equations is:

$$p = -\left(\frac{\mu}{K_p}\right)\ln(r) + B, \quad v = \frac{C}{r} \tag{6.21}$$

where B and C are integration constants, which should be determined using the boundary conditions for the pressure at the column edge, $r = R_c$, and at the circular edge of the wetted region inside the porous layer, $r = R(t)$ (139).

The boundary condition at the circular edge of the wetted region inside the porous layer is expressed as:

$$P = -P_{pm}, \;\; r = R(t), \tag{6.22}$$

where $P_{pm} \approx \frac{n\gamma}{R_{pm}}$ is the capillary pressure inside the pores of the porous layer, and R_{pm} is a characteristic scale of the pore radii inside the porous layer.

The other boundary condition is written as:

$$P = \frac{\gamma}{R_b}\left(4 - \frac{C}{C_1^{\frac{1}{2}}}\frac{\left(1-\varphi(H,t)\right)^{\frac{1}{3}}}{\varphi(H,t)^{\frac{1}{2}}}\right), \quad r = R_c. \tag{6.23}$$

Using the latter two boundary conditions, both integration constants, b and c, can be determined, which gives the following expression for the radial velocity according to Eq. 6.21:

$$v = \frac{K_p}{\mu}\frac{\Delta P}{r\ln\left(\frac{R}{R_c}\right)}, \tag{6.24}$$

where ΔP is given by Eq. 6.14.

The velocity at the circular edge of the wetted region inside the porous layer is:

$$\varepsilon\frac{dR}{dt} = v|_{r=R} \tag{6.25}$$

where ε is the porosity of the porous layer. Combination of the latter two equations gives the evolution equation for $R(t)$:

$$\frac{dR}{dt} = \frac{K_p}{\varepsilon\mu}\frac{\Delta P}{R\ln\left(\frac{R}{R_c}\right)} \tag{6.26}$$

Let us introduce the following dimensionless variables: $l \to \frac{R}{R_c}$, $\quad _1 \to \frac{t}{t_{00}}$ where t_{00} is a characteristic time scale of the imbibition into the porous substrate and R_c is the radius of the tube. Let us estimate ΔP according to Eq. 6.14 and Eq.6.18 as:

$$\begin{aligned}\Delta P = P_{pb} - P_{pm} &= \frac{4\gamma}{R_b}\left(1 - \frac{C}{4\cdot C_1^{\frac{1}{2}}}\frac{\left(1-\varphi(z=H,t)\right)^{\frac{1}{3}}}{\varphi(z=H,t)^{\frac{1}{2}}}\right) + \frac{n\cdot\gamma}{R_{pm}} \\ &= \frac{4\gamma(1+\alpha)}{R_b}\left(1 - \frac{C}{4\cdot C_1^{\frac{1}{2}}(1+\alpha)}\frac{\left(1-\varphi(z=H,t)\right)^{\frac{1}{3}}}{\varphi(z=H,t)^{\frac{1}{2}}}\right) \\ &= \frac{4\gamma(1+\alpha)}{R_b}\left(1 - \frac{{\varphi_f}^{1/2}}{\left(1-\varphi_f\right)^{1/3}}\right)\end{aligned} \tag{6.27}$$

Hence, according to Eq. 6.26 t_{00} can be estimated as:

$$t_{00} = \frac{R_b \quad R_c^2}{4 \quad K_p(1 + \quad)} \tag{6.28}$$

Using new variables, we can rewrite Eq. 6.26 as:

$$\frac{dl}{d\ _1} = \frac{1}{l \cdot \ln l}\left(1 - \frac{\sqrt[3]{\frac{\left(1-\varphi(\zeta=1,\tau)\right)}{\left(1-\varphi_f\right)}}}{\sqrt{\frac{\varphi(\zeta=1,\tau)}{\varphi_f}}}\right) \tag{6.29}$$

In the latter Eq. 6.29 the left-hand side depends on a new time $_1$while the right-hand site depends on . Relation between these two dimensionless time scales is: $= \frac{t_{00}}{t_0} \cdot\ _1$.

If we switch to the dimensionless time in Eq. 6.29, it results in:

$$\frac{t_{00} \cdot dl}{t_0 \cdot d} = \frac{1}{l \cdot \ln l}\left(1 - \frac{\sqrt[3]{\frac{\left(1-\varphi(\zeta=1,\tau)\right)}{\left(1-\varphi_f\right)}}}{\sqrt{\frac{\varphi(\zeta=1,\tau)}{\varphi_f}}}\right) \tag{6.30}$$

Let us define $\delta = \frac{t_{00}}{t_0}$, that is the ratio of characteristic time scale t_{00}, which is the time scale of the liquid imbibition into the porous layer and t_0, which is the time scale of the equilibration of liquid contents inside the foam:

$$\cdot \frac{dl}{d} = \frac{1}{l\ \ln l}\left(1 - \frac{\sqrt[3]{\frac{\left(1-\varphi(\zeta=1,\tau)\right)}{\left(1-\varphi_f\right)}}}{\sqrt{\frac{\varphi(\zeta=1,\tau)}{\varphi_f}}}\right) \tag{6.31}$$

3. Boundary conditions at the foam/porous layer interface

In our previous publication(19), it was assumed that the height of the foam remains constant during the contact with the vertical porous layer and it was possible to neglect the small changes in the foam height which occurs due to the drainage of the foam. It was possible to assume because penetration of the liquid into the vertical thick, porous medium was small enough. Situation is different in the case under consideration. That is, below the changes of the foam height due to the liquid drainage from the foam into the porous layer is taken into account.

Let us consider a mass conservation law of liquid within the column and porous layer, in the case when the free liquid layer does not form at the foam/porous layer interface:

$$\pi R_c^2 \left(\int_{H_1(t)}^{H} \varphi(z,t) dz \right) + \varepsilon \Delta \pi R^2(t) = V_0 = \pi R_c^2 \varphi_i \big(H - H_1(0) \big) \qquad (6.32)$$

Differentiating Eq. 6.32 with time results in:

$$\pi R_c^2 \left(\int_{H_1(t)}^{H} \frac{d}{dt} \varphi(z,t) dz - \varphi(H_1(t),t) \frac{dH_1(t)}{dt} \right) + 2\varepsilon \Delta \pi R(t) \frac{dR(t)}{dt} = 0 \quad (6.33)$$

Using Eqs. (6.1) and (6.2) the latter equation can be rewritten as:

$$\pi R_c^2 \left(Q\big(H_1(t)\big) - Q(H_2) - \varphi(H_1(t),t) \frac{dH_1(t)}{dt} \right) + 2\varepsilon \Delta \pi R(t) \frac{dR(t)}{dt} = 0 \qquad (6.34)$$

In the case under consideration formation of a free liquid layer at the foam/porous layer interface is impossible, hence, the bottom of the foam remains directly in contact with the porous layer and its position does not move during the drainage. Therefore, only the top of the foam can move because of the drainage. At the top of the foam there is no accumulation/source of liquid and, hence, $Q_f(H_1,t) = 0$. Let us introduce the flux of the liquid at the foam/porous layer interface as:

$$Q_f(H,t) = \pi R_c^2 Q(H,t)) = \pi R_c^2 \left(-\frac{C\gamma}{2\mu\beta} R_b \frac{\varphi^{\frac{1}{2}}(H,t)(1-\varphi(H,t)}{3} \frac{d\varphi(H,t)}{dz} \right) \qquad (6.35)$$

and the flux of the liquid inside the porous layer as:

$$Q_{pm}(t) = \frac{2\pi\Delta K_p}{\mu} \frac{\left(\frac{\gamma}{R_b} \left(4 - \frac{C}{C_1^{\frac{1}{2}}} \frac{\left(1-\varphi(H,t)\right)^{\frac{1}{3}}}{\varphi(H,t)^{\frac{1}{2}}} \right) + \frac{n\gamma}{R_{pm}} \right)}{\ln \frac{R}{R_c}} \tag{6.36}$$

Hence, Eq. 6.34 can be rewritten as:

$$\frac{dH_1(t)}{dt} = \frac{1}{\pi R_c^2 \varphi(H_1(t),t)} \left(Q_{pm}(t) - Q_f(H,t) \right) \tag{6.37}$$

Using dimensionless variables and co-ordinate as before: $\zeta \to \frac{Z}{Z_0}, l \to \frac{R}{R_0}, \tau \to \frac{t}{t_0}$, Eq. 6.37 can be rewritten as:

$$\frac{d\zeta_1(\tau)}{d\tau} = \frac{1}{\varphi(\zeta_1(\tau),\tau)} \begin{bmatrix} \left(\frac{2\varepsilon\zeta_\Delta}{l_c^2} \left(\frac{1}{\ln\frac{l}{l_c}} \left(1 - \frac{\sqrt[3]{\frac{(1-\varphi(\zeta_2,\tau))}{(1-\varphi_f)}}}{\sqrt{\frac{\varphi(\zeta_2,\tau)}{\varphi_f}}} \right) \right) \right) - \\ \left(-\frac{\varphi(\zeta_2,\tau)^{\frac{1}{2}} \left(1 - \frac{\varphi(\zeta_2,\tau)}{3}\right)}{(1-\varphi(\zeta_2,\tau))} \frac{d\varphi(\zeta_2,\tau)}{d\zeta} \right) \end{bmatrix}, \tag{6.38}$$

where $\zeta_\Delta = \Delta/z_0$.

Let us consider a mass conservation law of the gas phase within the foam in the case, when there is no bubble rupture at the top of the foam i.e. $\varphi(H_1,t) > \varphi_{cr}$ (φ_{cr} is a critical liquid volume fraction below which the coalescence/bubble burst begins) and $Q(H_1,t) = 0$:

$$\pi R_c^2 \left(\int_{H_1(t)}^{H_2} 1 - \varphi(z,t) dz \right) = cons \tag{6.39}$$

Differentiating Eq. 6.39 with time leads to the following expressions for the rate of the moving top boundary of the foam:

$$\frac{dH_1(t)}{dt} = \frac{1}{\pi R_c^2\left(1-\varphi(H_1(t),t)\right)} Q_f(H,t) \tag{6.40}$$

and in dimensionless form:

$$\frac{d\zeta_1(\tau)}{d\tau} = \frac{-1}{1-\varphi(\zeta_1(\tau),\tau)} \frac{\varphi(\zeta_2,\tau)^{\frac{1}{2}}\left(1-\frac{\varphi(\zeta_2,\tau)}{3}\right)}{(1-\varphi(\zeta_2,\tau))} \frac{d\varphi(\zeta_2,\tau)}{d\zeta} \tag{6.41}$$

Comparison of Eqs. 6.37 and 6.40 results in the following expression for the boundary condition at the foam/porous layer interface in the case, when the free liquid layer does not form:

$$Q_f(H,t) = (1-\varphi(H_1(t),t))Q_{pm}(t) \tag{6.42}$$

and in dimensionless form:

$$\begin{aligned} -\frac{\varphi(\zeta_2,\tau)^{\frac{1}{2}}\left(1-\frac{\varphi(\zeta_2,\tau)}{3}\right)}{\left(1-\varphi(\zeta_2,\tau)\right)} \frac{d\varphi(\zeta_2,\tau)}{d\zeta} \\ = \big(1 \\ -\varphi(\zeta_1(\tau),\tau)\big)\frac{2\varepsilon\zeta_\Delta}{l_c^2}\left(\frac{1}{\ln\frac{l}{l_c}}\left(1-\frac{\sqrt[3]{\left(1-\varphi(\zeta_2,\tau)\right)}}{\sqrt{\frac{\varphi(\zeta_2,\tau)}{\varphi_f}}}\right)\right) \end{aligned} \tag{6.43}$$

Note, in the above equations we supposed that the liquid volume fraction at $z = H_1$ is higher than φ_{cr}, there is no bubble collapsing/coalescence at the top of the foam and the top boundary condition is zero liquid flux, i.e $Q_f(H_1(t),t) = 0$. The suggested system of Eqs. 6.5, 6.24 with boundary condition (6.43) at foam/porous layer interface is valid when no free liquid layer is formed at foam/porous layer interface, i.e. if $\varphi(H,t) < \varphi_{max}$, which is always the case under microgravity conditions In this case

porous layer absorbs all liquid coming from the foam and the top boundary of the foam moves downward due to liquid drainage inside the foam according to Eq. 6.31. This case was referred to a fast or intermediate imbibition of the liquid into the porous layer(19). This is the only case in the case under microgravity conditions.

6.3 Experimental Procedure

Triton-X-100 is a nonionic surfactant purchased by Sigma-Aldrich(165). This surfactant was selected because it shows a relatively high liquid-air surface viscosity, and, hence, is close to the adopted above non-slip boundary conditions on the surface of Plateau borders. Standard solutions of Triton X-100 with concentration 50 CMC and 20CMC were made. The experiment was carried out in a glass tube, 9cm long with a 2.5cm outer diameter and 2.1cm inner diameter, with a porous substrate attached to one end. Four different filter paper grades were used as the porous substrate – Grades 1, 3, 5 and 601. The glass tube was positioned horizontally held by a clamp stand, ensuring its horizontal position using a spirit level, with one camera placed above the glass tube and a second camera facing the filter paper (Figure 6.1). Parafilm was used to cover the open end of the tube to prevent loss of foam due to evaporation.

The foam of uniform bubble size was created using a squeeze bottle to initial length equal to L=6cm measured considering the substrate as zero point. Two Pike Allied Vision Technologies Cameras: camera 1, Sony TV Lens 1:1.8 16mm (Figure 6.1) were used for capturing images of the experiment at regular time intervals.

The images captured were analyzed by ImageJ software measuring spreading radius. It was proven that the liquid drainage in the vertical direction inside the tube was negligible over duration of the experiments. Permeability of filter papers was measured by placing a strip of each grade in water recording the changes in height. The dependency between height squared against time was plotted with the gradient representing permeability. To find the porosity the glass tube was placed vertically on each filter paper grade and filled with water to a specified height. The volume of water was then divided by the wetted area resulting to the value of porosity. Initial volume fractions for each foam solution were obtained by weighing 50ml of foam. The initial volume fractions of foams (see below) were found by weighing a known volume of foam and dividing this weight by the volume of the foam and the liquid density, that is, $_i = \frac{M_i}{V_i}$, where M_i and V_i are initial weight and volume of the foam respectively; ρ is the liquid density.

Each experiment repeated at least 2-3 times. The variation between the experimental data values was quantified by standard deviation and presented in Figures. 6.5-6.6.

Initial liquid volume fraction for surfactants Triton X-100 – 50 CMC and Triton X-100 – 20 CMC was 8.56% and 10% respectively, which are below a critical volume fraction of ~12%, when the suggested theoretical approach could become questionable.

Table 6. 1: Filter Paper Properties: Thickness of filter paper, Δ , Average Pore Radius , R_{pm}, Porosity , ε Permeability, k_p, obtained from Whatman filter paper guide (166), (165). Source:(163)

Filter Paper Grade (FPG)	**1**	**3**	**5**	**601**
Thickness, Δ(m)	1.8×10^{-4}	3.9×10^{-4}	2×10^{-4}	1.6×10^{-4}
Average Pore Radius, R_{pm}(m)	5.5×10^{-6}	3.0×10^{-6}	1.25×10^{-6}	5.0×10^{-6}
Porosity, ε	0.48	0.77	0.54	0.90
Permeability, k_p(m²)	9.81×10^{-14}	1.57×10^{-13}	1.50×10^{-14}	1.67×10^{-13}

Table 6.1 shows that the thickness of the filter paper was varied more than twice, the pore radius was varied more than three times, porosity varied twice and the permeability varied more than 10 time for different filter papers used.

6.4 Results and Discussion: radius of the wetted area inside porous substrate

Capillary flow inside the foam and liquid imbibition inside the porous substrate are described by dimensionless Eq. (6.6) and Eq. (6.31), respectively, have been solved analytically using COMSOL software finite element method on one dimensional regular grid. A backward differentiation formula was used to solve time-dependent variables and time stepping was free taken by the solver with initial step size of 10^{-20}. Relative tolerance was set to 10^{-8}, whereas absolute tolerance was set to 10^{-10}. The values of foam/porous substrate systems parameters, K_p , Δ, average R_b, ε, μ, ρ, average pore size and initial liquid volume fraction, φ_i, have been incorporated in simulations based on the experimental data as shown in Table 6.1.

The imbibition into the porous substrate is characterised through measurements of wetted radius, $R(t)$, with initial value equal to the radius of the foam column $R(0) = R_c$ (see Figure 6.1). Experimentally, spreading radius was accurately measured due to the symmetry of the circular shape of the wetted area (please see Figure 6.3)

Figure 6. 3:Image of the spreading diameter on the filter paper for Triton X-100. Source:(163)

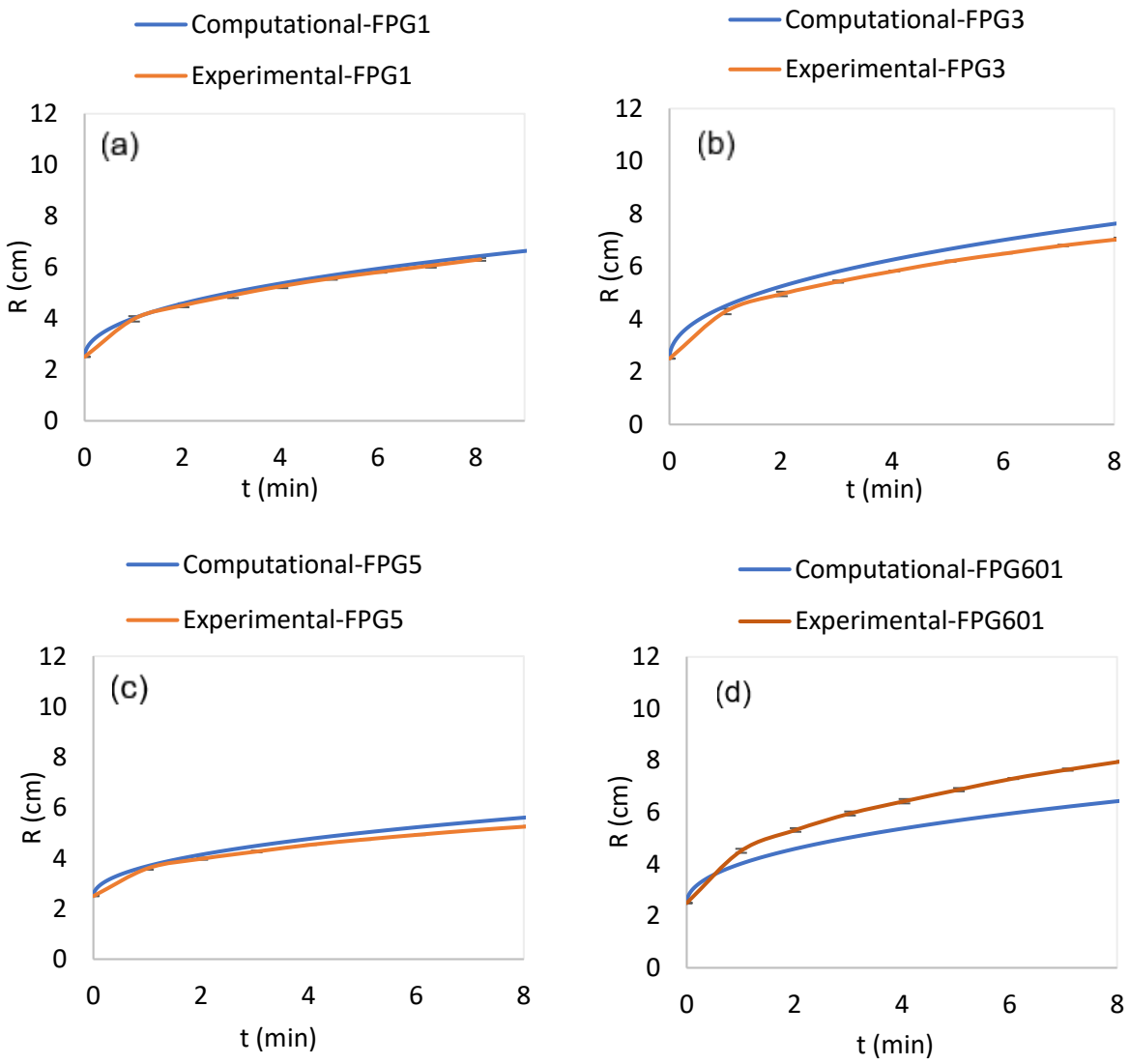

Figure 6. 4:Comparison between experimental and simulations results of time evolutions of spreading radius $R(t)$ for (a) Triton X-100-20CMC-Filter Paper Grade 1(FPG1) (b) Triton X-100-20CMC- Filter Paper Grade 3(FPG3) (c) Triton X-100-20CMC- Filter Paper Grade 5(FPG5) and (d) Triton X-100-20CMC- Filter Paper Grade 601(FPG601). Source:(163)

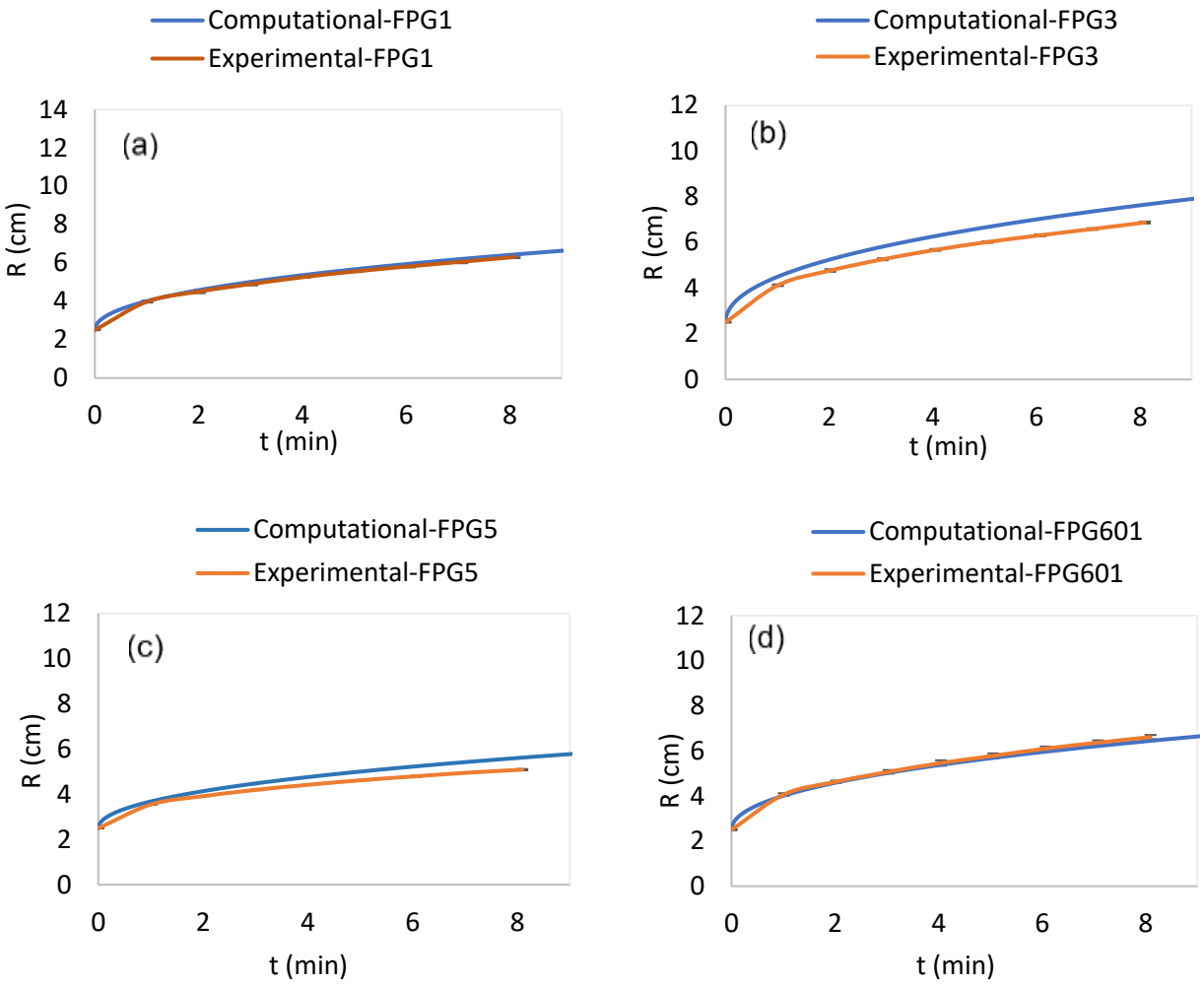

Figure 6. 5:Comparison between experimental and simulations results of time evolutions of spreading radius $R(t)$ for (a) Triton X-100-50CMC- Filter Paper Grade 1(FPG1) (b) Triton X-100-50CMC- Filter Paper Grade 3(FPG3) (c) Triton X-100-50CMC- Filter Paper Grade 5(FPG5) and (d) Triton X-100-50CMC- Filter Paper Grade 601 (FPG601). Source:(163)

Experimentally obtained time evolutions of spreading radius, R(t) [cm] inside porous layer are in a reasonable agreement with the theoretical predictions for all investigated surfactant solutions-filter paper systems, for both initial volume fractions of Triton-X-100 i.e 20CMC and 50CMC and for filter papers of four different grades, i.e. grade 1,3,5 and 601, as shown in Figures. 6.4-6.5.

If $\Delta P > 0$ then liquid from the Plateau border will penetrate the porous substrate. Spreading radius, $R(t)$, gradually increases until final liquid volume fraction at the foam/porous layer interface,φ_f, is reached (see Eq. 6.19), when the capillary drainage/imbibition process is completed, and there is no further liquid penetration into the porous substrate. When φ_f is reached, as expressed by Eq.6.16, the pressure inside the Plateau channels and the pressure inside the porous layer equilibrate.

Dimensionless parameter α, as expressed by Eq. 6.17 has shown a considerable effect to the rate of spreading $R(t)$. Any increase of parameter α results to an increase of the rate of spreading, $R(t)$.

Parameter α is a function of bubble radious, R_b and the pore radius of the porous layer, R_{pm}, and its value depends on calculated error in experimentall observations for both measured parameters. Dimensionless parameters φ_i, ε and ζ_Δ exibited a small effect to the rate of spreading, $R(t)$. The effect of small changes of dimensionless parameter α for Triton X-100-50CMC-FPG3 is presented in Figure 6.6.

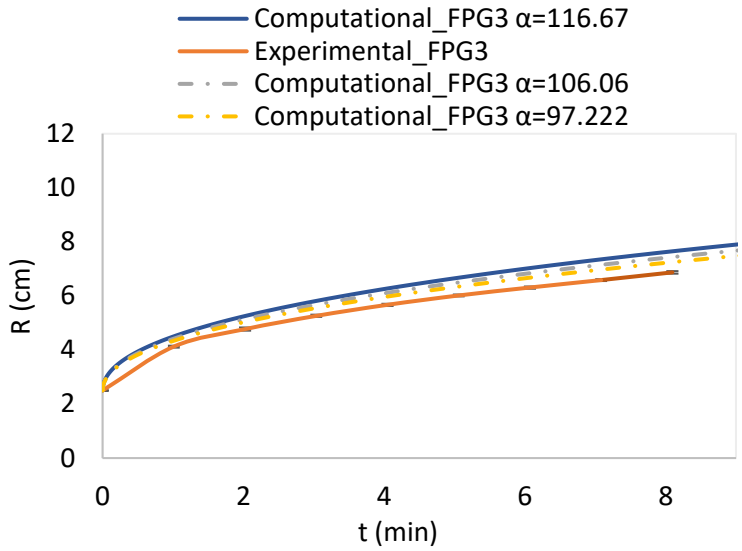

Figure 6. 6:Comparison between experimental and simulations results of time evolutions of spreading radius $R(t)$ for Triton X-100-50CMC- Filter Paper Grade 3(FPG3) for different values of dimensionless parameter α, as expressed by Eq. (6.17). Source:(163)

6.5 Conclusions

A new method of foams drying under microgravity conditions is suggested. A theory of the method was developed and compared with experimental measurements of the process. Comparison of the experimental data with a theoretical prediction are in very reasonable agreement.

Nomenclature 6

Δ	Thickness of porous layer
$R(t)$	Radius of the wetted area inside the porous layer
R_c	Radius of column
R_b	Bubble radius
R_{pb}	Plateau border radius
R_{pm}	Pore radius of porous media
φ	Liquid volume fraction
φ_i	Initial liquid volume fraction
φ_f	Final Liquid volume fraction at foam/ porous layer interface
φ_{cr}	Critical liquid volume fraction
φ_{max}	Maximum liquid volume fraction
$\varphi_{interface}$	Maximum liquid volume fraction at the foam/porous substrate interface
μ	Dynamic viscosity of liquid
μ_s	Surface viscosity
γ	Liquid-air interfacial tension
ρ	Liquid density
g	Gravity acceleration
n_p	Number of Plateau borders per bubble
C^2	0.161 (constant)
c	Velocity coefficient, $c = 0.5169$ for foams produced by Newtonian solutions
C_1	Geometrical coefficient, $\sim 0.378 - 0.972$ for foam with structures between bcc and fcc and bubbles of same size.
ζ	The dimensionless horizontal scale
ζ_H	The dimensionless length of the column
ζ_{1e}	The dimensionless position of the left-hand side of the foam at equilibrium
ζ_1	The dimensionless position of the left-hand side boundary of the foam
ζ_2	The dimensionless position of the foam/porous layer boundary

ζ_Δ	Δ/z_0
τ	The dimensionless time
τ_t	Dimensionless time required for completion of imbibition process
l	The dimensionless radius of the absorbed area into the porous area
l_c	The dimensionless radius of the column
Bo	Bond number
P_b	Pressure inside bubbles
P_c	Capillary pressure
P_{pm}	Mean capillary pressure inside capillaries in the porous layer.
τ_{max},	Maximum dimensionless time required for completion of capillary drainage/imbibition process
α	Ratio of capillary pressure in porous layer to capillary pressure in the bubbles
v	Velocity at circular edge of the wetted region inside the porous layer
ε	Porosity of porous layer
Q	Total volumetric flux through the Plateau borders
Q_f	Flux of the liquid at foam/porous layer interface
Q_{pm}	Flux of the liquid inside the porous layer
V_f	Volume of liquid inside the foam
λ_{cr}	Critical foam height

CHAPTER 7

Modelling of foamed emulsion drainage

Overview

In Chapter 6 a new method of foam drying under microgravity condition was proposed. In this chapter a theory of foam drainage of foams containing emulsified oil is developed and the effect of oil on foam stability is investigated both theoretically and experimentally. The results of this research study were published earlier in Colloids and Surfaces A: Physicochemical and Engineering Aspects and reused in this chapter with permission from corresponding author, Professor Victor M. Starov(v.m.starov@lboro.ac.uk).

Initially in this Chapter the experimental procedure is described and information for foamed emulsion preparation is provided. In section 7.3 a theory of foamed emulsion drainage is developed, and results are presented in section 7.4. In Results section comparison between experimentally obtained measurements and model predictions of time evolutions of both foam height and free liquid layer is provided for four investigated foamed emulsion systems.

7.1 Introduction

Emulsions are colloidal dispersions where one liquid (dispersed phase) is dispersed into another liquid (continuous phase) of different nature and composition. In most of emulsions one phase is usually oil and the other one is water, so that the two most common types of emulsions are oil-in water (O/W) or water-in -oil (W/O) where oil is the dispersed phase or water is the dispersed phase respectively. Other more complex cases are the so-called double emulsions which include oil-in-water-in oil (O/W/O) and water-in-oil-in-water(12) Emulsions are stabilised by surfactants/proteins(167). Formulating products as emulsions enables mixing the ingredients into a combined system with dramatic effect on their properties, for example as eggs and oil are mixed into mayonnaise.

Most of metastable emulsions contain oil, water and a surfactant which protects emulsions from separation into two phases(167). In general foams are composed of bubbles dispersed in a liquid, however the foam under consideration below consists of gas bubbles, an aqueous surfactant phase and dispersed oil droplets(167). As foams with oil droplets are notoriously unstable, emulsification is an interesting way of creating stable foams of various oil volume fractions(13,14).

These types of foams with oil are a commonplace in a wide range of products including food foams, pharmaceuticals, cosmetics, pulp and paper and water treatment processes where emulsions are used for the production of more stable foams and as antifoams(11). Food foams such as whipped cream, aerated deserts and mousses contain natural surfactants such as proteins (eggs or casein), polysorbates or carbohydrates which act as stabilisers increasing foam stability by significantly decreasing the drainage rate(11,45,168).

However, the effect of some types of oil or liquid fat droplets that surround air bubbles in food foam products can reduce or eliminate foam stability. Storage, handling and processing of these systems depend on their stability. Heating or freezing of food foams could cause destabilisation and decrease of shelf-life. Their rate of draining, disproportionation and coalescence is pivotal for their quality, textural behaviour and mouth feel(46).

In the pharmaceutical industry several foamed emulsions have been created for the effective delivery of active ingredients and controlled release for topical and oral applications for the provision of therapeutic benefits(11,12). The rheological properties of foamed emulsions must be controlled to suit the nature of a specific application.

In all of our investigated systems emulsion droplets surround the bubbles. A captured microscope image of SG10 emulsion (see the definition below) is shown in Fig.7.1.

Ross(169) described the mechanism of destabilisation based on two coefficients: the spreading and entering coefficients which are functions of the aqueous and oil phase surface tensions. Koczo et al(13) investigated the interaction between oil drops and foam lamella. They performed experiments of foam drainage in the presence of oil and showed that the presence of emulsified oil increased foam stability only if the pseudo emulsion film (the film between the oil droplet and the air/water interface) is stable. It was stated that when this film is stable oil droplets accumulate in the plateau borders (PBs) leading to hydrodynamic resistance(13) . At high packing fractions well stabilised drops have been shown to arrest foam drainage, until shear(170,171) restarts the drainage.

In a more recent experimental study Schneider et al(14) investigated foamed emulsion drainage and evaluated gas, liquid and oil volume fractions in the foam by a combination of electrical conductivity and surface photography. The authors emphasised the complexity of interactions between air bubbles and oil droplets and the necessity of further experimental and theoretical investigation of all parameters that affect the drainage process of foamed emulsion systems(14).

Usually two different scenarios for boundary condition at liquid-air interface are used: (i) Poiseuille flow (non-slip condition) or (ii) a plug flow (free slip condition)(40). The lifetime of foams and emulsions varies depending on the type of surfactant. Foam distraction occurs as a result of drainage, coarsening and coalescence(172,173). Viscosity effects in foam drainage have been previously studied in other types of foams made from non-Newtonian solutions (174,175): the transition from the regime with rigid surfaces to the regime with fluid surfaces was observed by increasing the viscosity of the bulk and bubble radius(174,175).

Below a surface viscosity of the foamed emulsion is used. The relation between the surface and bulk viscosities is characterised by Boussinesq number.

Boussinesq number, expressed as a function of surface viscosity, $B_{oussinesq} = \frac{\mu_s}{\mu R_{pb}}$, where R_{pb} is the Plateau border radius, μ is the liquid dynamic viscosity, μ_s is the surface shear viscosity quantifies the role of surface and bulk dissipations(174,175). The values of the inverse Boussinesq number can predict the boundary conditions and the flow type (176).Foam drainage of conventional two-phase foams consisting of gas bubbles and liquid surfactant solution have been previously investigated both experimentally and theoretically for various cases (31,33,37,90,133).

Drainage of foams placed on porous substrates has also recently been theoretically investigated by Arjmandi-Tash et al(19). This has been followed by a theory of foam drainage when placed on a wettable thin porous layer(40) where the rate of foam drainage and imbibition inside the porous layer

and other characteristics of the process were theoretically predicted and compared with experimental observations.

Drainage is driven by joint action of capillarity and gravity forces, and the liquid flows through both Plateau borders and nodes. As liquid drains within the foam body alterations in the local liquid volume fraction are created(40). Understanding changes in the local liquid fraction are important as it has a strong effect on the further evolution and stability of the foams.

Below a mathematical model of foamed emulsion drainage is developed assuming that the composition of the emulsion remains constant (no creaming of emulsion), this is true during the first stage of the drainage(14). Experimental observations of foam height, drained liquid layer and liquid volume fraction evolutions in time are compared with model predictions.

For the derivation of the model of foam drainage the following assumptions are adopted: (a) the main part of the liquid volume is located inside Plateau borders and the dry foam approximation is used for the drainage equations. It is assumed that the thickness of the foam layer at the bottom of the foam where Plateau border description is not applicable is thin as compared with the total foam height; (b) surface viscosity is taken into account, which results in an "effective slip" at the liquid-air interface.

The developed analytical model is capable of describing the drainage process of these multiphase complex systems by considering mobile surfaces and taking into account the presence of surface viscosity(142) on the liquid-air interfaces.

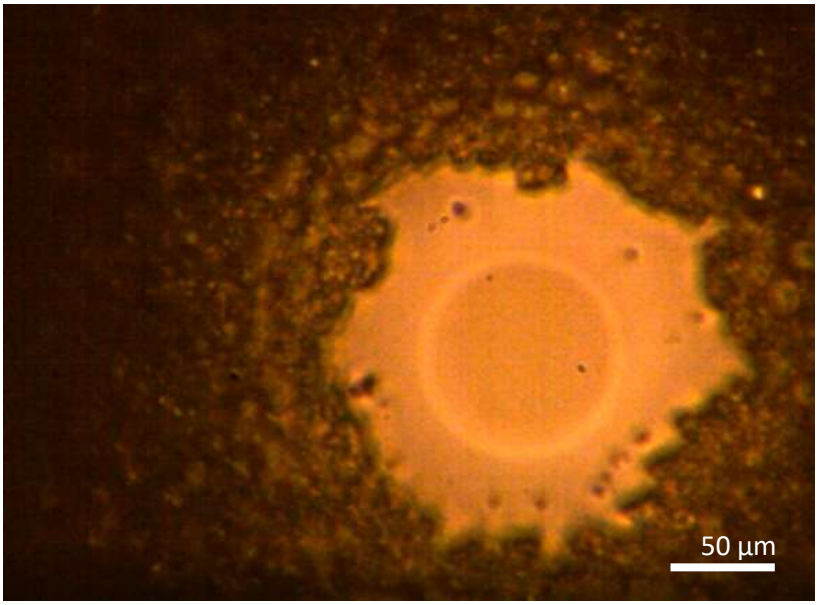

Figure 7. 1: Captured microscope image of a SG10 foamed emulsion (captured during the experiments). A gas bubble is surrounded by emulsified oil droplets of smaller diameter concentrated at the gas/liquid interface. Source: (15)

7.2. Materials and Methods

Emulsions of 30g/l sodium dodecyl sulphate (SDS) from Fisher stores, and rapeseed oil from Co-op are prepared using the double syringe method(177). For the preparation of each emulsion, SDS solution and rapeseed oil are passed from one syringe into the other through a plastic tube of 4mm internal diameter and 224 mm length leading to thorough mixing. The procedure is repeated until the mixture has been passed through the tube twenty times. Four different emulsions were prepared, and the proportions of each component are shown in table 7.1.

Table 7. 1: Proportions of 30g/l SDS and rapeseed oil used for each investigated emulsion. Source:(15)

Emulsion	Volume of SDS solution (ml)	Volume of Rapeseed oil (ml)	Oil volume fraction
SG10	45	5	0.1
SG20	40	10	0.2
SG30	35	15	0.3
SG40	30	20	0.4

The emulsions are deposited into a foam column, which has 19 capillaries at the bottom for bubbling gas to create bubbles with an internal diameter of 0.18mm. The foamed column used had an internal diameter of 3.8cm. Electrodes were connected with the foam column at various heights for measurements of the resistance [Ω].

Compressed air is injected into the system with a flow rate of 50L/min, creating foam within 2-4sec allowing measurements of the foam height, drained liquid height at the bottom and resistance time evolutions. The recorded resistance values [Ω] are then converted to conductivity values [S/m] and in turn in relative conductivity [dimensionless] by dividing with the conductivity of the emulsion used for foaming. This allows the liquid volume fraction to be calculated based on the following equation of relative conductivity σ versus liquid volume fraction φ at various heights of the foam column(164):

$$\sigma = \frac{1}{3}\left(\varphi + \varphi^{3/2} + \varphi^{2}\right)$$

The relative conductivity of a liquid foam relates to liquid volume fraction, indicating that for each conductivity value there are three possible solutions. The polynomial is extracted based on experimental data for a variety of surfactants. As liquid volume fraction falls between 0-1, a single value of liquid volume fraction is obtained for each conductivity(164).

7.3. Theory and Mathematical model

Let us consider foam composed of bubbles of uniform size and produced in a column of height H (Fig. 7.2). Drainage occurs in the vertical direction along the co-ordinate axis z directed downward, with z=0 at the top of the column. Time evolutions of the foam height and free liquid under the foam are $H_f(t) = H - H_1(t)$ and $H_l(t) = H - H_2(t)$, respectively (Figure 7.2). This means that changes in $H_f(t)$ are caused only by a decrease of the foam volume through coarsening or coalescence and not because of liquid drainage. It is assumed below that the bubble radius, R_b, increases over time, which is caused by coarsening, which for dry foams evolves as follows:

$$R_b(t) = R_{b0} + A\sqrt{t}, \tag{7.1}$$

where R_{b0} is the initial bubble radius and A is a constant(178).

Eq. (7.1) can be rewritten as:

$$R_b(t) = R_{b0}\left(1 + \sqrt{\frac{t}{t^*}}\right) \tag{7.2}$$

where t^* is a characteristic time of coarsening.

Below t^* will be calculated based on experimental data. Initial bubble radius has been measured at the beginning of foam formation by measuring bubble diameter of a sufficient number of bubbles (60-100) in the same area of the foam body for each investigated foamed emulsion and analysed using Image J. R_{b0} corresponds to the average value obtained. Bubble radius was also evaluated and measurements have been obtained for several time intervals during drainage process.

It is assumed that the dissipation occurs in the Plateau borders only and the contribution of the liquid flow in the films and nodes is neglected. Calculations show (see below) that the region at the bottom of the column where this approach is not applicable is thin as compared with the column height and can be neglected.

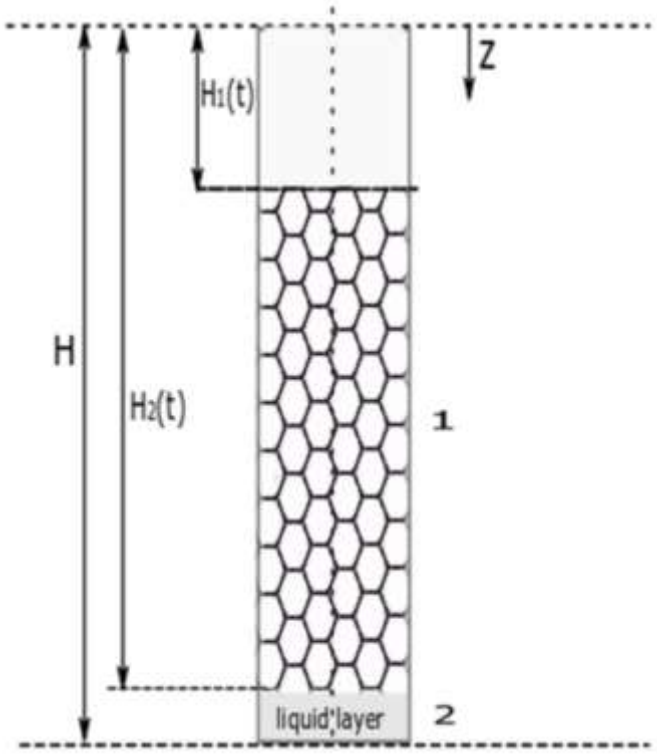

Figure 7. 2: Schematic presentation of the foam placed in a foam column . 1 – foam; 2 –liquid layer built at the bottom boundary resulting from drainage. Source: (15)

As shown in Figure 7.2, $z = 0$ is at the top of the foam column. It was determined in References(179,180) (and shown below) that in the case under consideration the presence of oil results in foaming solutions are non-Newtonian power-law liquids, which show a shear-thinning behaviour (please refer to section 3 of Appendix 7A). Based on our experiments the effective viscosity decreases with increasing shear rate for all investigated systems corresponding to non-Newtonian fluids. We assume that the emulsion does not evolve inside the foam, so that it flows as a shear-thinning fluid. For a power-law liquid dependence of the effective viscosity, μ_{eff}, on applied shear rate is given by the well-known Ostwald–de Waele relation:

$$\mu_{eff} = k\dot{\gamma}^{n-1} \qquad (7.3)$$

where k is ‘‘flow consistency index’’, n is the ‘‘flow behavior index’’ and $\dot{\gamma}$ is the shear rate. Please refer to the appendix for experimentally observed values for *k and n.*

A velocity profile for flow of a power-law fluid in a pipe of radius *R* with no-slip boundary condition is given by the following expression(181):

$$u(r) = \frac{n}{n+1}\left(\left|\frac{dP}{dz}\right|\frac{1}{2k}\right)^{1/n}\left(R^{1+1/n} - r^{1+1/n}\right), \quad (7.4)$$

where $\frac{dP}{dz}$ is the pressure gradient. According to Eq. 7.4, the average velocity, V, in a circular tube of cross-sectional area of A, identical to that of actual Plateau border, is determined as follows:

$$\mathrm{V} = \frac{n}{3n+1}\frac{1}{\pi^{1/2+1/(2n)}}\left(\left|\frac{dP}{dz}\right|\frac{1}{2k}\right)^{1/n} A^{1/2+1/(2n)}. \quad (7.5)$$

According to Wang and Narsimhan, (2006) the average velocity in the actual Plateau border geometry, v , is related to that given by Eq. 7.5 as (142):

$$v = c \cdot V, \quad (7.6)$$

where the coefficient c is (142):

$$c = a(n) + \beta \cdot b(n). \quad (7.7)$$

In the above equation (7.7) β is dimensionless inverse surface viscosity(142,182) and $a(n)$ and $b(n)$ are functions of flow behaviour index, n, and their values are presented in Table 7.2. Flow behaviour index is a rheological property which indicates the degree of non-Newtonian characteristics of an emulsion(183). For $0 < n < 1$ the fluid is characterised as Pseudoplastic. i.e the apparent viscosity decreases as the shear rate increases, while $n = 1$ indicates a Newtonian behaviour. In Eq. (7.7) surface viscosity is taken into account and it is assumed that the bubble interfaces are mobile.

Table 7. 2: Values of velocity coefficient for different values of flow behavior index, n (142). Source:(15)

n	1	0.8	0.6865	0.6	0.5	0.35
$a(n)$	0.5169	0.4851	0.459	0.434	0.3922	0.2942
$b(n)$	0.5446	0.5337	0.5248	0.5165	0.4999	0.4548

By incorporating Eq. (7A.16), Eq. (7A.18) mentioned in the Appendix 7A is rewritten as:

$$\frac{d\varphi}{d\tau}+\frac{d}{d\zeta}\left[\frac{2\cdot\sqrt{B_0}\cdot\left(1+B\cdot\sqrt{\varphi/(1-\varphi)^{2/3}}\right)^{n}\cdot\left(1+\lambda\sqrt{\tau}\right)^{n+1}\varphi^{\frac{3n+1}{2}}}{(1-\varphi)^{1/3}}\right.$$
$$-\left(1+B\cdot\sqrt{\varphi/(1-\varphi)^{2/3}}\right)^{n} \qquad (7.8)$$
$$\left.\cdot\left(1+\lambda\sqrt{\tau}\right)^{\mathrm{n}}\frac{\varphi^{\frac{3n-2}{2}}(1-\frac{\varphi}{3})}{(1-\varphi)}\frac{\partial\varphi}{\partial\zeta}\right]^{1/n}=0$$

where φ is liquid volume fraction, $\zeta \rightarrow z/z_0$, $\tau \rightarrow t/t_0$ dimensionless variables,

$\lambda=\sqrt{\frac{t_0}{t^*}}$, where t_0 *and* z_0 the characteristic time and length scales, respectively expressed by Eq. (7A.15) and Eq. (7A.17) in the Appendix, n the flow behaviour index, R_b the bubble of radius, $C^2 \approx 0.161$, C_1 a geometrical coefficient, $C_1 = 4\pi/(3n_p\delta \approx 0.378-0.972)$, where δ=0.718-1.108 and n_p=6-10, for a foam with structures between bcc (body-centred cubic) and fcc (face-centred cubic) and bubbles of the same size.

$B=\frac{b\,\mu\,R_b}{\alpha\mu_s}\sqrt{\frac{C_1}{C^2}}$ where, μ_s the surface viscosity. Surface viscosity, μ_s, is taken into account, according to Ref(142) which results in an "effective slip" at the liquid-air interface.

B_0 is the corresponding Bond number given by Eq. (7.9)

$$B_o=\frac{\Delta p_{grav}}{\Delta p_{cap}}=\frac{\rho g\frac{C_1^{1/2}}{C}R_{bo}}{\frac{\gamma}{\frac{C_1^{1/2}}{C}}}=\frac{C_1}{C^2}\frac{\rho g R_{bo}^2}{\gamma}. \qquad (7.9)$$

If the parameter <<1 in Eq. (7A.16) then coarsening can be neglected during the drainage.

For a fresh foam produced in the foam column, the liquid volume fraction profile is initially uniform, that is,$\varphi(\zeta,\tau=0)=\varphi_{\mathrm{i}}$ (84,178).

Boundary conditions

During drainage the liquid from the top of the foam drains to the lower parts of the foam. Therefore, the liquid volume fraction at the top, F_{top}, decreases over time. There is a critical liquid volume fraction, φ_{cr} below which the coalescence/bubble burst begins(145,184).

The value of this critical liquid volume fraction is a function of the nature of the surface-active substances (polymer and/or surfactant) and their concentration and also by a possible contribution of disjoining pressure action(91,185,186).

However, in Ref. (145) a mechanism based on a critical film dilatation is proposed for the onset of coalescence and critical liquid content in draining foams, which we will adopt in our model below. Based on the theory of critical liquid volume fraction, there are two possible scenarios for the boundary condition at the top of the foam (i.e. $z = H - H_1$ or $\zeta = \frac{H}{z_0} - \zeta_1$):

(i) If the liquid volume fraction at $z = H - H_1$ is higher than φ_{cr}, then there is no bubble collapse at the top of the foam (i.e. $\frac{dH_1}{dt} = 0$) and the top boundary condition is zero liquid flux:

$$Q(H_1, t) = 0 \qquad (7.10)$$

or in dimensionless form:

$$Q(\zeta_1, \tau) = 0 \qquad (7.11)$$

(ii) If the foam continues to dry and the liquid volume fraction at $z = H - H_1$drops to the value of φ_{cr}, then the bubbles at the top of the foam start to rupture and the height of the foam decreases from the top (i.e. $\frac{dH_1}{dt} > 0$). In this case the boundary condition at the top of the foam is a constant liquid volume fraction:

$$\varphi(H_1(t), t) = \varphi_{cr}$$

Or in a dimensionless form:

$$\varphi(\zeta_1(\tau), \tau) = \varphi_{cr} \qquad (7.12)$$

and the rate of foam collapse, $\frac{dH_1}{dt}$, can be expressed according to the following equation(91):

$$\frac{dH_1(t)}{dt} = \frac{1}{\varphi_{cr}} Q(H_1, t), \qquad (7.13)$$

or in dimensionless form:

$$\frac{d\zeta_1(t)}{dt} = \frac{1}{\varphi_{cr}} Q(\zeta_1(\tau), \tau). \quad (7.14)$$

After the onset of the drainage, the boundary condition at the bottom of the foam is a constant liquid volume fraction, φ_{cr}~0.36, which corresponds to random packing limit for spherical particles in three dimensions(91). However, as we consider a uniform initial liquid volume fraction along the foam height (i.e.$\varphi_{cr} << \varphi(\zeta, \tau = 0) = \varphi_i < \varphi_{max}$, the boundary condition at the bottom of the foam should be zero liquid flux during a very early stage of the drainage until the liquid volume fraction at the bottom of the foam reaches $\varphi_{max} = 0.36$.

As the foam drains the solution accumulates under the foam and the interface between the foam and emulsion, $z = H_2$, moves up. The rate of this movement can be found using a mass conservation law of the emulsion within the whole column (see Appendix 7A):

$$\frac{dH_2(t)}{dt} = -\frac{1}{1-\varphi_{max}} Q(H_2(t), t), \quad (7.15)$$

or in dimensionless form:

$$\frac{d\zeta_2(t)}{d\tau} = -\frac{1}{1-\varphi_{max}} Q(\zeta_2(\tau), \tau). \quad (7.16)$$

The above equations could be easily deduced from the fact that the product of the front velocity with the density difference of the two sides of the front is equal to the flux.

7.4 Results and Discussion

The model of foam drainage described by dimensionless Eq. (7.8) have been solved using COMSOL software, finite element method on a one-dimensional regular grid. The derived equations for foam drainage were solved using the boundary conditions described in Section 7.3 to obtain the evolution of liquid volume fraction inside the foam. The experimentally obtained data for investigated emulsions $n, \mu_s, k, R_{b0}, \gamma, \rho$, and initial liquid volume fraction, φ_i, have been incorporated in model calculations as shown in (Table 7.3). Values of calculated model parameters t_0, z_0, Bo, and B are listed in Table7. 4. The values of the model calculated parameters t_0 *and* z_0 are derived based on Eq. (7A.17), Eq. (7A.15) respectively presented in Appendix 7A. The corresponding Bo is based on Eq. (7.9) mentioned above in section 7.3 and is dependent on the initial bubble radius, R_{b0}, the emulsion density, ρ, and the liquid-air interfacial tension, γ, all experimentally obtained parameters presented in table 7.3.

The low values of Bo mentioned in table 7.4 indicate that surface tension dominates towards gravitational forces, which has a pronounced effect on the rate of drainage.

Table 7. 3: Values of experimentally obtained parameters: flow behavior index, n, flow consistency index,k,density, ρ ,liquid-air interfacial tension, γ,initial bubble radius, R_{b0}, initial liquid volume fraction, φ_i, and surface viscosity, μ_s, for all investigated foaming solutions. Source:(15)

	n	k	ρ[kg/m^3]	γ [N/m]	R_{b0} (m)	φ_i	μ_s [Pa s](187)
SG10	0.69	0.0151	991	0.029	0.00043	0.15	0.0001
SG20	0.555	0.0276	982	0.029	0.00045	0.15	0.0001
SG30	0.515	0.0522	973	0.029	0.00048	0.15	0.0001
SG40	0.569	0.0788	964	0.029	0.00047	0.15	0.0001

Table 7. 4: Calculated model parameters: Bond number, B_o,characteristic time, t_0, characteristic length, z_0, and parameters t^* and B for all investigated foaming solutions Source:(15)

	B_o	t_0	z_0	t^*	B
SG10	0.32393	0.27966	0.0017271	1287.7	3.3464
SG20	0.35389	0.17622	0.001735	696.19	0.96784
SG30	0.35065	0.36746	0.001743	2853	2.0939
SG40	0.3151	1.0942	0.0017512	2434.2	2.5151

The theoretical predictions and experimental measurement of the time evolution of both the foam height, $H_f(t) = H - H_1(t)$ and free liquid layer $H_l(t) = H - H_2(t)$ are shown in Fig. 7.3 for the four different foamed emulsions studied . All experimentally obtained values have been normalised and fitted in polynomials using MATLAB software for the determination of average foam height and free liquid layer values as a function of time for comparison with simulation results.

The average initial foam heights determined were 0.216m, 0.21569m, 0.2223m and 0.222m, for systems SG10, SG20, SG30 and SG40 respectively.

There is no measurable change in the height of the foam as captured both by the experiments and simulations during the timescale of the study. Liquid drainage out of the foam can be measured and the amount of liquid drained is higher with the highest concentration of oil SG40, again shown both by experiments and simulations. This is because of the highest viscosity of the sample.

When liquid volume fraction at bottom of the foam (at the porous substrate interface) reaches the maximum value, $\varphi_{\max}$, a free liquid layer starts to accumulate at the bottom of the foam column. Figures 7.3(a)-7.3(d) show that there is a very good agreement of the dynamics of the foam height evolutions and free liquid layer accumulation both qualitatively and quantitatively during all stages of the drainage process.

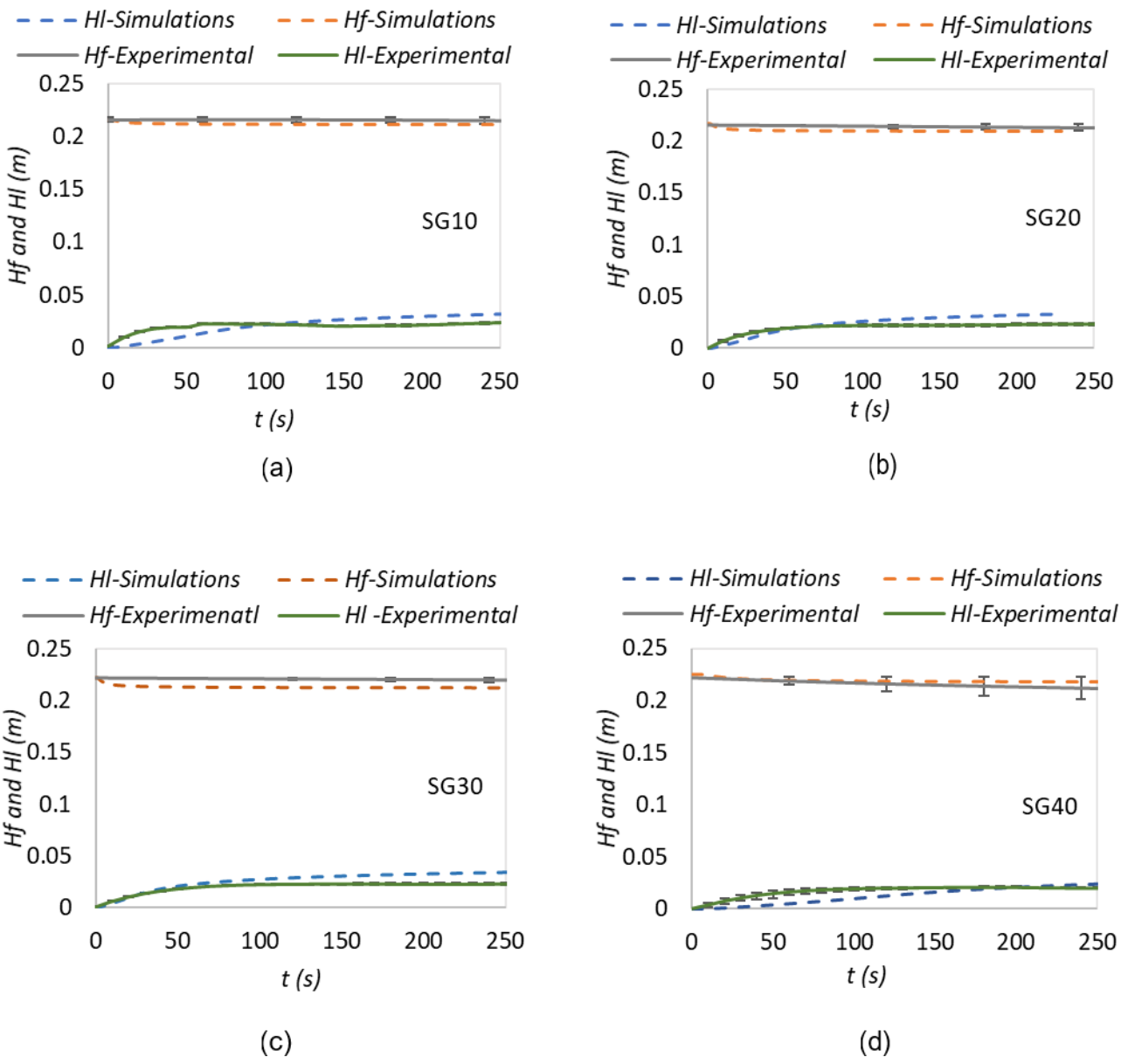

Figure 7. 3:Time evolutions of foam height, $H_f(t) = H - H_1(t)$ and free liquid layer $H_l(t) = H - H_2(t)$ for Foamed emulsion made of foaming emulsion (a) SG10 (b) SG20 (c) SG30 and (d) SG40. Source:(15)

Experimental evaluation of liquid volume fraction both at top of the foam boundary and at the foam/liquid layer interface through measurements of liquid conductivity are shown in Figure 7.4 for the four foaming solutions: SG10, SG20, SG30 and SG40.

The liquid fraction at the top of the foam remains relatively high, which is probably why there is no coalescence observed and there is almost no change in the foam height in Figure 7.3.

The initial rapid drainage predicted by simulation results and shown in Figures 7.3(a)-7.3(d) which corresponds to the initial increase of liquid volume fraction from $\varphi_i = 0.15$ to $\varphi_{max} = 0.36$ was not

possible to observe experimentally due to the evolution of the liquid fraction during generation(188) .Therefore, experimentally observed initial liquid volume fraction at the top of the foam was lower than φ_i corresponding to a dry foam with a value shown in Figure 7.4 for each investigated system. During the experiments, the initially observed liquid volume fraction at the foam/liquid layer interface had already reached the theoretically predicted maximum value, φ_{max}. Drainage starts immediately before the initial foam height is reached leading to very dry foam at the top and wet foam at the bottom.

The experimental results are reasonable when considering immediate drainage while foam is being generated. To observe the theoretically predicted behaviour described by model calculations, as presented in Figure 7.4 a uniform foam is required which would mean producing foam very quickly or limiting the effect of gravity,(e.q drainage under microgravity conditions) in an attempt to capture the foamed emulsion behaviour at the very beginning of the drainage process.

Regardless the absence of experimental measurements of liquid volume fraction at the top and bottom boundaries of the foam for the initial short rapid drainage period theoretically predicted, comparison between experimental results and model calculations are in reasonable agreement as shown in Figures 7.4(a)-7.4(d).

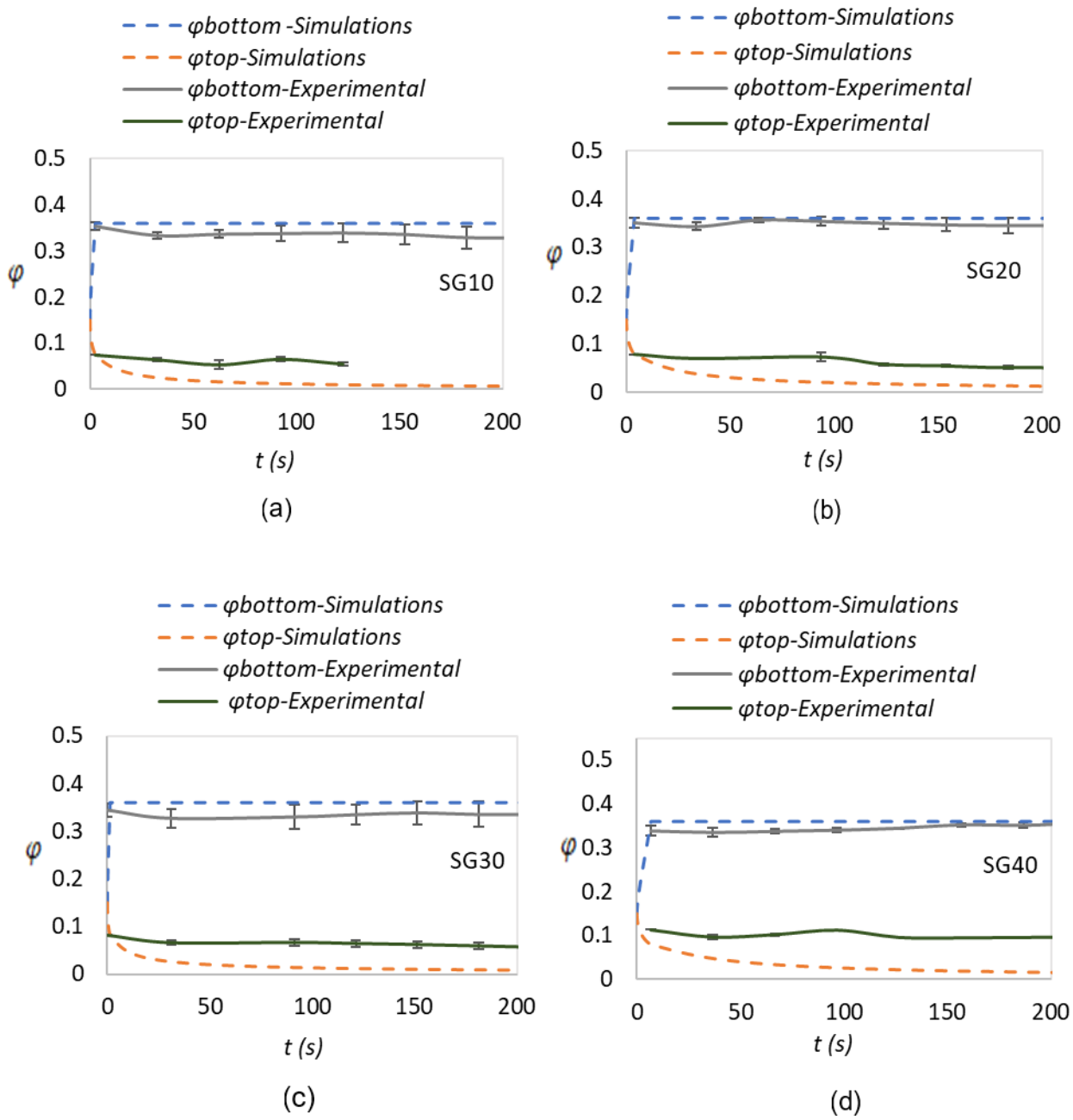

Figure 7. 4: Time evolutions of liquid volume fraction of the top and bottom boundaries for Foamed emulsion made of Foaming emulsions (a) SG10; (b) SG20; (c) SG30 and (d) SG40. Source:(15)

7.5 Conclusions

These types of systems are frequently used in a variety of cleaning, food and cosmetic products and the developed theory of foam drainage will find a wide range of industrial applications. The drainage of foamed emulsions of various oil volume fractions is experimentally investigated. The drainage of emulsion foam is investigated using mixture of sodium dodecyl sulphate and oil, which were prepared using the double syringe method. In the course of drainage both the foam height and the thickness of the free liquid layer accumulated at the bottom of the foam were measured. A mathematical model was developed, taking into account of both the non-Newtonian behaviour of the foamed emulsion and surface viscosity. The model is capable of describing the time evolutions of both the foam height and the thickness of the drained layer. The model predictions are compared with experimental observations of the drainage process for four different foamed emulsion systems of SDS surfactant and rapeseed oil generated using the double syringe emulsification technique and a bubbling through capillaries in a foam column. Comparison showed a reasonably good agreement between the theory predictions and experimental observations. Drainage is observed during foam formation before the initial foam height is reached leading to dry foam at the top and wet foam at the foam/liquid layer interface. A free liquid layer starts to accumulate at the bottom boundary of the foam when the maximum value of liquid volume fraction, $\varphi_{\max}$, is reached at the bottom.

Nomenclature 7

α	Velocity coefficient
A	Plateau border cross-sectional area, m^2
Bo	Bond number
c	Velocity coefficient
C	Geometrical coefficient
C_1	Geometrical coefficient
f_n	Drag coefficient
g	Gravity acceleration, m/s^2
H	Column height, m
H_f	Foam height, m
H_l	Drained liquid height, m
H_l	Position of the foam
H_1	Position of the top of the foam boundary
H_2	Position of foam/liquid interface boundary
ζ	The dimensionless vertical coordinate
ζ_1	The dimensionless position of the foam boundary,
ζ_2	The dimensionless position of the foam/liquid layer interface boundary,
ζ_{1e}	The dimensionless position of the foam boundary at equilibrium,
k	Flow consistency index, Pa s^n
μ_{eff}	Effective viscosity [Pa s]
$\dot{\gamma}$	Shear rate, s^{-1}
l	Length of the Plateau border, m
n	Flow behaviour index
n_p	Number of plateau borders per bubble
N	Number of bubbles per unit volume, $1/m^3$
σ	Relative conductivity
$\frac{dP}{dz}$	Pressure gradient
p	Pressure, Pa

P	Modified pressure, Pa
q_{pb}	Flow rate in Plateau border, m^3/s
Q	Total volumetric flux through the Plateau borders, m/s
φ	Liquid volume fraction
R	Radius, m
R_b	Radius of bubbles, m
R_{Pb}	Curvature radius of Plateau border, m
t	Time, s
t_0	Characteristic time scale, s
v	Average velocity in Plateau border, m/s
V	Average velocity in a circular tube, m/s
z	Co-ordinate axis, m
z_0	Characteristic length scale, m
φ_i	Initial liquid volume fraction
φ_{cr}	Critical liquid volume fraction
φ_{max}	Maximum liquid volume fraction
ρ	Emulsion density kg/m^3
ρ_{oil}	Oil density kg/m^3
γ	Liquid-air interfacial tension N/m
Boussinesq	Boussinesq number

Appendix 7A

7A.1 Mathematical model

We can substitute Eq. 7.5 into Eq.7. 6 of the main text and multiply by the Plateau border cross-section to obtain the flow rate, q_{pb}, in a Plateau border as follows:

$$q_{pb} = c\frac{n}{3n+1}\frac{1}{\pi^{1/2+1/(2n)}}\left(\left|\frac{dP}{dz}\right|\frac{1}{2k}\right)^{1/n} A^{3/2+1/(2n)}. \quad (7A.1)$$

The quantity P in Eqs. (7.4,7.5 and 7A.1) is referred to as modified pressure and it is an abbreviation for the sum of the capillary pressure and gravitational contributions. Accordingly, the driving force for Plateau border drainage $\frac{dP}{dz}$ is:

$$\left|\frac{dP}{dz}\right| = \rho g + \frac{d}{dz}\left(\frac{\gamma}{R_{pb}}\right), \quad (7A.2)$$

where γ is the liquid-air interfacial tension, R_{pb} is the radius of curvature of Plateau border; ρ and g are the liquid density and the gravity acceleration, respectively. According to (164) the cross-sectional area of a plateau border can be written as:

$$\mathrm{A} = \frac{V_b}{n_p \cdot l}\frac{\varphi}{(1-\varphi)} = C^2 R_{pb}^2 = \mathrm{C}_1 \cdot R_b^2 \cdot \frac{\varphi}{(1-\varphi)^{2/3}}, \quad (7A.3)$$

where φ is liquid volume fraction, V_b is the volume of a bubble of radius R_b, l is the length of the Plateau border, n_p is the number of plateau borders per bubble; $C^2 \approx 0.161$, C_1 a geometrical coefficient, $C_1 = 4\pi/(3n_p\delta \approx 0.378 - 0.972)$ for a foam with structures between bcc (body-centred cubic) and fcc (face-centred cubic) and bubbles of the same size.

The length of a plateau border is given by Eq. (7A.4) (164):

$$\mathrm{l} = \delta \cdot R_b \cdot (1-\varphi)^{-\frac{1}{3}}, \quad (7A.4)$$

where δ=0.718-1.108 and n_p=6-10(164).

Hence, the volume of a bubble with radius R_b can be expressed as:

$$V_b = C_1 \cdot R_b^2 \cdot n_p \cdot l \cdot \frac{(1-\varphi)}{(1-\varphi)^{2/3}} = C_1 \cdot R_b^2 \cdot n_p \cdot \delta \cdot R_b \cdot (1-\varphi)^{-1/3} \cdot \frac{(1-\varphi)}{(1-\varphi)^{2/3}} \quad (7A.5)$$
$$= C_1 \cdot R_b^3 \cdot n_p \cdot \delta$$

Substituting Eq.(7A.3) and Eq.(7A.2) into Eq.(7A.1) results in the following expression of flow rate in a plateau border:

$$\mathrm{q}_{pb} = c\,\frac{n}{3n+1}\,\frac{1}{\pi^{\frac{1}{2}+1/(2n)}}\,\frac{1}{2^{1/n}}\left(\frac{\rho\cdot \mathrm{g}}{k}\cdot A^{\frac{3n+1}{2}} - \frac{C\gamma}{2\mathrm{k}}\cdot A^{\frac{3n-2}{2}}\cdot\frac{\partial A}{\partial z}\right)^{1/n}. \quad (7A.6)$$

If we define:

$$\frac{1}{f_n} = \left(c\,\frac{n}{3n+1}\,\frac{1}{\pi^{\frac{1}{2}+1/(2n)}}\,\frac{1}{2^{1/n}}\right)^n. \quad (7A.7)$$

Then, from E.q (7.5) and Eq. (7.6) in the main text it is possible to conclude:

$$\mathrm{q}_{pb} = \left(\frac{\rho\cdot \mathrm{g}}{k\cdot f_n}\cdot A^{\frac{3n+1}{2}} - \frac{C\gamma}{2\mathrm{k}\cdot f_n}A^{\frac{3n-2}{2}}\frac{\partial A}{\partial z}\right)^{1/n} \quad (7A.8)$$

The total volumetric flux through the plateau borders is given by Eq. (7A.9), Ref. (91)(189):

$$Q = \frac{4}{15}\cdot N\cdot n_p\cdot R_b\left(\frac{\rho\cdot \mathrm{g}}{k\cdot f_n}\cdot A^{\frac{3n+1}{2}} - \frac{C\gamma}{2\mathrm{k}\cdot f_n}A^{\frac{3n-2}{2}}\frac{\partial A}{\partial z}\right)^{1/n}, \quad (7A.9)$$

where N is the number of bubbles per unit area and is given by Eq.(7A.10):

$$\mathrm{N} = \frac{(1-\varphi)}{V_b} = \frac{(1-\varphi)}{C_1\cdot R_b^3\cdot n_p\cdot\delta}. \quad (7A.10)$$

The mass conservation law for liquid inside plateau border channels is:

$$\frac{\partial \varphi}{\partial \mathrm{t}} + \frac{\partial Q}{\partial z} = 0. \tag{7A.11}$$

Substituting Eq. (7A.9) into Eq. (7A.11) results in:

$$\frac{\partial \varphi}{\partial \mathrm{t}} + \frac{\partial\left(\left(\frac{4}{15}\right)^n \cdot N^n \cdot {n_p}^n \cdot {R_b}^n \frac{\rho \cdot g}{k \cdot f_n} A^{\frac{3n+1}{2}} - \left(\frac{4}{15}\right)^n \cdot N^n \cdot {n_p}^n \cdot {R_b}^n \frac{C\gamma}{2k \cdot f_n} A^{\frac{3n-2}{2}} \frac{\partial A}{\partial z}\right)^{1/n}}{\partial z} = 0. \tag{7A.12}$$

Substitution of Eq. (7A.3) into Eq. (7A.12) gives:

$$\frac{\partial \varphi}{\partial \mathrm{t}} + \frac{\partial\left(\frac{{C_1}^{\frac{1}{2}} \cdot \rho \cdot g}{k \cdot a_n} \cdot {R_{b0}}^{n+1} \cdot \left(1+\sqrt{t/t^*}\right)^{n+1} \cdot \frac{\varphi^{\frac{3n+1}{2}}}{(1-\varphi)^{1/3}} - \frac{C \cdot \gamma}{2 \cdot \mathrm{k} \cdot a_n} \cdot {R_{b0}}^n \left(1+\sqrt{t/t^*}\right)^n \frac{\varphi^{\frac{3n-2}{2}}\left(1-\frac{\varphi}{3}\right)}{(1-\varphi)} \cdot \frac{\partial \varphi}{\partial z}\right)^{1/n}}{\partial z} = 0, \tag{7A.13}$$

where:

$$\frac{1}{a_n} = \left(c \cdot \frac{n}{3n+1} \cdot \frac{1}{\pi^{1/(2n)}} \cdot \frac{1}{2^{(1/n)-3}} \cdot \frac{1}{3^{3/2} \cdot 5} \cdot \frac{1}{\delta^{3/2}} \cdot \frac{1}{{n_p}^{1/2}}\right)^n =$$
$$\left(\alpha \frac{n}{3n+1} \frac{1}{\pi^{1/(2n)}} \frac{1}{2^{1/n-3} 3^{3/2}} \frac{1}{\delta^{3/2}} \frac{1}{{n_p}^{1/2}}\right)^n \left(1 + B\sqrt{\frac{\varphi}{(1-\varphi)^{2/3}}}\right)^n = \frac{1}{\beta_0}\left(1 + B\sqrt{\frac{\varphi}{(1-\varphi)^{2/3}}}\right)^n \tag{7A.14}$$

and $c = a(n) + \beta \cdot b(n) = \alpha + b\left(\frac{\mu R_{pb}}{\alpha \mu_s}\right) = \alpha\left(1 + B\sqrt{\frac{\varphi}{(1-\varphi)^{2/3}}}\right)$

where $B = \frac{b\,\mu\,R_b}{\alpha \mu_s}\sqrt{\frac{C_1}{C^2}}$.

In above equations interfacial mobility, through surface viscosity, μ_s, is taken into account, according to Ref.(142), which results in an “effective slip” at the liquid-air interface. Interfacial mobility is a surface rheological property describing the rheological behaviour of bubble surfaces. More specifically, the elastic modulii and viscocities will be small for a mobile surface and high for a rigid surface although this is not intrinsic(190).

Non-dimensionalisation of Eq.(7.A13) is undertaken as follows.

Let us introduce the following dimensionless variables and parameters:

$\zeta \to z/z_0, \tau \to t/t_0$

where,

$$z_0 = \sqrt{\frac{\gamma}{\rho \cdot g}}. \tag{7A.15}$$

And we can compare the characteristic time-scales of drainage and coarsening as:

$$\lambda = \sqrt{\frac{t_0}{t^*}} \tag{7A.16}$$

and:

$$t_0 = \left(\frac{{z_0}^{n+1} \cdot 2 \cdot k \cdot a_n}{{R_{b0}}^n \cdot C \cdot \gamma}\right)^{1/n} = \left(\frac{\left(\sqrt{\frac{\gamma}{\rho \cdot g}}\right)^{n+1} \cdot 2 \cdot k \cdot a_n}{{R_{b0}}^n \cdot C \cdot \gamma}\right)^{1/n} = \left(\frac{2 \cdot k \cdot \beta_0}{\gamma^{\frac{1-n}{2}} {R_{b0}}^n \cdot C \cdot (\rho g)^{\frac{n+1}{2}}}\right)^{1/n}, \tag{7A.17}$$

where

$$\frac{1}{\beta_0} = \left(\alpha \frac{n}{3n+1} \frac{1}{\pi^{1/(2n)}} \frac{1}{2^{1/n-3} 3^{3/2}} \frac{1}{\delta^{3/2}} \frac{1}{{n_p}^{1/2}}\right)^n$$

Substitution of equations (7A.16) and (7A.17) into (7A.13) results in:

$$\frac{\partial \varphi}{\partial(\tau)} + \frac{\partial\left(\left(\frac{t_0}{z_0}\right)^n \frac{C_1^{\frac{1}{2}} \cdot \rho \cdot g}{k \cdot a_n} \cdot {R_{b0}}^{n+1} \cdot \left(1+\sqrt{t/t^*}\right)^{n+1} \cdot \frac{\varphi^{\frac{3n+1}{2}}}{(1-\varphi)^{1/3}} - \frac{{t_0}^n}{{z_0}^{n+1}} \cdot \frac{C \cdot \gamma}{2 \cdot \mathrm{k} \cdot a_n} \cdot {R_{b0}}^n \left(1+\sqrt{t/t^*}\right)^n \frac{\varphi^{\frac{3n-2}{2}}\left(1-\frac{\varphi}{3}\right)}{(1-\varphi)} \cdot \frac{\partial \varphi}{\partial \zeta}\right)^{1/n}}{\partial(\zeta)} = 0 \quad (7A.18)$$

7A.2 Equilibrium profile

The equilibrium profile for liquid content inside the foam is reached when the gravity and capillary gradient forces equilibrate each other inside the foam. The equilibrium profile can be found by assuming zero liquid flux across the foam height. Integration of Eq. (7A.12) in this case using the boundary condition at the bottom of the foam, $\varphi(H_2(t), t) = \varphi_{max}$, results in:

$$\frac{2C_1^{1/2}\rho g R_b}{C\gamma}\int_{\zeta}^{2e} \partial z = \int_{\varphi_{eq}}^{\varphi_{max}} \varphi^{-\frac{3}{2}}(1-\varphi)^{-\frac{2}{3}}(1-\varphi/3)\partial\varphi \quad (7A.19)$$

And

$$\left(1-\varphi_e(z)\right)^{\frac{1}{3}}\varphi_e^{-\frac{1}{2}}(z) = (1-\varphi_{max})^{1/3}\varphi_{max}^{-1/2} + \frac{C_1^{\frac{1}{2}}\rho g R_b}{C\gamma}(H_{2e}-z). \quad (7A.20)$$

Eq.(7A.20) can be rewritten as the following dimensionless form:

$$\left(1-\varphi_e(\zeta)\right)^{\frac{1}{3}}\varphi_e^{-\frac{1}{2}}(\zeta) = (1-\varphi_{max})^{1/3}\varphi_{max}^{-1/2} + \sqrt{B_0}(\zeta_{2e}-\zeta). \quad (7A.21)$$

If $\zeta = \zeta_{1e}$ is substituted in the above equation (we suppose that ζ_{1e} is the dimensionless position of the top of the foam at equilibrium), then the equilibrium liquid volume fraction at the top of the foam can be deduced. The latter is a function of the foam height at equilibrium, $\zeta_{2e} - \zeta_{1e}$ and can be calculated as:

$$\left(1-\varphi_e(\zeta_{1e})\right)^{\frac{1}{3}}\varphi_e^{-\frac{1}{2}}(\zeta_{1e}) = (1-\varphi_{max})^{1/3}\varphi_{max}^{-1/2} + \sqrt{B_0}(\zeta_{2e}-\zeta_{1e}). \quad (7A.22)$$

The dependency of the equilibrium liquid volume fraction at the top of the foam on the foam height (according to Eq. (7A.21)) is schematically illustrated in Figure 7A.1. As shown in Fig. 7A.1, $\varphi_e(\zeta_{1e})$ increases to φ_{max} as the final foam height, $\zeta_{2e} - \zeta_{1e}$, decreases. Substituting $\varphi_e(\zeta_{1e}) = \varphi_{cr}$ in Eq. (7A.21) allows determining a critical foam height, λ_{cr}. This critical foam height is shown in Fig. 7A.1 where $\varphi_e(\zeta_{1e}) = \varphi_{cr}$.

If the initial foam height, $\zeta_2(\tau = 0) - \zeta_1(\tau = 0) = \zeta_{2i} - \zeta_{1i}$, is less than λ_{cr}, then over duration of the whole process the liquid volume fraction at the top of the foam remains above the φ_{cr} and the top part of the foam does not move, that is $\zeta_1(\tau) = \zeta_{1i}$. However, if $\zeta_{2i} - \zeta_{1i}$ is bigger than λ_{cr} then two possibilities can be predicted:

(1) over duration of the whole drainage process the liquid volume fraction at the top of the foam remains above the φ_{cr}, which is exactly the same as before,

(2) at some moment in time, τ_{cr}, $\varphi(\zeta_1, \tau_{cr}) = \varphi_{cr}$. After that moment the apparent boundary of the foam at the top starts to decrease according to Eq. (7.14) in the main text.

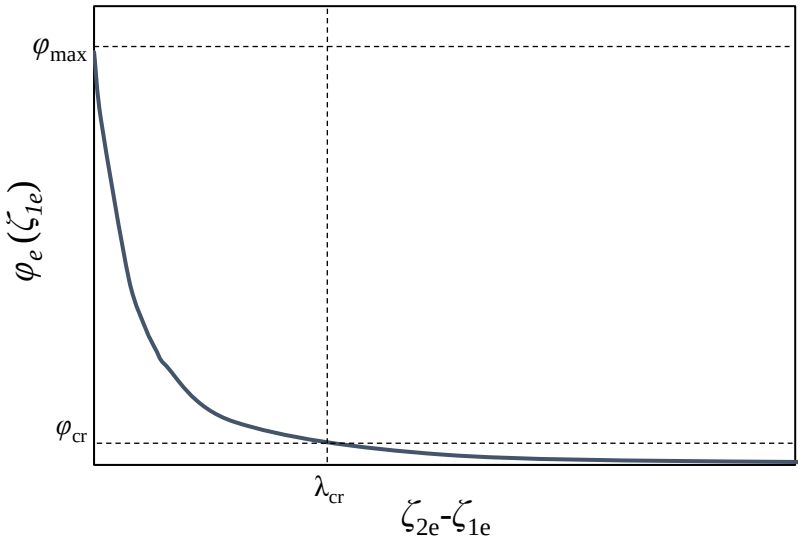

Figure 7A. 1:The dependency of the equilibrium liquid volume fraction at the top of the foam on the foam height. Source:(15)

Therefore, the foam height will decrease from both top and bottom boundaries while $\varphi(\zeta_1, \tau) = \varphi_{cr}$. This reduction in foam height continues until the time when it reaches equilibrium. According to Eq. (7A.22) and Fig. 7A.1, the final height of the foam in this case is fixed and equal to the critical foam height, $\zeta_{2e} - \zeta_{1e} = \lambda_{cr}$. Considering a mass conservation of the solution within the whole column at initial and final state of the process, it is possible to predict which of the two above mentioned possibilities will occur:

$$\varphi_{\mathrm{i}}(H_{2i} - H_i) + H - H_{2i} = \int_{H_{1e}}^{H_{2e}} \varphi_{\mathrm{e}}(H)dH + H - H_{2e}. \qquad (7A.23)$$

The left-hand side of the equation shows the initial amount of the liquid presented within the whole column while the right-hand side of the equation determines the final liquid content at equilibrium. Eq. (7A.23) can be rewritten as the following dimensionless form:

$$\varphi_{\mathrm{i}}(\zeta_{2i}-\zeta_{1i})-\zeta_{2i}=\int_{\zeta_{1e}}^{\zeta_{2e}}\varphi_{\mathrm{e}}(\zeta)d\zeta-\zeta_{2e}. \qquad (7A.24)$$

If we suppose that during the drainage the liquid volume fraction at the top of the foam drops to the value of φ_{cr} (i.e. the second possibility occurs), then as mentioned above$\zeta_{2\mathrm{e}}=\zeta_{1e}+\lambda_{\mathrm{cr}}$. Substituting this expression into Eq. (7A.24) results in:

$$\varphi_{\mathrm{i}}(\zeta_{2i}-\zeta_{1i})-\zeta_{2i}=\int_{\zeta_{1e}}^{\zeta_{1e}+\lambda_{cr}}\varphi_{\mathrm{e}}(\zeta)d\zeta-(\zeta_{1e}+\lambda_{cr}). \qquad (7A.25)$$

From the above equation:

$$(\zeta_{1e}-\zeta_{1i})=(\zeta_{2i}-\zeta_{1i})-\varphi_i(\zeta_{2i}-\zeta_{1i})+\int_{\zeta_{1e}}^{\zeta_{1e}+\lambda_{cr}}\varphi_{\mathrm{e}}(\zeta)d\zeta-\lambda_{cr}. \qquad (7A.26)$$

Since the foam height decreases from the top in this case, $\zeta_{1e}-\zeta_{1i}>0$ and the right-hand side of Eq. (7A.26) should be also a positive value:

$$\varphi_i<1-\frac{\lambda_{cr}-\int_{\zeta_{1e}}^{\zeta_{1e}+\lambda_{cr}}\varphi_e(\zeta)d\zeta}{(\zeta_{2i}-\zeta_{1i})}, \qquad (7A.27)$$

Or

$$\varphi_i<1-\frac{\lambda_{cr}-\int_{0}^{\lambda_{cr}}\varphi_e(\zeta)d\zeta}{(\zeta_{2i}-\zeta_{1i})}=\varphi_t, \qquad (7A.28)$$

A comparison between the values of φ_i and φ_t for each foaming solution can predict the state of the top of the foam during the drainage. The integral in Eq. (7A.28) (to find the values of φ_t) can be calculated numerically using Eq. (7A.21) for different values of B_o number and it is identical to the area under the equilibrium curve from $\zeta_{2e}-\zeta_{1e}=0$ to $\zeta_{2e}-\zeta_{1e}=\lambda_{cr}$ in Fig. A1. Therefore, in the case in which the initial foam height, $\zeta_{2i}-\zeta_{1i}$, is bigger than λ_{cr} the foam height decreases from the top boundary only if the condition specified in Eq. (7A.28) is satisfied for the value of initial

liquid volume fraction. Otherwise the liquid volume fraction at the top of the foam remains above the φ_{cr} and the top boundary of the foam does not move.

7A.3 Rheological properties of foamed emulsions-Obtained experimental data

7A.3.1 Effective Viscosity as a function of shear rate

Power law fits for the viscosity as a function of the shear rate $\mu_{eff} = k\,\dot{\gamma}^{n-1}$,

where k is ‘‘flow consistency index’’, n is the ‘‘flow behavior index’’ and $\dot{\gamma}$ is the shear rate.

Table 7A. 1: Values of experimentally obtained parameters: flow consistency index, k and flow behavior index, n for all investigated emulsions. Source:(15)

	k	n
SG10	0.0151	0.69
SG20	0.0276	0.555
SG30	0.0522	0.515
SG40	0.0788	0.569

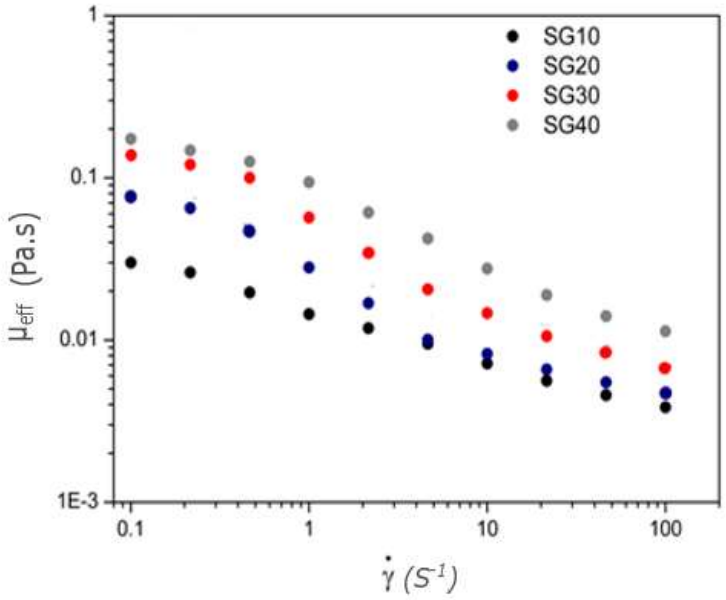

Figure 7A. 2:Effective viscosity [Pa.s] versus shear rate [S^{-1}] for emulsions SG10, SG20, SG30 and SG40. Source:(15)

7A.3.2 Density and surface tension of the liquids

Given the value of the Oil density, $\rho_{oil} = 0.91$ kg/m^3

we can calculate the emulsion density based on the following expression:

$$\rho = \phi\rho_{oil} + (1-\phi)\rho_{water,} \qquad (7A.29)$$

where, ρ_{oil} the oil density, ρ the emulsion density, ϕ the liquid volume fraction and ρ_{water} the water density.

Table 7A. 2: Values of calculated emulsion density, ρ, and liquid-air interfacial tension, γ. Source:(15)

	ρ [kg/m^3]	γ [N/m]
SG10	991	0.029
SG20	982	0.029
SG30	973	0.029
SG40	964	0.029

CHAPTER 8

Research Limitations

The studies presented in Chapters 3-7 have potential limitations related to the adopted methodologies and assumptions undertaken. Although careful consideration of all physicochemical factors and parameters has been taken during the design of our methodologies and development of mathematical models these limitations may have slightly influenced our estimates and conclusions. More specifically, the following research limitations can be identified for each Chapter:

1. Jacobi's condition of equilibrium was investigated and verified for the first time in Chapter 3. The action of the Disjoining/Conjoining pressure in the vicinity of the three-phase contact line was considered to act simultaneously with capillary pressure yielding the equilibrium profile of a droplet on a deformable substrate. A simplified linear Disjoining/Conjoining pressure isotherm was adopted to obtain an analytical solution which captures the essential properties of the real smooth isotherm: (i) it has a short range of surface forces action (ii) corresponds to partial wetting at the proper selection of parameters, (iii) corresponds to stable thin liquid films in the whole range of surface forces action. The adoption of the simplified Disjoining/Conjoining pressure isotherm with two regions may be considered as a study limitation with possible minor quantitative effects on results. In a future study an alternative Disjoining/Conjoining pressure isotherm with four regions could be introduced for comparison and results evaluation.
2. In Chapter 4 hysteresis of contact angle for droplet on deformable substrate was theoretically investigated and the effect of model parameters on the values of static advancing and static receding contact angles was presented. Model results where qualitatively verified with previously obtained results on various polymer substrates. The study's primary limitations concentrate on the adoption of a simplified linear Disjoining/Conjoining pressure isotherm with specific isotherm parameters, adopted in order to obtain an analytical solution. An additional limitation is related to the assumption of negligible substrate surface tension adopted for simplification, which may have had a possible quantitative effect on the values of contact angles. These limitations can be avoided in future research via the adoption of a real Disjoining/Conjoining isotherm and via consideration of substrate's surface tension, where full scale computations will be required.
3. A new theory of foam drainage placed on a thin porous layer is developed in Chapter 5 and theoretical predictions on the process kinetics are compared with experimental findings with good agreement. There may be some possible limitations in this study related to the methodology and assumptions for model development. More specifically, we investigated foam produced by SDS surfactant of 4CMC placed on a thin porous substrate of known properties and assumed that all bubbles are of uniform size. The limitations of the study could be related to the restricted selection of surfactant type and concentration and investigated porous substrate. Research limitations can be eliminated in future research with consideration of bubble size distribution and a wider selection of surfactants and porous layers.
4. A new theory of foam drying under microgravity conditions is presented in Chapter 6 where model predictions on time evolutions of spreading radius of foam in contact with porous layer are presented and compared with experimental results. We considered foam produced by a Newtonian surfactant solution in a column positioned horizontally and attached to a thin porous layer and assumed that all bubbles are of uniform size during the duration of the experiments. The limitations

of this study are related to the specific selection of one type of surfactant solution and the assumption of uniform bubble radius. In future research these limitations could be eliminated by investigating multiple surfactant solutions with low liquid-air surface viscosity for comparison and with consideration of bubble size distribution.

5. In Chapter 7 foamed emulsion drainage was investigated theoretically and experimentally. A new mathematical model was developed taking into account the non-Newtonian behaviour of foamed emulsion systems and the effect of surface viscosity was considered. Time evolutions of foam height, liquid layer and liquid volume fractions were theoretically predicted and compared with experimental results with good agreement. Foamed emulsions were created by SDS surfactant and rapeseed oil of various proportions with the double syringe emulsification method. The research limitations identified during this study are: i) the specific emulsification method used for emulsion preparation which does not allow comparison between different methods and their effect on the stability of foamed emulsions ii) the selection of one type of surfactant solution and of oil for emulsion preparation. Additionally, it was observed during the experiments that drainage of foamed emulsion systems occurs at the very beginning of foam formation before the initial foam height was reached. The absence of experimental measurements of liquid volume fraction at the top and bottom of the foam for the initial short rapid drainage theoretically predicted entails an identified study limitation which can be eliminated in a future research of foamed emulsion drainage under microgravity conditions.

CHAPTER 9

Conclusions and Future work

9.1 Conclusions

Wetting phenomena and Foam drainage on complex substrates have been investigated and discussed in the following areas:

1) Equilibrium droplets on deformable substrates: Equilibrium conditions
2) Hysteresis of Contact Angle of Sessile Droplets on Deformable Substrates: Influence of Disjoining Pressure
3) Foam drainage placed on a thin porous layer
4) Drying of Foam under Microgravity Conditions
5) Modelling of foamed emulsion drainage

Equilibrium conditions of droplets on deformable substrates were investigated in Chapter 3. A piece-wise linear disjoining/conjoining pressure isotherm was adopted to obtain an analytical solution and low slope approximation was used for all calculations. The fundamental principle of a minimum value of excess free energy for both profiles of the droplet and the deformable substrate was considered to derive the profiles of the droplet and the deformable substrate. The two Jacobi's equations deduced were investigated and it was shown that are always increasingly positive for the bulk part of the droplet and for the transitional region where disjoining/conjoining pressure is predominant. It was proven for the first-time using Jacobi's sufficient condition that the derived profiles of the droplet and the deformable substrate really correspond to equilibrium.

According to Kelvin's equation, to reach equilibrium contact angle the droplet should be at the equilibrium with oversaturated vapour. Therefore, only non-equilibrium contact angles (static advancing and static receding contact angles) can be observed experimentally. A theory of contact angle hysteresis of sessile liquid droplets on deformable/soft substrate was developed in Chapter 4. Calculations showed that advancing and receding contact angles of a droplet on smooth, homogeneous deformable substrate depend on droplet volume, and the elasticity of the substrate. Both advancing and receding contact angles decrease with increasing substrate elasticity. Hysteresis of contact angle was proven to be lower for deformable substrates than that for non-deformable. For model derivation, a simplified disjoining pressure isotherm was adopted, which allows direct calculations of static advancing/receding contact angles on deformable substrates, and Winkler's model was considered to account for the elasticity of the substrate.

In Chapter 5 a theory of foam drainage of foam produced from a Newtonian surfactant solution placed on a thin porous layer (completely wettable) was developed and surface viscosity was taken into account. The derived equations of foam drainage and liquid imbibition into the porous layer were solved using boundary conditions and describe the evolution of liquid volume fraction inside the foam. Theoretical predictions of foam height and wetted area time evolutions are compared with experimentally obtained results and the effect of model parameters on the kinetics of the drainage/imbibition process were investigated.

A new method of drying foams in the absence of gravitational field is presented in Chapter 6 where foam is suggested to be placed on a porous support, which will absorb the liquid from foam based on capillary forces only. Triton-X100 at concentrations above CMC on four types of filter papers, i.e. grade 1,3,5 and 601 were investigated. The experiments were conducted in the laboratory where the effect of gravity was eliminated by using a foam column placed horizontally, in contact on one end on a thin porous substrate. Theoretical model predictions of wetted radius inside the porous substrate were compared with experimental observations and comparison showed a reasonable agreement for all investigated foam/porous substrate systems.

The process of foam drainage emulsion foam was investigated in Chapter 7. Four different foamed emulsion systems of SDS surfactant and rapeseed oil were prepared using the double syringe emulsification technique and a bubbling through capillaries in a foam column. A theoretical model was developed, taking into account the effect of surface viscosity and non-Newtonian behaviour of the foamed emulsion and the kinetics of the process were predicted. Model predictions of time evolutions of foam height, free liquid layer formation, and liquid volume fraction for investigated foamed emulsion systems of various oil volume fractions were compared with experimental observations. The results showed no measurable change of the foam height while a free liquid layer starts to accumulate at the bottom boundary of the foam after an initial rapid increase of liquid volume fraction to the maximum value at the bottom of the foam. Comparison between experimental observations and model calculations showed a reasonable agreement.

9.2 Future work

Recommendations for future investigations in the area of wetting phenomena and foam drainage on complex substrates are provided in this section, taking into consideration the areas investigated above, assumptions undertaken and obtained results.

1. Equilibrium conditions of droplet on deformable substrate were investigated and presented in Chapter 3. The action of disjoining/ conjoining pressure was considered to act simultaneously with capillary pressure yielding the equilibrium liquid profile and a piece-wise linear disjoining/conjoining pressure isotherm was adopted which retains the main important properties of the real s-shaped isotherm. The validity of the Jacobi's sufficient condition was verified for the first time which sets an area for further investigation. The study made a significant contribution to our understanding of equilibrium conditions of droplets on deformable substrates, presented a new method of verification of the obtained solution via the development of a mathematical model and will initiate the development of new studies in the area of interfacial science. Therefore, any previously obtained solution of equilibrium should be checked using Jacobi's sufficient condition and their validity is yet to be confirmed. Additionally, droplet on deformable substrate and Jacobi's necessary condition of equilibrium can be investigated in a future research in the case of a simplified disjoining/conjoining pressure isotherm with four regions, a, b, c and spherical as shown in Figure 9.1.

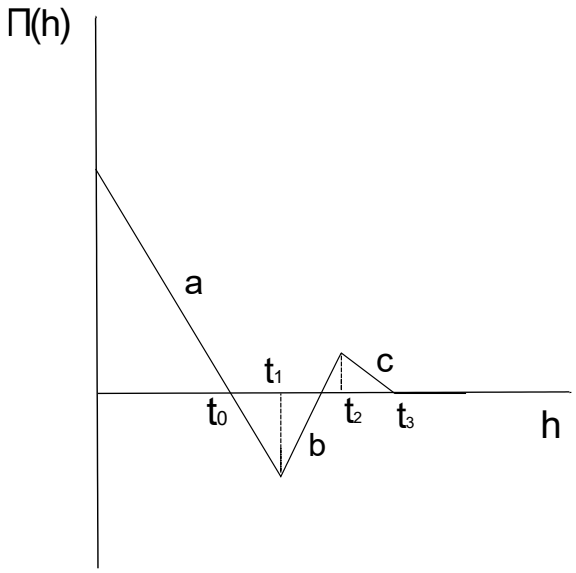

Figure 9. 1: Piece-wise linear Disjoining/Conjoining pressure isotherm with four regions, a, b, c and spherical.

Jacobi's condition should identify the only possible/stable solution at region "b" where oscillatory solution is possible.

2. Hysteresis of contact angle of droplet on deformable substrate was theoretically investigated in Chapter 4. The theoretical model of contact angle hysteresis was developed in terms of a simplified disjoining pressure isotherm to obtain an analytical solution, which accounts for the action of surface forces in the vicinity of the three-phase contact line. Both advancing and receding contact angles on smooth and homogenous deformable substrates where proven to depend on the action of the Disjoining/Conjoining pressure, the droplet volume and the elasticity of the substrate. The results of the study were qualitatively verified with previously experimental obtained results on various polymer substrates. The action of the Disjoining/Conjoining pressure is predominant at the vicinity of the three-phase contact line and cannot be ignored. The research presented in Chapter 4 entails a fundamental study which aims to increase our understanding on the parameters that affect the values of advancing and receding contact angles for droplets on elastic substrates. The developed mathematical model can be adopted in future research studies on contact angle hysteresis and suggests consideration of the action of the Disjoining/Conjoining pressure near the three-phase contact line where surface forces become predominant. Considering the assumptions undertaken, it is suggested that the research could be extended in the future by considering the case of the real s-shaped isotherm where full scale computer simulations will be necessary. In addition, a comparison of theoretical predictions with experimentally obtained results is suggested for future investigation.
3. Simultaneous foam drainage and imbibition of liquid from foam into thick porous substrate was only previously theoretically investigated by Arjmandi-Tash et.al (19) where a system of two interconnected differential equations was derived to describe the kinetics of foam drainage and

penetration into the porous substrate. However, it is difficult to experimentally investigate the kinetics of wetted area on thick, porous substrate. In Chapter 5 the rate of drainage and the rate of penetration and wetted area was investigated for the first time both theoretically and experimentally, for the case on foam drainage/imbibition into thin, porous substrate. The process investigated (40) allowed the development of a new system of differential equations able to describe the rate of liquid volume fraction inside the foam and the rate of wetted area inside the thin porous layer. The mathematical model developed was experimentally verified and comparison showed reasonable agreement. The suggested methodology and obtained results of the study demonstrate significance contribution to our understanding on the factors and parameters that affect the process of simultaneous foam drainage and imbibition into thin porous layers with multiple industrial and medical applications where the substrate is porous (such as skin and hair). For a thin, porous layer, the saturation in the vertical direction occurs much faster that in the horizontal direction. The properties of the substrate which determine this function are yet to be experimentally researched. As a future investigation the difference between thin and thick porous substrates is proposed where multiple porous layers will be investigated.

4. In Chapter 6 the previously developed theory of foam drainage on thin porous material (40), has been modified to be applied to foams drying on porous material in microgravity conditions. Experiments of foam made by TritonX-100– 50 CMC and Triton X-100 – 20 CMC placed in a horizontal column attached to thin porous layers of different grades were conducted in the laboratory while the effect of gravity was eliminated and results obtained were compared with model predictions. Investigating foam drainage under microgravity conditions allows exclusive investigation of capillary flows and helps overcoming the instability barriers imposed by gravity. In addition, it allows gaining information and understanding of foam stability, rheology and liquid distribution in microgravity conditions. The study suggests a new method of foam drying under microgravity conditions and entails a pioneering study on the parameters that affect the interaction of foams with thin porous material in the absence of gravity. The developed theory and mathematical model can be adopted on future research and could have significant academic, medical and industrial impact for foam related processes where gravity is not desirable or should be eliminated for product investigation and improvement. Considering the adopted methodology and assumptions undertaken, the developed theory can be extended in the future for foam produced by surfactants with low liquid-air surface viscosity and bubble size distribution could be considered.
5. A theory of foamed emulsion drainage has been presented in Chapter 7 where time evolutions of both the foam height and the thickness of the free liquid layer are evaluated. Theoretical predictions of rate of drainage, free liquid layer formation, foam height and liquid volume fraction for foamed emulsion systems made of SDS solution and oil of various oil volume fractions (rapeseed oil) are compared with experimental observations. These types of systems are frequently used for the production of multiple food, cleaning, cosmetic and pharmaceutical products and the study could have a significant academic and industrial impact for foamed emulsion related projects and product development. Considering the undertaken methodology, it is suggested that a different type of emulsification method is used for emulsion preparation, such as sonication, and the effect on foam stability and the kinetics of the process can be investigated theoretically and experimentally. In addition, foamed emulsion drainage/imbibition into porous layers can be investigated in the future for pharmaceutical applications and the effect of system parameters on the interaction can be evaluated through integration analysis. During the duration of the experiments it was observed that an initial short rapid drainage occurs which does not

allow experimental evaluation of liquid volume fraction at the top and bottom of the foam. In a future research the effect gravity can be eliminated by performing experiments under microgravity conditions.

REFERENCES

1. Brannick J, Kirshtein A, Liu C. Dynamics of Multi-Component Flows: Diffusive Interface Methods With Energetic Variational Approaches. Vol. 2, Reference Module in Materials Science and Materials Engineering. Elsevier Ltd.; 2016. 1–7 p.
2. Ronald Young F. Fizzics: The Science of Bubbles, Droplets, and Foams. The Johns Hopkins University Press; 2011. 1–70 p.
3. Starov VM, Velarde MG. Wetting and Spreading Dynamics, Second Edition. CRC Press Taylor and Francis Group; 2019. 1–157 p.
4. Bonn D, Eggers J, Indekeu J, Meunier J. Wetting and spreading. Rev Mod Phys. 2009;81(2):739–805.
5. Koehler SA, Hilgenfeldt S, Stone HA. Generalized view of foam drainage: Experiment and theory. Langmuir. 2000;16(15):6327–41.
6. Dias MM, Wilkinson D. Percolation with trapping. J Phys A Gen Phys. 1986;19(15):3131–46.
7. Kessler DA, Koplik J, Levine H. Geometrical models of interface evolution. III. Theory of dendritic growth. 1985;31(3):1712–7.
8. Zhao Y, Jones SA, Brown MB. Dynamic foams in topical drug delivery. Jpp. 2010;62:678–84.
9. Housman T, Mellen B, Rapp S, Fleischer AJ, Feldman S. Patients with psoriasis prefer solution and foam vehicles: a quantitative assessment of vehicle preference. Cutis. 2002;70(6):327–332.
10. Arzhavitina A, Steckel H. Foams for pharmaceutical and cosmetic application. Int J Pharm. 2010;394(1–2):1–17.
11. Schramm LL. Emulsions, Foams, and Suspensions: Fundamentals and Applications. New York: Wiley-VCH; 2006.
12. Garti N, Bisperink C. Double emulsions: Progress and applications. Curr Opin Colloid Interface Sci. 1998;3(6):657–67.
13. Koczo K, Lobo LA, Wasan DT. Effect of oil on foam stability: Aqueous foams stabilized by emulsions. J Colloid Interface Sci. 1992;150(2):492–506.
14. Schneider M, Zou Z, Langevin D, Salonen A. Foamed emulsion drainage: Flow and trapping of drops. Soft Matter. 2017;13(22):4132–41.
15. Koursari N, Johnson P, Parsa M, Schneider M, Trybala A, Starov VM. Modelling of foamed emulsion drainage. Colloids Surfaces A Physicochem Eng Asp. 2020;600.
16. Bhakta AR, Khilar KC. A Network Simulation for Drainage of Static Foam Columns. Langmuir. 1991;7(8):1827–32.
17. Purdon CH, Haigh JM, Surber C, Smith EW. Foam Drug Delivery in Dermatology. Am J Drug Deliv. 2003;1:71–5.
18. Huang X, Tanojo H, Deng H, Lenn J, Krochmal L. A novel foam vehicle for delivery of topical corticosteroids. J Am Acad Dermatol. 2005;53(1):S26–38.
19. Arjmandi-Tash O, Kovalchuk N, Trybala A, Starov V. Foam drainage placed on a porous substrate. Soft Matter. 2015;11(18):3643–52.
20. Carre A, Shanahan MER. Viscoelastic Braking of a Running Drop. Langmuir. 2001;17(10):2982–5.

21. Jerison ER, Xu Y, Wilen LA, Dufresne ER. The Deformation of an Elastic Substrate by a Three-Phase Contact Line. 2011;2–5.

22. Park SJ, Weon BM, Lee JS, Lee J, Kim J, Je JH. Visualization of asymmetric wetting ridges on soft solids with X-ray microscopy. Nat Commun. 2014;5:1–7.

23. Pericet-Camara R, Auernhammer GK, Koynov K, Lorenzoni S, Raiteri R, Bonaccurso E. Solid-supported thin elastomer films deformed by microdrops. Soft Matter. 2009;5(19):3611–7.

24. Andreotti B, Bäumchen O, Boulogne F, Daniels KE, Dufresne ER, Perrin H, et al. Solid capillarity: When and how does surface tension deform soft solids? Soft Matter. 2016;12(12):2993–6.

25. Lester G. Contact angles of liquids at deformable solid surfaces. J Colloid Sci. 1961;16:315–326.

26. Style RW, Dufresne ER. Static wetting on deformable substrates, from liquids to soft solids. Soft Matter. 2012;8(27):7177–84.

27. Sell P -J, Neumann AW. The Surface Tension of Solids. Angew Chemie Int Ed English. 1966;5(3):299–307.

28. Tamarkin D, Friedman D, Shemer A. Emollient foam in topical drug delivery. Expert Opin Drug Deliv. 2006;3(6):799–807.

29. Kahanek N, Gelbard C, Hebert A. Desonide: a review of formulations, efficacy and safety. Expert Opin Investig Drugs. 2008;17(7):1097–104.

30. Exerowa, D., Kruglyakov, P. M., Möbius, D. & Miller R. Foam and foam films: theory. Experiment Application. Marcel Dekker. 1998;

31. Hudales JBM, Stein HN. The influence of solid particles on foam and film drainage. J Colloid Interface Sci. 1990;140(2):307–13.

32. Verbist G, Weaire G. A soluble model for foam drainage. Epl. 1994;26(8):631–4.

33. Verbist G, Weaire D, Kraynik AM. The foam drainage equation. J Phys Condens Matter. 1996;8(21):3715–31.

34. Jun S, Pelot DD, Yarin AL. Foam consolidation and drainage. Langmuir. 2012;28(12):5323–30.

35. Goldfarb II, Kahn K, Schreiber I. . Izv Akad Nauk SSSR. 1987;

36. Goldshtein V, Goldfarb I, Schreiber I. Multiphase Flow at press. Int J. 1996;

37. Koehler SA, Stone HA, Brenner MP, Eggers J. Dynamics of foam drainage. Phys Rev E - Stat Physics, Plasmas, Fluids, Relat Interdiscip Top. 1998;58(2):2097–106.

38. Cox SJ, Verbist G. Liquid flow in foams under microgravity. Microgravity Sci Technol. 2003;14(4):45–52.

39. Caps H, Cox SJ, Decauwer H, Weaire DL, Vandewalle N. Capillary rise in foams under microgravity. Colloids Surf, A,. 2005;261:131–4.

40. Koursari N, Arjmandi-Tash O, Johnson P, Trybala A, Starov VM. Foam drainage placed on thin porous layer. Soft Matter. 2019;15:5331–44.

41. Caps H, Soyez G, Chevalier M-L, Decauwer H, Ausloos M, Vandewalle N. Foam imbibition in microgravity. Eur Phys J B - Condens Matter. 2003;33(1):115–9.

42. Banhart J. Foam Metal: The Recipe. Europhys news. 1999;30(17).

43. Hart D, Hansen N, Legros J-C, Schramm LL. Microgravity, industry related research for oil recovery. Am Inst Phys. 1997;387(761).

44. Vandewalle N, Caps H, Delon G, Saint-Jalmes A, Rio E, Saulnier L, et al. Foam stability in microgravity. J Phys Conf Ser. 2011;327(1).

45. Xu W, Nikolov A, Wasan DT, Gonsalves A, Borwankar RP. Foam film rheology and thickness stability of foam-based food products. Colloids Surfaces A Physicochem Eng Asp. 2003;214(1–3):13–21.

46. Kokini J, Van Aken G. Discussion session on food emulsions and foams. Food Hydrocoll. 2006;20(4):438–45.

47. Arjmandi-Tash O, Kovalchuk NM, Trybala A, Kuchin I V., Starov V. Kinetics of Wetting and Spreading of Droplets over Various Substrates. Langmuir. 2017;33(18):4367–85.

48. Young T. An Essay on the Cohesion of Fluids. Vol. 95. Philosophical Transactions of the Royal Society of London; 1805. 65–87 p.

49. Koursari N, Ahmed G, Starov VM. Equilibrium Droplets on Deformable Substrates: Equilibrium Conditions. Langmuir. 2018;34(19):5672–7.

50. Derjaguin BV, Churaev NV, Muller VM. Surface Forces. Springer, Boston, MA; 1987.

51. Donaldson SH, Røyne A, Kristiansen K, Rapp M V., Das S, Gebbie MA, et al. Developing a general interaction potential for hydrophobic and hydrophilic interactions. Langmuir. 2015;31(7):2051–64.

52. Starov VM. Equilibrium and hysteresis contact angles. Moscow Inst Food Technol. 1992;39:147–73.

53. Starov VM, Velarde MG, Radke CJ. Wetting and Spreding Dymanics. CRC Press Taylor and Francis Group; 2007.

54. Attinger D, Moore C, Donaldson A, Jafari A, Stone HA. Fluid dynamics topics in bloodstain pattern analysis: Comparative review and research opportunities. Forensic Sci Int. 2013;231(1–3):375–96.

55. Eral HB, 'T Mannetje DJCM, Oh JM. Contact angle hysteresis: A review of fundamentals and applications. Colloid Polym Sci. 2013;291(2):247–60.

56. Rusanov A. Theory of wetting of elastically deformed bodies .1. Deformation with a finite contact-angle. Colloid J USSR. 1975;37(4):614–622.

57. Rusanov AI. On the Thermodynamics of Deformable Solid Surfaces. 1978;63(2).

58. Shanahan ME. The spreading dynamics of a liquid drop on a viscoelastic solid. J Phys D Appl Phys. 1988;21:981.

59. Shanahan M, de Gennes P. The ridge produced by a liquid near the triple line solid/liquid/fluid. Compt Rend Acad Sci Paris. 1986;302:517–52.

60. Chen L, Bonaccurso E, Gambaryan-Roisman T, Starov V, Koursari N, Zhao Y. Static and dynamic wetting of soft substrates. Curr Opin Colloid Interface Sci. 2018;36:46–57.

61. Neumann F. Lectures on the Theory of Capillarity. Teubner; B G Teubner Leipzig, Ger. 1894;

62. White LR. The contact angle on an elastic substrate . 1 . The role of disjoining pressure in the surface mechanics. 2003;258:82–96.

63. Ahmed G, Kalinin V V., Arjmandi-Tash O, Starov VM. Equilibrium of droplets on a deformable substrate: Influence of disjoining pressure. Colloids Surfaces A Physicochem Eng Asp. 2017;521:3–12.

64. Ahmed G, Koursari N, Kuchin I V., Starov VM. Hysteresis of Contact Angle of Sessile Droplets on Deformable Substrates: Influence of Disjoining Pressure. Colloids Surfaces A Physicochem Eng Asp. 2018;546(March):129–35.

65. Style RW, Che Y, Wettlaufer JS, Wilen L, Dufresne ER. Universal deformation of soft substrates near a contact line and the direct measurement of solid surface stresses. 2013;1–5.

66. Pericet-Cámara R, Best A, Butt HJ, Bonaccurso E. Effect of capillary pressure and surface tension on the deformation of elastic surfaces by sessile liquid microdrops: An experimental investigation. Langmuir. 2008;24(19):10565–8.

67. Lubbers LA, Weijs JH, Botto L, Das S, Andreotti B, Snoeijer JH. Drops on soft solids: Free energy and double transition of contact angles. J Fluid Mech. 2014;747:1–12.

68. Bico J, Reyssat É, Roman B. Elastocapillarity: When Surface Tension Deforms Elastic Solids. Annu Rev Fluid Mech. 2017;50(1):629–59.

69. Style RW, Hyland C, Boltyanskiy R, Wettlaufer JS, Dufresne ER. Surface tension and contact with soft elastic solids. Nat Commun. 2013;4:1–6.

70. Shuttleworth R. The Surface Tension of Solids. Proc Phys Soc Sect A. 1950;63(444).

71. Keddie JL, Jones RAL, Cory RA. Size-dependent depression of the glass transition temperature in polymer films. Epl. 1994;27(1):59–64.

72. Forrest JA, Dalnoki-Veress K, Stevens JR, Dutcher JR. Effect of free surfaces on the glass transition temperature of thin polymer films. Phys Rev Lett. 1996;77(10):2002–5.

73. Winkler E. The theory of elasticity and strength with special reference to their application in the art for polytechnics, building academies, engineers, mechanical engineers. Archit Etc H Dominicus. 1867;

74. Style RW, Jagota A, Hui C-Y, Dufresne ER. Elastocapillarity: Surface Tension and the Mechanics of Soft Solids. Annu Rev Condens Matter Phys. 2017;8:99–118.

75. Kuchin I V., Starov VM. Hysteresis of the Contact Angle of a Meniscus Inside a Capillary with Smooth, Homogeneous Solid Walls. Langmuir. 2016;

76. Kuchin I, Starov V. Hysteresis of contact angle of sessile droplets on smooth homogeneous solid substrates via disjoining/conjoining pressure. Langmuir. 2015;

77. Kerr AD. Elastic and Viscoelastic Foundation Models. J Appl Mech. 1964;

78. Ahmed G, Koursari N, Trybala A, Starov VM. Sessile Droplets on Deformable Substrates. Colloids and Interfaces. 2018;2(4):56.

79. Purewal T, Grant D. Metered Dose Inhaler Technology. Buffalo Grove Interpharm Press. 1998;97–99.

80. Mazzotta A, Esposito M, Carboni I, Schipani C, Chimenti S. Clobetasol propionate foam 0.05% as a novel topical formulation for plaque-type and scalp psoriasis. J Dermatolog Treat. 2007;18(2):84–7.

81. Franz TJ, Parsell DA, Halualani RM, Hannigan JF, Kalbach JP, Harkonen WS. Betamethasone Valerate Foam 0.12%: A Novel Vehicle with Enhanced Delivery and Efficacy. Int J Dermatol. 1999;38(8):628–632.

82. Germick RJ, Amardeep SR, Narsimhan G. Experimental investigation of static drainage of protein stabilized foams — Comparison with model. J Food Eng. 1994;23(4):555–78.

83. Ramani M V., Kumar R, Gandhi KS. A model for static foam drainage. Chem Eng Sci. 1993;48:455–

465.

84. Magrabi SA, Dlugogorski BZ, Jameson GJ. Free drainage in aqueous foams: Model and experimental study. AIChE J. 2001;47(2):314–27.

85. Koehler SA, Hilgenfeldt S, Stone HA. Generalized view of foam drainage: Experiment and theory. Langmuir. 2000;16(15):6327–41.

86. Bhakta AR, Khilar KC. A Network Simulation for Drainage of Static Foam Columns. Langmuir. 1991;7(8):1827–32.

87. Hutzler S, Weaire D, Saugey A, Cox SJ, Peron N. The physics of foam drainage. SEPAWA-Kongress 2005. 2005;191–206.

88. Sharma MK, Shah DO, Brigham WE. The influence of temperature on surface and microscopic properties of surfactant solutions in relation to fluid. AIChE J. 1985;31(2):222.

89. Exerowa D, Kruglyakov PM. Foams and foam films: theory, experiment, application. Elsevier. 1998;

90. Gururaj M, Kumar R, Gandhi KS. A Network Model of Static Foam Drainage. Langmuir. 1995;11(4):1381–91.

91. Bhakta A, Ruckenstein E. Decay of standing foams: drainage, coalescence and collapse. Adv Colloid Interface Sci. 1997;70(1).

92. Lodge RA, Bhushan B. Wetting properties of human hair by means of dynamic contact angle measurement. J Appl Polym Sci. 2006;102(6):5255–65.

93. Zviak C. The Science of Hair Care; Marcel DekkerNew York. 1986;

94. Bureiko A, Trybala A, Kovalchuk N, Starov V. Current applications of foams formed from mixed surfactant–polymer solutions. Elsevier. 2015;222:670–7.

95. Kornev KG, Neimark A V., Rozhkov AN. Foam in porous media: thermodynamic and hydrodynamic peculiarities. Vol. 82, Advances in Colloid and Interface Science. 1999. 127–187 p.

96. Huang X, Tanojo H, Lenn J, Deng CH, Krochmal L. A novel foam vehicle for delivery of topical corticosteroids. J Am Acad Dermatol. 2005;53(1 SUPPL.):26–38.

97. Trybala A, Koursari N, Johnson P, Arjmandi-Tash O, Starov V. Interaction of liquid foams with porous substrates. Curr Opin Colloid Interface Sci. 2019;39:212–9.

98. Bureiko A, Arjmandi-Tash O, Kovalchuk N, Trybala A, Starov V. Interaction of foam with a porous medium: Theory and calculations. Eur Phys J Spec Top. 2015;224(2):459–71.

99. Lubarda VA. Mechanics of a liquid drop deposited on a solid substrate. Soft Matter. 2012;8(40):10288–10297.

100. Deryagin BV, Starov VM, Churaev NV. Pressure on a Wetting Perimeter. Colloid J. 1982;44:770−775.

101. Shanahan M, de Gennes P. Adhesion 11. Springer. 1987;2:517–521.

102. Gielok M, Lopes M, Bonaccurso E, Gambaryan-roisman T. Droplet on an elastic substrate : Finite Element Method coupled with lubrication approximation. Colloids Surfaces A Physicochem Eng Asp. 2017;521:13–21.

103. Shanahan MER. On the form of a locally perturbed liquid/solid/fluid triple line. J Phys D Appl Phys. 1990;23(6):703–5.

104. Style RW, Che Y, Ji S, Mook B, Ho J, Hyland C, et al. Patterning droplets with durotaxis. 2013;

105. Limat L. Straight contact lines on a soft , incompressible solid. 2012;1–13.

106. Marchand A, Das S, Snoeijer JH, Andreotti B. Capillary Pressure and Contact Line Force on a Soft Solid. 2012;1–5.

107. Schulman RD, Dalnoki-veress K. Liquid Droplets on a Highly Deformable Membrane. 2015;115:1–5.

108. Shanahan MER, Garré· A. Viscoelastic Dissipation in Wetting and Adhesion Phenomena. Langmuir. 1995;11(4):1396–402.

109. Gelfand IM, Fomin S V. Calculus of Variations. Prentice-Hall, Inc, Englewood Cliffs, N.J; 1963. 117–120 p.

110. Starov VM. Static contact angle hysteresis on smooth, homogeneous solid substrates. Colloid Polym Sci. 2013;

111. Li J, Miller R, Wüstneck R, Möhwald H, Neumann AW. Use of pendent drop technique as a film balance at liquid/liquid interfaces. Colloids Surfaces A Physicochem Eng Asp. 1995;96(3):295–9.

112. Thoma M, Möhwald H. Monolayers of dipalmitoylphosphatidylcholine at the oil-water interface. Colloids Surfaces A Physicochem Eng Asp. 1995;95(2–3):193–200.

113. Li J, Miller R, Möhwald H. Characterisation of phospholipid layers at liquid interfaces. 2. Comparison of isotherms of insuloble and soluble films of phospholipids at different fluid/water interfaces. Colloids Surfaces A Physicochem Eng Asp. 1996;114:123–30.

114. Kumar G, Prabhu KN. Review of non-reactive and reactive wetting of liquids on surfaces. Adv Colloid Interface Sci. 2007;133(2):61–89.

115. Miller R, Krägel J, Wüstneck R, Wilde PJ, Li JB, Fainerman VB, et al. Adsorption kinetics and rheological properties of food proteins at air/water and oil/water interfaces. Nahrung - Food. 1998;42(3–4):225–8.

116. Bormashenko E, Bormashenko Y, Whyman G, Pogreb R, Musin A, Jager R, et al. Contact angle hysteresis on polymer substrates established with various experimental techniques, its interpretation, and quantitative characterization. Langmuir. 2008;24(8):4020–5.

117. Rioboo R, Voué M, Adão H, Conti J, Vaillant A, Seveno D, et al. Drop impact on soft surfaces: Beyond the static contact angles. Langmuir. 2010;26(7):4873–9.

118. Kristen N, Von Klitzing R. Effect of polyelectrolyte/surfactant combinations on the stability of foam films. Soft Matter. 2010;6(5):849–61.

119. Sita Ram Sarma DSH, Pandit J, Khilar KC. Enhancement of stability of aqueous foams by addition of water-soluble polymers-measurements and analysis. J Colloid Interface Sci. 1988;124(1):339–48.

120. Stevenson P. Foam Engineering: Fundamentals and Applications. West Sussex, United Kingdom: John Wiley & Sons, Ltd.; 2012. 7–12 p.

121. Lioumbas JS, Georgiou E, Kostoglou M, Karapantsios TD. Foam free drainage and bubbles size for surfactant concentrations below the CMC. Colloids Surfaces A Physicochem Eng Asp. 2015;487:92–103.

122. Schramm LL. Foams: Fundamentals and applications in the petroleum industry. Washington DC: ACS Advances in Chemistry Series No. 242 (Am. Chem. Soc.); 1994.

123. Koehler SA, Hilgenfeldt S, Stone HA. Foam Drainage in 2D: Comparison of Experiment and Theory. Am Phys Soc Div Fluid Dyn Meet New Orleans, USA. 1999;

124. Plateau J. Statique Expe ´rimentale et The ´orique Des Liquides Soumis Aux Seules Forces Mole ´culaires. Paris: Gauthier-Villars; 1873.

125. Weaire D, Hutzler S, Cox S, Kern N, Alonso MD, Drenckhan W. The fluid dynamics of foams. J Phys Condens Matter. 2003;15(1).

126. Carn F, Colin A, Pitois O, Vignes-Adler M, Backov R. Foam drainage in the presence of nanoparticle-surfactant mixtures. Langmuir. 2009;25(14):7847–56.

127. Gubes M, Keskin Y, Oturanc G. Numerical solution of time-dependent Foam Drainage Equation (FDE). Methods Differ Equations. 2015;3(2):111–22.

128. Pitois O, Fritz C, Vignes-Adler M. Liquid drainage through aqueous foam: Study of the flow on the bubble scale. J Colloid Interface Sci. 2005;282(2):458–65.

129. Hutzler S, Cox SJ, Wang G. Foam drainage in two dimensions. Colloids Surfaces A Physicochem Eng Asp. 2005;263(1-3 SPEC. ISS.):178–83.

130. Koehler SA, Hilgenfeldt S, Stone HA. Foam drainage on the microscale: I. Modeling flow through single Plateau borders. J Colloid Interface Sci. 2004;276(2):420–38.

131. Neethling SJ, Lee HT, Cilliers JJ. A foam drainage equation generalized for all liquid contents. J Phys Condens Matter. 2002;14(3):331–42.

132. Hilgenfeldt S, Koehler SA, Stone HA. Dynamics of coarsening foams: Accelerated and self-limiting drainage. Phys Rev Lett. 2001;86(20):4704–7.

133. Koehler SA, Hilgenfeldt S, Stone HA. Liquid flow through aqueous foams: The node-dominated foam drainage equation. Phys Rev Lett. 1999;82(21):4232–5.

134. Cox SJ, Weaire D, Hutzler S, Murphy J, Phelan R, Verbist G. Applications and generalizations of the foam drainage equation. Proc R Soc London Ser A Math Phys Eng Sci. 2000;456:2441–64.

135. Weaire DL, Hutzler S, Verbist G, Peters E. Advances in Chemical Physics. Adv Chem Physics, ed I Prigogine S A Rice, John Wiley Sons, Inc, Hoboken, NJ, USA. 1997;

136. Sun Q, Tan L, Wang G. Liguid Foam Drainage:An Overview. Int J Mod Phys B. 2008;22:2333–54.

137. Hutzler S, Weaire D. Foam coarsening under forced drainage. Philos Mag Lett. 2000;80(6):419–25.

138. Gottlieb AB, Ford RO, Spellman MC. The efficacy and tolerability of clobetasol propionate foam 0.05% in the treatment of mild to moderate plaque-type psoriasis of nonscalp regions. J Cutan Med Surg. 2003;7(3):185–92.

139. Starov VM, Kostvintsev SR, Sobolev VD, Velarde MG, Zhdanov SA. Spreading of Liquid Drops over Dry Porous Layers: Complete Wetting Case. Langmuir. 2002;252(25):397–408.

140. Wierenga PA, Gruppen H. New views on foams from protein solutions. Curr Opin Colloid Interface Sci. 2010;15(5):365–73.

141. Kruglyakov PM, Karakashev SI, Nguyen A V., Vilkova NG. Foam drainage. Curr Opin Colloid Interface Sci. 2008;13(3):163–70.

142. Wang Z, Narsimhan G. Model for Plateau border drainage of power-law fluid with mobile interface and its application to foam drainage. J Colloid Interface Sci. 2006;300(1):327–37.

143. Arjmandi-Tash O, Trybala A, Mahdi FM, Kovalchuk NM, Starov V. Foams built up by non-Newtonian polymeric solutions: Free drainage. Colloids Surfaces A Physicochem Eng Asp. 2017;521:112–20.

144. Saint-Jalmes A. Physical chemistry in foam drainage and coarsening. Soft Matter. 2006;2(10):836–

49.

145. Carrier V, Colin A. Coalescence in draining foams. Langmuir. 2003;19(11):4535–8.

146. Camlab. Whatman filter paper and more | Camlab UK [Internet]. 2018. Available from: https://www.camlab.co.uk/whatman-filter-papers-for-technical-use

147. Petkov JT, Danov KD, Denkov ND, Aust R, Durst F. Precise Method for Measuring the Shear Surface Viscosity of Surfactant Monolayers. Langmuir. 2002;12(11):2650–3.

148. Carrier V, Destouesse S, Colin A. Foam drainage: A film contribution? Phys Rev E - Stat Physics, Plasmas, Fluids, Relat Interdiscip Top. 2002;65(6):1–9.

149. Schramm LL. Emulsions, Foams, and Suspensions: Fundamentals and Applications. Wiley-VCH; 2005.

150. Banhart J, Weaire TD. On the road again:Metal Foams find favor. Am Inst Phys. 2002;37–42.

151. Dubois F, Joannes L, Dupont O, Dewandel JL, Legros JC. An integrated optical set-up for fluid-physics experiments under microgravity conditions. Meas Sci Technol. 1999;10(10):934–45.

152. Smirnov NN, Nikitin VF, Ivashnyov OE, Maximenko A, Thiercelin M, Vedernikov A, et al. Microgravity investigations of instability and mixing flux in frontal displacement of fluids. Microgravity Sci Technol. 2005;15(2):35–51.

153. Smirnov NN, Legros JC, Nikitin VF, Istasse E, Schramm L, Wassmuth F, et al. Filtration in artificial porous media and natural sands under microgravity conditions. Microgravity - Sci Technol. 2003;14(2):3–28.

154. Van Vaerenbergh S, Legros JC. Soret Coefficients of Organic Solutions Measured in the Microgravity SCM Experiment and by the Flow and Bénard Cells. J Phys Chem B. 1998;102(22):4426–31.

155. Touzet M, Galliero G, Lazzeri V, Saghir MZ, Montel F, Legros JC. Thermodiffusion: From microgravity experiments to the initial state of petroleum reservoirs. Comptes Rendus - Mec. 2011;339(5):318–23.

156. Prodi F, Santachiara G, Travaini S, Vedernikov A, Dubois F, Minetti C, et al. Measurements of phoretic velocities of aerosol particles in microgravity conditions. Atmos Res. 2006;82(1–2):183–9.

157. Divinis N, Karapantsios TD, Bruijn R de, Kostoglou M, Bontozoglou V, Legros JC. Lateral motion and interaction of gas bubbles growing over spherical and plate heaters. Microgravity - Sci Technol. 2006;18(3–4):204–9.

158. Smirnov NN, Nikitin VF, Legros JC, Istasse E, Schramm L, Wassmuth F. Microgravity investigations of capillary-driven imbibition and drainage in inhomogeneous porous media. Acta Astronaut. 2004;54(1):39–52.

159. Cox SJ, Weaire D, Verbist G. Comment on “foam imbibition in microgravity. An experimental study” by H. Caps, H. Decauwer, M.-L. Chevalier, G. Soyez, M. Ausloos and N. Vandewalle. Eur Phys J B. 2004;40(1):119–21.

160. Saint-Jalmes A, Cox SJ, Marze S, Safouane M, Langevin D, Weaire D. Experiments and simulations of liquid imbibition in aqueous foams under microgravity. Microgravity - Sci Technol. 2006;18:108–11.

161. Zhao Y, Brown MB, Jones SA. Pharmaceutical foams: are they the answer to the dilemma of topical nanoparticles? Nanomedicine Nanotechnology, Biol Med. 2010;6(2):227–36.

162. Farajzadeh R, Andrianov A, Krastev R, Hirasaki GJ, Rossen WR. Foam-oil interaction in porous media: Implications for foam assisted enhanced oil recovery. Adv Colloid Interface Sci. 2012;183–184:1–13.

163. Koursari N, Arjmandi-Tash O, Trybala A, Starov VM. Drying of Foam under Microgravity Conditions. Microgravity Sci Technol. 2019;31(5).

164. Weaire, D. and Hutzler S. The Physics of Foams. Univ Press Oxford. 1999;

165. Sigma-Aldrich (MERCK). Product results [Internet]. Available from: https://www.sigmaaldrich.com/catalog/search?term=FILTER+PAPERS&interface=All&N=0&mode=match partialmax&lang=en&region=GB&focus=product

166. Camlab. Quantitative Ashless Filter Papers [Internet]. 2019. Available from: https://www.camlab.co.uk/quantitative-ashless-filter-papers-c3583.aspx

167. Schramm LL. Emulsions, Foams, and Suspensions: Fundamentals and Applications. New York: Wiley-VCH; 2005. 223–321 p.

168. Wilde PJ. Interfaces: Their role in foam and emulsion behaviour. Curr Opin Colloid Interface Sci. 2000;5(3–4):176–81.

169. Ross S. Inhibition of Foaming. II1,2A Mechanism for the Rupture of Liquid Films by Antifoaming Agents. J Phys Colloid Chem. 1950;54(3):429–36.

170. Goyon J, Bertrand F, Pitois O, Ovarlez G. Shear induced drainage in foamy yield-stress fluids. Phys Rev Lett. 2010;104(12):4–7.

171. Salonen A, Lhermerout R, Rio E, Langevin D, Saint-Jalmes A. Dual gas and oil dispersions in water: Production and stability of foamulsion. Soft Matter. 2012;8(3):699–706.

172. Georgieva D, Cagna A, Langevin D. Link between surface elasticity and foam stability. Soft Matter. 2009;5(10):2063–71.

173. Monroy F, Giermanska Kahn J, Langevin D. Dilational viscoelasticity of surfactant monolayers. Colloids Surfaces A Physicochem Eng Asp. 1998;143(2–3):251–60.

174. Safouane M, Saint-Jalmes A, Bergeron V, Langevin D. Viscosity effects in foam drainage: Newtonian and non-newtonian foaming fluids. Eur Phys J E. 2006;19(2):195–202.

175. Gauchet S, Durand M, Langevin D. Foam drainage. Possible influence of a non-newtonian surface shear viscosity. J Colloid Interface Sci. 2014;449:373–6.

176. Saint-Jalmes A, Langevin D. Time evolution of aqueous foams: Drainage and coarsening. J Phys Condens Matter. 2002;14(40 SPEC.):9397–412.

177. Gaillard T, Roché M, Honorez C, Jumeau M, Balan A, Jedrzejczyk C, et al. Controlled foam generation using cyclic diphasic flows through a constriction. Int J Multiph Flow. 2017;96:173–87.

178. Magrabi SA, Dlugogorski BZ, Jameson GJ. Bubble size distribution and coarsening of aqueous foams. Chem Eng Sci. 1999;54(18):4007–22.

179. Bureiko A, Trybala A, Huang J, Kovalchuk N, Starov V. Effects of additives on the foaming properties of Aculyn 22 and Aculyn 33 polymeric solutions. Colloids Surfaces A Physicochem Eng Asp. 2014;460:265–71.

180. Degré G, Joseph P, Tabeling P, Lerouge S, Cloitre M, Ajdari A. Rheology of complex fluids by particle image velocimetry in microchannels. Appl Phys Lett. 2006;89(2):1–4.

181. Bird RB, Stewart WE, Lightfoot EN. Transport Phenomena (revised second ed.). New York: John Wiley & Sons, Ltd.; 2007.

182. Desai D, Kumar R. Flow through a plateau border of cellular foam. Chem Eng Sci. 1982;37(9):1361–

70.

183. Erçelebi EA, Ibanoğlu E. Rheological properties of whey protein isolate stabilized emulsions with pectin and guar gum. Eur Food Res Technol. 2009;229(2):281–6.

184. Rio E, Biance AL. Thermodynamic and mechanical timescales involved in foam film rupture and liquid foam coalescence. ChemPhysChem. 2014;15(17):3692–707.

185. Bibette J, Morse DC, Witten TA, Weitz DA. Stability criteria for emulsions. Phys Rev Lett. 1992;69(16):2439–42.

186. Khristov K, Exerowa D, Minkov G. Critical capillary pressure for destruction of single foam films and foam: Effect of foam film size. Colloids Surfaces A Physicochem Eng Asp. 2002;210(2–3):159–66.

187. Stevenson P. Remarks on the shear viscosity of surfaces stabilised with soluble surfactants. J Colloid Interface Sci. 2005;290(2):603–6.

188. Yazhgur P, Rio E, Rouyer F, Pigeonneau F, Salonen A. Drainage in a rising foam. Soft Matter. 2016;12(3):905–13.

189. Narsimhan G. A model for unsteady state drainage of a static foam. J Food Eng. 1991;14(2):139–65.

190. Exerowa D, Gochev G, Platikanov D, Liggieri L, Miller R. Foam Films and Foams: Fundamentals and Applications. London: CRC Press Taylor and Francis Group; 2019.